Laboratoire de Constructions Hydrauliques
Ecole Polytechnique Fédérale de Lausanne

Communication 12

Stability of linings by concrete elements for surface protection of overflow earthfill dams

Pedro de Almeida Manso

Editeur : Prof. Dr A. Schleiss

Lausanne, 2002

Communications du Laboratoire de constructions hydrauliques
Ecole Polytechnique Fédérale de Lausanne
Editeur: Prof. R. Sinniger

N° 1 1986 W. H. Hager
Discharge measurement structures

N° 2 1988 N. V. Bretz
Ressaut hydraulique forcé par seuil

N° 3 1990 R. Bremen
Expanding stilling basin

N° 4 1996 Dr R. Bremen
Ressaut hydraulique et bassins amortisseurs, aspects hydrauliques particuliers

N° 5 1997 Compte-rendu du séminaire à l'EPFL
Recherche dans le domaine des barrages, crues extrêmes

Communications du Laboratoire de constructions hydrauliques
Ecole Polytechnique Fédérale de Lausanne
Editeur: Prof. Dr A. Schleiss

N° 6 1998 N. Beyer Portner
Erosion des bassins versants alpins suisse par ruissellement de surface

N° 7 1998 G. De Cesare
Alluvionnement des retenues par courants de turbidité

N° 8 1998 J. Dubois
Comportement hydraulique et modélisation des écoulements de surface

N° 9 2000 J. Dubois, J.-L. Boillat
Routing System - Modélisation du routage de crues dans des systèmes hydrauliques à surface libre

N° 10 2002 J. Dubois, M. Pirotton
Génération et transfert des crues extrêmes - Le logiciel Faitou

N° 11 2002 A. Lavelli, G. De Cesare, J.-L. Boillat
Modélisation des courants de turbidité dans le bassin Nord du Lac de Lugano

N° 12 2002 P. de Almeida Manso
Stability of linings by concrete elements for surface protection of overflow earthfill dams

Laboratoire de Constructions Hydrauliques
Ecole Polytechnique Fédérale de Lausanne

Communication 12

Stability of linings by concrete elements for surface protection of overflow earthfill dams

Pedro de Almeida Manso

Editeur : Prof. Dr A. Schleiss

Lausanne, 2002

PREFACE

One third of all the identified dam failures in the world are caused by uncontrolled overtopping due to the insufficient capacity of spillways. There exist a large number of small and medium sized earthfill and rockfill dams up to 30 m for which the spillway was designed on the basis of too optimistic hydrological conditions and simplified models. For these dams, a promising solution to increase the spillway capacity is to provide an erosion resistant lining of the downstream face and to allow controlled overtopping. Several lining systems have been developed for embankment dams such as grass, riprap, paving, gabions, geo-textiles, concrete slabs and roller compacted concrete (RCC).

In the present communication, Mr. Pedro de Almeida Manso describes the result of a study regarding the stability of concrete macro-roughness linings for surface protection of overflow earthfill dams. Systematic hydraulic model tests were carried out with alternative macro-roughness concrete blocks placed on the downstream face of an embankment dam. Based on the observed flow characteristics and failure modes of the investigated types of lining elements, Mr. Manso developed a stability model to compute the safety factors for the surface protection lining. Synoptic design charts were derived for 1:3 dam slopes, allowing a rapid determination of the required dimensions and weight of the macro-roughness concrete blocks for a given design unit discharge and safety factor.

With his study, Mr. Manso gives very helpful information for all design engineers, who have the task to rehabilitate spillways of existing dams or to design new dams up to 30 m as well as for the protection of cofferdams.

Prof. Dr Anton J. Schleiss

PREFACE

Un tiers de toutes les ruptures de barrage dans le monde ont pour origine un déversement non-contrôlé par-dessus le couronnement dont la cause est une capacité insuffisante des ouvrages d'évacuation des crues. Il existe aujourd'hui un grand nombre de petits et moyens barrages en remblai d'une hauteur inférieure à 30 m, dont les évacuateurs de crues ont été dimensionnés sur des bases hydrologiques trop optimistes et des modèles trop simplifiés. Une solution prometteuse pour résoudre cette difficulté consiste à protéger le parement aval par un revêtement résistant à l'érosion et de permettre un déversement contrôlé lors des crues. Plusieurs types de revêtement ont été développés comme par exemple une protection végétale, des enrochements et empierrements, des gabions, des géotextiles, des dalles et blocs en béton ainsi qu'un revêtement en béton compacté au rouleau (BCR).

Dans la présente communication, M. Pedro de Almeida Manso décrit les résultats d'une étude concernant la stabilité de revêtements en béton constituant une macro-rugosité hydraulique sur le parement aval d'un barrage en remblai. Des essais systématiques ont été effectués sur un modèle physique avec plusieurs types d'éléments en béton. Sur la base des caractéristiques de l'écoulement observé et du mode de rupture des types de revêtement étudiés, M. Manso a développé un modèle de stabilité pour le calcul des coefficients de sécurité de la protection de surface. Des abaques de dimensionnement ont ainsi pu être obtenus pour des parements aval de barrages en remblai de pente 1:3. Ces courbes permettent d'estimer rapidement les dimensions et poids nécessaires pour des blocs en béton de différentes formes et pour différents coefficients de sécurité.

Avec son étude, M. Manso fournit des informations utiles pour tous les ingénieurs ayant pour mission d'assainir des barrages en remblai existants et de concevoir de nouveaux barrages jusqu'à 30 m de hauteur ainsi que des batardeaux de dérivation provisoire.

Prof. Dr Anton J. Schleiss

TABLE OF CONTENTS

Index of Figures

Index of Tables

Index of Photos

Appendices

ABSTRACT

The research work concerns the study of a macro-roughness lining system made of isolated concrete elements for protection of earth embankment dams during overflow. Uncontrolled overtopping of dams has proven to be one of the most important causes of dam failure, mainly in the case of embankment dams, which are more prone to failure by flow-driven erosion. Overflow is the use of controlled overtopping for flood management. Earth dams are considered the target group for this matter as they make up for the large majority of dams up to 30 m. Furthermore, they are a first-line development feature in developing regions and will have the largest construction rate in the forthcoming years. The developed macro-roughness lining system is focused for the rehabilitation of existing dams, for the design and construction of spillways of low height dams (up to 30 m), as well as for overflow cofferdams. The main feature of these concrete element linings is to have their stability during overflow assured mainly by their self-weight. For such elements the flow is said to run over regular macro-roughness.

Several configurations of elements were compared for their stability on a typical dam slope of 1/3 (V/H) under increasing flow discharges till failure was reached. For that purpose, an experimental facility was designed and built, and experimental tests were performed. Stability of the elements was evaluated for different foundation drainage conditions, for different shear conditions between the elements and their foundation, and for different joint alignments. Observation of flow conditions and measurement of flow characteristics were done for quasi-uniform flow conditions. Straightforward measuring devices were used. Remarks on their adequacy for the study of flow characteristics over regular macro-roughness surfaces are included.

Based on the experimental results, a stability model was developed to allow computation of a design safety factor. The experimental results were rendered dimensionless so that similar proportional elements could be designed with different dimensions and weight, respecting the failure conditions identified in the laboratory. The model is based on the governing overturning equation, identified as the dominant failure mechanism, and on assumptions concerning the hydrodynamic forces, the hydrostatic lift and the air concentration on the flow. Computation tools were developed and are described herein. Synoptic design charts were obtained with these tools, allowing the rapid estimate of the lining characteristics (dimensions and weight) for a certain withstood design unit discharge, for various margins of safety. Recommendations are made for the design of a lining system, including suggestions for crest, toe and drainage.

RESUME

La présente dissertation concerne l'étude d'un système d'éléments en béton pour la protection superficielle de barrages en terre en cas de déversement. Le déversement accidentel est une des plus importantes causes la rupture de barrages et en particulier de celles en remblais, plus vulnérables à l'érosion par l'écoulement sur le parement aval. Néanmoins, rendre un barrage submersible en admettant un déversement contrôlé, peut être une alternative pour maîtriser les crues. Les barrages en terre sont le groupe-cible pour ce système de protection, puisque celles-ci sont la majorité des barrages jusqu'à 30 m, dont les ouvrages de contrôle de crues sont fréquemment déficitaires ou représentent une partie considérable du coût global. En plus, les barrages en terre sont des éléments de première ligne du développement régional et auront le taux de construction le plus élevé dans les prochaines années, à l'échelle mondiale. Le système de protection superficielle présenté dans ce travail est envisagé pour la réhabilitation d'aménagements existants, pour le dimensionnement et construction d'évacuateurs de crues pour des barrages jusqu'à 30 m, et pour des batardeaux submersibles.

Les principales caractéristiques de ces éléments sont d'être stables pendant le déversement sous l'action prépondérante de leur poids propre et d'engendrer un écoulement sur macro-rugosités. Plusieurs géométries d'éléments ont été comparées du point de vue de leur stabilité sur une pente typique d'un barrage en terre de 1/3 (V/H), lorsque soumises à débits croissants jusqu'à la rupture du système. Dans ce cadre, une installation expérimentale a été dimensionnée et construite, et des essais ont été réalisés. La stabilité des éléments a été évaluée pour différentes conditions de drainage de la fondation, pour différentes conditions de frottement entre les éléments et la sous-couche de fondation, et pour différents alignements des joints. L'écoulement a été étudié et ses caractéristiques ont été mesurées pour des conditions de quasi-uniformité. Des techniques de mesure simples et robustes ont été choisies et leur adéquation pour l'étude de l'écoulement sur des macro-rugosités est commentée.

Basé sur les résultats obtenus dans les essais au laboratoire, un modèle analytique de stabilité a été développé pour le calcul d'un facteur de sécurité lors du dimensionnement des éléments. Les résultats ont été rendus non-dimensionnelles pour permettre le dimensionnement d'éléments similaires à ceux utilisés en laboratoire, mais de différente taille et poids. Le modèle a pour base l'équation du renversement, celui étant identifié comme le mécanisme de rupture dominante pendant les essais en laboratoire. Des hypothèses concernant les forces hydrodynamiques, l'impulsion hydrostatique et la concentration d'air dans l'écoulement ont été faites. Des outils de calcul ont été développés pour l'obtention d'abaques de dimensionnement ; ceux-ci permettent l'estimation rapide des caractéristiques d'une protection superficielle (taille, poids, débit spécifique de dimensionnement) pour différentes marges de sécurité. Finalement, des recommandations pour le dimensionnement sont faites, y incluant des suggestions pour la conception de la crête et le pied du barrage, ainsi que la couche de drainage.

RESUMO

A presente dissertação concerne o estudo de um sistema de macro-rugosidades para protecção superficial de barragens de terra galgáveis, composto de blocos em betão. O galgamento descontrolado é uma das principais causas de ruptura de barragens, e em particular de barragens de terra e de enrocamento. No entanto, o galgamento, quando controlado, pode ser uma alternativa interessante para a gestão de cheias. Este trabalho concentra-se em barragens em terra, por serem estas a maioria das barragens existentes até 30 m de altura, serem elementos de primeira-linha do desenvolvimento regional, e para as quais se prevê a maior taxa de construção nos próximos anos em termos mundiais. O sistema de protecção desenvolvido destina-se a ser utilizado na reabilitação de de barragens existentes, no projecto e construção de descarregadores de cheias de barragens até 30 m de altura em aproveitamentos de pequena dimensão e ainda para ensecadeiras galgáveis.

A principal característica dos elementos de betão é deverem a sua estabilidade durante o galgamento à acção predominante do seu peso próprio. Nestas condições, o escoamento realiza-se sobre macro-rugosidades. Várias geometrias de elementos são comparadas no que respeita à sua estabilidade num plano com uma inclinação típica de barragens de terra de 1/3 (V/H) quando submetidos a caudais crescentes até ser atingido o colapso. Para realização dos ensaios, foi dimensionada e construída uma instalação experimental. A estabilidade dos diversos sistemas de protecção superficial é avaliada para diferentes condições de drenagem da fundação, para diferentes condições de atrito entre os elementos e a superfície onde foram colocados e para diferentes alinhamentos das juntas. Os ensaios consistiram na observação e medição das características do escoamento, em regime *quasi*-uniforme. Foram utilizadas técnicas de medição expeditas, sendo ainda analisada a sua adequabilidade ao estudo de escoamentos sobre macro-rugosidades.

É apresentado o modelo analítico de estabilidade desenvolvido. Este modelo permite o cálculo do factor de segurança de dimensionamento utilizando os resultados dos ensaios laboratoriais. A adimensionalização dos resultados permite o dimensionamento de elementos de betão de geometria semelhante aos utilizados no laboratório mas de peso e dimensões diferentes, respeitando as mesmas condições de ruptura. O modelo de estabilidade baseia-se na equação de derrubamento, identificado como o mecanismo de ruptura dominante, de acordo com hipóteses assumidas para as forças hidrodinâmicas, para a impulsão hidrostática e para a concentração de ar no escoamento. Baseadas neste modelo, foram desenvolvidas ferramentas de cálculo computacional para o dimensionamento dos elementos em betão. Estas ferramentas foram utilizadas para a produção de ábacos de dimensionamento que possibilitam a rápida estimativa das características dos elementos (dimensão, peso, caudal unitário de dimensionamento) para diferentes margens de segurança. São ainda apresentadas recomendações para o projecto de um sistema de protecção superficial, incluindo sugestões constructivas para o coroamento e o pé da barragem, bem como para a camada de drenagem subjacente.

1 INTRODUCTION

1.1 BACKGROUND

Over the last decades the international engineering community became more and more engaged in assessing dam safety as the rate of new constructions reduced. Dam failures have happened in the past and their causes and origins are not fully mastered. Current engineering practice and safety standards have evolved considerably and in a way that many existing dams are no longer considered safe. Evaluation of dam safety was initiated in the 1970's by the analysis of past failures, searching for trends on the most common accidents and incidents. The exhaustive data collection and processing aims at the improvement of design codes and the promotion of more stringent surveillance and maintenance policies.

According to the International Committee on Large Dams[1-2] (Bulletin 99, 1995), one third of the total identified failures was caused by dam overtopping, mainly due to insufficient spillway capacity. The reasons being pointed out for this are the inadequacy of formerly used hydrological methods to estimate extreme floods and the specifications for the selection of the spillway design conditions. The first steps to revert this trend are the recent advances on hydrology and on climatic processes, which have allowed obtaining better estimations of extreme flood events. Still, at numerous locations on the planet the estimates are quite rough. Therefore, the difficulty to master hydrological uncertainties has placed overtopping at the centre of research concerns. Known technical solutions privilege avoiding and controlling overtopping, depending on the available hydrological data, funding and characteristics of the dam. Progress on this topic is of utmost importance for dam construction and rehabilitation.

From all dams types, those made of embankment are the most widespread. Overtopping of such dams can result in partial or complete failure, due to their granular constitution. Furthermore, they represent the majority of Large Dams less than 30 m high. These dams are used mainly for irrigation, water supply and flood management. For many regions on the globe they represent the first step in regional development.

The present study concentrates on the effects of overtopping in embankment dams, as they presently represent the large majority of new built dams (ICOLD 1997). Low height dams are often designed with little financing and few hydrological data, with frequent underestimation of spillway capacity. Today, providing protection against erosion by overtopping is a primary goal of design or rehabilitation. For this purpose, the downstream slope of the embankment dam can be protected to withstand frontal overflow. If the protection lining is properly designed,

[1] ICOLD

[2] According to the ICOLD Bulletin 109 (1997), « Large » dams are those with more than 15 m of height, or those that having heights between 10 and 15 m have either (1) more than 1 000 000 m^3 of storage volume or (2) more than 500 m long or (3) were designed to discharge floods of more than 2000 m^3/s or (4) have unusual characteristics.

controlled overtopping (overflow) of the dam body can be a possible answer to ensure dam safety and manage floods (Lafitte, 1985).

For existing dams, increasing the discharge capacity can be achieved by the construction of an auxiliary overflow spillway. For new dams, conventional reinforced concrete spillways may even be dismissed, depending on the hydrological climate, the behaviour of the overflow structure and the consequences of flooding of downstream areas.

However, allowing for frontal overtopping of the embankment, even if controlled, raises suspicion amongst engineers, more accustomed to side-spillways. In fact, an embankment constitutes a non-stable foundation for rigid concrete structures. If the foundation is not stable, settlement occurring during the first years of operation might uneven the spillway joints, with obvious risks of infiltration and internal erosion of the embankment. Thus, technical solutions for overflow normally exclude conventional concrete structures.

Presently, the design procedures try to closely combine site features with risk analysis. Risk is the *combination* of the probability of a given event with its consequences. If an extreme flood event (action) causes a dam to be overtopped and fail (reaction) but the resulting wave propagating downstream does not threat human lives or property values, overtopping does not represent a danger. Thus, overtopping can no longer be considered *a priori* the direct and isolated cause of a catastrophe.

On the other hand, in cases where the consequence can be severe, the duration of the overflow and the extension of dam erosion play an important role. Dam erosion mainly depends on the overtopping duration and magnitude, and on the characteristics of the embankment. Hence, a lining protection of the downstream surface might keep the dam from failing or, at least, delay its failure, allowing for the alarm to be given.

As an example, resistance to failure by overtopping is presently considered as one criterion for dam safety evaluation in the United States (Hagen, 1982). Decreasing risk is assigned to projects where rockfill dams have been designed for overtopping, or where earth embankments were resistant to surface flow erosion. In the United Kingdom (Minor, 1998), overtopping is considered acceptable by legislation, under some conditions. A dam (concrete, embankment or other) can be overtopped intentionally, remaining structurally intact or even failing, as long as the consequences are not severe.

Discussion on the acceptability of overflow structures is well under way. The engineering community faces a dilemma, between refusing unconditionally any idea of flood discharge over embankments, or accepting the construction of spillways over embankments according to local conditions and design features. Overflow spillways might soon become either an economical alternative or a safety complement to conventional spillways, mainly in the case of dams less than 30 m high.

Moreover, overflow structures can also be economically advantageous (Pinheiro and Relvas, 1998) when compared with conventional spillways. The latter traditionally consists of an intake structure, usually on the abutment, an overflow concrete weir, a waterway (chute or gallery) and the restitution works (energy stilling basin, roller bucket or sky jump). Most of these works are normally made in reinforced concrete. A large lump of the spillway construction cost concerns the excavation works and the reinforced concrete works. Savings can be achieved by replacing a side channel or gallery by a frontal overflow spillway. The reduction in excavation cost and

construction duration might be considerable. Significant cost reduction in the flood discharge or diversion works can thus be achieved, which might render a project economically feasible, particularly in the case of low height dams.

Additional savings might also be achieved if the geometry of the energy dissipation basin is reduced. In fact, overflow protections or linings can be designed to dissipate energy along the slope. Depending on the lining geometry (roughness) and on the created flow pattern, energy will be reduced along the slope, thus reducing the remaining energy at the restitution. In consequence, the geometry (and cost) of the stilling basin is diminished or even omitted.

Several lining systems including grass, riprap, geo-textiles, geo-membranes, concrete slabs, rolled compacted concrete (RCC) have already been developed for embankment dams. Systems made of concrete elements are studied herein.

1.2 PURPOSE OF THE WORK

This work aims to contribute to the definition of a lining system for overflow earthfill dams made of loose concrete elements. These elements are conceived to be self-stable and to enhance energy dissipation along the dam's downstream slope by creation of a complex flow pattern. When compared to previously developed systems, advantages in performance and fabrication procedure are expected, due to the block's weight and geometry. The system consists of a layer of concrete blocks, placed side by side, from downstream to upstream, separated from the embankment by a foundation/drainage layer.

The surface created by the alignment of the concrete blocks will be similar to a cascade of regular shape. The geometry of the elements will be chosen so that the system can operate under flow depths of the same order of magnitude as the bottom irregularities. Hydraulically, this corresponds to a **flow over a macro-roughness bottom**, where the flow surface is highly influenced by the bottom configuration.

The work was **predominantly experimental** and intended to characterise the flow pattern and the **stability** of the lining along the embankment **slope** for different flow conditions. Particular attention was given to the influence of the geometry of the elements and to the drainage conditions.

The key questions which this work aimed to answer to, were:

- What kind of concrete element protection has the best performance in terms of stability?
- For a given concrete protection element and given slope, what is the critical specific discharge leading to failure?

The stability of the lining largely depends on the discharge, the downstream face slope of the dam, the foundation upon which the lining is set (including drainage and filter layers) and the concrete element's geometry (weight, surface, roughness, shape, joints, interlocking systems, etc.), which were taken as the main parameters under study. The design of the embankment itself was not analysed; it should be the object of particular studies.

The research work consisted of the following steps:

- literature review of existing overflow concepts and lining systems for overflow earthfill dams, as well as an introduction to the hydraulics of flow over macro-roughness;
- geometrical definition of the individual concrete elements;

- design and construction of an experimental facility;
- definition of the hydraulic experiment procedure, similarity conditions and instrumentation;
- analysis of the element stability, including the evaluation of the drainage efficiency;
- study of the flow pattern over the created macro-roughness surface, for different flow conditions and different bottom configurations;
- establishment of a methodology for the stability design of a lining composed of the conceived concrete elements.

The work was developed within the research group on overflow dams at the Laboratory of Hydraulic Constructions (LCH) of the Swiss Institute of Technology in Lausanne (EPFL). Two subjects are being developed, one concerning the stability behaviour of loose macro-roughness blocks placed on a typical embankment slope (Manso and Schleiss, 2002) and the other concerning high velocity flows over macro-roughness (André, 2000; André *et al.*, 2001).

Key words: overflow dams, erosion protection, linings, macro-roughness, stability, drainage and spillways.

1.3 SIGNIFICANCE OF THE PROJECT

This research work develops the concept of an alternative lining system made of loose concrete blocks for embankment dams, which aims to enable localised and controlled overtopping and to prevent damage to the downstream slope of the dam. It should also contribute to a considerable reduction of the remaining (residual) energy at the dam toe. Such a lining system can be considered for:

- the **rehabilitation of dams**, in the form of auxiliary spillways for schemes with reduced flood discharge capacity;

- the **design of spillways for low height dams** according to present safety standards, being an easy to make and less costly alternative to a conventional concrete spillway, particularly if little hydrological data is available and flood estimates are barely reliable;

- the **protection of overflow cofferdams**, to reduce the frequency of the design discharge of the diversion works, thus reducing its dimensions and cost, and also to accommodate unexpected hydrological events.

A broad field of application exists on the **rehabilitation of dams**. In what concerns flood discharge, existing dams are often under-designed, as testified by recent safety assessment studies. A common outcome of these studies is the need to increase the capacity to overpass floods, in order to satisfy the more stringent present safety standards. More reliable flood estimates can now be obtained due to the existence of longer hydrological records and improved prediction tools. On the other hand, overflow spillways can provide an interesting alternative for flood discharge when lack of space for interventions is a critical design feature.

For **low height dams**, lack of safety concerns not only the insufficient discharge capacity but, in some cases, also the own existence and operating conditions of the spillway. The problem goes far beyond the scope of hydrological uncertainties or ancient design practices, and concerns the main decision point of most small dam projects: the cost of the appurtenant structures. As an example, in order to create a reservoir of some 100 000 m^3 for irrigation purposes a promoter will consider the construction of a 10-30 m high earthfill dam with available local material,

including an intake, a simple culvert bottom outlet and a conventional spillway for a few cubic meters. Surprisingly or not, the cost of the flood control structures, including excavation and concrete dumping, can amount to 45-50 % of the overall budget (ICOLD, 1997; Olivier, 1967)[3]. Such an investment is sometimes difficult to justify, especially if the consequences of dam failure by overtopping are low.

As far as **cofferdams and diversion works** are concerned, the controlled overflow of these structures is of interest. The probability that a flood with a return period larger than the diversion works design flood arrives during the couple of years of construction is not negligible. In fact, in a two year construction period, the risk for downstream populations may be greater than that accepted for the whole lifespan of the dam (Lempérière, 1993). However, it is neither wise nor economically feasible to avoid this by increasing enormously the diversion's dimensions. Thus it is not uncommon that diversion works are subject to floods events for which they are seriously under-estimated. If such a flood arrives, the cofferdam is likely to be overtopped after a certain time, flooding the construction site. Unexpected and uncontrolled overtopping can, in certain cases, lead to failure of the cofferdam. This causes long delays in the construction, which considerably increases the cost of the project. Major damage can still be avoided if the cofferdam, though overtopped, does not fail. What's more, by reducing the energy of the overflows severe damage on the site can be prevented. In fact, if the cofferdam is designed to withstand overflow of a given duration and magnitude (acting as an auxiliary spillway), the possibility to reduce the diversion works dimensions may even be considered, despite a possible increase in the frequency of site flooding. A direct consequence would be the lowering of the cofferdam height. This height is normally defined to create the necessary backwater level (and head) to discharge the estimated flood through the diversion. Savings in construction duration by reduction in the time needed for both the construction of the diversion and the cofferdam may reveal significant, these advantages being proportionally increased with the increase of the overflow unit discharge.

In conclusion, overflow linings seem to have a promising future in embankment dams. As the great majority of tomorrow's dams between 10 m and 30 m high will be earth embankments, especially those on small watersheds or where a good rock foundation is not available, **this work concentrates on earth embankments,** rather than rock embankments. Rock fill dams are quite rare in dams less than 30 m high, except in a few countries like Norway, Canada and Australia (ICOLD 1997).

1.4 ORGANISATION OF REPORT

The dissertation starts with this introduction, where the background for the most recent developments on dam safety is highlighted and the motivation for the current research project explained. The main objectives of the project and a resume of the proposed research approach are presented. The potential field of application of the developed lining system is also clarified.

In Chapter 2, a review of the concept of controlled overtopping (overflow) of dams, as well as its evolution and applications, is made. The characteristics of alternative existing systems and the hydraulics of flow over macro-roughness surfaces are also studied. Conclusions are drawn on which should be the present priorities in terms of research developments and practical applications.

[3] According to the Bulletin 109 (ICOLD, 1997), for schemes with a reservoir volume less than 10 hm^3, construction costs are around 1 USD/m^3 of storage volume.

Chapter 3 includes a description of the experimental work led. The selected lining elements and the design of the experimental set-up are presented. Furthermore, the experimental objectives are highlighted and the experimental tests and the instrumentation used are described. The test plan and outcome are presented.

The experimental results are analysed in Chapter 4, for the different experimental tests set-up. Comparison between the different lining systems is done, concerning mainly the generated flow pattern and the measurements obtained. A balance on the adequacy of the used instrumentation for the study of flow over regular macro-roughness surfaces is included.

In Chapter 5 a detailed result analysis is presented, focusing on the stability of each one of the different linings used in the experiments. A stability model for the computation of both minimum and recommended safety factors is presented. Design tools are included. A design example is presented i**n section 5.7**. In the following Chapter 6, recommendations for the design of a lining made of concrete elements are presented.

Finally, in Chapter 7, conclusions are drawn on the evolution of the overflow concept and on the performance of the designed lining system, in terms of stability and created flow pattern. Recommendations for follow-up studies are also included.

2 LITERATURE REVIEW

2.1 INTRODUCTION

An overview of the past research and technical developments on the concept of overflow embankments is made in this chapter. Dam stability is reviewed, as well as the behaviour of known linings. The main features of the hydraulics of high-velocity flows over macro-roughness are highlighted.

2.2 STATISTICS ON DAM FAILURES AND ON EMBANKMENT DAMS

Large-scale dam safety evaluation started with the classification of dams and failures, in terms of height, of type and of reservoir dimensions. An exhaustive data collecting, organising and analysing work led by Prof. Laginha Serafim resulted in an inventory of past failures of Large Dams, published in Bulletin 99 of ICOLD in 1995. Data from China and the URSS were not considered. Some conclusions presented in that publication are presented hereafter:

- "in absolute terms, most failures involve **small[4] dams**, which do however make up the greatest proportion of dams in service";

- "in earth and rock fill dams, the **most common cause of failure is overtopping** (31 % as primary cause and 18 % as secondary cause[5]), followed by internal erosion in the body of the dam (15% as primary cause and 13% as secondary cause) and in the foundation (12% as primary cause and 5% as secondary cause)";

- "where the appurtenant works were the seat of the failure, the most common cause was **inadequate spillway capacity** (22 % as primary cause and 39 % as secondary cause)".

In particular, (Bulletin 109 from ICOLD 1997, Lempérière 1993, Serafim 1981):

- embankment dams are the most widespread type of dam construction around the world; they account for the majority of the overall world total number of dams;

- around 70 per cent of known failures concern Large Dams less than 30 m - Table 2.1**;**

- for the estimated existing 100 000 small dams not classified as large dams, failures have been reported, but hardly any statistics are available and it is not certain that the failure rate is any lower or higher than for Large Dams. The majority of these are embankment dams;

[4] the expression "small" stands here for low Large dams, meaning those with storage volumes larger than 1 million m^3 and lower than 30 m.
[5] Primary cause is taken as the main cause of failure and secondary cause as the complementary cause.

- for China precise statistics are not available, although China alone has more large embankment dams than the whole of the rest of the world. Overtopping is considered to be the cause of most failures of Chinese dams;

- overtopping has been the most frequent cause of embankment dam failures, accounting for more than 50 per cent of the cases, frequently due to an under-estimated flood discharge capacity.

Table 2.1 - Statistic of dam failures (adapted from Serafim, 1981)

Ruptured dams of over 15 m (1851-1979)										
Height	**Concrete**			**Embankment**			**Other materials**			**Total**
	Gravity	**Butress**	**Arch**	**Rockfill**	**Earth**	**Earth/rock fill**	**Timber**	**Metallic**	**Gabions**	**N°of dams**
15-20	6	4	3	3	33				1	50
20-25	4	1		1	15	1		1	1	24
25-30	1	1		1	11	1	1			16
30-35	3	2		1	7		1			14
35-40	2			3	5					10
40-45	4				3					7
45-50				1	1	1				3
50-55	1			1	2					4
55-60				1						1
60-65			1	1	2					4
65-70										
70-75										
75-80										
80-85					1					1
85-90										
>90				1	1					2
Total	21	8	4	14	81	3	2	1	2	136

From the previous, it is evident that low height dams, meaning those less than 30 m high (Large or not[6]) deserve a closer look. In fact:

- their failure is said to have caused a total number of victims ten (10) times higher than failures of very high dams (Bulletin 109, ICOLD, 1997) where the percentage of embankment dams is not so significant;

- amongst these, there are around 35 000 Large Dams, 90 per cent of which are embankment dams and have ungated spillways[7];

- there are around 1000 dams 10-30 m high, impounding more than 0.1 hm^3 being built around the world every year, from which 200 to 300 dams can be classified as Large Dams.

An increase in the safety of dams within this range of heights is thus urgent. These dams play a major role in the economical life of vast areas of the planet, in water supply, in irrigation and in

[6] Outside the domain of Large Dams, a total of approximately 100 000 dams with less than 30 m is estimated to exist (Bulletin 99, ICOLD 1995).
[7] According to Bulletin 109 (ICOLD, 1997), their cost is normally less than 1 million USD.

flood management. A large percentage is constructed without good engineering design and construction practices. The majority was built or will be built in rapidly developing regions, with reduced financial resources and scarce hydrological data. A low safety standard is a common outcome. Once more, overflow might be a good and less costly solution for flood management.

The international effort to assess dam safety and improve design standards and construction procedures is paying off. Indeed, the failure rate for dams built after 1950 has been considerably reduced, in comparison with the period before that date (Serafim, 1981; Lafitte, 1985).

2.3 EMBANKMENT DAMS SUBJECT TO OVERFLOW

2.3.1 The concept of overflow fill dams

In most dams floods are managed by varying the reservoir level and the operational conditions of the discharge structures (spillway, orifices, etc.). A freeboard is normally compulsory between the maximum operation level (MOL) and the crest, in order to account for the flood-driven rise of the reservoir level, for wave run-up and for wind set-up. International standards for Large Dams advise considering a freeboard such that in case of extreme floods the crest is not overtopped, or at least not in a large extent. The limiting event is called the safety check flood.

In opposition, an overflow fill dam is designed to allow, intentionally, flow spilling over the crest at a previously defined location. The magnitude and the duration of the overtopping design flood should not endanger the overall stability of the dam. In such case, overtopping is made in a controlled way and is usually named overflow. Erosion of the dam along its downstream face or at the toe is either disabled by protective measures, or limited and of acceptable extension.

The concept of an overflow embankment was born from river closure works. Loose stones and gravel would be dumped in a river at a rate higher than the transport capacity of the river flow, enhancing deposition. Izbach and Khaldre (1959) extensively studied this process; the formulae presented in that publication are used worldwide. Parkin (1943) developed the concept of dams with built-in spillways, where flow-through the dam body would start after rising above the top of the impervious upstream face blanket. Some years later, Olivier (1967) developed the concept of through and overflow rock-fill dams. These structures have simple geometry and should withstand both seepage (trough) flow and overflow till a certain extent; in this case the grain size of the rock fill limited the through flow, being the overflow predominant[8].

Nowadays, rockfill and earthfill overflow dams are separately studied. The main difference concerns the role of infiltration in the overall embankment stability. In rock fill dams significant infiltration might be acceptable, whereas in earth fill dams drainage of the infiltrated flows is of utmost importance to prevent major changes in the formerly established seepage flow net.

There are some remarkable examples of overflow embankments as the Bearspaw dam in Canada, the Henshaw dam in the USA, the Loerie dam in South Africa, the Stanford dam in the Great Britain, and the Toktogul cofferdam and the Dnestrovskaya, Denstrovsky, Dnieper and Ust-Khantaysky dams is the former Soviet Union (Lafitte, 1985).

In brief, overtopping can either lead to failure, or to flood discharge with limited damage, or even to safe flood discharge. Controlled overtopping renders overflow fill dams an interesting

[8] Martins and Maranha das Neves. (1993) presented another concept: the flow-through flow or percolating dams, with no impervious element and without overflow, mostly used to raise the upstream water level.

solution to reduce dam construction (and rehabilitation) costs with safe flood management.

Furthermore, overflow dams may prove economically advantageous in the cases of cofferdam construction, as well as in the construction of low height dams or in the rehabilitation of existing dams. Economical advantages will be created in the form of reduction in cofferdam height or diversion dimensions, both causing significant reduction in the construction duration and deadline for commissioning. Other vectors for savings are the reduction on the quantities of reinforced concrete structures to be used (spillway, energy dissipation basin) or the non-construction of galleries and tunnels.

2.3.2 Hydraulics of an overflow event

2.3.2.1 General

Overflow will go through the stages presented in Figure 2.1 (Powledge and Sveum 1988, Powledge *et al.* 1989):

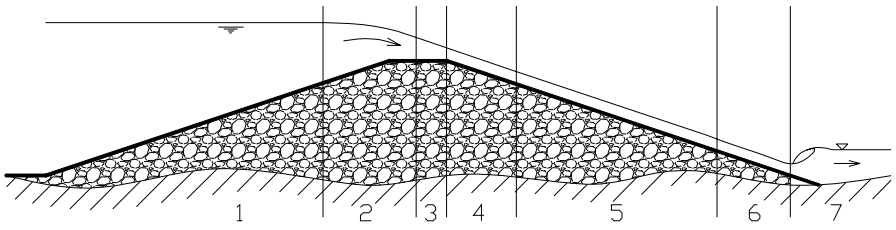

1. Subcritical flow while approaching the crest (approach flow)
2. Transition from subcritical flow to supercritical flow, passing through the critical flow depth
3. Rapidly accelerating varied flow, with development of the bottom boundary layer and increasing turbulence
4. Region of clear water flow and boundary layer development (clear water), until the Inception point, where the turbulent bottom boundary layer reaches the flow surface. From this section on the flow will be aerated (two-phase flow) and named white water flow.
5. Partially aerated flow region, with increasing air entrainement;
6. Fully aerated flow region, in quasi-uniform flow regime
7. Transition from supercritical uniform flow to subcritical river flow through a hydraulic jump at the toe of the dam.

Figure 2.1 – Hydraulic characteristics of overflow

The location of the transitions between the different flow regimes depends on the overflow head, on the roughness of the dam surface (at the crest, along the slope and at the toe) and on the

infiltration rate (reducing surface flow). The flow will be supercritical along the downstream slope and progressively more turbulent due to the surface roughness. Air will be entrained gradually from the surface after the inception point and, if the slope is sufficiently rough and long, uniform conditions might be attained. The location of the hydraulic jump near the toe of the dam should be considered the most critical point, as the energy being dissipated can erode the toe of the dam and thus endanger the dam stability by back erosion (Lafitte, 1985).

2.3.2.2 Over the crest

Along the crest the flow transits from subcritical to supercritical regime. The location of the critical depth section depends on the overflow head and on the crest shape. Erosion is expected to start only downstream of the critical velocity section, due to the increase of the shear velocity and to the development of uplift pressures in the embankment. The discharge over the crest is a function of the upstream face slope, the abutment geometry (for short crest lengths), the crest width and the approaching head.

Critical flow height (rectangular section) can be computed from equation 2.1 and the unit discharge, as in the case of a non-submerged broad crested weir (or *Bélanger* weir), from equation 2.2 (Quintela, 1981), where C=0,385.

$$h_{cr} = \sqrt[3]{\frac{q_w^{\,2}}{g}} \tag{2.1}$$

$$q_w = C \cdot \sqrt{2g} \cdot H^{\frac{3}{2}} \tag{2.2}$$

Depending on the magnitude of the event, the overflow nappe will create positive or negative pressures on the transition region between the downstream edge of the crest and the initial reach of the downstream face. Similarly to what occurs in conventional WES[9] spillways crests, the detachment of the under-nappe from the boundary (crest and face surfaces) being non aerated, negative pressures will be generated which will accelerate the erosion processes. Strong protection is advised at this location.

2.3.2.3 Along the slope

After the transition to the slope the flow will rapidly accelerate. A turbulent boundary layer created by separation of the main flow from the physical boundary (dam) will progress across the flow depth until it reaches the surface; an external observer would see clear water. The boundary layer reaches the surface at the inception point, downstream of which an external observed will see white water, characteristic of an air-water mixed flow. The air concentration in the flow will increase with distance until uniform conditions are reached.

Depending on the discharge, full aeration of the flow will require a shorter or longer length. Therefore, a proportional relation exists between the dam height and the face slope needed for a given discharge to reach uniform conditions. Considered should also be the surface roughness. In uniform conditions, equilibrium between gravity and shear forces is obtained and the energy line slope is constant.

The distance to the crest needed to reach uniform conditions is normally one of the major doubts both researchers and engineers have. This distance is of utmost importance when designing laboratory experimental facilities if observation and study of the flow pattern in uniform regime

[9] Waterways Experimental Station

is envisaged. The only estimate or thumb rule found in literature is the one of Pravdivets and Slissky (1981) who stated that for a stepped surface of regular macro-roughness, uniform flow would be attained in a distance not larger than 20 times the critical flow depth at the crest.

Computation of flow depth, velocity and energy along the slope still cannot be accurately made. A rough estimate of the energy head can be obtained using Bernoulli's energy equation for free surface gradually varied flow, only valid for water flow. Major uncertainties are related with the role of air in the mixed flow and its influence on friction (and thus on velocity). Advances made mainly during the 1990's for smooth concrete spillways have brought some indications that have been recently tried out for regular macro-roughness stepped surfaces (Chanson, 1994, Matos, 2000, Boes, 2000). This subject is out of this research work's range.

2.3.2.4 At the toe of the dam

High flow velocities characterise the flow pattern at the downstream part of the slope and at the dam toe. In uniform regime or not, the flow will surely be highly aerated, supercritical and have a high erosion potential. Depending on the tailwater conditions (level and velocity), the transition between the arriving supercritical flow and the flow regime downstream, made via a hydraulic jump, will be located on the downstream part of the slope or over the dam toe. Thus, the toe transition should be designed in order to protect the embankment from erosion and to provide a good transition between the descending flow and the tailwater, for different operational combinations of the latter. The situation of a submerged hydraulic jump occurring on top of the lining upstream from the toe structure should be definitely avoided. Therefore, detailed design of the toe structure is closely depending on the computation of the hydraulic jump features for different hydraulic scenarios.

2.3.3 Stability of an embankment dam when overtopped

2.3.3.1 Notions of structural safety of embankments

The stability of an embankment dam depends on the structural behaviour of both the embankment and the foundation. The acting loads include the self-weight, the varying reservoir water level, the up-lift pressures in the foundation, the seepage flow pressures and eventually earthquake driven loads. In design scenarios are normally included boundary conditions as limit stability state at the end of construction, the steady fully-developed-seepage-flow-net state with full reservoir, the rapid draw-down of the reservoir, the reservoir level correspondent to an extreme flood, and others. Structural failure of an embankment occurs normally by sliding of large volumes of material, by cracking or by settlement (Singh and Varshney, 1995). The causes of failure can be internal, as those related with the sealing element or the fill material characteristics, or external, as an extreme event, either a flood or an earthquake. The most common causes of failure can be reduced to just two:

1) Internal erosion,
Occurring whenever there is an excess of seepage flow, typically when the impervious element fails, either during first filling or when the reservoir reaches abnormal levels for the first time. The fine particles of the embankment are washed out and the upper fill layers settle. This failure mode is more frequent for earth embankments than rock embankments. Seepage flow will likely emerge at the interfaces between areas with different compaction degrees, mainly in the transition between embankment and concrete works.

2) Overtopping,

Uncontrolled overtopping is often caused by insufficient discharge capacity of the spillway structure for a given flood event. However, responsibility for the incapacity to accommodate and safely pass the expected design flood entering the reservoir has to be shared between storage capacity and spilling capacity. When overtopping of the crest occurs, water flows along the dam downstream face itself, endangering its own integrity by both erosion and creation of up-lift pressures in the embankment. If persistent in time, it can lead to breaching of the embankment.

2.3.3.2 Modes of failure of embankments subject to overtopping

Once water starts flowing over the crest two kinds of flow develop: an **infiltrating flow** through the dam's body and a **free-surface flow** along the dam's face. Depending on the **embankment constitution**, on the **duration of overflow** and on the **magnitude of the overtopping event**, the relation between these two types of flows changes considerably resulting in very different failure evolutions. Magnitude is defined has the head over the crest or the head rise rate.

To illustrate the evolution of a failure event, an example concerning a homogeneous earthfill is hereforth described. Questions related to the foundation are not discussed. Differences to the failure of other types of embankments, both in earthfill or rockffill are merely overviewed for completion and comparison, without the pretension of an exhaustive analysis. In fact, the failure of a homogeneous earth fill dam with drainage prism is the simplest case, allowing the explanation of the more general overtopping features. It is schematically presented in Figure 2.2.

During normal operation of the reservoir a water saturation line will be established across the embankment. A drainage prism in the downstream toe of the dam, preventing the saturation line to reach the downstream face surface, collects the seepage flow. The establishment of a steady state seepage flow corresponding to a given reservoir level is a long-term process when compared with the short duration of most overtopping events, in the order of hours.

Depending on the magnitude and on the duration of overtopping, different situations can occur:

1. For low flows the entire overflow might be infiltrated. If the event is of short duration there will be hardly any rise in the saturation line.

2. When the overflow increases more rapidly than the infiltrating flow, water will run along the dam slope. Free-surface flow will progressively erode the slope and the dam toe.

3. For event of long duration, infiltration might occur during time enough to raise the saturation line, leading to internal erosion and shallow surface sliding. Water will spring out along the downstream face of the dam, *independently* of the magnitude of free-surface flow. The destabilising up-lift pressures generated in the embankment by this seepage flow will unbalance the equilibrium of some parts of the embankments that will subsequently slide.

Often, the critical place in terms of stability is the downstream toe, where free-surface flow reaches its maximum velocity and thus its maximum erosion potential. Further, the seepage flows resulting from the intersection of the wet front with the elevated saturation line will also emerge about in this region.

a) short duration

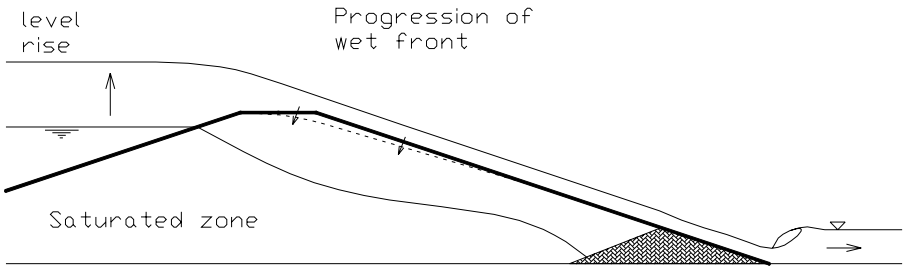

b) increasing duration

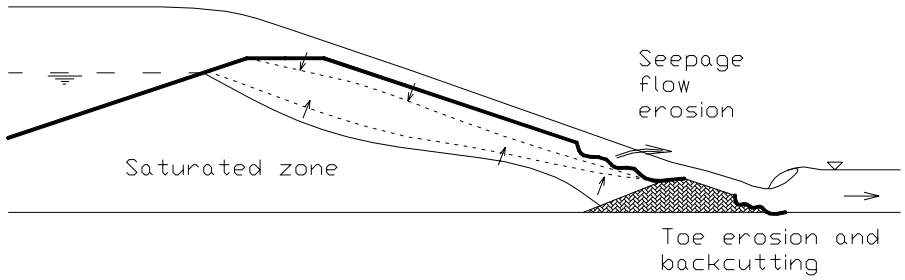

c) long duration overtopping

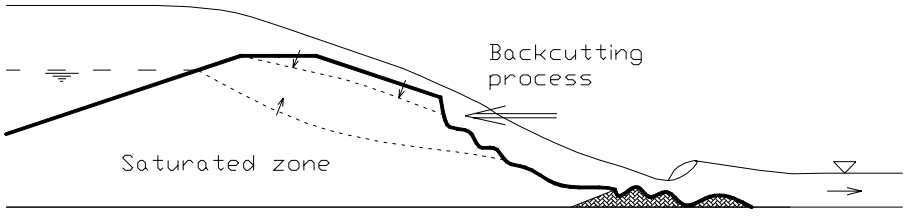

Figure 2.2 – Schematic representation of the failure mode of an homogeneous earth fill dam subject to overtopping (with hydraulic jump at the toe)

Starting at the toe, erosion will progress upstream, by deepening the free-surface flow channel, generating also bank slides; it will eventually end up by breaching completely the embankment. This process is often called back-cutting or retrogressive erosion. This process is accelerated if there is an hydraulic jump over the toe.

Homogeneous earth fill dam with inclined/chimney drain
This case is quite similar to the previous explained. Nevertheless, the existence of a more extensive drainage of the embankment, including a chimney drain and a drainage blanket, will delay the rise of the saturation line on the downstream part of the embankment. However, once these elements are exposed to free-surface flow, erosion will progress faster.

Zoned earth fill with clay core
A low-permeability central clay core assures the water-tightness of the dam. The upstream part of the embankment (shoulder) is almost totally saturated when the reservoir is at its maximum operational level, contrarily to the almost dry downstream shoulder. Preventing the saturation of the downstream part is important, as it endangers the overall stability. The failure occurs by erosion of the downstream slope by the same processes described above, until it is almost totally eroded, or at least enough to render the inner core unstable and exposed. From this stage onwards, stability is severely endangered due to the absence of the downstream support. The core and the upstream shoulder will be eroded by back-cutting and under-cutting. Total breaching and rapid drawdown of the reservoir follow, which will further cause the remaining upstream slope to slide (Odendaal and Zyl, 1979).

Rock fill with artificial upstream face sealing
The permeability of rockfill material is higher than that of the preceding earth fill examples, notably for quite large uniformly sized rock fill material. Therefore, in standard cases, once the face-sealing element is overtopped infiltration will increase rapidly. Water infiltrating the embankment will wash out the finer particles. Settlement and bank sliding will follow. Whenever the overflow unit discharge exceeds the seepage capacity of the rock fill, saturation will be achieved and overflow will be predominant. The weight of the rockfill will be considerably reduced by saturation. The stability of these embankments depending mainly on their own dry self-weight, such reduction might cause failure.

Zoned rock fill with clay core
The difference to earthfill-zoned dams is that the transition layers between the stabilising shoulders and the sealing element have to be conceived to span over a broader range of grain sizes and permeability. After core overtopping, saturation presents the same dangers for dam stability as seen previously for rockfill dams with artificial upstream face sealing. However, the higher permeability of the downstream shoulders, comparatively to zoned earth dams, might avoid or will delay saturation, depending on the granular distribution of the rock fill material.

Concluding remarks
It can be said that for a given overtopping event (given magnitude and duration):

- Failure of embankments dams due to overtopping depends mainly on the magnitude of the overtopping event, the duration of the overtopping event, the relative disposition of the various structural elements of the embankment on the cross section (drainage, filters, impervious element, stabilising shoulders, etc.) and on the geotechnical characteristics of the material of each of these elements of the embankment;

- In particular, erosion of the dam's downstream surface depends strongly on:
    a) the concentration of the flow at one particular section or its uniform distribution over a larger section (defining the unit discharge);
    b) the flow velocity, function of the dam height, the face slope, the unit discharge and the surface lining roughness;
    c) the existence of surface irregularities that might enhance turbulence and scouring;
    d) the presence and height of the tailwater level;
    e) the dam toe resistance to erosion by high velocity flows or up-lift pressures.

- The free-surface flow driven erosion is the results from a higher erosion potential of the overtopping flow (acting shear stress) comparatively to the surface resistance to erosion (resisting shear stress).

- The infiltrating flow starting conditions and the progression rate of the wet front depend mainly on the characteristics of the earth embankment.

- The more cohesive is the fill (unprotected) the better it will resist to overtopping, due to a comparatively lower permeability and higher surface resistance.

- The commonly used transition layer between the embankment material and the surface protection, normally made for filtering purposes and to act as a drainage layer for rain water, have little to no influence in the reaction of the dam system to the overtopping event. Its drainage capacity will likely be insufficient for overflow infiltration flows.

- Homogeneous fill dams are less prone to erosion by overflow than other types of embankment dams. Changes in the seepage flow are slow and the cohesiveness of the material delays surface erosion. These dams seem to be the more indicated to withstand overflow of low magnitude and any duration, for heights up to 20 m. The breach caused by free-surface flow erosion is generally smaller than for zoned embankments (and increases slower), thus reducing the outgoing flood flows (ICOLD, 1997).

2.3.4 Evolution of overflow lining construction over embankments

The engineering community has never been very fond of neither embankment overtopping not of placing rigid concrete structures, such as a conventional spillway, on top of a mobile foundation. In fact, prudence is advisable, but perhaps not more than for any other engineering work. Traditionally the idea of overflow has been associated with the dangers of setting a rigid concrete spillway over an embankment. The most frequent arguments for scepticism have been:

- the limited resistance of an exposed embankment to the shear forces of overflow;

- the mobility of the embankment (and of the foundation) and the implications it might have on the integrity and operation of the spillway channel (assumed as rigid);

- the creation of destabilising up-lift pressures, capable of displacing concrete slabs, rock fill blocks, etc., due to the lack of knowledge on how to control and manage seepage flows;

- the difficulty in estimating the design condition for the restitution, considered as the key point of the whole structure, as well as the most expensive component (Albert and Gautier, 1992).

Still recently, solutions that include overflow have been ruled out from rehabilitation of flood discharge structures. Costly modifications to existing spillways or then heightening of the embankment have been preferred. However, in some cases it has revealed physically or economically unfeasible to accommodate floods without allowing some overtopping. Low-cost overtopping protections, once further studied, have a vast range of potential applications.

Some examples have already been built, mostly in low dams at low risk locations, as wisdom advises before starting large-scale application. Overflow lining are being used either as a reinforced surface protection acting as an auxiliary spillways or as a permanent spillway.

2.4 PROTECTION LINING SYSTEMS FOR OVERFLOW EARTHFILL DAMS

2.4.1 Purpose of linings

A lining system for an overflow earth fill dams can be designed to fulfil fully or partially the following demands:

1. Safely discharge floods (either as main or auxiliary spillway);
2. Protect the embankment face (and body) from the erosion generated by high-velocity free surface flows;
3. Drain the infiltrated water;
4. Reduce the remaining energy at the toe of the dam;
5. Force air entrainment along the face of the dam, reducing the negative pressures;
6. Improve the integration of the dam in the landscape by covering the lining with vegetation.

2.4.2 Lining systems for surface protection of overflow earthfill dams

The first structures built were typically constituted of an impervious lining. The crest and the channel surface would be as smooth as possible, in order to limit the friction and prevent surface erosion. A conventional energy dissipation structure and a more extended drainage of the embankment were normally included. The most frequent applications have been made in concrete and in reinforced soil. Some variations with or without reinforcement, with or without joints, and anchored or not, have been made. These systems are still in use and they all have something in common: the embankment should have finished to settle once the spillway is constructed.

A different approach considering a permeable lining placed over a draining foundation has also been tried. The water overflowing the dam will thus infiltrate through the joints of the lining. For rockfill dams, the material grain size distribution and an eventual reinforcement should guarantee the stability of the lining and of the dam. For earthfill dams, the infiltrated water should be collected in a drainage layer placed between the lining and the embankment.

Numerous references exist on protection measures for overflow dams. Nevertheless, most of the existing design guidelines, as well as construction experience, concern the use of overflow linings for protection against erosion; almost no experience concerning the potential to dissipate energy exists. For prevention of overflow erosion the most frequently used protective systems are (Powledge *et al.*, 1988; Frizell *et al.*, 1996):

- **Grass**, planted on the surface of cohesive embankments;

- **Geo-textile lining**, consisting of a wide range of manufactured fabrics, mats, or large scale cells;

- Cement linings, used for **soil-cement** or for **roller-compacted concrete** (RCC)[10] protections;

- **Concrete blocks**, specially shaped, pre-cast concrete blocks that are designed to mechanically interlock or are tied together by cables, which are run through the interior of the blocks. Mechanically interlocking blocks are hand-placed, while cable-tied blocks are laid in mats on the embankment surface and secured with soil anchors;

- **Rip-rap**, consisting of well-graded stone of a specified mean diameter placed on the embankment surface to a specified thickness, tied up together (reinforced rip-rap) or loose;

- **Gabion**, made of uniformly graded stone placed in wire mesh cells on the embankment surface.

The main features of each of these systems are presented in Table 2.2, together with valid references for further consultation. Other systems are also included although little to no information exists about them. Concluded can be that:

- These systems have been used mostly for dams under 30 m of height;

- The stability of the lining system is often ensured by anchoring it in the embankment;

- RCC, soil cement and reinforced concrete slab linings are only economical in the case of large quantities (Frizell *et al.*, 1996), requiring easy site access and needing heavy machinery;

- Grass, geotextile, gabions and polymeric covers are very prone to vandalism;

- Several systems for overlapping, mechanical interlocking or artificial interlocking have been tried, in order to bind together loose elements (rip-rap, concrete elements);

- The systems using pre-cast concrete blocks with weight around 160 kg/m^2 have reached an advanced stage of development and can be used for mild slopes, specific discharges under 3 m^2/s and velocities of up to 13 m/s. Examples in Russia go considerably beyond. Commercial applications exist and will be further analysed in section 2.4;

- The pre-fabricated systems (concrete blocks, gabions) are particularly suited environmentally sensitive locations, where local production (in a batch plant) or the use of large machinery has to be excluded.

- Some systems are covered with vegetation after construction, mainly those that have cavities;

- Little information exists about energy dissipation potential of the existing systems.

10 In fact, when building an RCC dam each new concrete layer will be reduced in width, when compared with the underlying layer, resulting from this procedure a traditional gravity dam profile with a stepped downstream surface. The same procedure is being used over embankments.

Table 2.2 - Selected examples of surface protection systems for embankment dams. Data from experimental work and prototype operation observations.

System	Slope (V/H)	Velocity (m/s)	Discharge ($m^3/s/m$)	Overflow depth at crest (m)	Energy dissipation	Built Examples	Features	References
Grass		3.7	<2				Data from short duration events over cohesive fills	ICOLD (1997)
	1/2.5; 1/20	<1.8 m/s	0.6; 1.85				Prone to vandalism	
Reinforced Rip Rap			66.7			Ust-Khantaysky	Including crest; Observed results	MIKHAILOV *et al.* (1985)
	1/5		3.7				Grain size: 15-60 cm	FRIZELL *et al.* (1996)
Geotextile	1/2; ¼	6.7	2.25				With and without cover; failure due to poor anchorage or poor stretching of the material	FRIZELL *et al.* (1996)
Gabions	½ 1/3	<8	<3		Between 40% and 90%		Laboratorial results	PEYRAT *et al.* (1991) FRIZELL *et al.* (1996)
Reinforced concrete			12	3.7		Lebna dam (Tunisia)	Conventional spillway	SCHOBER (1991); ALBERT *et al.*(1992)
						Dnestrovskaya dam (ex-URSS)		ICOLD (1993) MIKHAILOV *et al.* (1985)
Reinforced soil (*Terre armée*)				1.0	Vertical Fall ~100%	Vallon de Bîmes (France)	Dam height = 9 m	ALBERT *et al.* (1992) ICOLD (1993)
			12			Taylor Draw Dam (USA)	Dam height = 22.5 m	ALBERT *et al.* (1992) ICOLD (1993)
Soil cement				1.2	Low		Laboratory results USBR; protection against erosion is a function of the thickness ; deterioration problems	POWLEDGE *et al.* (1989) FRIZELL et al. (1996)
RCC lining			<10					LEMPÉRIÈRE (1993)
			<10	4.3 m during 4-5 days	Between 40% and 90%	Brownwood Country Club Dam (USA)	Dam height = 5.79 m	POWLEDGE *et al.* (1989)
			<0.5		<90%			ALBERT and GAUTIER (1992)
			8-10		~70%	M'Bali dam	Dam height = 23,5 m	ALBERT and GAUTIER (1992)

System	Slope (V/H)	Velocity (m/s)	Discharge ($m^3/s/m$)	Overflow depth at crest (m)	Energy dissipation	Built Examples	Features	References
RCC lining	1/1.5	17	11.3	3.7		Ashton dam (steps 0.6 m high and 0.9 m wide)	Rehabilitation of earth/rock fill dam spillway for PMF. Crest protected by concrete cap. Chute height = 15 m; Crest length = 61 m The spillway has never been operated. Idaho, USA	NIGUS et al. (2000)
Concrete blocs and slabs			<50	3– 4		Cabora-Bassa Cofferdams (Mozambique)	During operation. Upstream cofferdam was protected with blocs of 400 kg. Downstream cofferdam had concrete slabs of 7 x 7x 2.5 m, without water-tightness system to prevent up-lift pressures	ICOLD (1984)
Reinforced concrete blocks cast in situ			12			Toktogul (ex-URSS)	Drop of 20 m, observed discharge	MIKHAILOV *et al.* (1985) LAFITTE (1985)
Cable tied concrete blocks		7.9				Jackhouse Dam (UK)	135-160 kg/m^2, under layer of geotextiles, anchored, cohesive subsoil, observed discharge without failure	POWLEDGE *et al.* (1989)
		8.6					With grass cover; anchored; products like ARTIOFLEX, PETRAFLEX, TRI-LOCK with intensive use for river protection	FRIZELL *et al.* (1996)
Pre-cast concrete blocks	1/ 6.5; 1/ 4.5; 1/ 6.5	17-23; -; -	60; 13; 5		-	Dnieper; Dneister cofferdam; Moscow water supply scheme (ex-URSS)	Designed upon ratio block thickness /unit discharge; 3rd example was under 2 m^2/s during one month without damage (dam height=12 m)	PRAVDIVETS and SLISSKY (1981) PRAVDIVETS (1987)
Pre-cast concrete blocks	1/3	3-3.5	0.92		n ~ 0.03-0.04	Brushes Clough dam	Prototype tests A design manual has been published by CIRIA	BAKER *et al.* (2000) HEWLETT *et al.* (1997)
Pre-cast concrete blocks	½	<13	<2.88		f=0.11 in uniform flow		Better than equivalent smooth surface; cost decrease of about 60% when compared with conventional structures	FRIZELL et al. (1996)
Pre-cast concrete pyramids						Leithen dam	Built in 1983 in Linz, Austria. Small watershed < 5 km2, Dam height = 15 m; Crest length of ~30 m Never experienced overtopping.	BOSSHARD (1991).
Geo-membrane	0.17 (~1/6)	6-8					Observed results; sensible to mechanical damage and deterioration	TIMNLIN Jr. et al. (1988)

Until now the use of such linings has been limited to velocities below ~8 m/s, unit discharges lower than 2-3 m^2/s and dams up to 10 m high, with some exceptions.

2.4.3 Crest design

The overflow crest may or may not be the full length of the dam and be located:

- close to either one of the abutments for cases where the dam is planned to breach with limited damages, thus reducing the vertical distance to be eroded and rapidly reaching the more solid foundation;

- in the central part of the dam if the dam should withstand overflow without breaching, corresponding to the highest section and the longest face length, thus providing a longer distance to dissipate energy.

In every case the site should be examined and the length and position of the controlled overflow selected to ensure the best use of the natural features and peculiarities of the site. Flow concentration at low points of the crest should be avoided as it may lead to higher erosion rate than expected. It may sometimes be necessary to provide a rigid crest, especially if negative under-nappe pressures are expected during overflow. According to Fritz and Hager (1998) the width and shape of the crest should be analysed, as the discharge coefficient for overflow dam crest is normally higher than that of a standard broad-crested weir with vertical faces.

The crest can thus consist of (Frizell *et al*. 1996, Pravdivets and Slissky 1981, Pravdivets 1987):

- Conventional protections of embankment crests, as asphalt roads or rip-rap layers;

- A rigid concrete cap, as a transition to the face lining;

- A trapezoidal approach channel covered with rip-rap, followed by a smooth-crested concrete weir (conventional design) slightly elevated above the approach channel, being the transition to the core constituted by a filter of suitable gradation.

2.4.4 Core design

A conventional core of clay material can be protected, for instance, by placing a synthetic filter cloth between the core and the sand filter (Odendaal and Zyl, 1979). Easy and low cost solutions can be realised by:

1. Using sheet piles as a sealing element (cut-off), placing them directly from the crest (if large enough for machinery), with proper treatment to prevent deterioration, either to link the crest and the core, or as a core itself in the case of low dams;

2. Creating a mixed barrier of impervious and partially pervious sheet piles, being the latter ones used for the establishment of the long-term saturation line, thus preventing rapid rise of the saturation line in the downstream part of the embankment during overflow events.

The sealing (water tightness) element should reach the crest, otherwise even a small incipient overflow event might lead to failure. Examples exist where dams fail before significant overtopping started, due to internal erosion on the transition zone between the core and the crest (ICOLD, 1997).

2.4.5 Toe protection design

Toe protection should avoid or reduce scouring, preventing damages to the dam body and foundation. The construction of a conventional concrete structure is the most common solution. When macro-roughness linings are used the reduction of the amount of energy being dissipated along the slope, by increase of the friction losses, can be envisaged to reduce the conventional concrete energy dissipation basin's size and cost.

The design of a toe protection depends largely on the quality of the foundation and on the tailwater level. The descending flow jet will reach high velocities at the toe, having high erosion potential. The transition from supercritical to subcritical regime is made through a hydraulic jump, the geometry and location of which is highly dependent on the tailwater level.

For a low tailwater level, the flow energy will be dissipated directly on the riverbed where erosion can occur, depending on the quality of the foundation. On the contrary, for high tailwater levels, such transition will be made on top of the face protection. Attention should be given to the oscillating pressure pattern of the hydraulic jump. At a certain instant, the resulting pressure can act as an upward destabilising force that conjugated with the foundation's up-lift pressures can cause the surface protection to lift and fail. Therefore, a compromise location for the hydraulic jump should be reached in order to place and design a toe protection that will avoid any of the above-described damages.

Hence, the main criteria are:

1. For **erodible foundations**, a protective rigid structure (reinforced concrete) should be designed in a way to assure that for limiting design scenarios the hydraulic jump is located within the structure. The limiting design scenarios will correspond to the minimum and maximum expected tailwater levels. The conventional dissipation basin is sized according to the residual energy to be dissipated at the toe;

2. For **non-erodible foundations**, a bucket can be envisaged, to launch the flow further downstream where the foundation is sufficiently resistant.

In practical terms, Frizell *et al.* (1996), Pravdivets (1987), Pravdivets *et al.* (1989) and Hewlett *et al.* (1997) proposed:

1. The construction or placement of a heavier/larger protection at the toe, receiving not only a significant component of the lining's weight on the tangential direction to the slope, but also the hydrodynamic pressures dues to the hydraulic jump transition;

2. The use of massive downstream toe concrete blocks fixed to the foundation;

3. The construction of a conventional energy dissipation basin, with protection of the downstream riverbed by means of a rip-rap protection;

4. The reduction of the slope to 1/6 (V/H) at the slope so that an elongated-surface hydraulic jump with reduced erosion potential can develop.

2.5 EXISTING PROTECTION LININGS BY CONCRETE ELEMENTS

2.5.1 General description

Prefabrication of structural elements for civil engineering works has been a trend over the last decades. The aim is to reduce the demand for reinforced concrete and labour cost. Such linings are of economical interest in case of multiple repetition, simplicity of geometry (reflecting in form-work complexity) and low transport cost. Some systems of prefabricated concrete elements have been already been developed and are presented in the following sections.

2.5.2 Overlapping wedge-shaped concrete blocks

The lining system using pre-cast wedge-shaped concrete blocks has been developed over the last 20 years, in the ex-URSS[11], in the United Kingdom (CIRIA[12]) and in the United States of America (USBR[13] and CSU[14]). The main goal is to provide protection against erosion caused by high velocity flows on embankments subject to overflow, for slopes milder than 1V/2H. The developed linings comprise a layer of free draining, angular, gravel filter material, upon which is placed a row of overlapping concrete blocks - Figure 2.3.

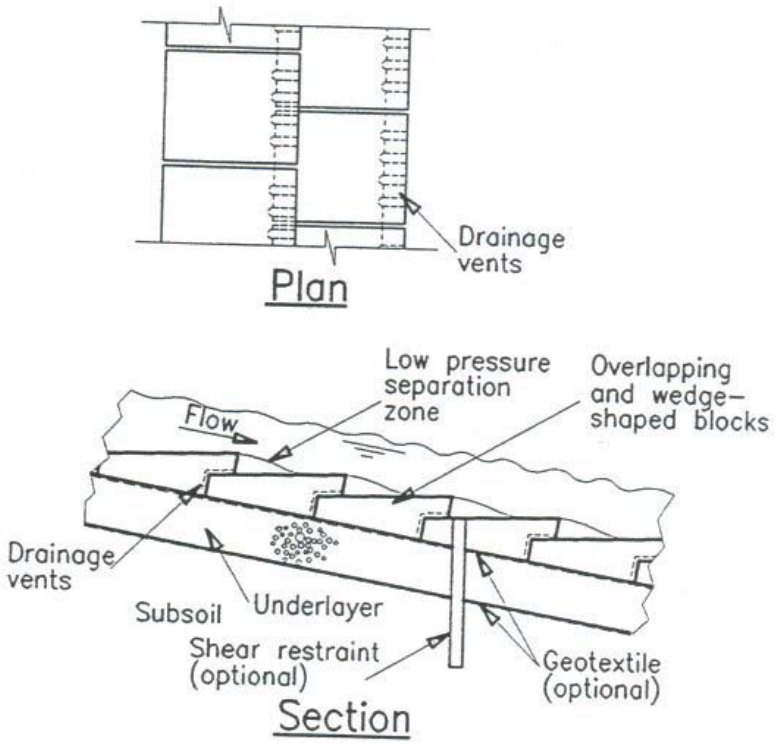

Figure 2.3 – Concrete element defined by Hewlett *et al.* (1997) for the design of a stepped-block spillway

[11] Moscow Institute of Civil Engineering, Moscow, Russia.
[12] Construction Industry Research and Information Association, in collaboration with the Salford University, United Kingdom.
[13] Bureau of Reclamation of the U.S. Army Corps of Engineers, USA.
[14] Colorado State University, USA.

The stability of these blocks is ensured by a combination of hydraulic forces, namely the impact on the step surface and the reduction of the up-lift pressures in the foundation by water extraction. Fixed concrete blocks are placed at the toe of the dam, normally beneath the tailwater level, to support the overlapping block rows that are placed along the slope.

Optimisation of the water extraction performance made during the nineties (Frizell et al., 1996; Hewlett et al., 1997) allowed to decrease the weight of the elements and to prefabricate them industrially. This system has proven to be stable for a wider range of flow velocities than those existing before. The stability of the stepped concrete lining was further improved by providing continuous aspiration of seepage flow through the joint openings (vents)[15], profiting from the low-pressure region created in the backstretch of the stepped surface. Despite some small differences, the concrete elements are basically similar to those described in the Design Guide edited by Hewlett et al., 1997. Some of this system's advantages are (Baker, 2000):

1. the upstream edge of each block is shielded from the flow, thus eliminating the risk of stagnation pressure forming against any offset, being transferred to the foundation and generating up-lift pressures (common failure mechanism for flat block systems).

2. the blocks shape is said to be self-stable in uniform flow; if a block lifts then the curving flow streamlines will generate a downward force that pushes the block back into place.

3. the stepped surface contributes to the reduction of flow velocity and to the size of any energy-dissipating device at the toe.

4. the wedge-shaped block offers the *most stable solution for the minimum weight* of concrete (Baker, 1989).

2.5.3 Pyramidal concrete blocks

A different concept characterises the system used in Leithen since 1983 in the municipality of Weibern, Province of Linz, in Austria (Bosshard, 1991) – Figure 2.4.

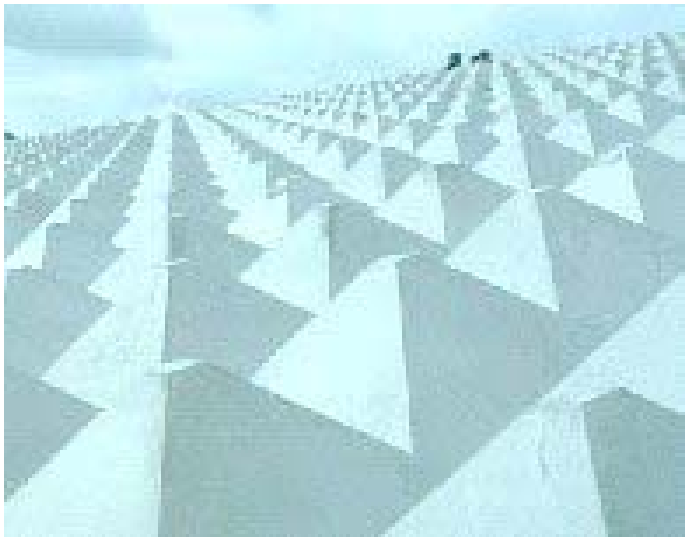

Figure 2.4 – L**ining of downstream face of Leithen Dam in Austria (*in* Bosshard, 1991) with pyramids**

[15] The dimensions of the slots have been optimise to a standard of 2,8 % of the vertical step face area, for a given surface slope of +11° in relation to the embankment slope.

The embankment dam is part of a flood retention scheme, also used for leisure activities. The dam has a height of around 15 m and the pyramid lining has been placed over a distance of approximately 50 m of width, acting as main spillway. This spillway has never operated since commissioning. The pyramids seem to be stable due to their own weight. Unfortunately, it was not possible to study any documentation on this pyramid system during this research work.

2.5.4 Stability of concrete element linings

2.5.4.1 Introduction

Being the wedge-shaped block system the most documented one, this section will focus on this system's stability and on constructive measures adequate to its reinforcement.

2.5.4.2 Main forces acting on an isolated element

The acting forces on a concrete block submit to flow on a sloped surface are a function of the flow conditions, the block characteristics and of its surroundings. They can either be stabilising or destabilising, according to the failure mechanism and failure flow conditions. The shape of the block plays a relevant role on the distribution of the hydrodynamic (flow-driven) forces and on the definition of the gravity centre location, relatively to the destabilising forces directions. In most cases, acting forces in a concrete block can be reduced to:

- The self weight of the block,
- The hydrostatic lift of the fluid (water and air) where the element is submerged,
- The hydrodynamic forces due to the overrunning flow, that can be decomposed in a Drag component, parallel to the flow direction, and a Lift component, normal to the flow.

The CIRIA wedge-shaped block system makes use of the hydraulic forces to assure stability, by difference of pressures in the upper side of the element and in the foundation. The system of acting forces upon one single concrete element, decomposed in surface contact forces, is presented in Figure 2.5. Quantification of some of the forces is not straightforward due to their variability in both time and space, as for the hydrodynamic loads.

The hydrodynamic loads vary in time and space. They can be decomposed on a steady mean component and a fluctuating component, being failure a probabilistic event occurring when the pressure fluctuations coincide in the most unfavourable way. The extreme values are frequently higher than the mean values (Sánchez Juny *et al.*, 2000).

From laboratory tests the *most significant factor* affecting CIRIA's block stability was found to be the inter-block forces. These forces allow the hydrodynamic pressures to be more evenly distributed across the channel, delaying the failure of a specific block (Baker, 1989).

Frizell *et al.* (2000) did not consider the block weight in their stability analysis, as it seems not to be relevant, as long as the equilibrium of pressures between the flow side and the foundation side is established. Blocks of any weight are believed to be possible to build. Overlapping and interlocking effects can further reinforce stability.

The most critical place down the slope is the region where up-lift pressures achieve their maximum value. The up-lift pressures are the component of the hydrostatic pressures acting on the element foundation. From a certain location downstream these pressures no longer increase, being kept constant by quasi-uniform flow conditions and regular performance of the water-extraction mechanism.

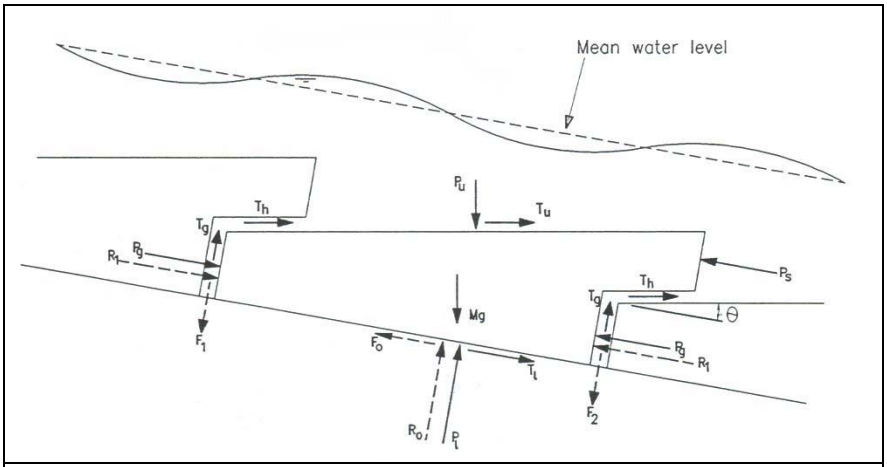

- normal pressure force on upper surface of block (P_u)
- shear force on upper surface (T_u)
- normal pressure force on step (P_s)
- normal forces on ends of block due to pressure in gaps (P_g)
- shear forces on blocks due to flows in gaps (T_g, T_h)
- uplift pressure force on lower surface of block (P_l)
- normal reaction forces from adjacent blocks (R_1)
- frictional forces resisting vertical movement of block (F_1, F_2)
- shear force due to seepage flow beneath block (T_l)
- normal reaction from underlayer (R_o)
- frictional force from underlayer resisting movement (F_o).

Figure 2.5 – Acting forces on a wedge-shaped block (*Mg* = weight, *in* Hewlett *et al.*, 1997)

In what concerns quantitative results some references were found in literature, namely:

- Pravdivets and Slissky (1981) evaluated the hydrodynamic load on the upper element surface in approximately 10 per cent of the kinetic head.

- Frizell et al. (1996) obtained the net force per meter of block width by integration of the pressure profile on the step horizontal surface and the measured filter layer pressure.

The system developed in Austria appears to make use of the weight as the main stabilising force, not considering, as far as it was possible to investigate, any water extraction mechanism.

2.5.4.3 Failure mechanisms

Past lining systems have been conceived under a simple basic criterion: *the block size (thickness, length) and weight are set in accordance with a unit design discharge*. Therefore, the unit discharge corresponding to failure conditions should be known *a priori* for each type of block geometry.

The most likely failure mechanisms are:
1. Lift of elements, by conjugated action of up-lift pressures and other acting forces;
2. Sliding of elements, due to insufficient downstream resistance capacity;
3. Overturning of elements;

4. Sub-layer failure either by settlement caused by internal erosion of the subsoil or by sliding.

Failure might the result of a single mechanism or a combination of these mechanisms. Predominance of one of the mechanism is expected. As an example, Frizell *et al.* (1996) presented lift as the most common failure mechanism, by rise of pressures in the lining foundation. Failure by lift is more likely to occur at the toe and when it can happen by departure of an individual block or by lifting of a wave-like group of blocks.

2.5.4.4 Constructive measures to improve the stability of the lining. General review.

The stability of the lining system can be improved by enhancing the connection between the blocks and/or by reinforcing the connection between the lining and the underlying embankment - Figure 2.6. Connection can be made by:

a) **overlapping**, where a single block will be under the stabilising influence of the self-weight of one or more neighbouring blocks, doing the same to the following;

b) **mechanical interlock**, where the elements do not just overlap but really lock each other (e .g male-female connections);

c) **artificial interlocking or binding,** made by cable-tying the blocks or by placing connecting pins between consecutive elements. The lining will then be laid in mats on the embankment surface and secured with soil anchors. This procedure is commonly used, at least, for the most downstream blocks, more likely to operate under fluctuating pressures due to the presence of an eventual hydraulic jump.

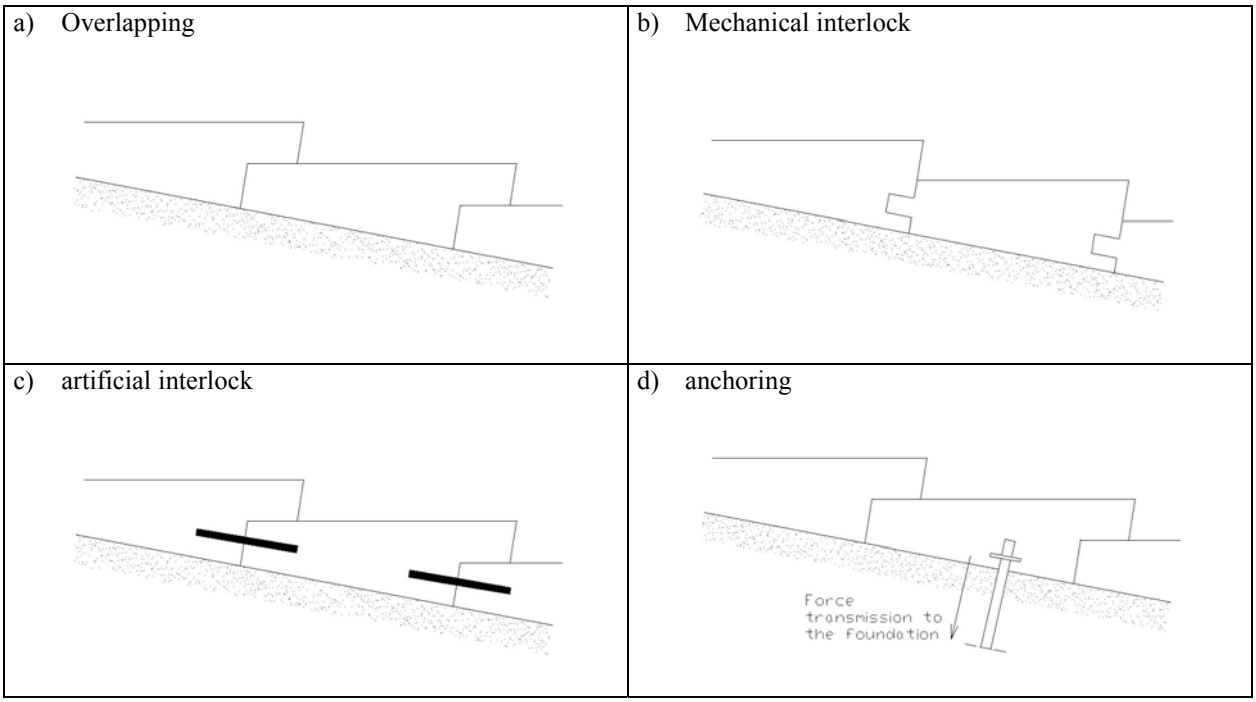

Figure 2.6 – Constructive measures to improve the stability of the lining

These procedures can be used to increase the stability of a lining for a given design discharge, or, in the opposite sense, to allow the use of lighter blocks for higher velocities and flows, for which they would initially be considered unsafe.

Further, spaced **anchoring** of the lining along the slope will improve the connection between the lining system and the embankment itself, also preventing element sliding. Critical are the choices made for the spacing, the resistance and the geometrical definition of the anchors, in accordance with the expected stability conditions. Other measures to improve stability are the use of larger blocks in the stilling area or the construction of a mass concrete anchor block, complemented or not with the construction of a conventional dissipation structure (Hewlett *et al.*, 1997, 1994).

2.5.5 Transition and Drainage layers

The long and reliable operation of the overflow spillway depends primarily on keeping up-lift pressures from reaching destabilising magnitudes. Secondly, the embankment stability should not be threatened by eventual internal erosion driven by the infiltrated flow. Hence, drainage of the element foundation and proper transition between the lining's foundation and the embankment are key elements in the overall overflow lining performance.

Drainage should efficiently collect and guide the infiltrated water downstream to a toe collecting drain (placed across the valley), thus avoiding the build up of up-lift pressures under the lining concrete elements. Further, the drainage layer acts as a regulating layer (foundation) to assist construction. If the infiltrated flow is not rapidly evacuated, due to insufficient drainage capacity or because it has reached the seepage saturation line, then up-lift pressures will be build up.

Infiltrating flow depends mainly on the overtopping flow and on the concrete element joint geometry and joint opening. Drainage layers are often designed according to Terzaghi's principles for filter layers (Strobl, 2000, Singh and Varshney, 1995):

a) To ensure flowing conditions, $D_{15}/d_{15} > 4\text{-}5$ (2.3)

b) To assure a geometrical barrier, $D_{15}/d_{85} < 4\text{-}5$. (2.4)

However, a closer insight should be provided in order to quantify the effective drainage flow, in terms of percentile fraction of the overflow discharge, for intermediate operation or failure conditions. The thickness of the drainage layer plays an important role in its efficiency. From literature some references were collected:

1. Frizell *et al.* (1996), present a drainage layer consisting on a 0.5 ft (approximately 15 cm) layer of free draining, angular, gravel filter material.

2. Pravdivets *et al.* (1996) advised the placing of 2 or 3 layers of drainage filter, their thickness being 3-4 times the d_{85} or more, but not less than 0,20 m.

Beneath the drainage layer a transition layer is normally placed, which separates the embankment material from the lining components. This layer should prevent the migration of fine particles from the underlying embankment, thus protecting the subsoil from internal erosion (piping). Alternative systems can be used to make this transition - Figure 2.7.

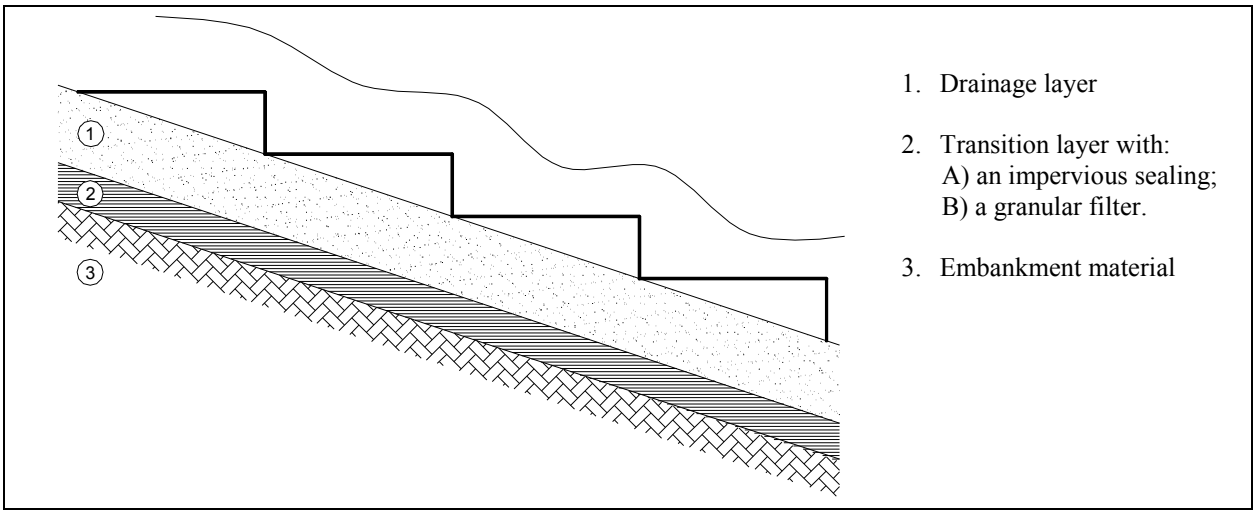

Figure 2.7 – Schematic representation of the transition and drainage layers

An impervious sealing creates a thinner transition comparatively to a granular filter, despite its higher cost. On the other hand, the granular filter thickness depends on the size difference between the separated materials. As a compromise, Pravdivets (1989) advises the eventual use of geotextiles to improve the filtering performance and prevent internal erosion of the embankment.

From observations at a large-scale laboratory flume, it is expected that fines and dirt will be flushed out from the drainage layer one overtopping starts (Frizell *et al.*, 1996). Initial settlement of the embankment should be expected and accounted for. Prof. Pravdivets (Baker, 2000) reported one example of failure caused by drain layer erosion, at Jelyvski in the Ukraine.

2.6 HIGH VELOCITY FLOWS OVER MACRO-ROUGHNESS

2.6.1 Introduction

Flow over macro-roughness will be herein divided in flows over irregular macro-roughness, as rip-rap and large boulders, and uniform macro-roughness, as stepped surfaces created by RCC dams, wedge-shaped blocks or pyramids as presented in the previous section 2.3. The following section concentrate almost exclusively on the latter type of surfaces. Exceptions are highlighted.

2.6.2 Roughness

The notion of roughness is a major player in most hydraulic research at least since Chézy. From the initially studied smooth surfaces, Nikuradse progressed to the notion of **equivalent absolute roughness**, k [L]. In this concept, the energy loss a flow suffers when running over a surface of irregular roughness is equal to the one produced over another surface covered with fictitious regular shaped roughness elements of height k. Afterwards, roughness was discovered to depend not only from surface roughness but also from the flow depth. This dependency is reflected in the parameter of **relative roughness**, ε [-] or k/D, where D is the diameter of the pipe, substituted by D_h (the hydraulic diameter) for free-surface flow. The characteristics of a running flow are closely influenced by the roughness of the boundaries or, from a different angle view, by the friction between the flow and the boundaries. The relation between flow energy variations and boundary roughness can be synthesised in a friction factor.

Flow regime classification is also based on roughness, and friction, being summarised in the known Moody-Stanton aback. Hydraulic engineers use these notions by means of the worldwide

known Colebrook-White and Darcy-Weisbach formulae for the computation of energy friction losses in closed pipes or open channels. However, this aback is only available for relative roughness values up to 0.05.

The type of flow understudy is classified as flow running over **macro-roughness**. Empirically, it corresponds to the situation when the water depth is of the same order of magnitude of the elements creating the roughness, meaning the flow surface is disturbed by the bottom configuration (Bathurst 1978, Dubois 1998). In general this condition is assumed for high values of the relative roughness and is normally expressed in the following way for granular material:

$$D_{84}/h \geq \frac{1}{4} \tag{2.5}$$

which can also be presented as a "relative roughness":

$$h/D_{84} \leq 4 \tag{2.6}$$

In such case, "roughness" is assumed to be a function of a characteristic diameter. For uniformly repeating surface geometry, the height of the roughness element measured perpendicularly to the slope, *ks*, as been unanimously adopted – Figure 2.8.

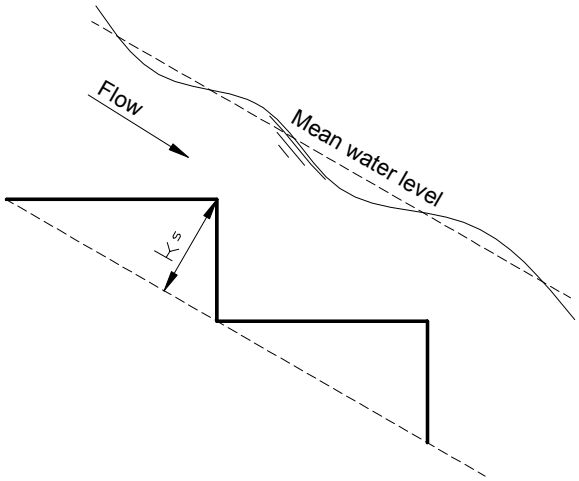

Figure 2.8 – Definition of the characteristic roughness height, *ks*, in stepped surfaces.

The majority of common cases in open channel hydraulics concern turbulent rough flows, where friction depends exclusively from the relative roughness:

$$f = F(\varepsilon) = F(\frac{k}{D_h}) \tag{2.7}$$

For flows over macro-roughness this relation is thus:

$$f = F(\frac{k_s}{4 \cdot h}) \tag{2.8}$$

substituting the hydraulic diameter by 4 times the hydraulic radius of a rectangular channel[16].

[16] When *B>>d* the hydraulic radius is assumed as the flow depth, *d*.

In resume, flows over macro-roughness are outside the range of the Moody-Stanton aback. In fact, when analysing the influence of roughness on the flow pattern, three relative roughness domains can be identified (Samora, 1993; Martins *et al.*, 1996):

- **high relative roughness**, where the roughness height influences the surface profile, friction is mainly a function of the **form** of the bottom surface;

- **intermediate relative roughness**, where the individual roughness elements will have progressively less influence on the flow pattern;

- **low relative roughness**, where the roughness height is very small in comparison to the flow depth, as flow in smooth surfaces or pipes. In such case the effect of the roughness will be felt only in a narrow depth range close to the boundary, not interfering with the main flow – this is called **skin friction**;

The same authors have limited the high relative roughness domain to $\varepsilon>0.05$, precisely the limit of the frequently used aback. Therefore, for flows over macro-roughness ($\varepsilon>0.25$) friction depends mainly on the bottom configuration.

2.6.3 Internal flow features

2.6.3.1 Flow regimes over uniform macro-roughness

Two main flow regimes are observed over regular macro-roughness surfaces (Chanson, 1994), similar to what will be created over the concrete elements presented in this work (Figure 2.9):

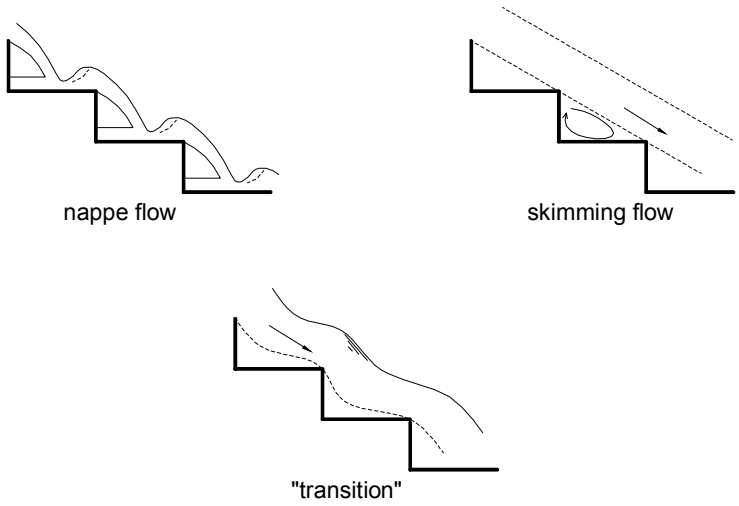

Figure 2.9 – Flow regimes over stepped surfaces

1. Nappe flow - for low discharges, the flow jumps from element to element (step to step). As the flow increases the cavity between the roughness tips will be progressively filled up. The flow jet impinging the element surface will limit the extent of the separation zone thus entrapping a volume of air;

2. Skimming flow - for large discharges, the water flows as a coherent stream, "skimming" over the elements. The separation line will unite the roughness tips creating a pseudo-

bottom. An entrapped vortex will occupy most of cavity between consecutive roughness tips. Friction is said to depend on the momentum exchanges between the over-running flow and the re-circulating entrapped flow underneath.

Nappe flow and skimming flow can still be divided in several sub-regimes, with isolated nappe or partial nappe (Pinheiro and Fael, 2000), with fully developed hydraulic jump or not, as a wake-step interference (Chanson 1994), etc., which are considered not to be so relevant to review at this stage of the development of the herein presented lining system concept.

2.6.3.2 Onset of skimming flow

The transition from nappe flow to skimming flow has been deeply studied for regular stepped surfaces, for which several theories for analytical evaluation of the conditions of onset of skimming flow are available (Chanson 1994, Pinheiro and Fael, 2000). However, and as the scope of the present review is broader than just stepped-like surfaces, the concept of the onset conditions of skimming flow can empirically be understood as "the disappearance of the cavity beneath the free-falling nappes" (Chanson, 1994). Still, this definition is only appropriate for regular macro-roughness elements with a *constant linear development* through the channel width.

In opposition, for elements like the pyramids used in Austria, there is a strong 3D effect on the flow pattern, which renders inadequate the definition of nappe flow, and thus of the onset of skimming flow. Nevertheless, skimming flow conditions are quite clear to identify for large discharges – the flow will undoubtedly stream over the elements. Yet, it is not clear if the pseudo bottom has a regular geometry throughout the channel width, which poses difficulties to the definition of a flow depth. For low discharges, there is not a consensual definition. The like for irregular macro-roughness surfaces.

2.6.3.3 Flow regions

Taking as example the most studied regular macro-roughness surfaces till present – stepped slopes – the following flow regions are identified (see Figure 2.10):

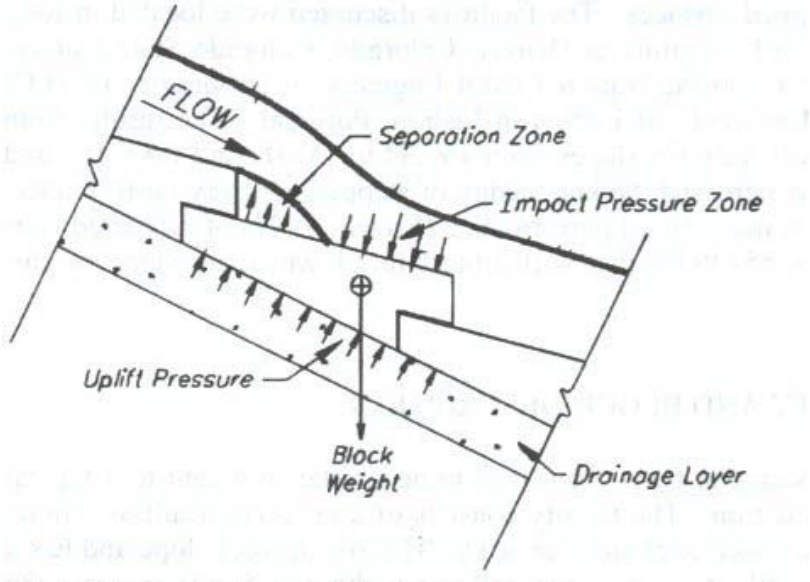

Figure 2.10 – Flow regions (*in* Hewlett *et al.*, 1997)

1. **A separation zone** created at the inner-side (step height) of the element tip (step tip) as the flow separates from the physical boundary (separation zone);

2. **An impact zone**, on the upstream face of the macro-roughness element (step horizontal surface), where the separation line reattaches with the physical boundary.

In the wedge-shaped lining systems, air vents located in the separation zone enhance the extraction of water from the drainage layer, decreasing the up-lift pressures and sucking the block into the embankment.

For increasing discharges, air will be entrapped underneath the separation line. For skimming flow conditions, the separation line develops into a pseudo-bottom, underneath which circulating currents occupy the cavities. Entrapped three-dimensional vortexes are created, the geometry and volume of which depend on the flow discharge. An irregular pressure field results from these circulating vortexes. Minimum pressures do not attain cavitation levels, at least not in the fully developed flow region (Júny *et al.*, 2000, André *et al.*, 2001).

Design should not be made considering the average value of these pressures, as the most critical stability conditions will correspond to the extreme values, either stabilising or destabilising, which can be several orders of magnitude higher than the mean values. On the other hand, in the "impact zone" the hydrodynamic pressures also vary with the unit discharge and the flow regime. For low discharges, the impinging jet in nappe flow will impact the element surface, to which corresponds an irregular spectre of pressure. For higher discharges, the impinging jet will progress towards the outer tip.

2.6.3.4 Flow aeration

In regular macro-roughness surfaces as the ones corresponding to a stepped slope, air entrainment starts at the surface from the inception point (Figure 2.11). Comparatively with a smooth chute the inception point is located further upstream. However, the mechanisms of air entrainment are believed to be similar both in conventional smooth chutes and stepped chutes (Chanson, 1994). Further, quasi-uniform flow is reached when the air concentration profile becomes constant (Henderson 1966). Therefore, once skimming flow becomes fully developed (constant air profile), a stepped surface behaves in the same way as a non-stepped one (Chanson, 1994).

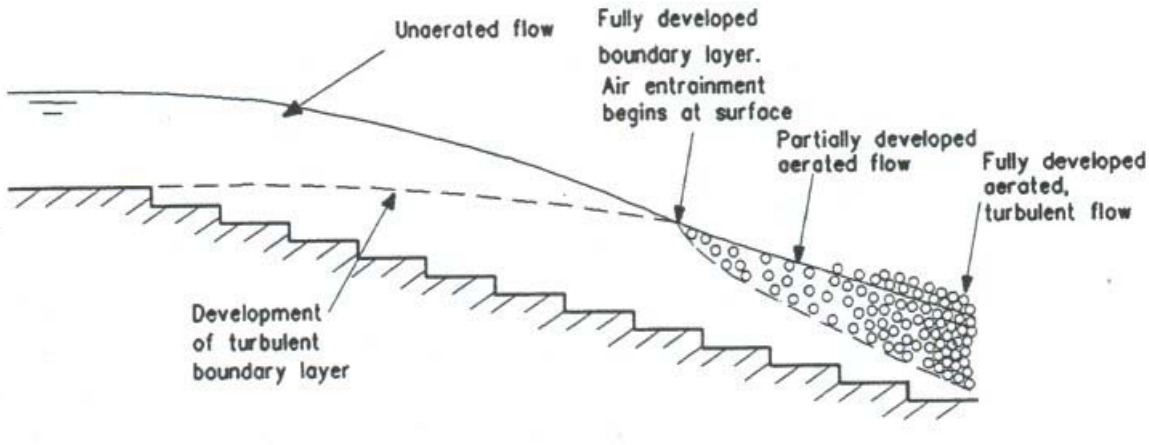

Figure 2.11 - Boundary layer development for a stepped surface (in Hewllet et al. , 1997)

The characteristics of the main flow "skimming" over the pseudo-bottom are, in fully developed quasi-uniform conditions, similar to that over a smooth chute. The entrapped vortexes below do not interfere with the air concentration of the main flow, but rather in the energy dissipation mechanisms (described in the following sections).

One commonly used parameter that quantifies the air content on the flow is the mean depth-averaged air concentration, C_{mean}. From the previous statement, the mean air concentration is assumed to be equal to that of a smooth spillway of identical slope (Frizell *et al.*, 2000). It can be computed from the following equations:

a) for uniform flow on smooth chutes or quasi-uniform skimming flow over regular macro-roughness

$$C_{mean} = 0.9 \cdot \sin\alpha \qquad \text{(Chanson 1994, } \alpha<50°\text{)} \qquad (2.9)$$

$$\text{or} \quad C_{mean} = 0.76 \cdot \sin\alpha^{0.82} \qquad \text{(Matos 1999)} \qquad (2.10)$$

b) for natural rip-rap surfaces (e.g mountain rivers)

$$C_{mean} = 1.44 \cdot \sin\alpha - 0.08 \qquad \text{(Hartung and Scheuerlein, 1970)} \qquad (2.11)$$

In all presented formulae the mean air concentration depends uniquely on the channel slope.

For macro-roughness surfaces, there seems to be more air in the flow at the bottom than in the case of a conventional non-aerated spillway, reducing the risk of cavitation damage. However, and giving the example of a stepped cascade, safety against cavitation damage might be assured only at a distance from the inception point larger than six times the equivalent clear water depth at that location (Matos *et al.*, 2000).

2.6.4 Flow depth

The highly aerated turbulent flow conditions do not allow an accurate measurement of the flow depth (Olivier 1967). In fact, the identification of the flow depth or the flow velocity is not straightforward in two-phase flows. Standard equations for clear-water flow have to be corrected on the basis on air-water mixture density. The discussions on what to assume, how to measure and what to correct are far from finished. Some standardisation has been achieved in the last years for stepped surfaces, but outside this domain each author tends to assume its own reference values.

In nappe flow regime, where the flow jumps freely from element to element, the depth and the velocity at critical flow over the roughness element tip, are normally used as a reference. However, this is only possible when a fully developed hydraulic jump over each element is observed.

For increasing discharges, most of the flow will be running over the roughness tips. The entrapped water volume underneath barely participates in the main over-running flow. Therefore, for skimming flow regime one can say that:

- Upstream from the inception point, the flow depth measured perpendicularly to the slope and from the element tip is identical to the one measured in an identical smooth chute;

- In the partially aerated flow region, the flow depth varies in every section and its definition is clearly dependent from the varying air content. For both conventional and stepped surfaces, the representative water depth to which corresponds a local air concentration of 90 per cent Y_{90} is generally considered as reference (Wood 1991, Matos 2000);

- In quasi-uniform conditions, a pseudo bottom can be identified and depth can be measured from that reference using (Andre 2000, Matos 2000) either:

  A) Direct methods, as the visual observation of a mean surface elevation (also with video) or by estimating the water depth from measured air concentration profiles, more suitable for highly aerated flows (white water).

  B) Indirect methods, by computation of the conjugated hydraulic jump flow depth. This method provides only an equivalent clear-water depth at the upstream end of the hydraulic jump, that is to say, a non-realistic estimate of the mixed air-water flow depth at the dam face downstream toe. It can also be used to evaluate indirectly the energy dissipation along the dam face.

Matos (2000) concluded that the mean observed flow depth h_{obs} in fully aerated quasi-uniform flow conditions, is approximately the depth Y_{90}. This conclusion allows the computation of an equivalent clear-water depth, *hw* (eq. 2.12), for stepped-like macro-roughness surfaces, once observations measurements are available and the mean air concentration can be estimated.

$$h_w = h_{obs} \cdot (1 - C_{mean}) \tag{2.12}$$

2.6.5 Flow velocity

For uniform flow in open channels a logarithmic law is considered to be a good first assumption for the velocity distribution over the entire flow depth (Graf and Altinakar, 1998). However, for high velocity flows over smooth or macro-roughness surfaces, a clear-water velocity profile does not account for the air entrainment and thus is not accurate.

Nevertheless, design engineers commonly assume clear-water flow characteristics when designing concrete smooth chutes. Such simplification allows the use of gradually varied clear-water flow Bernoulli's equation that give, at least, an order of magnitude of the main hydraulic parameters. Corrections to account for the effects of air entrainment in the flow depth, flow velocity and energy dissipation are afterwards introduced.

In the case of flows over macro-roughness surfaces, flow conditions vary considerably according to the discharge. For low discharges, the flow pattern is highly complex and three-dimensional. No general velocity profile principle can be established. For increasing discharges, the flow is divided between the main skimming flow and the underneath entrapped flow in the cavities. For the main flow, the velocity profile is somewhat similar to that on a smooth chute, particularly in uniform flow conditions (Figure 2.12). The velocity profile follows the power law:

$$\frac{V}{V_{90}} = \left(\frac{y}{Y90}\right)^{1/N} \tag{2.13}$$

where N is believed to vary between 3.5 and 4, being 6 for smooth chutes (Chanson, 1994).

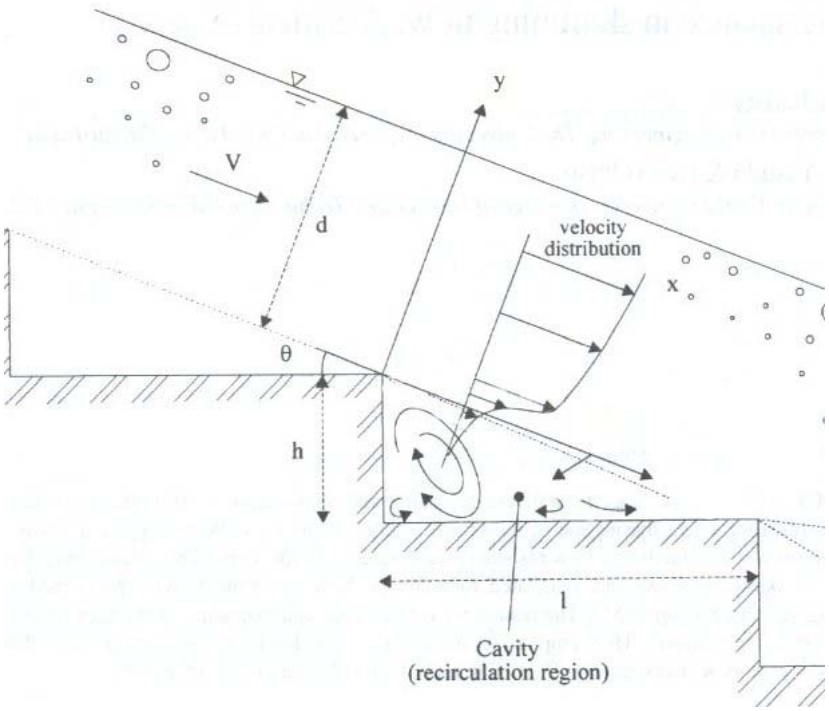

Figure 2.12 – Velocity profile (adapted from Chanson *et al.*, 2000)

However, if a more accurate velocity profile is to be established measurements of air concentration across the flow depth are needed. As an example, for stepped surface the reference velocity is normally assumed as that corresponding to a local air concentration of 90 percent. The influence of the interface (pseudo-bottom) between main flow and cavity flow has not yet been fully investigated. In fact, measurements have not been made in the 10 per cent of the flow depth, *h*, close to the bottom.

In quasi-uniform flow condition over regular/irregular macro-roughness an equivalent mean clear-water velocity can be computed from eq. 2.13.

$$V_w = \frac{q_w}{h_w} \tag{2.13}$$

For wide channels the mean (depth-averaged) velocity V_w is approximately equal to the mean velocity over the liquid section U_w except close to the boundaries.

2.6.6 Energy dissipation mechanisms

Each of the described flow regimes has different energy dissipation efficiency. For simplicity the following explanation will concern macro-roughness element in the form of a step. For other regular roughness shapes, differences concern mainly the macro-turbulence pattern and its influence on the flow regimes.

For low discharges with fully developed hydraulic jump, energy dissipation is approximately the loss of potential energy correspondent to the step height, as in the case of a drop structure – Figure 2.13; its efficiency is almost 100 per cent.

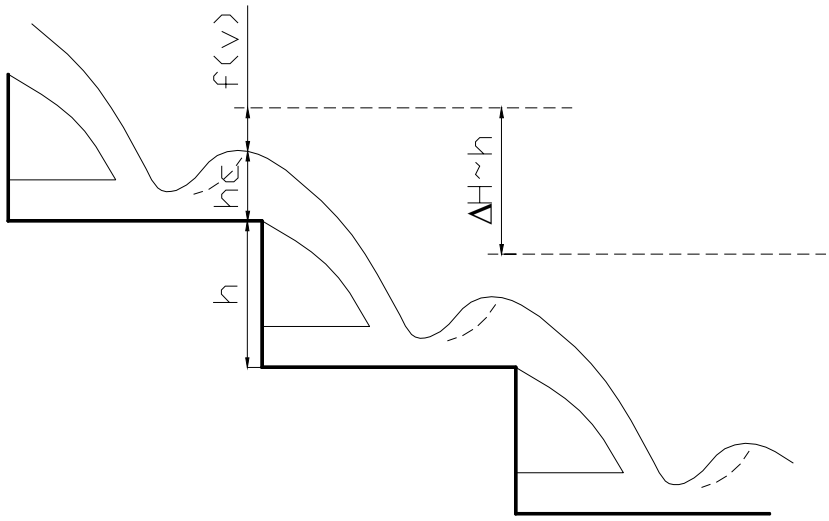

Figure 2.13 – Energy loss in successive drops (where *h* is the step height, h_c the critical depth, *f(V)* is the kinetic head, function of the critical velocity, and ΔH is the head loss at each step)

In general terms, energy dissipation in nappe flow regime is mostly made through jet break-up in the air, jet impact on the step and possibly due to the formation of the hydraulic jump (André *et al.*, 2001).

For increasing discharges, the impinging jet will impact the step surface further downstream and a large percentage of it will bounce back to the main flow. Energy dissipation will be made by means of impact against the surface and collision of bouncing flow with over-running flow (flow that does not even enter the cavity).

For a fully developed skimming flow regime over steep slopes, energy dissipation corresponds to the friction losses created by the momentum exchanges at the pseudo-bottom interface between the (over-running) flow and re-circulating vortex flow (Chanson 1994), as well as to the head loss associated with the internal bouncing jet formed near the outer edge of the steps (André *et al.* 2001).

In quantifiable terms, the energy loss in uniform flow is equal to the potential energy loss. For a given discharge, the highest dissipation efficiency is attained exactly for the highest velocity along the slope: the uniform velocity.

Spillway chutes of equal slope and length can be compared for their dissipation efficiency by means of the uniform velocity. The one having lower velocity at the toe is likely to have dissipated more energy along the slope. In this conditions, macro-roughness surface are likely to dissipate more energy than smooth surfaces, allowing for significant cost savings in the energy dissipating structure.

2.6.7 Energy dissipation evaluation on wedge-shaped element linings

The previously presented stepped-blocks systems have not been developed having energy dissipation as the main requirement. However, the existing experience shows also a reduction in

flow velocities (and flow energy). Some indications of the friction factor along a stepped slope were found in literature, being resumed in Table 2.3.

Frizell et al. (1996), computed the Darcy-Weisbach friction factor, *f*, along the slope, based upon velocity profile measurements, corrected for air concentration. Though being variable down the slope, the friction factor stabilise at a value of 0.11 for uniform flow. The mean air concentration in the same condition was of 34 %, meaning that the sidewalls of the spillways channel should be raised of the same percentage in comparison to the calculation performed for a smooth chute. An additional safety factor can always be added if deemed necessary.

Table 2.3 – Computed friction factors for stepped-block spillways

Reference	**Uniform flow**			
	$f_{Darcy\text{-}Weisbach}$	$n_{Manning}$ (s/m$^{1/3}$)	C_{mean}	*Slope*
Frizell et al. (1996)	0.11	0.033	0.34	Typical earth fill dam
Baker (2000)		0.03-0.04 (Chézy of 5.9-6.3) (equivalent smooth surface)		1/3
Frizell et al. (2000)	f_{mean} =0.08	(equivalent smooth surface)	0.41	Typical earth fill dam

Baker (2000) computed the Manning and Chézy's coefficients from field tests on the stepped-block prototype at Brushes Clough dam (UK).

Frizell et al. (2000), computed the mean value of the Darcy-Weisbach friction factor along the slope of an equivalent slope smooth surface for skimming flow regime, considering that in quasi-uniform flow the air concentration distribution along the depth is identical for both surfaces.

A review of friction laws for skimming flow over macro-roughness is presented in Appendix 1, as a complement to the present work.

2.6.8 Estimation of the energy dissipation efficiency in laboratory

Estimating the capacity of a certain lining to dissipate energy can be made by:

a) Developing extensive research for each geometry and establishing experimental friction laws from observed laboratory model measurements;

b) Obtaining a relation of energy reduction by meter of length of a certain surface, as a result of the application of the Euler theorem (equation of conservation of momentum) between two sections where flow energy is known (approach taken by André at the LCH).

The first proposal has been advised for slopes of less than 20° (Chanson *et al.*, 2000*).* However it is very time consuming and should only be used once one type of geometry has already proven to be sufficiently interesting for massive use. The second methodology is presently being followed by André at the LCH, for selection of the most promising macro-roughness surface in view of energy dissipation.

2.7 SYNTHESIS AND DISCUSSION

2.7.1 State-of-the-art synthesis

1. Embankment dams are the large majority of both existing and to-be-built dams in the near future. Failure of embankments accounts for around 70 % of known failures, most of them by overtopping due to insufficient flood discharge capacity. Controlled overtopping (overflow) of embankments present itself nowadays as a potentially good alternative for flood management.

2. Overtopping of an embankment dam should no longer be associated blindly to dam failure. Many existing dams have experienced overtopping and while some of them did breach some other, though, have suffered no damage or just limited damage. Controlled overtopping (overflow) can be considered for situations where the failure risk[17] is low.

3. Embankment erosion can be caused by free-surface flow erosion or infiltrated flow erosion. It is generally initiated at, or near, the downstream toe, where the flow velocities are the highest. If the duration and magnitude of the overflow events is long enough, erosion will progress upstream until, eventually, the crest is reached and a breach is opened.

4. There has been consistent research on the topics of overflow embankment dams during the last 40 years, and some surface lining systems have been developed, mainly for erosion prevention purposes.

5. Linings made of pre-cast concrete elements allows for a higher degree of mechanisation and use of prefabricated elements in earth dam construction.

6. Different existing systems of pre-cast stepped concrete elements differ mainly in weight and existence or not of interlocking cables or pins. Their stability principle is the same, comprising reduction of foundation up-lift, by water extraction through slots linking the drainage foundation to the inner step low pressure zone (Frizell *et al.* 1996, Hewllet *et al*. 1997)

7. Progress in other fields, mainly in flow over stepped spillways made on RCC dams and gabion weirs, seems to be to some extent applicable to the domain of overflow earth fill dams lined with concrete elements.

8. The flow regimes of nappe flow with fully developed hydraulic jump and fully developed skimming flow, are the most documented in literature. For this type of nappe flow, criteria for the definition of flow depth and flow velocity in drop structures can be used. For this type of skimming flow, progress is due to research on stepped spillways. The flow features have also been studied and are well documented.

9. Most of the existing stepped surfaces have been designed for fully developed skimming flow conditions on slopes of typical concrete gravity dams. Some examples are known where nappe flow conditions were used for gabion linings.

[17] Failure risk is the combination of the probability of a given flood event and the consequences (damages, human life losses) that it will have upon the dam system and the valley downstream.

10. For earth fill dams lined with concrete elements physical modelling of the lining system is required for visual observation of the failure conditions.

11. Concrete element lining's stability depends on the **element configuration**, on the **flow velocity** (as the hydrodynamic pressures depend on the square of the velocity), on the **rate of flow increase** and on the **governing failure mechanism**.

2.7.2 Discussion

1. The lining systems presented in the previous sections are not yet being used in large-scale. In particular, the wedge-shaped block solution has been thoroughly developed (Pravdivets and Slissky 1981, Hewlett *et al.* 1997, Frizell *et al.* 1996) in what concerns the hydraulics of the lining, but still raises some doubts about its performance.

2. Till present, the interaction of the lining system with the embankment was not yet been fully ascertained. Or, at least, not in an extent enough to overcome the reluctance of the engineering community to accept overflow spillways.

3. In what concerns stability, the wedge-shaped blocks have yet not proven to be a long-term efficient solution. Of course, the scarce number of existing constructed examples does not allow for extensive prototype operation analysis. The dependency of the lining stability from the water-extraction performance raises suspicion that with time the small slots (air vents), will be filled up with earth and vegetation. Ultimately these slots might be clogged. Regular maintenance seems thus compulsory, which might not be reasonable for isolated and/or low-budget schemes.

4. The wedge-shaped blocks have a complex geometry (e.g. the air vents), requiring elaborated formwork. Their fabrication might be economically interesting if close to a plant, or when a plant can be installed and multiple cast-forms developed. Fabrication efficiency depends considerably on the number of forms. Displacement, expatriation or overseas shipping of these forms might pose an additional obstacle to low-budget schemes.

5. Baker (1989) stated that "the wedge-shaped block offers the *most stable solution for the minimum weight* of concrete". Such statement is conceptually correct though quite dependent from the efficiency of the developed stability concept, submit to discussion in the previous items.

6. The existing stepped-block systems experience is limited to unit discharges up to 2-3 m^2/s, head of around 1.0 m and velocities up to 8 m/s (with some exceptions, see Table 2.2).

7. Alternative systems to the existing ones are needed, that withstand more severe hydraulic conditions, have a less complex stability concept and whose geometry is simple and easy to make in a batch plant with simple formwork.

3 EXPERIMENTAL WORK

3.1 INTRODUCTION

The developed lining system consists of a layer of concrete blocks, placed side by side, from downstream to upstream, separated from the embankment by a foundation/drainage layer of coarse material. A transition layer placed between the embankment material and the drainage layer will prevent the migration of the finer particles towards the surface.

The main purpose of the present research work is to evaluate the stability of the concrete elements when placed on a surface representing the downstream slope of a typical earthfill dam and submitted to overflow. To reach that purpose, an experimental facility was conceived and experimental tests were led. Observations focused mainly on the fully aerated quasi-uniform flow region. This chapter includes a description of the experimental facility, including a brief overview of its components. The experimental procedure used to study the lining's stability is presented, as well as the studied variants. Lastly, the experimental tests conducted and the measurements taken are described.

3.2 SELECTION OF CONCRETE ELEMENT GEOMETRY

3.2.1 General

Three conception principles were defined:

1. The stability of the elements should be ensured, primarily, by the own self-weight and, secondly, by some kind of interlocking effect;

2. The lining should not only protect the foundation from eroding but should also contribute significantly for energy dissipation;

3. The lining surface over the embankment should be similar to a stepped surface, enabling the comparison with former research on the hydraulics of flow over those surfaces.

Contrarily to the previous works of Pravdivets (1987), Hewllet *et al.* (1997) and Frizell (1997), no system to extract water from the foundation or to reduce the up-lift pressure by air-ventilation is previewed, nor prefabrication is demanded. The foreseen elements defined herein should be possible to cast *in situ*. In fact, site construction of simple shaped blocks might be, in itself, a big advantage where labour cost and concrete cost are not the critical economical factor.

The concrete elements conceived should, as first goal, withstand the same overflow conditions of existing lining systems. A second objective is to extend these limiting conditions. Extra capacity to dissipate energy is looked for herein, even if not as a main research goal. Energy dissipation and friction laws for some of the selected geometries are under study at the LCH.

3.2.2 Reference design conditions

3.2.2.1 Conceptual Demands

The elements were conceived to fulfil the following requisites:

1. Stability should depend mainly on their own weight;

2. The macro-roughness surface should create a complex flow pattern, which by impact and deflection of jets will increase the energy dissipation efficiency,

3. The element's weight should allow for their site handling, transportation and placing (for instance, a standard site crane can handle up to 1-2 tons with ease, being 3 tons the maximum load possible to carry);

4. Their geometry should be simple, to reduce the cost of form-work and allow its repetitive use;

5. The elements dimensions should prevent them from being endangered by vandalism (the elements should not be to small), being the minimum dimensions set by the handling conditions,

6. The lining's geometry should allow for a good integration in the surrounding landscape, which can be achieved, for instance, by placement of a vegetation cover.

7. Their dimensions should be such that experimental model work could be led in the laboratory, using a reasonable scale reduction from prototype. The model should not be too big, which would not be economically efficient, nor too small, which would pose difficulties in handling and increase the influence of scale effects in flow analysis. In fact, smaller dimensions tend to distort the role of, for instance, pressures in the joints or shear with the foundation, in the transition from model to prototype.

8. It should be possible to use a given element geometry in different slopes.

Furthermore, close attention was given to the definition of details, such as those related with the stability and drainage, as joint design by overlapping or interlocking. In the following sections the selected geometries are presented, as well as the assumptions made for their definition.

3.2.2.2 Laboratory restrictions

The geometry and size of the elements was defined in order to have the best observation and working conditions while performing the experimental tests. The placement of, at least, 5 elements across the channel width was desirable, so that measurements could be made over the middle element, away from the side walls were velocity is somewhat reduced. A channel of less than 1.5 m of width was envisaged, to limit the number of necessary elements to be produced. The elements should not weight more than around 10 N, to allow proper handling in the laboratory. On the other hand, their smallest dimension was kept to a minimum of 10 mm, to assure their integrity during casting, transport and placement.

3.2.2.3 Similarity conditions

The experimental tests in the laboratory were performed under Froude similarity conditions. Dynamic similarity between the observation in model and in prototype is, for free surface flows,

governed by gravity and pressure forces (Yalin 1971, Quintela 1981). A geometrical scale factor, λ_L, of 10 was chosen. The correspondent scale factors for other parameters as velocity, discharge, etc., are presented in Appendix 2.1.

The envisaged prototype lining elements will be made in concrete. In order to assure that the elements used in the laboratory behave in the same way as in prototype, the elements need to have the same geometry, weight and inertia, and thus the same gravity centre co-ordinates.

As a corollary of the previous, the laboratory elements have to be *homogeneous* (of only one material as in prototype) and the ratio of fluid and element densities has to be equal in both circumstances. Hence, the elements used in the laboratory also have to be made of concrete.

3.2.3 Element catalogue

3.2.3.1 Principles

The investigated concrete elements were divided into two parts: an *upper part* exposed to flow and a *lower part* as the foundation slab. The flow-exposed surface defines the macro-roughness and is responsible for the flow pattern created and correspondent energy losses. The foundation part is responsible for the good connection with the neighbouring elements. Stability concerns both parties.

The surface created by the loose concrete elements resembles that of RCC stepped spillways. In fact, different step configurations have been under study in recent years, focusing on their effects on the flow pattern and on the energy dissipation efficiency. Steps with flat slope, inclined slope, negative slope and with end sill have been studied previously for RCC chutes or gabion cascades (Peyras et al. 1991, Pinheiro and Fael 2000, André *et al.* 2001). The use of end sill, with/without an intermediate fill for RCC spillways is presently under study at the LCH (André *et al.* 2001) – Figure 3.1. However, these bottom configurations had never been tried in loose concrete elements.

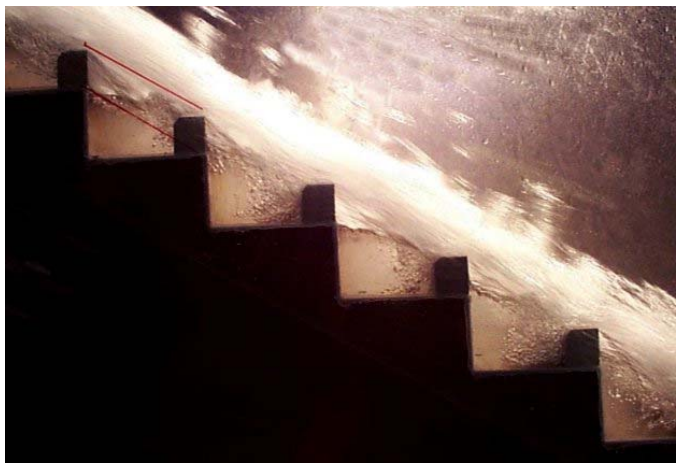

Figure 3.1 - Flow on a stepped chute equipped with end sill. Stepped spillway facility at LCH, Switzerland, slope of 30°, q= 17.7 l/s, steps of 104x60 mm (courtesy of Ms. André)

Three stepped–like configurations were chosen, for both embankment dams and RCC steps. For observation of a more complex 3-dimensional flow pattern, a pyramidal configuration was also included, despite not being adequate for construction over RCC dams.

3.2.3.2 Stepped-like elements

A step shape was obtained by detaching a single step from the existing stepped chute at LCH, having steps of 104 by 60 mm, and placing it over an embankment slope as an individual loose block – Figure 3.2.

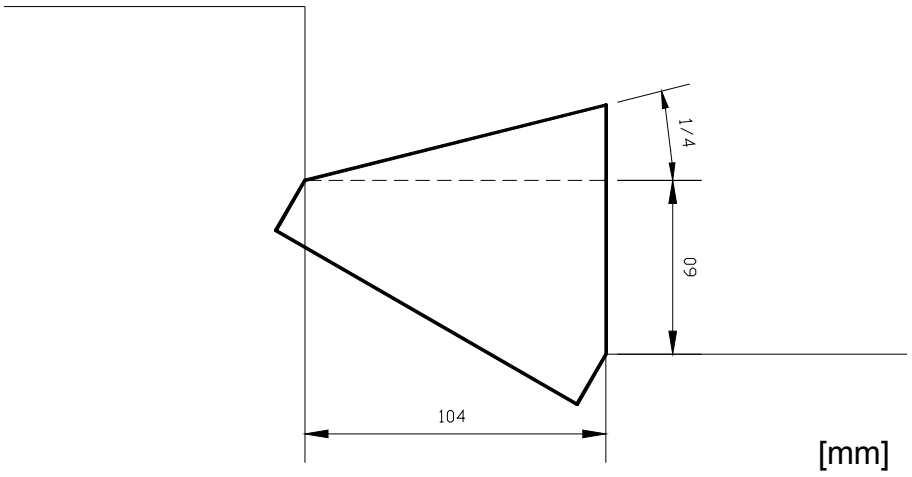

Figure 3.2 - Construction of the 44° negative step (Type 1), from LCH stepped chute

Element Type 1 corresponds to a step to which a ramp of ¼ slope was added. Element Type 2 is equivalent to a simple 30° negative step, whereas element Type 2 +ES has an end sill of 21 x 21 mm on the edge of the upper surface.

3.2.3.3 Pyramidal-like elements

The Pyramids are elements Type 3, having a base length of 100 mm and a side slope of 45°.

3.2.3.4 Foundation geometry

The interface between elements was set perpendicularly to the slope (and not vertically), to allow the use in different slopes. The use of a given element for slopes different than that for which the element was designed (1/3) has to take into consideration that the stability limit changes[18].

For a given unit discharge, extra safety can be provided either by choosing a heavier (but bigger) block or by increasing the foundation slab thickness (without changing the *upper part* geometry). The second alternative might reveal advantageous in terms of concrete saving, when compared to the first alternative. The flow pattern would remain identical, as it depends only on the *upper part* geometry. In what concerns stability, the additional weight will be stabilising and the element's gravity centre lowered.

3.2.3.5 Definition of the concrete elements dimensions

Different combinations of dimensions for each type of element were tried, respecting all the restrictions listed above. The weight was calculated for a concrete density of 2400 kg/m^3. The chosen element dimensions are presented in Table 3.2. Drawings are presented in Appendix 2.2. For all element types, the initial weight was set lower than 30 kN, to leave some margin for further foundation thickening. The initial foundation thickness in model was set to 10 mm.

[18] The hydrodynamic forces application point will have a different location relatively to the gravity centre.

3.2.3.6 Fabrication

Initially, element production was planned for LCH using simple formwork, which would be extensively and repetitively used. However, due to the uncommonly small dimensions difficulties to outcast the elements, keeping their regular shape and integrity, were faced. Therefore, a specialised company in pre-cast concrete was contracted to produce the stepped-like elements, being the pyramidal elements (easier to outcast) produced at LCH (formwork in Photo 3.1)[19]. The elements were made of Portland concrete, have smooth surfaces on the formwork side (excluding base) and dimensions precise at mm scale - Table 3.1.

Table 3.1 - Characteristics of the produced concrete elements

Type	base	width	foundation height	roughness height	cross section	volume	weight	ρ_s
	[mm]	[mm]	[mm]	[mm]	[mm^2]	[mm^3]	[N]	[kg/m^3]
44° negative step (Type 1)	120	100	10	74	5640	564000	13.6	2411
30° negative step (Type 2)	120	100	10	52	4320	432000	10.4	2407
30° negative step with end sill (Type 2+ES)	120	100	10	70	4761	476100	11.0	2310
45° pyramid (Type 3)	100	100	10	50	-	266667	5.7	2138

Photo 3.1 - Formwork for pyramid production in PVC

3.2.3.7 Particular construction features

To further improve the stability, several measures can be taken during construction, comprising the male-female joints, hollow joints (as in concrete dam block construction) or other overlapping and interlocking systems (as described in Chapter 2, section 2.5.4.4.). Chamfering of the element's exposed edges might prevent localised damages that endanger the element's integrity and performance.

[19] Due to the increased formwork complexity, pyramid production has unit cost double of that for stepped-like elements.

Table 3.2 – Resume of concrete element characteristics (ρ=2400 kg/m^3). The coloured results correspond to the built elements.

Steps	Main dimensions													Canal of 0.80 m					
	Prototype													Model					
1040/600 mm	scale factor	hf	s	hd	tan (β)	L_B	hs	ss	hc	width	area	volume	weight	hf	ks	ss	Base	width	#elements
	λ_L	(m)	(m)	(m)	(-)	(m)	(m)	(m)	(m)	(m)	(m^2)	(m^3)	(kN)	(m)	(m)	(m)	(m)	(m)	per width
44° negative step	**10**	**0.10**	**1.04**	**0.60**	**0.25**	**1.20**				**1.0**	**0.5672**	**0.5672**	**13.6**	**0.010**	**0.074**		**0.120**	**0.100**	**8**
(type 1)	10	0.20	1.04	0.60	0.25	1.20				1.0	0.6872	0.6872	**16.5**	0.020	0.074		0.120	0.100	8
	10	0.30	1.04	0.60	0.25	1.20				1.0	0.8072	0.8072	**19.4**	0.030	0.074		0.120	0.100	8
	10	0.40	1.04	0.60	0.25	1.20				1.0	0.9272	0.9272	**22.3**	0.040	0.074		0.120	0.100	8
30° negative step	**10**	**0.10**	**1.04**	**0.60**		**1.20**				**1.0**	**0.4320**	**0.4320**	**10.8**	**0.010**	**0.052**		**0.120**	**0.100**	**8**
(type 2)	10	0.20	1.04	0.60		1.20				1.0	0.5521	0.5521	**13.8**	0.020	0.052		0.120	0.100	8
	10	0.30	1.04	0.60		1.20				1.0	0.6722	0.6722	**16.8**	0.030	0.052		0.120	0.100	8
	10	0.40	1.04	0.60		1.20				1.0	0.7923	0.7923	**19.8**	0.040	0.052		0.120	0.100	8
30° negative step + end sill	**10**	**0.10**	**1.04**	**0.60**		**1.20**	**0.21**	**0.21**		**1.0**	**0.4753**	**0.47526**	**11.9**	**0.010**	**0.070**	**0.021**	**0.120**	**0.100**	**8**
(type 2+ES)	10	0.20	1.04	0.60		1.20	0.21	0.21		1.0	0.5954	0.59540	**14.9**	0.020	0.070	0.021	0.120	0.100	8
	10	0.30	1.04	0.60		1.20	0.21	0.21		1.0	0.7155	0.71546	**17.9**	0.030	0.070	0.021	0.120	0.100	8
	10	0.40	1.04	0.60		1.20	0.21	0.21		1.0	0.83055	0.83553	**20.9**	0.040	0.070	0.021	0.120	0.100	8
45° pyramid	**10**	**0.10**			**1.00**	**1.00**			**0.50**	**1.0**		**0.2767**	**6.7**	**0.010**	**0.050**		**0.100**	**0.100**	**8**
(type 3)	10	0.20			1.00	1.00			0.50	1.0		0.3767	**9.2**	0.020	0.050		0.100	0.100	8
	10	0.30			1.00	1.00			0.50	1.0		0.4767	**11.7**	0.030	0.050		0.100	0.100	8
	10	0.40			1.00	1.00			0.50	1.0		0.5767	**14.2**	0.040	0.050		0.100	0.100	8

hf	height of foundation
s	top surface of (base) step
hd	height of (base) step
β	angle between upstream element surface and dam face slope
L_B	length of element's foundation in slope direction
hs	end sill height
ss	end sill top surface
hc	height of the highest point (perpendicular to dam face)
ks	total height of element perpendicular to dam face
width	length of element foundation in the transversal direction to the flow

3.3 EXPERIMENTAL FACILITY

3.3.1 General

To perform the stability tests an experimental facility was built at the Laboratory of Hydraulic Constructions of the Swiss Institute of Technology in Lausanne (EPFL) – Photo 3.2.

3.3.2 Head tank and overflow weir

A 2 m^3 PVC head tank provides the proper tranquillity condition at the entrance of the chute. The tank is inside a metallic frame (square profiles of 40 x 40 mm). A dividing wall was built inside the tank, separating the highly turbulent arrival from the constant level pool close to the weir – Photo A3.1 (A3 stands for Appendix 3).

The entrance to the chute is made *via* a 70 cm-width sharp crest weir. The flow contracts over the weir, to immediately expand on the transition to the channel (80 cm of width). The transition assures good aeration conditions of the under-nappe cavity. On the upstream side of the weir, the approaching walls follow closely the approach flow streamlines – Photo A3.2.

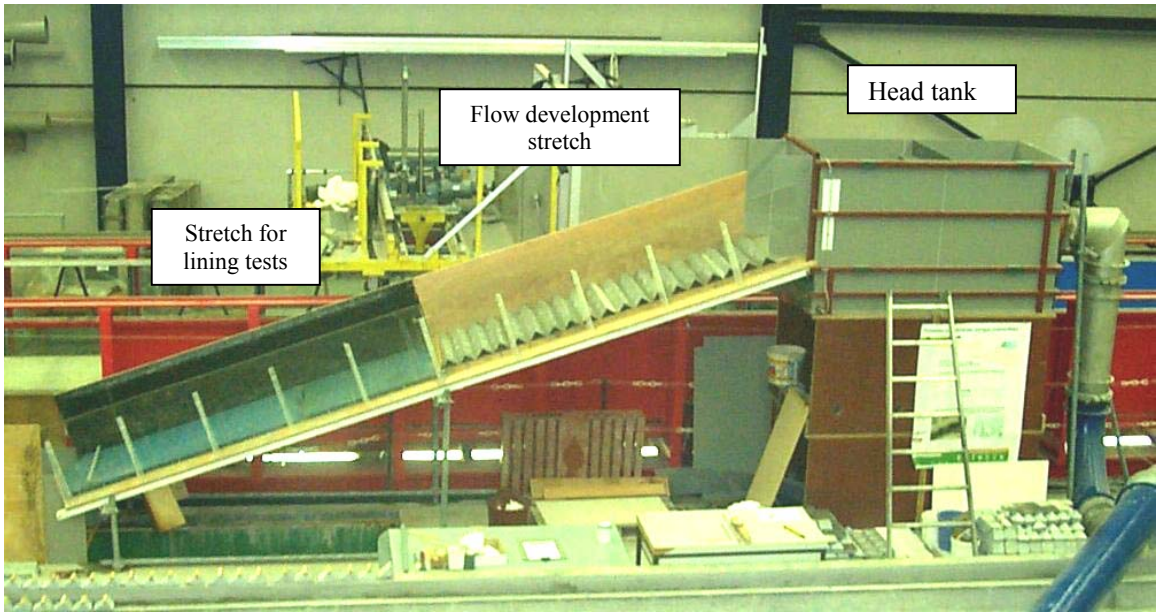

Photo 3.2 – General view of the experimental facility at LCH laboratory.

3.3.3 Channel

The dam face is simulated by a 6.0 m long, 0.80 m wide wooden chute of 1/3 (V/H) of slope. The chute was installed on top of a UPN80 metallic frame. Computation of static stability considered the loading of the self-weight of the structure, the weight of the elements (all along the channel) and a maximum water depth of 25[20] cm. The structure stood during the tests, behaving accordingly to expectations.

[20] Superior to a rough estimate of flow depth made for Q= 250 l/s and taking a Strickler's coefficient value of 10 $m^{1/3}/s$.

The upstream half of the channel was used for bottom turbulent boundary layer development, being the downstream stretch prepared for the lining stability tests. Triangular metallic profiles were placed throughout the upstream stretch, creating a macro-roughness surface similar to the tested linings (Photo A3.3). For the range of discharges available, the flow along the 3.0 m of the downstream part of the channel is either in fully or partially aerated conditions.

The 60 cm high sidewalls allow for proper flow observation (transparent Plexiglas wall) and provide adequate contrast conditions between the black wooden background and the flow region. The sidewalls were fixed using a series of triangular reinforcements, which contribute also for the stability to the whole chute. The height of the sidewalls included a 15 cm minimum freeboard, which proved to be largely sufficient.

At the toe, a large wooden beam simulates the lining's toe block, being fixed to the channel and preventing the lining elements from sliding – Photo A3.4. A wire mesh was placed in the collecting channel to prevent the elements from heading down to the sump

3.3.4 Hydraulic circuit

A centrifugal pump supplies the experimental facility *via* a ϕ300 pipeline. The pump maximum capacity is 250 l/s for a 15.0 m head. Due to the super-elevation of the tank and to the head losses on the circuit, the maximum observed discharge is of 228.5 l/s. The pump was operated at a displaced computer terminal close to channel.

Te pump has a variable behaviour in the range of flows from 20 l/s to 230 l/s. It was regulated to work in stable condition above 100 l/s, for which failure of the tested linings was expected. Below 100 l/s, the pump works in unstable conditions, the instantaneous flow varying of ± 10 l/s. Due to the storage capacity of the head tank, the variability of pump discharge did not influence the entering conditions to the chute, as shown by piezometer observations made in the calm water zone in the head tank.

3.3.5 Drainage set-up

For tests including drainage, the following changes were introduced to the facility (Photo A3.5):

i) The concrete elements were placed on top of the 4.0 cm thick drainage foam,
ii) The upstream metallic profiles were also raised of 4.0 cm,
iii) Three circular holes of 10 cm of diameter were made to evacuate the infiltrated flow, 5.50 meters downstream on the chute,
iv) A PVC basin was placed under the holes to collect the infiltrated water,
v) A triangular weir was installed inside the collecting basin to measure the infiltrated flow.

3.4 EXPERIMENTAL TEST PROCEDURE

3.4.1 Failure flow evaluation

Stability of the linings was evaluated by submitting the elements to increasing flow discharges until failure was reached. The limit equilibrium state discharge is hereforth named failure flow.

The inflow hydrograph was made in steps of increasing discharge, lasting a minimum of 2 minutes, in order to achieve stable flow and constant pressure conditions below the elements.

3.4.2 Test configuration for drainage

In order to evaluate the relation between the element's stability and the under-drain layer pressures, three alternative conditions were simulated:

a) **without drainage**, being the elements placed directly on the channel bottom and the downstream toe water-tightened (Photo 3.3a);

b) **with drainage layer**, being the elements placed on top of a highly draining layer (foam layer of 40 mm and estimated $K_{Darcy} \approx 10^{-3}$m/s), reducing or eliminating the lift pressures on the element's foundation (Photo 3.3b);

c) **with blocked drainage**, being placement similar to that of tests with drainage, but where no drainage flow was allowed, by closing the drainage water-relief holes at the toe of the channel.

The experimental tests with drainage allowed evaluating the infiltration rate through the lining joints. Flow collected through the drainage layer was separately measured. The foam having such a high permeability, about 10^2 higher than common drainage layer values, the collected infiltration flow is much higher than what will be observed in prototype. However, these test conditions allowed to assume the almost complete elimination of up-lift pressures in the foundation.

In prototype, the drainage conditions will be intermediate between those of a) – maximum up-lift pressures – and those of b) – nearly 100% efficient drainage and meaningless up-lift pressures in the foundation.

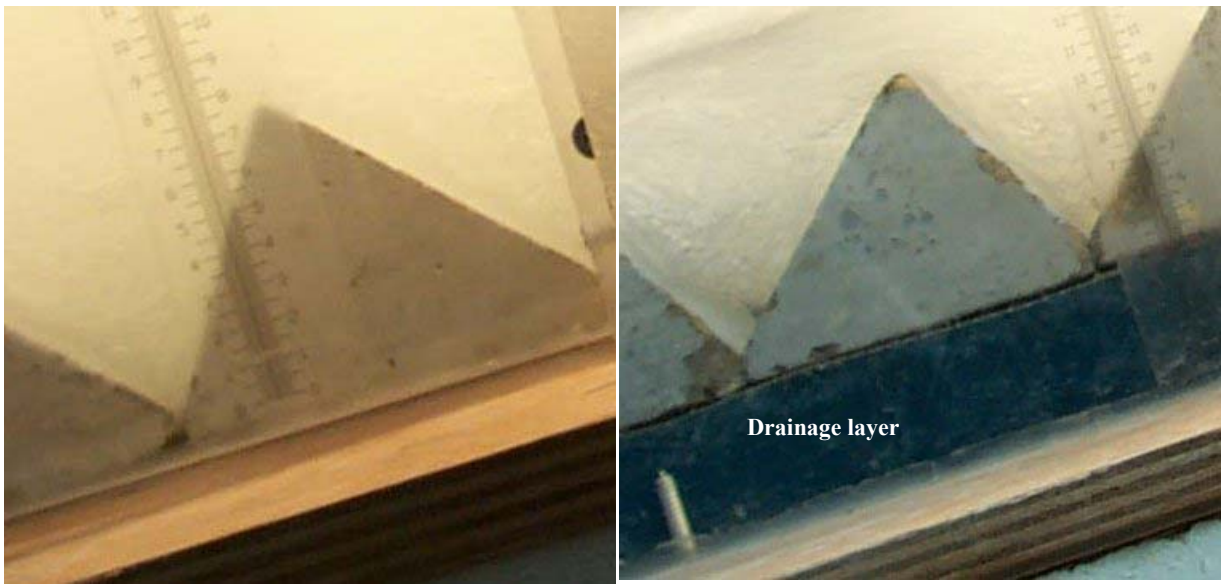

Photo 3.3 – Drainage conditions: a) without drainage layer, b) with drainage layer

3.4.3 Test configuration for foundation surface

In prototype, the concrete elements will be placed over a transition layer of granular material, as described in Chapter 2, section 2.5.5. The irregularity of the interface where the elements are set might play an important role in the stability of the lining. If neighbouring elements are slightly

tilted, one of the elements might be more exposed to the flow, favouring failure. The irregularity of the transition layer surface is related with the relative dimensions of the granular material to the concrete surface roughness. In model, uncompressible foundation conditions were simulated by the channel's smooth wooden surface for test without drainage, and by a metallic perforated sheet for the tests with drainage, which was placed on top of the drainage foam.

The perforated metallic sheet was initially used to prevent tilting of the elements and reduce the shear between those and the foam drainage layer. However, the metallic sheet was severely damaged after some failure tests and was removed. The elements were placed directly over the drainage foam. The only perceptible difference is the not so thigh longitudinal packing, as the shear between elements and foundation is higher.

3.4.4 Test configuration for joint alignment

Failure occurs by displacement of a first element, exposing the neighbouring ones and triggering a massive departure. For observation of the departure pattern, the placement order was changed. First, the elements were evenly placed (aligned longitudinal joints) and, afterwards half elements were introduced at the sidewalls every two rows (uneven longitudinal joints).

3.5 INSTRUMENTATION AND MEASUREMENTS

3.5.1 Introduction

Measurements were done for:

- The flow discharge,
- The flow velocity in quasi-uniform conditions for, at least, failure flow conditions,
- The flow depth,
- The permeability of the lining's joints, by measurement of the infiltrated flow.

For the proposed experiments, measurements techniques were defined, considering both the principles of redundancy and accuracy.

3.5.2 Flow discharge measurements

The automatic regulation system of the laboratory pumps includes an electromagnetic flowmeter to measure discharge. Furthermore, a calibrated piezometer was placed upstream of the overflow weir to observe flow oscillations in unstable pump functioning conditions as explained in paragraph 3.4.4 - Photo 3.4. The discharge was then computed using equation 3.1 (Henderson 1966) and compared with the automate indications.

$$Q = C \cdot L \cdot \sqrt{2g} \cdot H^{\frac{3}{2}} \tag{3.1}$$

where C is given by equation 3.2

$$C = \frac{2}{3}(0.611 + 0.08 \cdot \frac{h}{p}) \tag{3.2}$$

taking p = 0.52 m (vertical distance from crest to tank bottom), L=0.703 m (crest length) and assuming the velocity approach head to be negligible ($H \approx h$) in still water conditions. The water level in the piezometer varied within a short range, but corresponding discharge variations are

smaller than those showed by the automate system's computer, confirming the regulating effect of the upstream storage tank. Results were considered fairly accurate.

3.5.3 Surface levels measurements

As described in Chapter 2, section 2.6.4 there is not a consensus on how to measure or even evaluate surface levels in highly aerated free-surface flows. In the present work, the surface level was estimated only for quasi-uniform flow conditions in skimming flow regime. For that purpose, photos were taken 5.00 m downstream from the upstream weir, twice for each flow tested and for each lining configuration.

Photo 3.4– Upstream *Bazin* weir during tests. Calibrated piezometer on the right side.

Metric scales were placed along the chute at regular distances, to visually estimate the surface level from the photos and to check if uniform flow conditions were attained. The black painted background and the use of a spot light provided the adequate contrast conditions.

By taking several measurements for each discharge it was expected to obtain an accurate estimate of the observed flow depth. However, photo readings have a deviation from middle-of-channel conditions as they represent the flow conditions close to the wall, where surface tension and side splash increase slightly the observed flow surface (less than 5% as time average deviation).

3.5.4 Flow velocity measurements

In a similar way to flow depth, the evaluation of water flow velocity in two-phased free surface flows is not straightforward. Measurements were made:

I) using a currentmeter in the centre of the channel for the stepped-like elements,

- to measure the local velocity at 2.0 cm for the element tip (distance corresponding to 30 to 50% of the mean flow depth),
- to obtain velocity profiles for 100, 150 and 200 l/s whenever failure was still not attained, by measurement of local velocities at 10 different flow depths spaced of 0.5 cm,

II) by analysis of video film made for every element type, identifying a mean depth-averaged velocity *Vv*, of a coloured dye front propagation.

Currentmeter readings only register water velocity and can only be considered representative of water-flow velocity where the air concentration is low (close to the bottom). Local velocity readings were taken at a constant depth just to have an order of magnitude of the velocities. The chosen depth, 2.0 cm from the element's tip, intends to be a compromise for low and high discharges. For the range of discharges tested, water is still the predominant fluid at this depth.

Two different currentmeters were used (Photo 3.5), one automatic and another mechanical. Readings are averaged local velocities corresponding to exposure periods of 6 s for the automatic currentementer and 20 s for the mechanical one. Measurements were taken half way and 5.30 m (assumed quasi-uniform flow region) down the channel. The velocity profiles were taken to compare simple currentmeter readings with more sophisticated instrumentation readings, as the optic probe used by Boes (2000) and a modified Pitot tube used by Matos (1999).

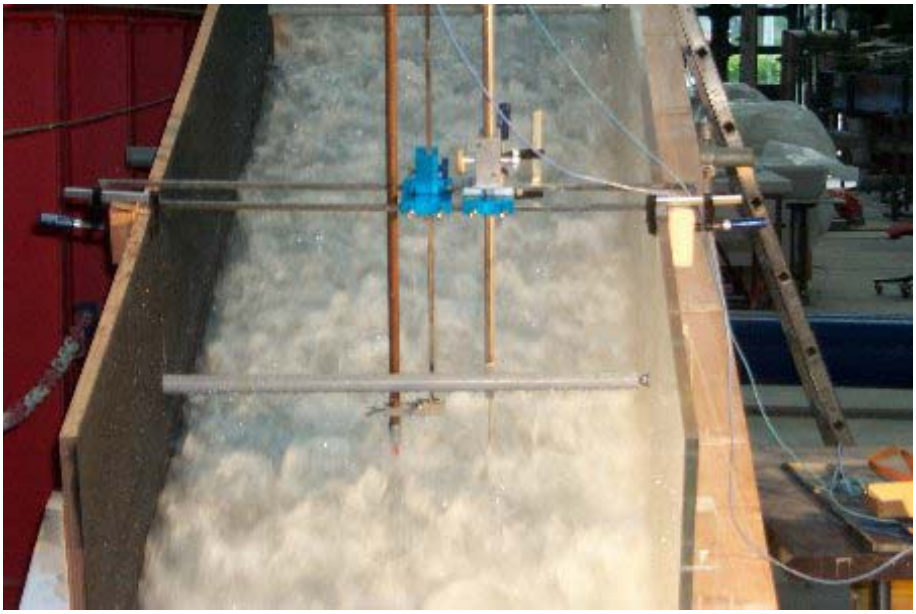

Photo 3.5 – Currentmeters at section 530. Test with elements Type 1, Q=20 l/s.

Video was recorded for several discharges, including the limit equilibrium state discharge (failure flow). Coloured blue dye[21] was dumped on the fluid, generating a moving front. Even if mixing is fast, the dumped quantities, about 1/3 of a 20 ml glass, allow a clear identification of a coloured front. Dumping was repeated at least three times for each recorded discharge. Video was taken a commercial digital video camera and the film was analysed using digital video software. The camera records 25 images (frames) per second with a resolution of 800 000 pixels. The velocity taken from these video films represents a mean front velocity in the reach between section at 4.50 m and 5.50 m downstream. It is considered as a fairly good estimate of the skimming flow mean velocity,

3.5.5 Infiltrated/drained flow measurements

The infiltrated flow through the joints was collected in a basin and measured using a triangular weir - Photo 3.6. The energy head on the weir was measured using a point gauge station, placed in still waters at a distance larger than 5 times the head.

[21] Water and dissolved Methylthioninium chloratum DAB7.

The weir is an 60° triangle with 0.407 m of side length. Discharge was computed using equation 3.3 (Henderson 1966).

$$Q = \frac{8}{15}.C.\sqrt{2g}.tg\frac{\theta}{2}.H^{\frac{5}{2}} \qquad (3.3)$$

where C=0.62, θ = 60° (in radians) and H is the overflow head (in meters).

Photo 3.6 – Detailed view of drainage basin, including the triangular weir and point gauge station for drainage flow measuring.

3.6 EXPERIMENTS PERFORMED

3.6.1 Types of linings

With the 4 types of elements selected, 8 different linings were created. Four linings correspond to the four element types (1, 2, 2ES and 3) and three others were obtained by inverting the elements, swapping the role of the upstream and downstream surfaces (1/a, 2/a and 2+ES/a).

The eighth type was developed by adding a metallic steel plate of 3 mm of thickness to the pyramid, simulating a 10 mm increase in the concrete foundation thickness (3+). The extra plate adds 2.5 N (or kN at prototype scale) to the pyramid weight. The characteristics of the tested linings are presented in Table 3.3.

A total of 23 different combinations were tested and are presented in Table 3.4, together with the failure flow results obtained. The measurements taken are highlighted. Detailed information for each test is presented in Chapter 4 and Appendix 4. Not all measurement procedures were used in every test, to reduce repetition, shorten the duration of each test and allow further tests within the time available. The tests are of the destructive type, being quite time consuming. Preparation of each test might take between 0.5 and 3.0 hours depending on the extension of failure damage.

For each lining configuration, a preliminary test was done, where general behaviour was observed and photos were taken, until the failure discharge was achieved and the lining would

collapse. After putting the whole system back in the channel, at least two more tests were done to confirm the value of the failure flow and to complete the measurements.

Table 3.3 - Characteristics of the tested lining systems

type	base	width	foundation height	roughness height	cross section	volume	weight	ρ_s
	[mm]	[mm]	[mm]	[mm]	[mm^2]	[mm^3]	[N]	[kg/m^3]
1	120	100	10	74	5640	564000	13.6	2411.3
1/a	120	100	10	74	5640	564000	13.6	2411.3
2	120	100	10	52	4320	432000	10.4	2407.4
2/a	120	100	10	52	4320	432000	10.4	2407.4
2+ES	120	100	10	70	4761	476100	11.0	2310.4
2+ES/a	120	100	10	70	4761	476100	11.0	2310.4
3	100	100	10	50	-	266667	5.7	2137.5
3+	100	100	20	50	-	366667	8.2	2236.4

3.6.2 Placement procedure and test preparation

During the first test of each lining, setting problems often appeared. These are mainly related with the facility, but disturb the resemblance between model and prototype conditions. For instance, if the blocks are not tightly packed in the longitudinal direction, packing by sliding will occur as soon as the flow starts running. The most upstream rows of blocks, placed immediately after the metallic profiles, become loose, and, of course, depart. To avoid such problem, good initial longitudinal packing was always envisaged and the most upstream rows were fixed.

On the other hand, if the element would be laterally too tight, in comparison with expected prototype placing conditions, failure might be delayed or might even not be attained. Thus, during placement stiff paper squares were placed in the lateral joints, being removed just before the beginning of the test.

Table 3.4 - Experiments carried out, with failure discharge and the measurement taken.

Lining Type	Uncompressible Foundation			Compressible Foundation				Measurements					
	Without Drainage		With Drainage	Blocked drainage		With Drainage		Photos		Dye Film		Current-meter	Drainage flow
	Aligned Joints	Unaligned joints	Aligned Joints	Aligned Joints	Unaligned joints	Aligned joints	Unaligned joints	With Drainage	Without Drainage	Without Drainage	With Drainage		
Type 1 44° negative step	**1** (>228.5 l/s)	**2*** (>228.5 l/s)	**12** (>228.5 l/s)		**15*** (100 l/s)	**20** (>228.5 l/s)	**14*** (150 l/s)	x	x	x (200/Qmax)	x (100/120/140/ 150/ 200/Qmax)	x	x
Type 1/a inverted type 1	**6** (100 l/s)	**5*** (70 l/s)	**13** (120 l/s)					x	x	x (90/100 l/s)	-	x	x
Type 2 30° negative step	**7** (>228.5 l/s)			**17** (>228.5 l/s)		**18** (>228.5 l/s)			x	X (100/150/180 / 200/Qmax)	x (150/200/Qmax)	x	x
Type 2/a inverted type 2	**8** (50 l/s)					**19** (60 l/s)			x	x (50 l/s)	x (50 l/s)	x	x
Type 2 + ES 30° negative step with end sill	**9** (160 l/s)		**11** (>228.5 l/s)	**16**[22] (90 l/s)		**23** (190 l/s)		x	x	- 70/80/90	- (80-180 l/s)	x	x
Type 2 + ES/a inverted type 2+ES	**10** (70 l/s)								x	-		-	
Type 3 45° pyramid		**3** (60 l/s)	-				**21** (80 l/s)		x	x (40/60 l/s)	x (40/60/80 l/s)	-	
Type 3 + 45° pyramid with steel plate		**4** (80 l/s)	-				**22** (100 l/s)		X (up to 90 l/s)	x (80 l/s)	x (100 l/s)	-	x (up to 80 l/s)

[22] During the only trial of test 16 failure was caused by the toe block collapse and not by failure of the elements. It was used to make video film measurements to complete data of tests 9 and 11.

* Tests with elements 1, 2 and 2ES and unaligned joint do not provide consistent result due to early departure of half blocks close to the walls.

3.7 METHODOLOGIES FOR RESULT INTERPRETATION

3.7.1 Definition of flow regime

For all tested discharges (above 20 l/s), the observed flow conditions over stepped-like elements (in regular or inverse position) correspond to skimming flow regime (SK), according to the definition of onset of skimming flow presented in Chapter 2.

For pyramids such classification has yet never been applied. The surface non-linearity over the width contributes to a clearly visible three-dimensional flow pattern below the skimming layer. Furthermore, the pseudo-bottom is not as perceptible as in stepped-like elements. However, a three-dimensional flow pattern is also observed in stepped cavities (Matos 1999, Sanchez Júny 2001). Hence, flow over pyramids may be considered "of the skimming flow type", enlarging such classification to the field of non-linear-over-the-width regular macro-roughness.

3.7.2 Uniform flow conditions

Uniform flow conditions are attained when the flow is fully aerated. Since air concentration measurements were not in the scope of this work, the channel was made long enough (at least longer than 20 times the overflow head for the maximum discharge), to assume fully aerated conditions at the most downstream reach, at a distance between 5.0 to 6.0 m from crest where the measuring cross-sections were placed.

3.7.3 Observed flow depth

For most of the experiments, photos were taken every step of 10 l/s before failure, capturing the flow pattern at a particular moment in time. For each photo, the surface level was identified by means of the metric scales on the channel sidewall. The surface level is slightly overestimated due to the proximity of the sidewall. A total of 310 photos were analysed. Two surface levels were determined for each photo (Photo 3.7):

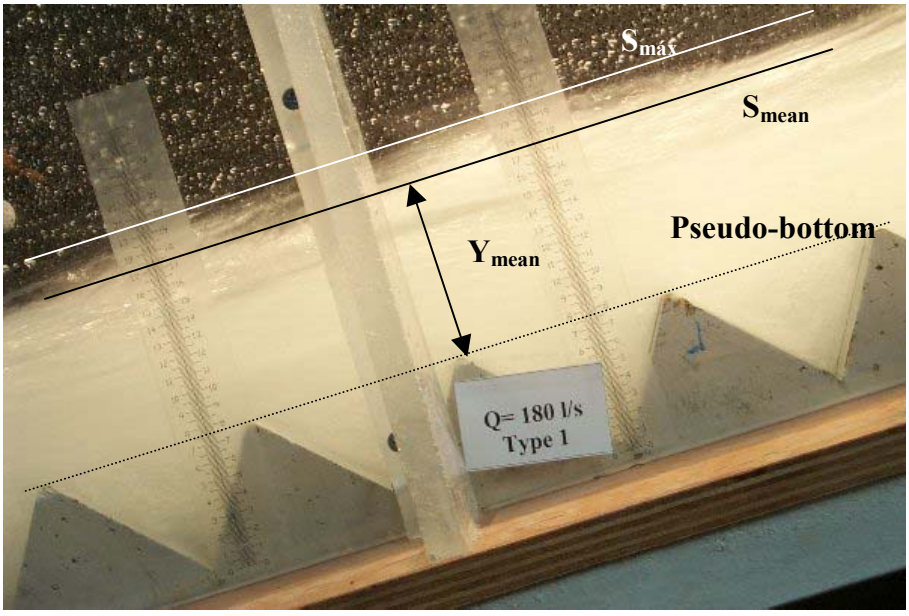

Photo 3.7 – Definition of mean and maximum surface level S_{mean} and S_{max}. Definition of mean flow depth, Y_{mean}. Photos taken during test n° 1, Q=180 l/s.

a) a mean surface level S_{mean}, neglecting the surface irregularities which tend to be less perceptible for high discharges;
b) a maximum surface level S_{max}, corresponding to the highest white-water surface irregularity (depending on the instant of the photo).

For a given discharge, the mean average flow depth Y_{mean} and the maximum flow depth Y_{max} were defined as the differences between the pseudo-bottom (defined by the element tips) and, respectively, the value of S_{mean} and S_{max}.

3.7.4 Equivalent clear-water flow depth

A fully developed skimming flow behaves similarly both over a stepped surface and on a non-stepped one (Chanson 1994), as seen in section 2.6.3.4. The characteristic flow depth h_w or equivalent clear-water depth (only water) is given by:

$$h_w = \int_0^{Y90} (1 - C) \cdot dz \tag{3.4}$$

where C is the local air concentration at depth z. The mean depth-averaged air concentration C_{mean}, is given by:

$$C_{mean} = \frac{1}{Y90} \int_0^{Y90} C \cdot dz \tag{3.5}$$

or

$$C_{mean} = 1 - \frac{h_w}{Y90} \tag{3.6}$$

where Y90 is the depth at which the local air concentration is 90 %. For flow over stepped-like elements, C_{mean} can be determined with equations 2.9 and 2.10. For slopes of 1/3 an average C_{mean} value of 0.30 is advised. For the pyramids, the relationship (2.11) derived by Hartung and Scheuerlein (1970) for C_{mean} computation in natural macro-roughness mountain rivers beds was considered more adequate.

The mean observed water level Y_{mean} can be considered equivalent to Y_{90} (Matos 2000), allowing the computation of h_w from equation 3.7 (or 2.12). Logically, $h_w < Y_{mean}$ due to both the entrained and entrapped air. The equivalent clear–water depth h_w is used in Chapter 5's stability calculations for computation of the acting forces.

$$h_w = Y_{mean} \cdot (1 - C_{mean}) \tag{3.7}$$

3.7.5 Analysis of flow velocity

Currentmeter measurements were made twice for each depth and discharge, using the average of both measurements for graphical presentation.

Velocity was also evaluated by digital video recording (see section 3.5.4). For discharges just before failure, coloured dye was dumped on the flow. Dumping was repeated at least 3 times for each discharge considered. Video film analysis consist on counting the number of frames, each corresponding to 1/25 of a second, needed for the coloured front to travel between two sections

distant of either 60 cm or 1.20 m - Photo 3.8. An averaged mean front velocity, V_v, was computed from equation 3.8:

$$V_v = \frac{1}{n}\sum_{i=1}^{n}\frac{\Delta x_i}{\Delta t_i} \tag{3.8}$$

being n the number of readings, Δt the number of frames/25 (in seconds) and Δx the travel distance (in metres). It provides a fairly good estimate of the mean depth-averaged skimming flow velocity. The accuracy of counting is estimated in 1/25, as the observer might fail to distinguish the exact frame at which the front crosses the reference sections. However, the difference of 1 frame out of a total of 4 or 5 represent a deviation in velocity estimates of about 16 %.

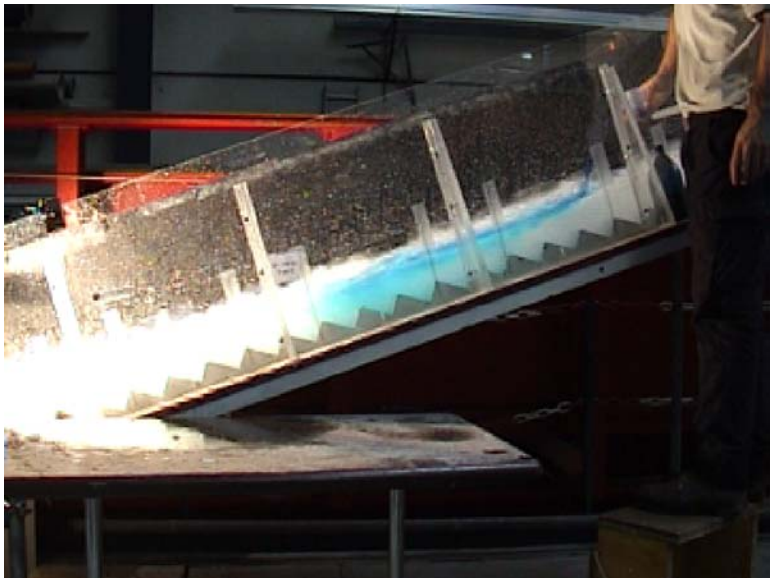

Photo 3.8 - Coloured front, example of one frame (Δt=1/25 s). Lining type 2, test n° 7, *Q*= 228.5 l/s.

For comparison, a mean water velocity, U_w, was computed from equation 2.12 (h_w from equation 3.7). This velocity is used for estimation of the hydrodynamic loads in Chapter 5. For tests with drainage, U_w is reduced accordingly.

4 ANALYSIS OF THE EXPERIMENTAL TESTS RESULTS

4.1 INTRODUCTION

A thorough analysis of each test is made in this chapter. Methodologies for treatment of measured data are exposed, as well as their outcome. Comparison of several parameters is presented. Remarks on the accuracy of the instrumentation and their adequacy and pertinence for the study of flow over macro-roughness surfaces, are made. The most representative results of the 23 tests are included; additional information (photos, figures) can be found in Appendix 4.

4.2 PRELIMINARY TEST SCREENING

Tests n° 2, 5, 14 and 15 (see Table 3.2) were not considered valid for stability analysis, after realising that tests with loose half elements did not guarantee reliable test conditions. Early departure of these halves is not representative of prototype linings' expected behaviour.

As an example, linings n° 14 and 20 should withstand similar discharges, contrarily to what was observed. Collapse of lining 14 was apparently triggered by departure of half elements close to the sidewalls. Albeit not being possible this for such high discharges (no visibility), comparison with tests done with aligned joints point out the non-alignment of the joints as the only reason for such incoherence. The like was concluded for test n°5, when compared with test n° 6. In future tests the halves should be somehow fixed to the sidewalls or to the channel bottom.

For seven of the remaining nineteen tests failure was not observed. The discharge causing failure of these lining is larger than the maximum discharge of the laboratory facility. The maximum available discharge in the laboratory was 228.5 l/s, corresponding to a unit discharge of 285.63 l/s (228.5/0.8) or, at prototype 1:10 scale of 9.03 m^2/s (285.63 x $10^{1.5}$). The remaining margin of security could not be evaluated. Stability of these linings is studied in Chapter 6 as if the failure flow was the corresponding to 228.5 l/s.

4.3 TESTS WITH DIFFERENT LINING SYSTEMS

4.3.1 Tests using the 44° NEGATIVE INCLINED STEP (Type 1)

Lining type 1 was submitted to 6 tests. Result of tests 1, 12 and 20, show that element type 1 withstood discharges of up to 228.5 l/s or q < 285.6 l/s/m. Comparison of tests 1 and 2 shows that stability does not depend on the joint alignment, at least not in the range of flows tested and for the most severe up-lift conditions (uncompressible foundation, without drainage). The influence of each test feature is highlighted in a standard comparison table – Table 4.1.

Table 4.1 – Comparison table for lining Type 1 (tests n° 1, 2, 12, 14, 15 and 20)

Item of comparison	Comments
Failure conditions *versus* (vs) Drainage	Drainage does not seem to play any role in stability for the observed range of discharges.
Failure conditions vs. Foundation	Failure was not attained in tests 1, 12 (uncompressible foundation) and 20 (compressible foundation). The (ir)-regularity of the foundation surface does not seem to play any role in stability for the observed range of discharges.
Failure conditions vs. Joint alignment	Tests are not conclusive due to early half-blocks departure (see §4.2).
Drainage vs. Flow depth	From tests 1 and 12 (and 20) drainage reduces the mean observed flow depth, Y_{mean}, by reduction of skimming flow discharge, as expected in supercritical regime – Figure 4.1
Drainage vs. Flow velocity	For any discharge, measurements with drainage at lower water depths (away from the tips) are always inferior to those without drainage, reflecting the reduction of main flow. In opposition, at high depths (close to the tips) higher local velocities can be observed, as a consequence of the reduction of Y_{mean} by drainage – Figure 4.2. Maximum velocities are quite alike, differing mainly in depth location. Video results are quite alike for tests with/without drainage. Differences between these values are of the same order of magnitude, one video frame (1/25 s), of the potential error made in visual film analysis. For tests with drainage, q_w was reduced proportionally to the measured drainage foam discharge. Values from tests with drainage are slightly higher than those of tests without drainage. These values should be taken as an order of magnitude. This conclusion is extensive for other linings.
Drainage vs. joint alignment	By comparing drainage measurements of tests 12 and 14, no significant differences are found – joint alignment has no influence on the amount of infiltrated flow. The opening of the joints has probably a larger influence.

The notion of range of validity as presented in Figure 4.2 is explained in §4.5 and corresponds to an evaluation of the limitations of currentmenter use for air-water flow velocity measurements.

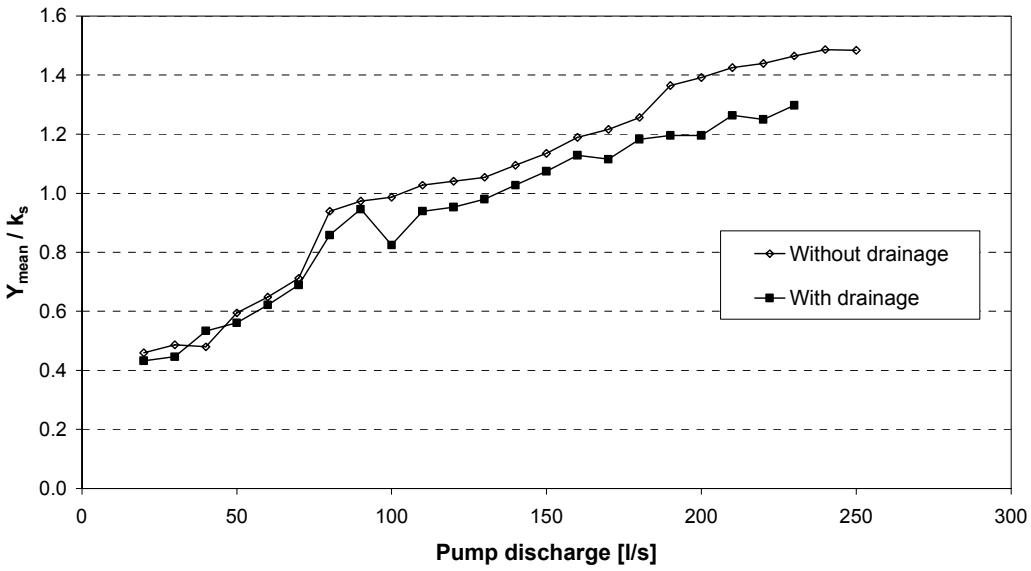

Figure 4.1 – Dimensionless mean flow depth Y_{mean}/k_s for different drainage conditions for the 44° NEGATIVE INCLINED STEP (Lining type 1, ks=74 mm). Measurements at section 500, from tests 1 and 12, without and with drainage. Channel slope of 1/3 (α=18.43°).

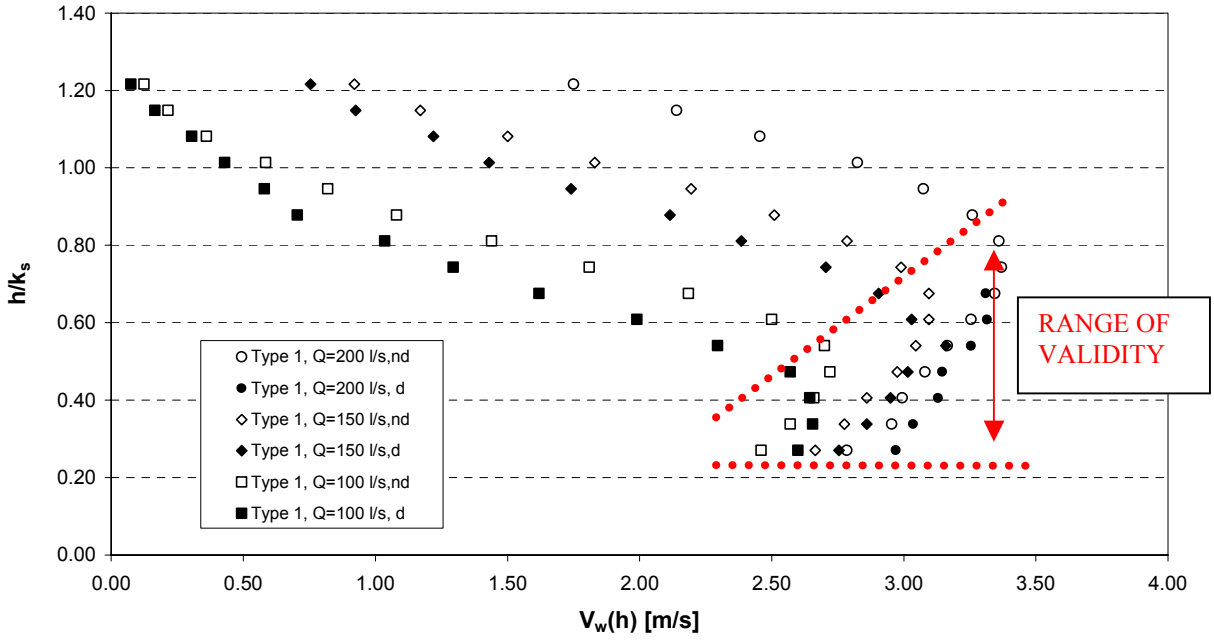

Figure 4.2 – Schematic velocity profiles for Q=100, 150 and 200 l/s, made with currentmeter measurements at several depths (zero at element tip). Comparison for different drainage conditions. 44° NEGATIVE INCLINED STEP (type 1, ks=74 mm). Measurements at section 530, from tests 1 and 12, without (nd) and with drainage (d). Channel slope of 1/3 (α=18.43°).

4.3.2 Tests using the INVERTED 44° NEGATIVE INCLINED STEP (Type 1a)

Elements of Type 1 were also used for lining type 1/a, for which tests n° 5, 6 and 13 were performed. Analysis of the different tests and set-up variants is presented in Table 4.2.

Table 4.2– Comparison table for lining Type 1a (tests n° 5, 6 and 13)

Item of comparison	Comments
Failure conditions vs. Drainage	Drainage delays failure, increasing the limit of stability from 100 to 120 l/s.
Failure conditions vs. Foundation	-
Failure conditions vs. Joint alignment	Tests with unaligned joint were generally considered not conclusive (see 4.2). However, failure flows were not so high in this case and the contribution of joint alignment could be highlighted. In fact, after departure of a first element, settings with aligned joints tend to fail by entire longitudinal rows, whereas in the unaligned settings elements become first just half exposed and tend to resist further (see photos in Appendix A4.6). Unaligned settings can apparently reduce the extent of damage.
Drainage vs. Flow depth	Similar to conclusions made for Type 1 – drainage reduces flow depth.
Drainage vs. Flow velocity	Neither currentmeter nor video recording were used in test n° 13.

4.3.3 Tests using the 30° NEGATIVE INCLINED STEP (Type 2)

Type 2 stepped-like elements were widely used. In tests n° 7, 17 and 18 the simplest geometry was used. Failure was not achieved within the tested range of discharges. The analysis of the different tests and set-up variants is presented in Table 4.3.

Table 4.3– Comparison table for lining Type 2 (tests n° 7, 17 and 18)

Item of comparison	Comments
Failure conditions vs. Drainage	For the observed range of discharges, drainage does not seem to play any role in stability.
Failure conditions vs. Foundation	Failure was not attained both in test 7 (uncompressible foundation) and in test 18 (compressible foundation). For the observed range of discharges, the foundation characteristics do not seem to play a major role in stability.
Failure conditions vs. Joint alignment	-
Drainage vs. Flow depth	No photos were taken during tests 17 or 18. Conclusions should be similar to lining type 1.
Drainage vs. Flow velocity	Video results are quite alike for tests with/without drainage. Differences between these values are of the same order of magnitude, one video frame (1/25 s), of the potential error made in visual film analysis. No currentmeter or photos readings were taken with drainage. Conclusions of comparison should be similar to those of lining type 1.

4.3.4 Tests using the INVERTED 30° NEGATIVE INCLINED STEP (Type 2a)

Inverted 30° negative step elements were used in tests n° 8 and 19. The analysis of the different tests and set-up variants is presented in Table 4.4.

Table 4.4 – Comparison table for lining Type 2a (tests n° 8 and 19)

Item of comparison	Comments
Failure conditions vs. Drainage	Drainage delays failure by reducing up-lift pressures in the foundation, which increases the limit of stability from 50 to 60 l/s.
Failure conditions vs. Foundation	The delay in failure from test 8 to test 19 is more likely related with draining efficiency than with the foundation rigidity or surface roughness. In what concerns the foundation surface characteristics, the tests were non-conclusive.
Drainage vs. Flow depth	No photos were taken during test 19. Conclusions should be similar to lining type 1.
Drainage vs. Flow velocity	Video results are quite alike for tests with/without drainage. Differences between these values are of the same order of magnitude, one video frame (1/25 s), of the potential error made in visual film analysis. No currentmeter or photos readings were taken with drainage. Conclusions of comparison should be similar to those of lining type 1.

4.3.5 Tests using the 30° NEGATIVE INCLINED STEP WITH END SILL (Type 2+ES)

Type 2+ES elements were obtained from type 2 elements by adding an end sill. For experimental work, the end sill was done with wood, glued to the surface of elements type 2. The analysis of the tests n° 9, 11, 16 and 23, is presented in Table 4.5.

Table 4.5– Comparison table for lining Type 2+ES (tests n° 9, 11, 16 and 23)

Item of comparison	Comments
Failure conditions vs. Drainage	Drainage delays failure from 160 to more than 228.5 l/s. Results of test 16 are considered erroneous as they are related with toe block collapse and not with element collapse. During test 23 the lining collapsed slightly earlier than expected (190 l/s). This might be related with the over-use of the drainage foam. In fact, the foam was already 0.5 cm compressed, being thus less efficient in draining and leading to higher up-lift pressures in the foundation than for previous tests.
Failure conditions vs. Foundation	Not conclusive (test 16 is not valid). However, the absence of the metallic sheet in test 23, can also explain the over-exposure of some blocks. In fact, this metallic sheet spreads the up-lift foundation pressures homogeneously in the foundation, delaying failure.
Drainage vs. Flow depth	Measurement of tests 9 and 11 show that drainage reduces the mean observed flow depth, Y_{mean}, by reduction of skimming flow discharge – Figure 4.3
Drainage vs. Flow velocity	Video measurements are available from test n° 16 and 23, confirming the order of magnitude of currentmeter readings. For currentmeter readings, conclusions are similar to lining type 1. The velocity profiles for both with/without drainage situations are presented in Figure 4.4. In what concerns the equivalent clear-water U_w, conclusions are similar to lining 1.

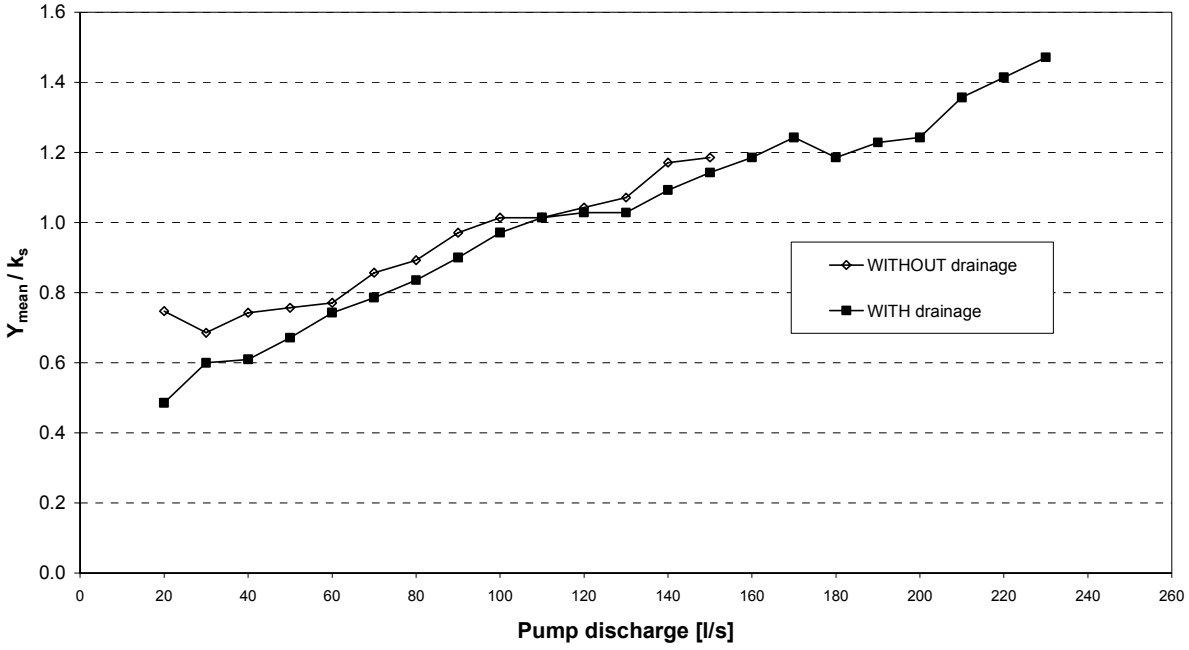

Figure 4.3 – Dimensionless mean flow depth Y_{mean}/k_s for different drainage conditions – 30° NEGATIVE INCLINED STEP WITH END SILL (type 2+ES, k_s=70 mm). Measurements at section 500, from tests n° 9 and 11, without and with drainage. Channel slope of 1/3 (α=18.43°).

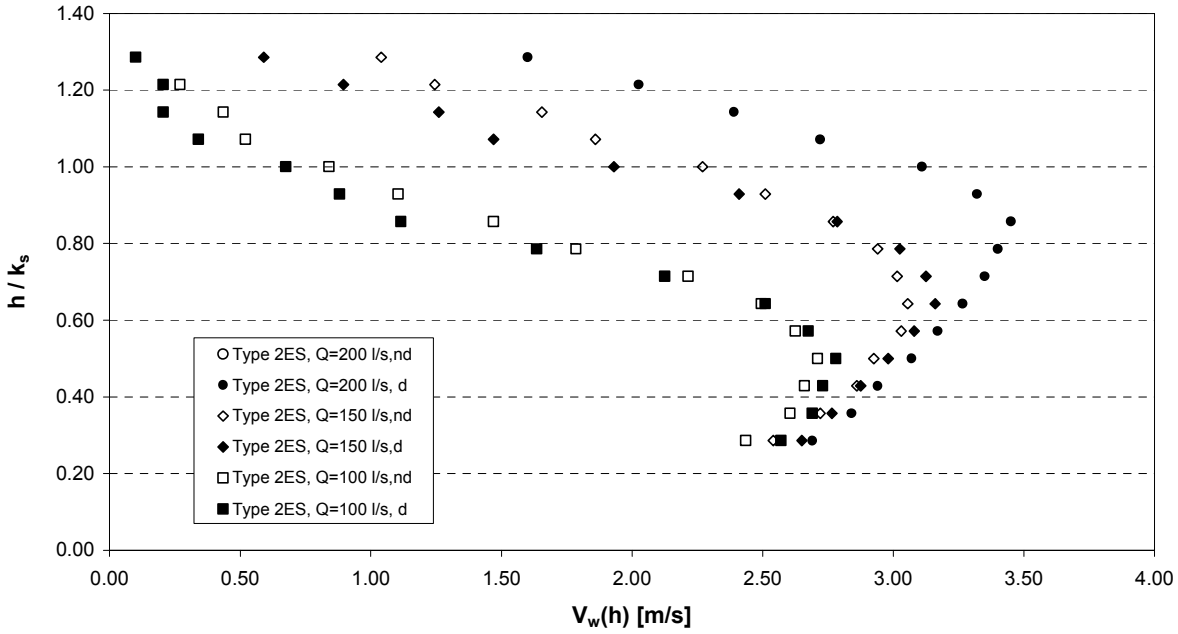

Figure 4.4 – Schematic velocity profiles for Q=100, 150 and 200 l/s, from currentmeter measurements (zero at element tip) – 30° NEGATIVE INCLINED STEP WITH END SILL (type 2+ES). Measurements at section 530, from tests n° 9 and 11, without (nd) and with drainage (d). Element type 2ES (ks=70 mm), channel slope of 1/3 (α=18.43°).

4.3.6 Tests using the INVERTED 30° NEGATIVE INCLINED STEP WITH END SILL (type 2+ES/a)

Elements type 2+ES were also used for lining type 2+ES/a in test n° 10. No variants were tested. In terms of stability, this solution is clearly not advantageous when compared to regular lining type 2+ES, since the failure discharge is considerably reduced for exactly the same geometry of lining and quantities of concrete.

4.3.7 Tests using the 45° PYRAMIDS (types 3 and 3+)

Tests using the pyramids (Table 4.6) were all done with uneven joint alignment, creating a highly complex pattern of flow. Lining type 3+ has exactly the same configuration, or *upper* (flow) part of the element, with a heavier foundation.

The flow pattern is highly diverse close to the element tips, rendering eventual currentmeter measurements inconsistent. This instrumentation device was not used. For increasing discharges, the flow pattern resembles skimming flow regime conditions allowing the definition of reference velocity values, as that of a mean coloured front velocity.

Lining type 3+ was developed to study the stability with an increased foundation weight, by adding a metallic steel plate to the foundation to simulate an increase in concrete thickness. To guarantee an equal behaviour of the element in the laboratory and in prototype, this method is limited to just one plate. If extra *n* plates were added, the displacement of the gravity centre (G) would be higher than what would correspond to *n*x10 mm of concrete. For just one plate, the difference in displacement of G is less than 5%. Further additional thickness has to have the same density of the element (as in prototype).

Table 4.6– Comparison table for lining Type 3/3+ (tests n° 3, 4, 21 and 22)

Item of comparison	Comments
Failure conditions vs. Drainage	Drainage contributes to delay failure, from 60 to 80 l/s in the case of lining type 3 or from 80 to 100 l/s in the case of lining type 3+, by reduction of up-lift pressures.
Failure conditions vs. Foundation	Not conclusive, since the foundation was changed simultaneously with the drainage layer.
Failure conditions vs. Joint alignment	-
Drainage vs. Flow depth	No photos were taken in tests 21 and 22. Conclusions should be similar to lining type 1.
Drainage vs. Flow velocity	Video measurements were made for all tests. However, due to the highly complex flow pattern and to the low discharges, accuracy in video analysis is more difficult to guarantee. No trend was identified relating the observed values and drainage.
Drainage vs. Joint alignment	-

4.4 COMPARISON OF ALL LINING SYSTEMS

4.4.1 Observed flow pattern

4.4.1.1 Effect of ramp (44° negative step) and end sill (30° negative step with end sill)

Elements type 1 and type 2+ES were developed from the simple negative step (type 2); they both have deeper and larger volume cavities than the initial step element.

For low discharges, the geometry of the cavities governs the flow development (Photo 4.1, Photo 4.3, Photo 4.5). The ramp and the end sill enhance an earlier submergence of nappe-flow and favour a fast transition to skimming regime. As the transition regime seems to be characterised by large pressure fluctuations (Chanson, 1994), reaching it at lower discharges may be favourable for stability. For such purpose, the end sill demands a lower volume of additional concrete than a ramp.

For larger discharges, differences in flow pattern are less perceptible just by visual observation. In principle, the skimming flow characteristics are similar the element types 1, 2 and 2ES (Photo 4.2, Photo 4.4, Photo 4.6). However, the volume and the geometry of the cavities being different, the entrapped vortexes have different configuration, rotating velocity and frequency. This difference in cavity flow pattern is important for energy dissipation efficiency comparison. In fact, one of the mechanisms of energy dissipation presented in Chapter 2 is precisely the momentum exchange at the pseudo-bottom interface. This subject represents an interesting field for further research.

Photo 4.1- 44° negative step: overflow of Q=30 l/s

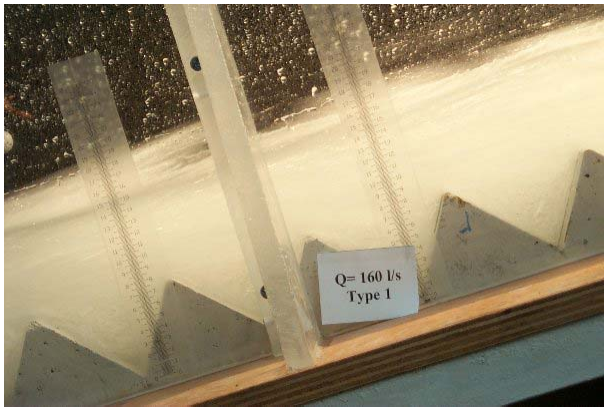

Photo 4.2 - 44° negative step: overflow of Q=160 l/s

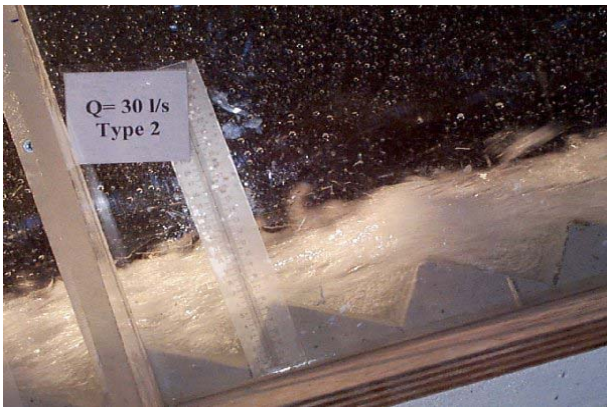

Photo 4.3 - 30° negative step: overflow of Q=30 l/s

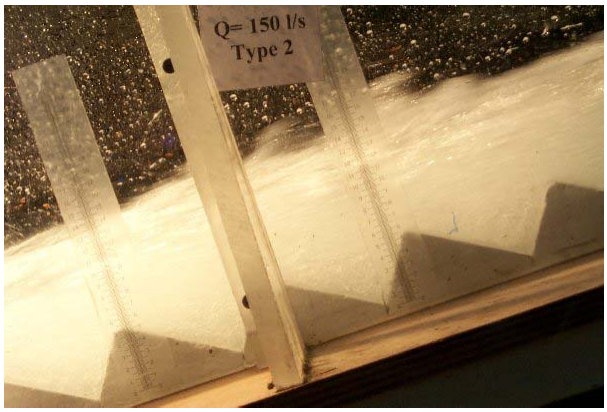

Photo 4.4 - 30° negative step: overflow of Q=150 l/s

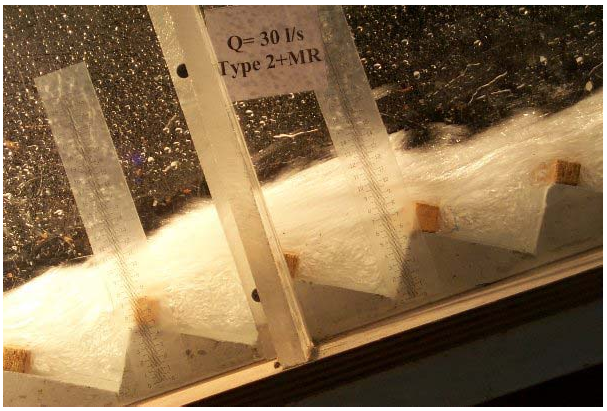

Photo 4.5 - 30° negative step with end sill: overflow of Q=30 l/s

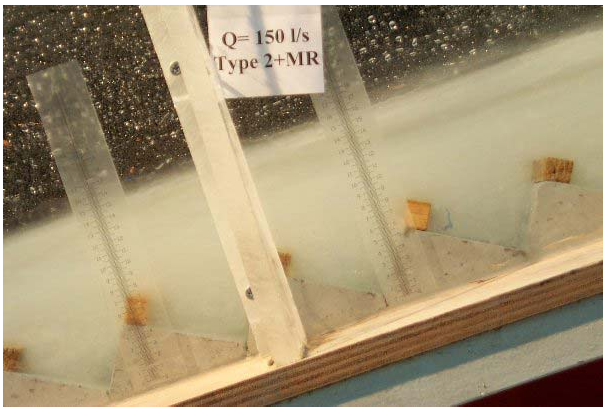

Photo 4.6 - 30° negative step with end sill: overflow of Q=150 l/s

4.4.1.2 Pyramid effect

The pyramids (Photo 4.7) create a more complex, diverse and three-dimensional flow pattern than stepped-like elements. This complex pattern is better observed for low discharges (Photo 4.8) before reaching a skimming flow type of regime (see §3.7.1, Photo 4.9 and Photo 4.10).

Photo 4.7 - Pyramidal bottom configuration (type 3)

Photo 4.8 - Lining type 3: overflow of Q= 15 l/s

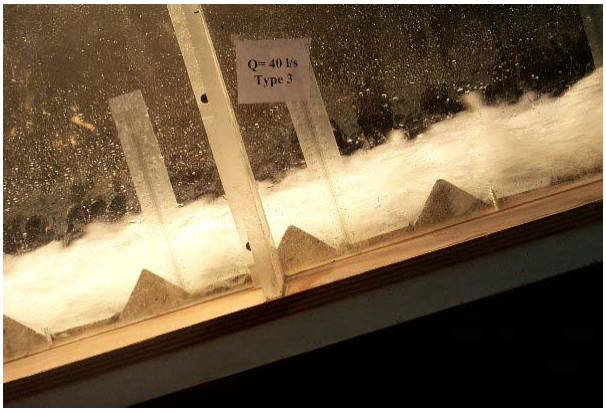

Photo 4.9 - Pyramids: overflow of low discharges (40 l/s)

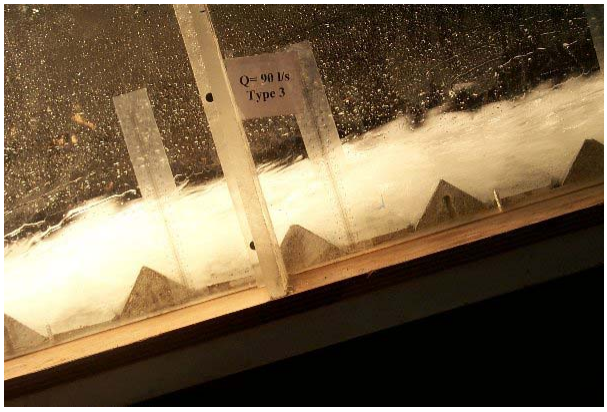

Photo 4.10 - Pyramids: overflow of high discharges (90 l/s)

4.4.1.3 Effect of inverting elements

By inverting the element a stepper upstream face was obtained (Photo 4.11 to Photo 4.16). Differences created concern the pattern of cavity flow and the pattern of the impinging-bouncing flow jets. In fact, the impact of impinging flow in the upstream surface is made at an angle closer to 90° than in previous cases, rendering these inverted elements unstable for lower discharges comparatively to regular elements. For increasing discharges, the flow impacts the element closer to the tip where it has its maximum overturning potential. Experimental results confirm this reasoning: failure flow results (Chapter 3) are always lower than for regular linings 1/2/2ES.

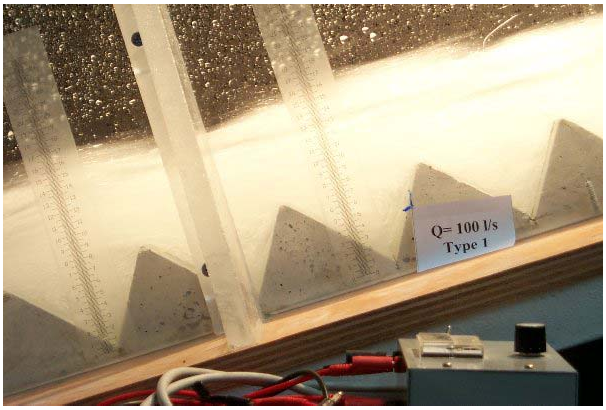

Photo 4.11 – Lining type 1, Q= 100 l/s

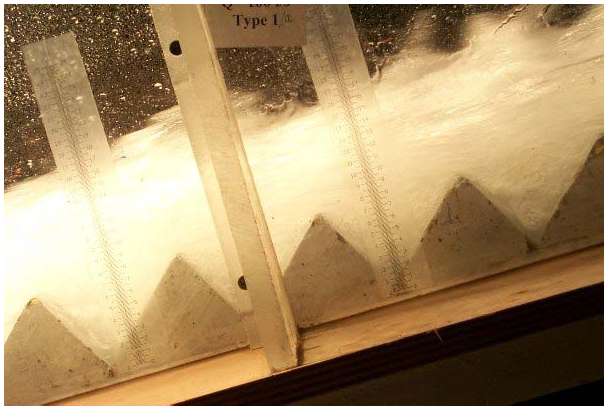

Photo 4.12 - Lining type 1/a, Q= 100 l/s

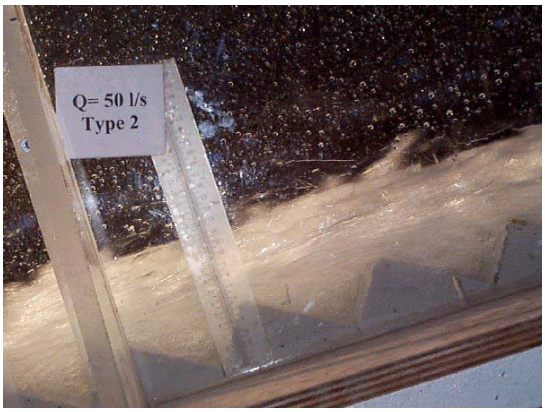

Photo 4.13 - Lining type 2, Q= 50 l/s

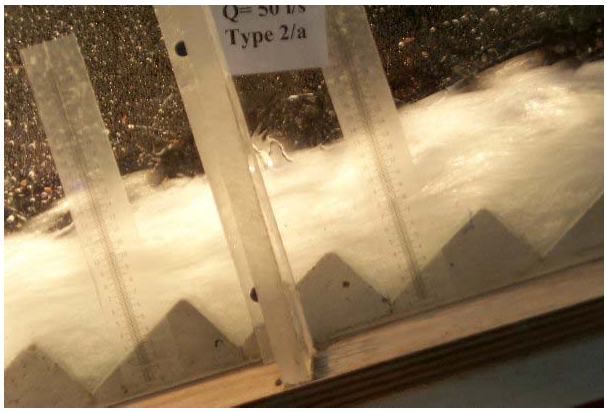

Photo 4.14 - Lining type 2/a, Q= 50 l/s

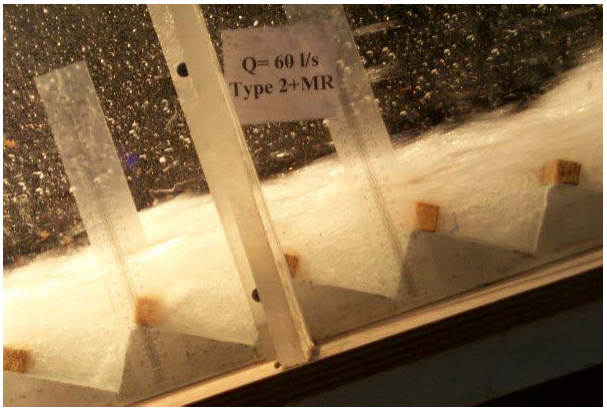

Photo 4.15 - Lining type 2ES, Q= 60 l/s

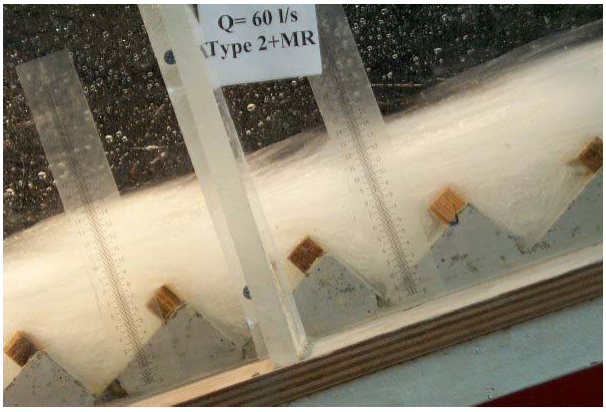

Photo 4.16 - Lining type 2ES/a, Q= 60 l/s

Surprisingly, elements 2ES/a withstood larger discharges than elements type 2/a. The additional gain has to be assigned to the only difference existing between both cases: the end sill. Apparently the characteristics of the vortex created are more favourable for stability.

4.4.2 Flow characteristics

4.4.2.1 Introduction

Differences in flow pattern obviously reflect on flow characteristics. For a given discharge, flow depth and flow velocity at the skimming layer vary with the lining configuration. In fact, each configuration's own cavity flow pattern influences the momentum exchanges at the pseudo-bottom interface and thus the friction losses, the flow depth and the flow velocity.

4.4.2.2 Flow depth

Figure 4.5 and Figure 4.6 present the mean flow depth as function of the unit discharge at model scale (plots for a prototype scale of 10 are presented in Appendix 4, dimensionless plots are presented in chapter 5). From interpretation of these figures it can be concluded that:

- When comparing regular element linings, as 1, 2 and 2ES with inverted element linings, as 1/a, 2/a and 2ES/a, a general trend can be identified, showing that for any given discharge Y_{mean} is generally higher for inverted elements. This results from the more direct impact of impinging flow.

- When comparing linings 1, 2 and 2ES between themselves, type 2 measurements are frequently higher than the remaining, probably due to the smaller cavity size. The differences are larger for lower discharges and tend to be attenuated for higher discharges. For equal conditions of discharge and mean air concentration, the mean depth-averaged flow velocity of lining type 2 should be lower than for the other linings (with corresponding higher energy dissipation efficiency). Such trend should be confirmed with more accurate measurement procedures. The end sill seems to contribute to a lowering of the surface level when compared to simple type 2 element values.

- Mean flow depth measurement for pyramids and 30° negative steps (type 2) are similar.

- Measurements taken during tests *with* drainage for 44° negative steps (1) and 30° negative step with end sill (2ES) agree better than equivalent measurements taken *without* drainage.

4.4.2.3 Local flow velocity

Comparison of the velocity profiles at section 530 for linings type 1 and type 2 for tests without drainage show great similarity throughout the flow depth (Figure 4.7). However, by plotting the same profiles in a dimensionless form, no relation can be highlighted (Figure 4.8).

These velocity profiles are only representative of mixed flow local velocity at low depths, where air concentration is low (see Range of Validity in Figure 4.2). The profile's shape changes abruptly at a depth that does not vary significantly with the type of lining but rather with the discharge. Hence, skimming flow characteristics observed 2.0 cm above the elements' tips seem to be similar for both linings and not to depend on the roughness height.

After placing the end sill (type 2ES), a similar velocity profile configuration was obtained (Figure 4.9). However, lower velocities were measured at lower depths, which might reflect a different pattern of momentum exchanges between the cavity- and skimming flows. Such influence, if any, can only be cleared out if measurements are done closer to the element's tip.

By inverting the elements, the velocities closer to the bottom are systematically lower than for lining type 1, probably due to a more direct flow impact on the element's surface (Figure 4.10). On the other hand, the observed flow depths increase. The air concentration profile is also likely to have changed. The former conclusions are similar for linings type 2-2/a and 2ES-2ES/a.

4.4.2.4 Flow in drainage layer

Infiltrated water was collected by a drainage layer and measured in a triangular sharp-crested weir. Drainage flow was plotted as a function of the pump discharge in Figure 4.11. The range of flows to be dealt with by the under-drain layer was approximately the same for all tested linings. During tests the infiltration depends mainly on the geometry of the joints. For low discharges, infiltrated flows represent about 20% of the overflow discharge. For increasing discharges, this percentage reduces considerably.

In prototype, the drainage layer permeability is more likely to be in the range of 10^{-5} m/s and drainage flows will be probably 10^{-2} times lower than those corresponding to the tests.

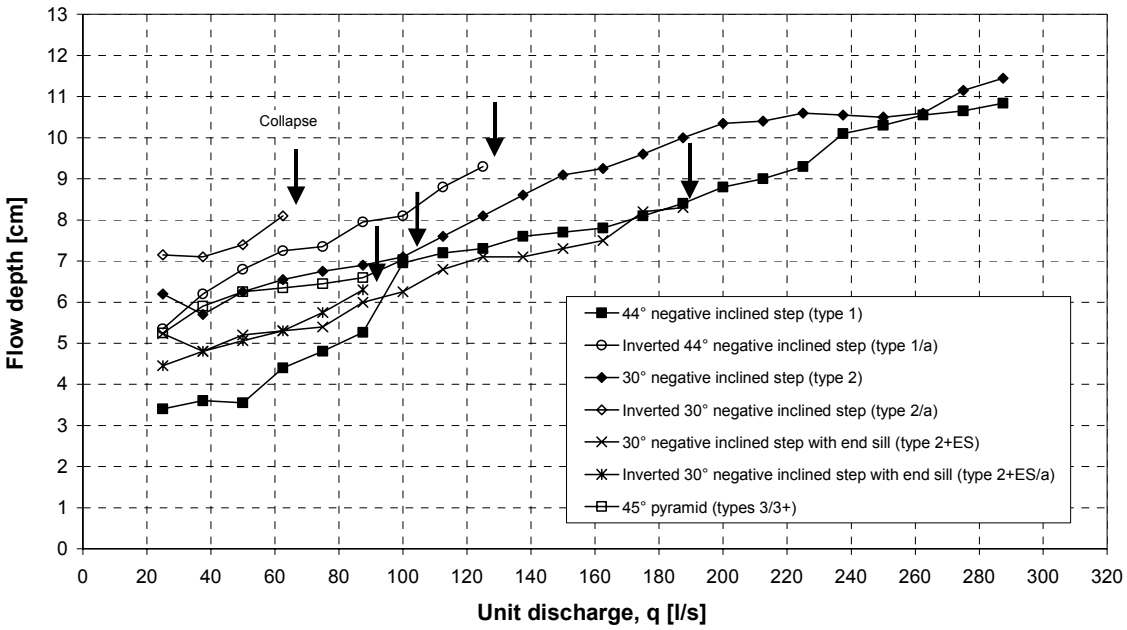

Figure 4.5 – Mean observed flow depth Y_{mean}, for all tested linings and discharges, WITHOUT DRAINAGE. Linings types 1/1a (k_s=74 mm, weight 13.6 N), types 2/2a (k_s=52 mm, weight 10.5 N), types 2ES and 2Es/a (k_s=70 mm, weight 11.0 N), types 3/3+ (k_s=50 mm, weight 5.7 N and 8.2 N).

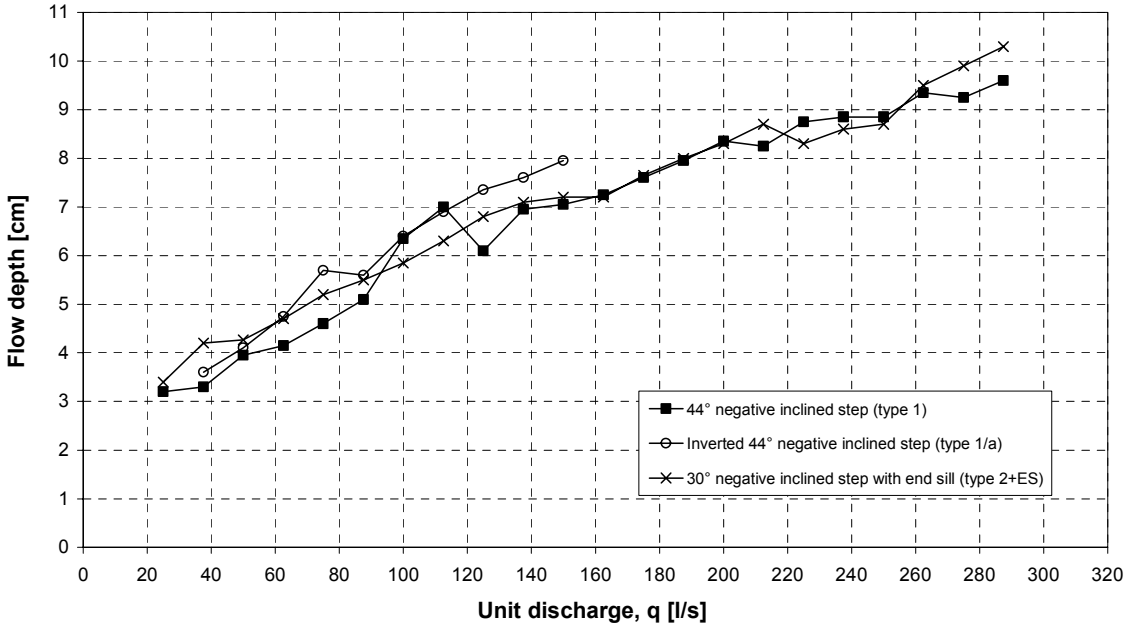

Figure 4.6 – Mean observed flow depth Y_{mean}, for all tested linings and discharges, WITH DRAINAGE. Linings types 1/1a (k_s=74 mm, weight 13.6 N), type 2ES (k_s=70 mm, weight 11.0 N).

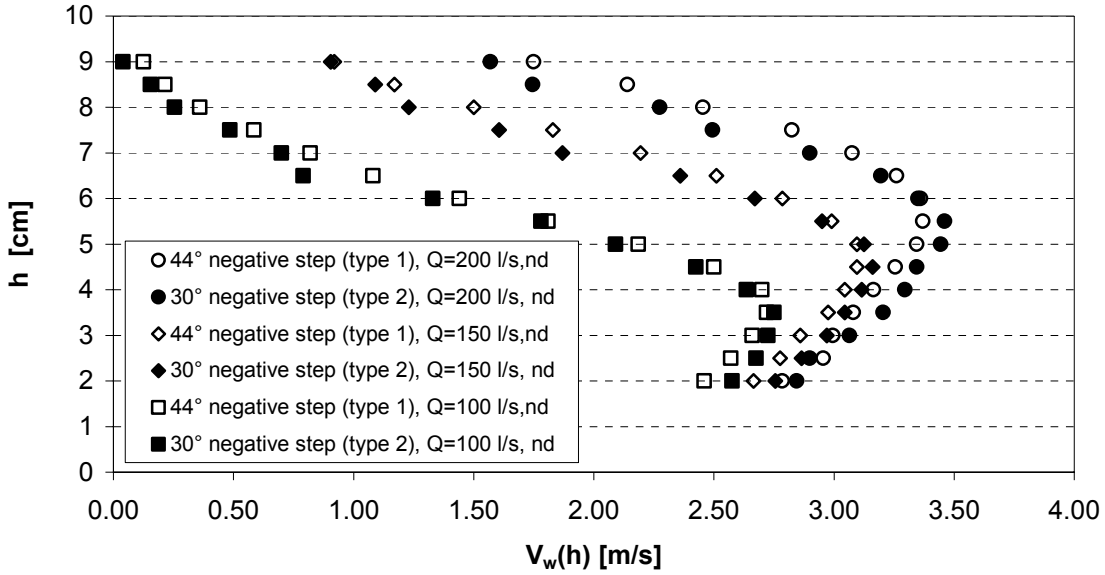

Figure 4.7 – Comparison of 44° NEGATIVE STEP (type 1 - test n°1) and 30° NEGATIVE STEP (type 2 – test n° 7) schematic velocity profiles for Q=100, 150 and 200 l/s made with currentmeter measurements at several depths (zero at element tip). Measurements at section 530, without drainage (nd). Element type 1 (k_s=74 mm), element type 2 (k_s=52 mm), channel slope of 1/3 (α=18.43°).

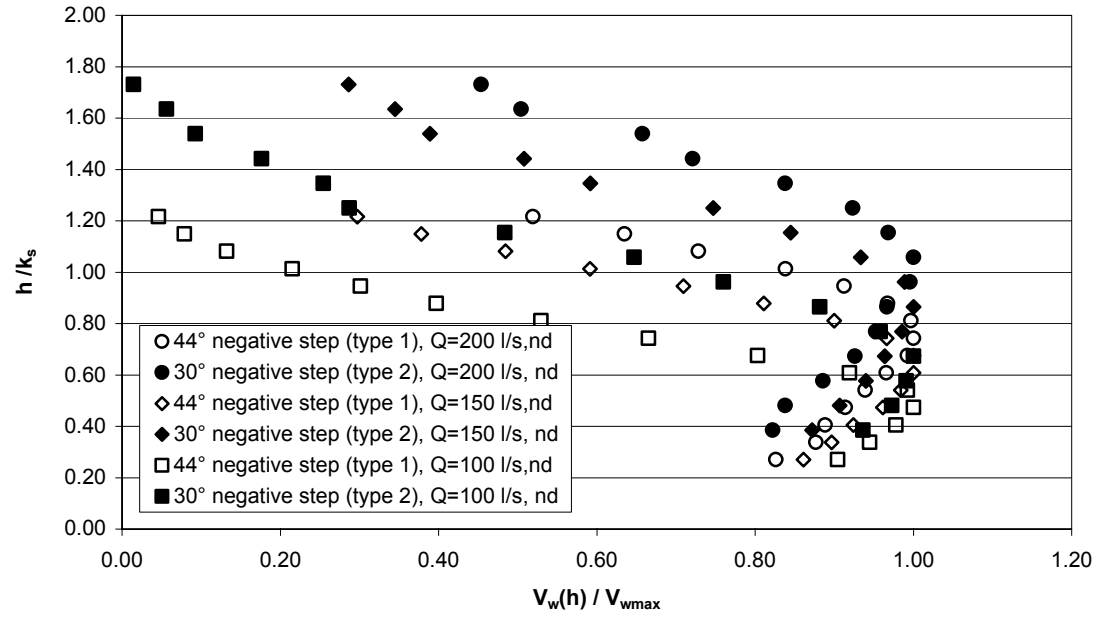

Figure 4.8 – Comparison of 44° NEGATIVE STEP (type 1 - test n°1) and 30° NEGATIVE STEP (type 2 – test n° 7) dimensionless schematic velocity profiles for Q=100, 150 and 200 l/s made with measurements at several depths (zero at element tip). Measurements at section 530, without drainage (nd). Element type 1 (k_s=74 mm), element type 2 (k_s=52 mm), channel slope of 1/3 (α=18.43°).

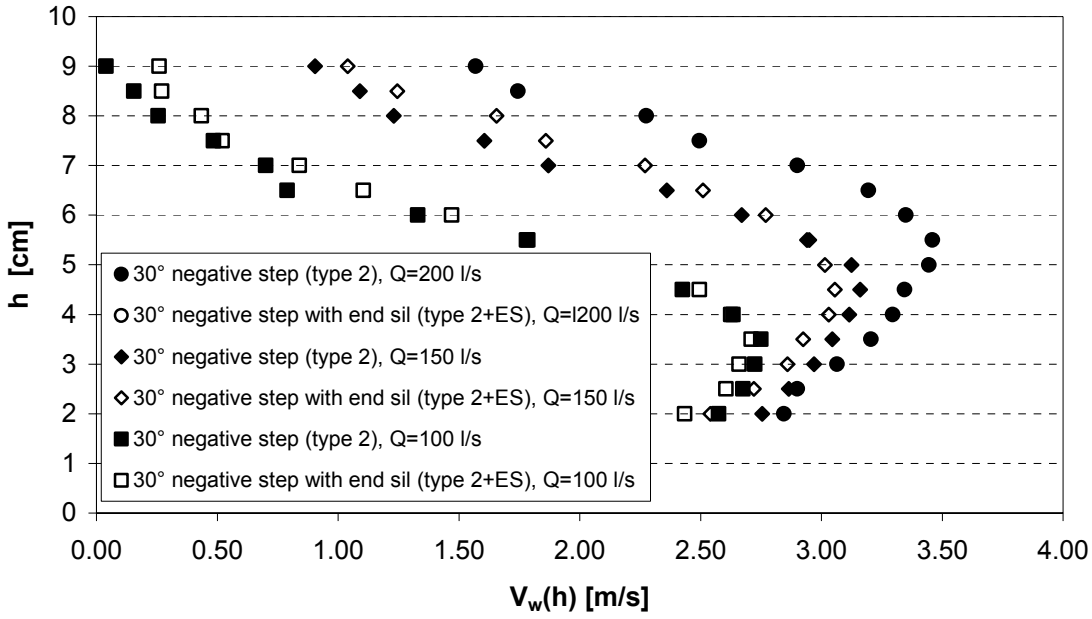

Figure 4.9 – Comparison of 30° NEGATIVE STEP (type 2 - test n°7) and 30° NEGATIVE STEP WITH END SILL (type 2+ES – test n° 9), schematic velocity profiles for Q=100, 150 and 200 l/s made with currentmeter measurements at several depths (zero at element tip). Measurements at section 530, without drainage (nd). Element type 2 (k_s=52 mm), element type 2ES (k_s=70 mm), channel slope of 1/3 (α=18.43°).

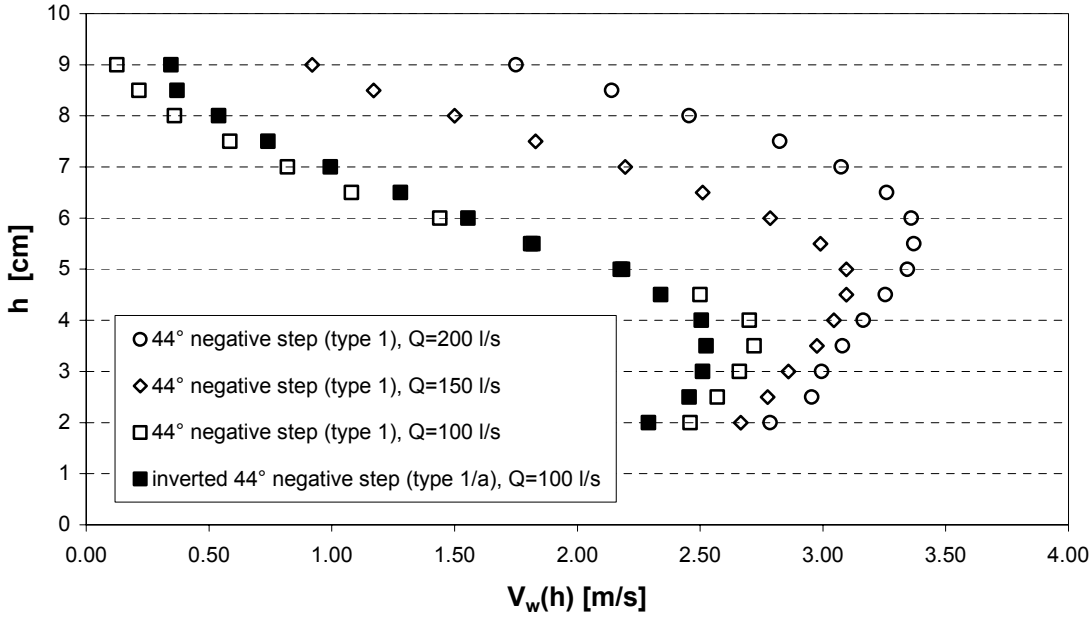

Figure 4.10 – Comparison of 44° NEGATIVE STEP (type 1 - test n°1) and INVERTED 44° NEGATIVE STEP (type 1/a – test n° 6), schematic velocity profiles for Q=100, 150 and 200 l/s made with currentmeter measurements at several depths (zero at element tip). Measurements at section 530, WITHOUT drainage. Element types 1 and 1/a (k_s=74 mm), channel slope of 1/3 (α=18.43°).

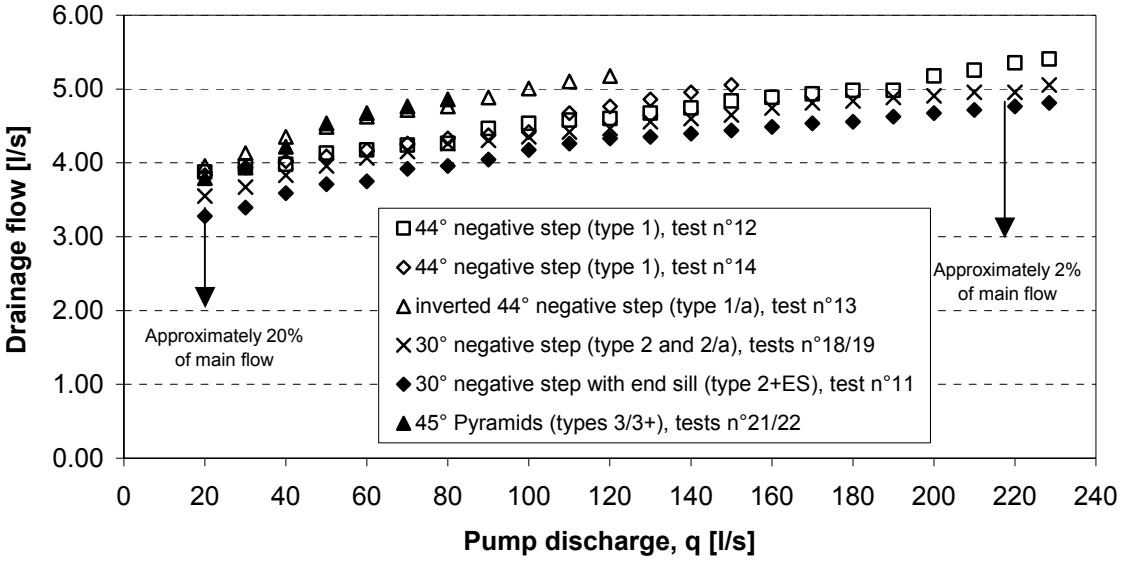

Figure 4.11 – Comparison of drainage measurement for all tests (with drainage)

4.4.3 Stability

The analysis presented in this section allows to concluded that:

a) Whenever the same element type was inverted (1 and 1/a, 2 and 2/a, and 2ES and 2ES/a) the lining failed for lower discharges. Thus, the inertia of the elements plays an important role in stability. The inverted linings (/a) revealed no improvements in the stability performance, most on the contrary.

b) For different lining surfaces, stability seems to depend mostly on the element's shape rather than on weight. As an example, linings type 3 and type 2/a failed for approximately the same discharge, though the latter having a double weight from the former. For linings type 1 and 2, conclusions are limited to the observed range of discharges.

c) For a given element type, stability clearly depends on the weight, as shown in tests with pyramids of different weight (3/3+) by increase of foundation slab thickness. The hydrodynamic loads acting on the flow-exposed surface remain unchanged.

d) The obtained failure flow discharges at prototype scale often surpass a unit discharge of $3m^2/s$ for all stepped-like elements (except the inverted elements). As an example, 44° and 30° negative inclined steps (types 1 and 2) should withstand to about 9 m^2/s at a prototype scale of 10. Linings using pyramids withstood unit discharges close to $3m^2/s$, despite having a weight approximately the half of the lightest stepped-like elements.

e) All linings withstood velocities of, at least, 1.5-2 m/s at model scale (approximately 6 m/s at a prototype scale of 10) for the most unfavourable conditions (highly inefficient drainage). Linings with elements 1 and 2 withstood up to ~3.5 m/s (11 m/s at a prototype scale of 10), whereas elements type 2 with the end sill did not fail before 3 m/s (10 m/s at prototype scale of 10).

4.5 DISCUSSION ON MEASUREMENTS TECHNIQUES

The method used to evaluate surface levels proved to be reliable and straightforward. Inaccuracy in visual observations was kept to the minimum by doing several photos for each situation, averaging the outcome. The error margin estimated for photo interpretation is of 5%.

Currentmeter readings concern uniquely one phase of the mixed flow, being representative of the flow local velocity at low depths where the air content is low. By consistency of the results, they allow the identification of trends and comparison of different macro-roughness linings.

The velocity profile shape obtained for the 30° negative step (type 2) was compared to those presented by Boes (2000) for a stepped spillway using optic probe measurements of local velocity and air concentration. The compared profiles are similar close to the bottom, diverging progressively for higher flow levels, where Boes' profile is almost vertical. The abrupt change of direction of the profiles obtained using the currentmeter testifies this method's inadequacy in the high air concentration region (see Range of Validity in figure 4.2).

Dimensionless velocity profiles are presented in Appendix 4, where the depth h is rendered dimensionless by division by the mean observed flow depth Y_{mean} (~Y90). Inflexion of the velocity profile shape occurs for $0.8Y_{mean}$ in the case of lining type 1, for $0.5Y_{mean}$ in the case of lining type 2 and for 0.5-0.6Y_{mean} in the case of lining type 2ES.

Video recording provided interesting results. Propagation of the coloured front could be followed. Accuracy in interpretation depends on the number of frames per second taken by the camera (own characteristic) and on the visual analysis of the film. The margin of error in frame counting is around 1/25 %. Consistency in the analysis depends considerably on the user. If the procedure is used repeatedly for the same discharge, the mean (depth-averaged) flow velocity might be fairly well estimated. However, the variation of just one frame can, in the case of 4 or 5 frames and 60 cm of travelling distance, result in velocity variations of ± 16,7%.

Although not providing the same information, the different measuring techniques allowed comparison between different linings and definition of the order of magnitude of flow velocity.

Furthermore, computed values of the mean (depth-averaged) clear-water velocity follow the same trends as the measured values (see Figures in Appendix 4). Clear-water computations are normally lower than values obtained with video recording. In fact, for some tests, like for experiments 1 and 12 computed and measured values are fairly close, mainly at high discharges. However, differences between values can mount to 20%, as in the case of tests using inverted elements (types 1/a and 2/a). In conclusion, equivalent clear-water velocities computed from flow depth (Figures 5.1 and 5.2) can provide a fairly good estimate (pre-design stage) of the mean flow velocity in quasi-uniform flow conditions over macro-roughness surfaces similar to a stepped surface. However, they should not be used for design purposes.

The electromagnetic flowmeter (part of the automatic regulation system of the laboratory pumps) has an estimated error margin in stable working conditions of 2 %. For discharges outside the stable working range, that is, for Q<100 l/s, the instantaneous discharge varies within a range of up to 10 %, being this variation considerably reduced by the storage capacity of the head tank.

Drainage measurements are considered to be within a 2% error margin due to visual interpretation of the point gauge station.

5 STABILITY ASSESSMENT OF LININGS BY CONCRETE ELEMENTS

5.1 INTRODUCTION

This Chapter deals with the stability of concrete elements placed on a slope, creating a regular macro-roughness bed, under uniform wide-channel flow conditions. This is the case of an overflow embankment dam having a downstream slope lined with large–scale concrete elements.

Stability can be evaluated using several different approaches, from those coming from sediment transport analysis using the notions of critical shear stress (or shear velocity), to those based on evaluation of individual acting forces and their stabilising or destabilising effect. However, independently of the used approach, it should be considered that:

1. Uniform conditions are assumed, corresponding to a fully developed turbulent boundary layer and constant profiles of velocity and air concentration.

2. Overturning is the governing failure mechanism, as observed during the experimental tests. A toe block, rigidly fixed to the dam foundation, prevents sliding.

3. Failure of the lining occurs when the *first* element is pulled out of a regular macro-roughness bed under gradually increasing strength of flow, as defined by Neill (1967).

Sediment transport theories define the critical equilibrium state of a particle as the condition when the acting shear stress equals the resistant shear. In simplified terms, the former depends on the flow characteristics and the latter on the boundary (grain) characteristics. However, for large-size particles, as boulders or riprap stones, this approach is not valid. Works by Neill (1967), Bathurst (1978), Maynord *et al.* (1989) and Samora (1993) show an evolution in the direction of adjusting the former theories, commonly associated with Shields, to coarse material and large size stones. Neill adapted the dimensional analysis theory to coarse material. The other authors made increasing advances to Shields' theories, notably by assuming corrections to the dimensionless Shields shear stress. All theories are based on *extensive laboratory data*, for different grain sizes and discharges.

For regular macro-roughness, such as the concrete elements presented in the present work, no formerly existing data was found in literature. Therefore, former approaches were simply not possible to follow and the return to a stability analysis based on the forces acting on an isolated element was compulsory.

A stability model was developed within this research work for the computation of a design safety factor. It is presented in the following sections. For failure conditions, this safety factor is naturally unity (1.0). The model assumptions concern the definition of the forces for the various design conditions and the air entrainment in the flow.

A spreadsheet was developed for the repetitive use of the conceived stability model. The assumptions were adjusted so that the stability model matched the experimental failure results. Design charts were computed with the developed model (section 5.5.3), presenting the safety factor as a function of the element's size and the unit design discharge. One example of application of the design model is presented in section 5.7.

5.2 MAXIMUM ALLOWABLE DISCHARGE FOR A GIVEN BLOCK WEIGHT

Limiting stability conditions can be represented by a dimensionless ratio between the discharge and the element characteristics. The chosen ratio relates the critical depth h_{cr} (equation 2.1) and the roughness height k_s. Figure 5.1 and Figure 5.2 present the dimensionless critical depth h_{cr}/k_s, versus the dimensionless mean flow depth Y_{mean}/k_s.

For each lining configuration, limit equilibrium state conditions (failure) correspond to the maximum value of h_{cr}/k_s (except for types 1 and 2 which did not fail). This relation can be used for elements of different dimensions than those used in tests, as long as the dimensionless ratio is respected. In order to design elements that maintain the proportionality to the tested elements but have different roughness heights, the drawings in Appendix 5.1 should be used (k_s in *cm* at prototype scale).

For equal density values, the maximum discharge that an element can withstand establishes the minimum size that element can assume and still be stable. The limiting sizes are mainly related with the capacity of site cranes. If the condition of $h_{cr}/k_{s\ max}$ is respected, larger dimensions can be used as long as the element's weight is acceptable. As an example, the limiting pairs of maximum discharge (q_{max}) and minimum roughness ($k_{s\ min}$) for elements limited to 30 kN at prototype scale, are presented in Table 5.1 (concrete density of 2400 kg/m^3; scale factor 10).

Table 5.1 – Example of maximum allowable discharge and minimum roughness height, for concrete elements of 30 kN of weight at prototype scale (scale factor 10).

Type	q_{max} [m^2/s]	$h_{cr}/k_{s\ max}$	k_s [m]	Volume [m^3]	Weight [kN]
1	13.30	2.74	0.96	1.2314	29.55
1a	5.85	1.58	0.96	1.2310	29.54
2	15.30	3.90	0.74	1.2450	29.88
2a	3.35	1.42	0.74	1.2275	29.46
2ES	9.50	2.19	0.96	1.2415	29.79
2ESa	4.40	1.32	0.96	1.2281	29.47
3	5.10	1.66	0.83	1.2365	29.67

($\rho_{concrete}$=2400 kg/m^3)

5.3 MAXIMUM ALLOWABLE FLOW VELOCITY

To estimate the flow velocity for a given discharge in prototype, a dimensionless ratio between the critical velocity and observed model values (V_{cr}/U) can be used. The mean allowable flow velocity U_{LES} was estimated from the model tests from the computed clear-water velocity, which closely agrees with the mean velocity values obtained by digital video analysis at failure flow conditions, i.e., at limit equilibrium flow conditions. Nevertheless, it should be considered as a gross estimate of the mean depth-averaged velocity (order of magnitude).

In Table 5.2, failure discharge and velocity are calculated with the above-mentioned relationships for prototype concrete blocks, for a scale 1:10 and for a maximum block weight of 30 KN for conditions without drainage.

Table 5.2 - Failure discharge and velocity in model and prototype for a scale 1:10, prototype example for maximum block weight of 30 kN (without drainage, $\rho_{concrete}$=2400 kg/m^3)

Lining type	Model data						Prototype data examples					
	Failure discharge q_{maxl}	Critical velocity for rectangular section V_{cr}	Measured flow velocity				Scale 1:10			Maximum block weight of 30 kN		
			Currentmeter $V_{currentmeter}$	Video V_V	Computed Vw	Faiilure velocity U_{LES}	Failure discharge q_{max}	Faiilure velocity U_{LES}	Weight	Scale	Failure discharge q_{max}	Failure velocity U_{LES}
	[l/s.m]	[m/s]	[m/s]	[m/s]	[m/s]	[m/s]	[m^2/s]	[m/s]	[kN]	[-]	[m^2/s]	[m/s]
1 (44° negative step)	285.6	1.21	2.89	3.75	3.76	3.76	9.03	**11.9**	13.6	1:13	13.3	**13.5**
1/a (inverted type 1)	125	0.92	2.29	2.65	1.92*	1.92*	3.95	**6.1***	13.6	1:13	5.85	**6.9***
2 (30° negative step)	285.6	1.21	2.86	3.83	3.56	3.56	9.03	**11.3**	10.4	1:14	15	**13.3**
2/a (inverted type 2)	62.5	0.73	1.71	2.14	1.10*	1.10*	1.98	**3.5***	10.4	1:14	3.35	**4.1***
2ES (type 2 with end sill)	187.5	1.06	2.54	-	3.23	3.23	5.93	**10.2**	11.0	1:13.7	9.6	**12.0**
2Es/a (inverted type 2ES)	87.5	0.82	2.1	-	1.98*	1.98*	2.77	**6.3***	11.0	1:13.7	4.4	**7.3***
3 (pyramids)	75	0.78	-	2.1	1.56	1.56	2.37	**4.9**	5.7	1:16.6	5.1	**6.4**

*For these concrete elements, C_{mean} is under-estimated, h_w is overestimated and U_{LES} is under-estimated.

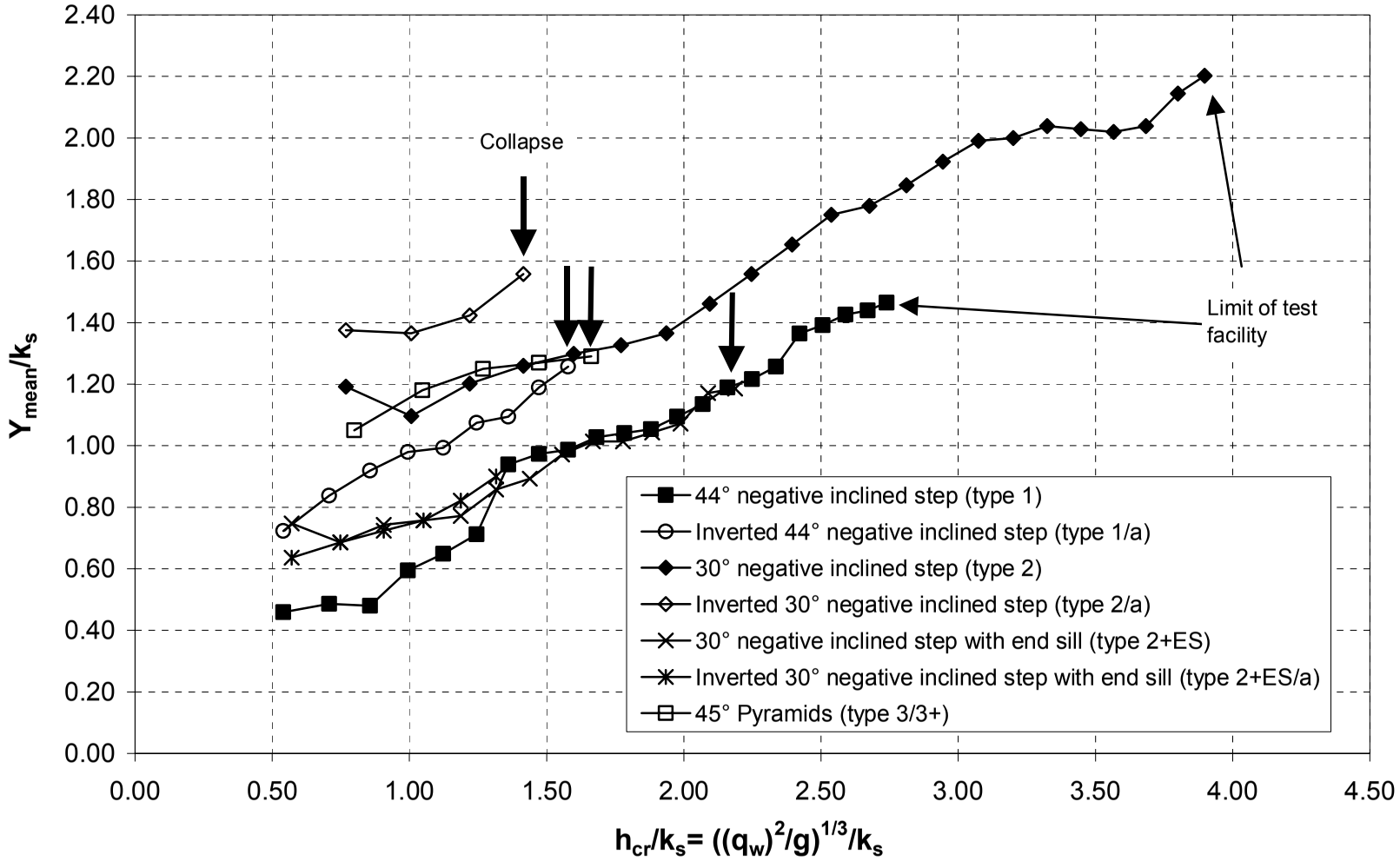

Figure 5.1 - Relation between dimensionless mean surface level (Y_{mean}/k_s) with the dimensionless clear-water critical depth (h_{cr}/k_s), for all types of linings tested in a 1/3-channel slope (α=18.43°). Flow depth measurements are relative to quasi-uniform flow conditions. Tests WITHOUT drainage.

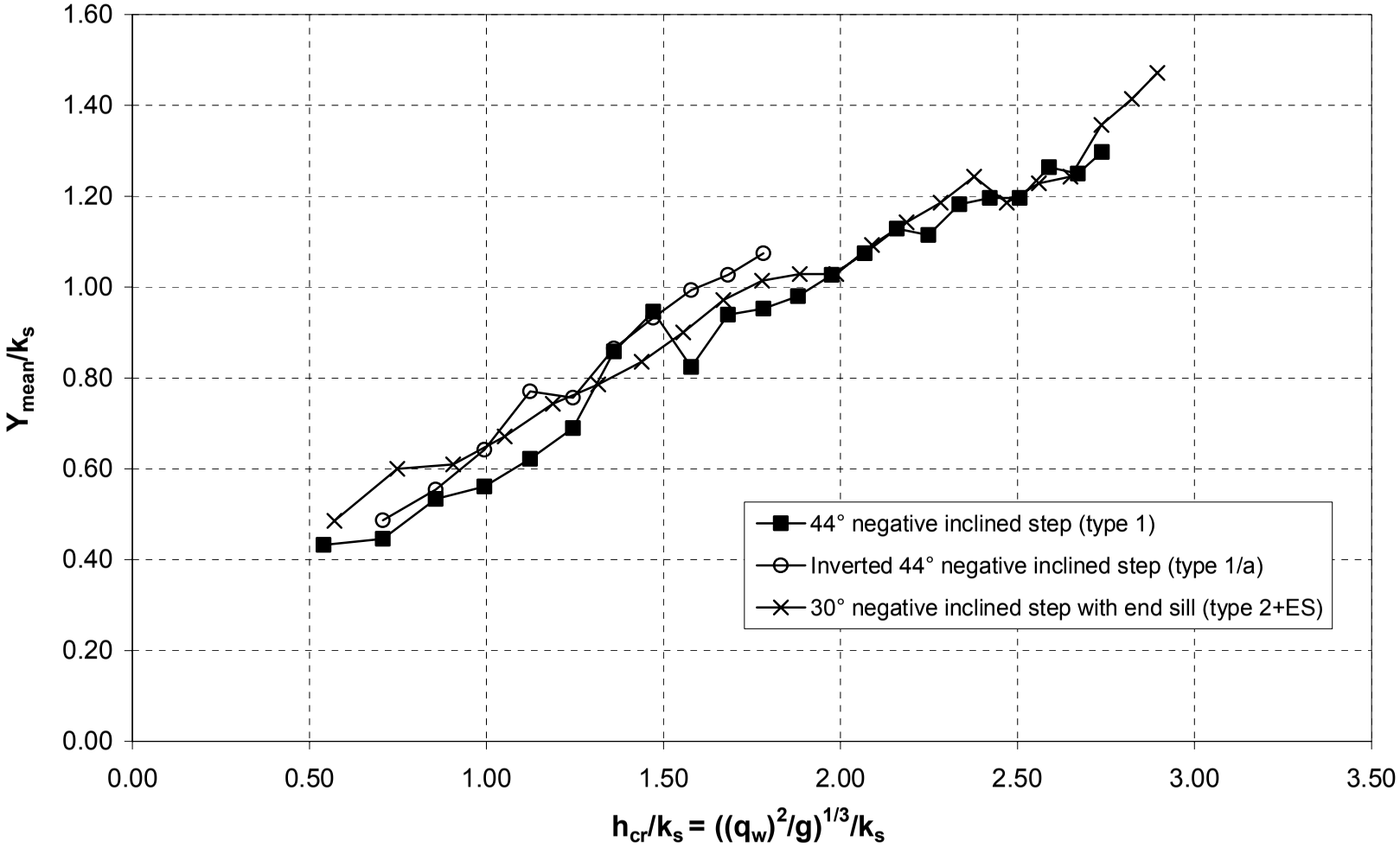

Figure 5.2 - Relation between dimensionless mean surface level (Y_{mean}/k_s) with the dimensionless clear-water critical depth (h_{cr}/k_s), for all types of linings tested in a 1/3-channel slope (α=18.43°). Flow depth measurements are relative to quasi-uniform flow conditions. Tests WITH drainage.

5.4 COMPUTATION OF SAFETY FACTORS

5.4.1 In Limit Equilibrium State (LES)

5.4.1.1 Basic stability equations

Stability is studied for the limit equilibrium conditions by solving a system of equations of forces and moments. In the present case failure is due to overturning, being the governing equation the sum of moments in relation to the overturning point, OP.

The stability equations can be developed using either the contact forces (as presented in Chapter 2, section 2.5.4) or the system of forces presented in Figure 5.3. This last one will be used.

If contact forces were to be taken one by one, a large number of components and points of application would have to be considered, resulting in a large system of equations to be solved. What's more, some of these forces have variable patterns. For instance, the hydrodynamic pressure forces acting on the flow-exposed surfaces have variable module, direction and sign, at every moment in time. Their distribution along the surfaces varies considerably, due to the re-circulating flow cells created in the cavities. Time-averaged values cannot be used, as pressure fluctuations can largely surpass the mean value. Extreme values are more suitable for stability analysis, but are unpractical to obtain.

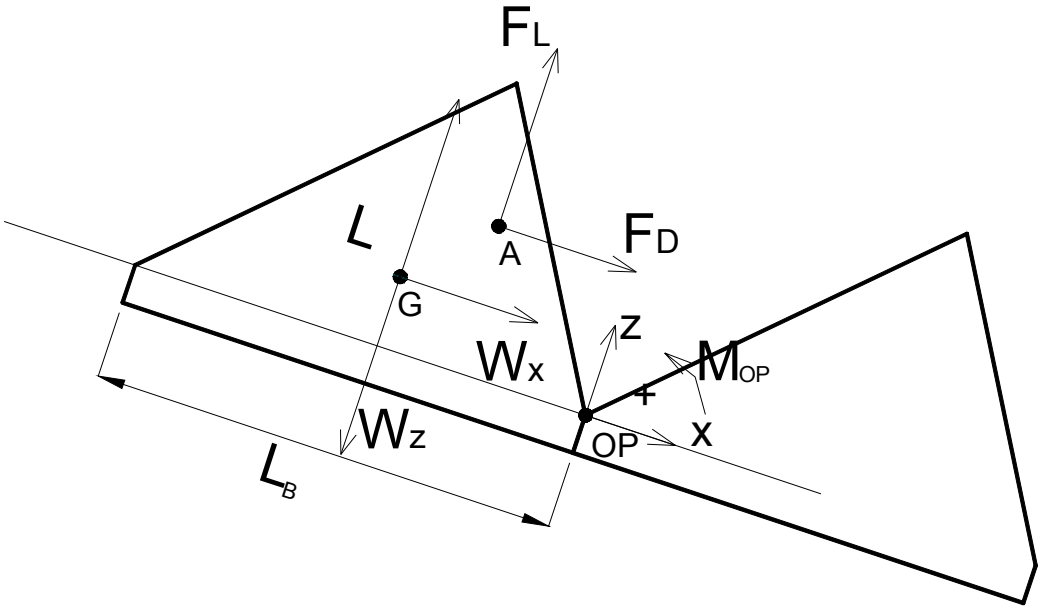

Figure 5.3 – Systems of forces considered for the stability analysis of regular-shaped concrete elements including drag and lift forces. Example of the 44° negative inclined step (type 1), without drainage.

The chosen system of forces is simpler to handle. It includes the weight of the element W, the hydrostatic lift L, and a resultant force of hydrodynamic pressures F_R. The number of unknowns and equations is thus reduced. The hydrodynamic force is decomposed in Drag F_D and Lift F_L according to the axis-directions. The hydrostatic lift is perpendicular to the slope as the hydraulic gradient is hydrostatic (in accordance with open-channel theory of Bernoulli).

The governing stability equation indicates that the moment created by the acting forces in relation to the overturning point OP is zero:

$$M_{OP} = 0 \tag{5.1}$$

that can be also written as

$$-W_x \cdot z_G + F_D \cdot z_A - F_L \cdot (b - x_A) + (W_z - L) \cdot (b - x_G) = 0 \tag{5.2}$$

The components of the weight (per meter of width) are computed from equations 5.3 and 5.4.

$$W_x = A \cdot \rho_s \cdot g \cdot \sin\alpha \tag{5.3}$$

$$W_z = A \cdot \rho_s \cdot g \cdot \cos\alpha \tag{5.4}$$

In sloped channel flow, a hydrostatic pressure gradient is assumed. In uniform flow conditions, the hydrostatic lift is perpendicular to the slope, the surface and the flow streamlines, as is the resultant of pressures acting on a body in the fluid. In open-channel flow, pressure is proportional to the distance to the surface measured perpendicularly to the slope, and converted to the equivalent water column (vertical) by multiplication of the *cos* α (α - angle of slope with horizontal plane) – equation 5.5:

$$L = \rho_w \cdot g \cdot A \cdot \cos\alpha \tag{5.5}$$

Drag is normally expressed as

$$F_D = C_D D^2 \tau \qquad \text{or} \qquad F_D = C_D \cdot A_D \cdot \rho_w \cdot g \cdot \frac{U_w^{\,2}}{2 \cdot g} \tag{5.6}$$

And lift as

$$F_L = C_L D^2 \tau \qquad \text{or} \qquad F_L = C_L \cdot A_L \cdot \rho_w \cdot g \cdot \frac{U_w^{\,2}}{2 \cdot g} \tag{5.7}$$

They are normally expressed in terms of the shear stress τ or of the kinetic energy head. The hydrodynamic coefficients C_D and C_L include form effects and its influence on the velocity depth-wise distribution.

The presented static system has 4 unknowns (C_D ,C_L, z_A, x_A) for just one equation. Solutions are quite dependent of the hydrodynamic forces values and on their application point (A). As knowledge of these is not straightforward, assumptions are compulsory.

Whittaker and Jäggi (1986) used this approach for large concrete spheres for river channel erosion protection, for which reasonable assumption on form factors values can be made. The authors solved the equilibrium momentum equation for overturning failure and expressed the result explicitly in terms of the critical (depth-averaged) velocity, which is of more practical handling than the shear stress (the shear stress depends on the square of the velocity). In the present case, limitations on form factor definition do not allow to follow the same procedure.

5.4.1.2 Assumptions for the stability model

5.4.1.2.1 <u>On the hydrodynamic loads</u>

From literature, scarce information was found concerning the location of the hydrodynamic forces application point (*A*). In fact, its location varies in time and space with the acting forces. For the tested concrete elements, *A* has to be somewhere in the *upper* part of the element. Using instantaneous values of Drag and Lift equation 5.2 defines two regions in the element. Limit equilibrium conditions correspond to having *A* over the division-line.

However, not having instantaneous values of F_D and F_L a first assumption is made, transposing both forces from *A* to the gravity centre *G*. A moment corresponding to this translation movement should be added at *G,* but for its computation the distance of *A* to *G* is needed (and thus the location of *A*). Hence, F_L and F_D were substituted by a pair of forces F_L* and F_D*, whose values applied in *G* create exactly the same moment in OP – Figure 5.4.

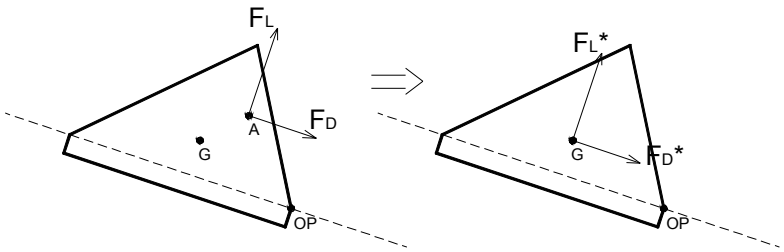

Figure 5.4 - Translation of hydrodynamic forces from *A* to *G* and substitution of F_D and F_L by F_D* and F_L*.

To eliminate the last unknown in excess, the resultant hydrodynamic force *F** was given the direction of the drag, application point at *G* and a value that causes exactly the same momentum in *OP* as before:

$$F^* = K^* \cdot A_D \cdot \rho_w \cdot g \cdot \frac{U_w^{\,2}}{2 \cdot g} \qquad (5.8)$$

where A_D corresponds to the roughness height.

In order to render the model coherent with the results analysis of Chapter 4, a last assumption is necessary. In fact, equation 5.8 needs a clear-water velocity input U_w. This velocity was computed with the equivalent clear-water height h_w. The latter results from the mean observed flow depth Y_{mean} from equation 2.12. Thus, only hydrodynamic pressures caused by the skimming flow are considered for the definition of U_w– Figure 5.5. In a similar way, pressures due to cavity flow were assumed to even themselves out in the slope-axis direction and to be of negligible additional effect in the perpendicular-to-the-axis direction. In conclusion, the present stability model depends only on the skimming flow kinetic head for *F** computation.

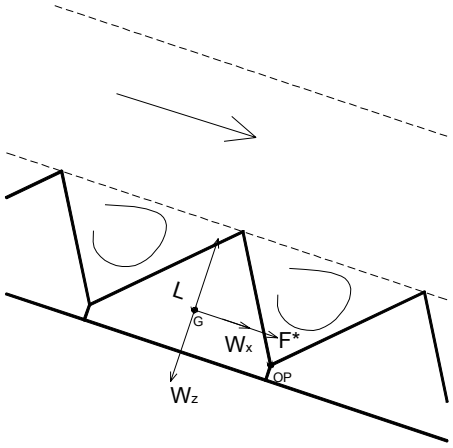

Figure 5.5 – System of forces acting on an isolated element – case of tests without drainage

5.4.1.2.2 On air entrainment

Air concentration has been previously reviewed in Chapters 2 and 3, which recommendations in are used hereafter. For computation of C_{mean}, an average of the values given by equations 2.9 and 2.10 is advised for stepped like elements, whereas the outcome of equation 2.11 is advised for the pyramidal elements.

Naturally, the air concentration on the mixed fluid flow reduces the hydrostatic lift, which can be considered by reducing the fluid's density (equation 5.9).

$$L = \rho_w \cdot (1 - C_{mean}) \cdot g \cdot A \cdot \cos\alpha \tag{5.9}$$

5.4.1.2.3 On drainage conditions

Drainage reduces the main flow discharge and, depending on its efficiency, may severely reduce or even eliminate the hydrostatic pressures in the foundation. In this case, the mean clear-water velocity is corrected by reducing q_w of C=10% in order to match the experimental results (equation 5.10).

$$U_w = \frac{q_w \cdot (1 - C)}{h_w} \tag{5.10}$$

In what concerns the hydrostatic lift, an example is used to present the changes caused by drainage - Figure 5.6. For a rectangular body in equilibrium over depth in moving waters, the hydrostatic lift is equal to the difference of acting pressures on the top and bottom surfaces. This difference equals to the component of the body's weight perpendicular to the slope (and streamlines direction). The value of lift is computed from:

$$L = g \cdot \rho \cdot L_B \cdot (h_{bottom} - h_{top}) \cdot \cos\alpha \tag{5.11}$$

where h_{bottom}-h_{top} = Dh, and L_B is the length of the top and bottom surfaces. When the body is placed on the bottom of the channel, supposed impervious, the same equilibrium of forces remains. This is the case of tests made without drainage.

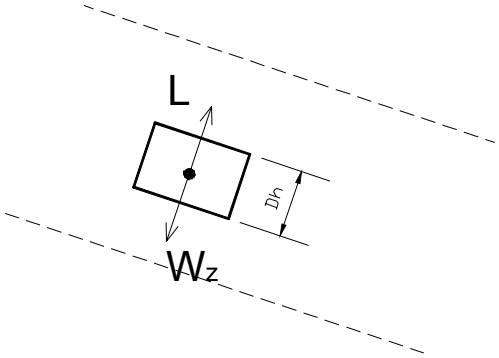

Figure 5.6 – Hydrostatic lift acting on a rectangular body in equilibrium over depth in free-surface flow in a sloped channel.

For tests with drainage, the bottom of the channel is no longer impervious. Due to the high permeability of the drainage foam the draining efficiency was considered 100%, eliminating the acting pressures on the bottom surface. Therefore, only the stabilising effect of the top surface pressures remains, which is in fact the weight of the water column on top of the element, W_w - Figure 5.7 (equation 5.12).

$$L_{with\_drainage} = -W_w = -g \cdot \rho_w \cdot L_B \cdot h_w \cdot \cos\alpha \tag{5.12}$$

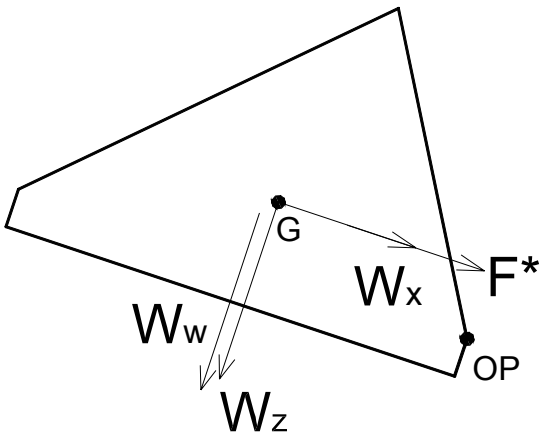

Figure 5.7 - System of forces acting on an isolated element – case of tests with drainage

5.4.1.3 Minimum safety factor definition (SF1)

The number of unknowns has been reduced to just one unknown: *F**. The resultant of all acting forces *R* is computed knowing its direction goes through *OP* at Limit Equilibrium State (LES).

The direction of *R* is given by:

$$\tan\theta = \frac{(z_G - z_{OP})}{(x_G - x_{OP})} = \frac{z_G}{(L_B - x_G)} \tag{5.13}$$

Being all forces in the normal (z) direction known, the component in the x-axis, R_x (Figure 5.8), can be computed from 5.14:

$$\frac{R_z}{R_x} = \tan\theta => R_x = \frac{R_z \cdot (L_B - x_G)}{z_G} \tag{5.14}$$

For computations without drainage, R_z is given by:

$$R_z = (W_z - L) \tag{5.15a}$$

whereas, for computations with drainage, L is substituted by $-W_w$:

$$R_z = (W_z + W_w) \tag{5.15b}$$

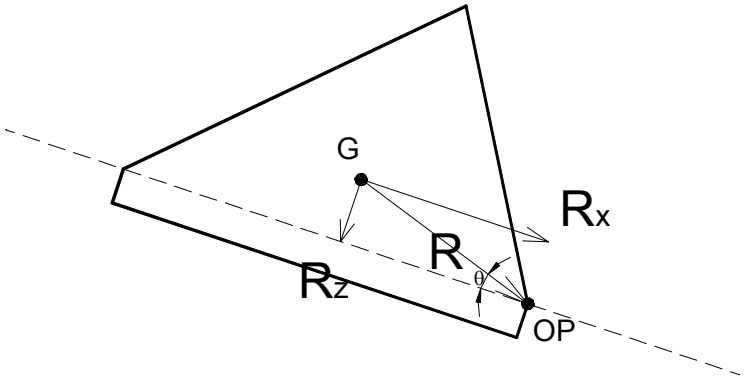

Figure 5.8 – Limit equilibrium state resultant of forces (decomposed in R_x and R_z)

From R_x, F* can be computed with 5.16:

$$R_x = W_x + F* \tag{5.16}$$

Having defined all the forces, a safety factor SF1 can be computed from equation 5.17.

$$SF1 = \frac{\sum M_{stabilising}}{\sum M_{Overturning}} \tag{5.17}$$

The sum of stabilising moments is given by (5.18):

$$\sum M_{stabilising} = R_z \cdot (b - x_G) \tag{5.18}$$

and the sum of overturning moments is given by (5.19):

$$\sum M_{Overturning} = (W_x + F*) \cdot z_G \tag{5.19}$$

Additionally, the value of K* can be computed using 5.8, being the mean flow velocity given by 5.10. K* will be of use for other design conditions, as explained in section 5.4.2.

For LES conditions, the safety factor is 1.0. For elements whose failure was not reached during the experimental tests (type 1 and 2), there is an additional safety margin that could not be quantified. As for all the other lining types, it is assumed that failure corresponds to h_{cr}/k_{smax}.

5.4.1.4 Recommended safety factor definition (SF2)

Design engineers will wish to have some additional margin of safety that can be quantified. Two possibilities exist for the *same overflow discharge*:

1. Increase the element size, by increasing the roughness height, computing the safety factor for below-LES conditions (to be seen in section 5.4.2);

2. Maintain the same roughness height and increase the element's weight by increasing the thickness of the foundation.

On the other hand, in LES conditions engineers are sure to have the least quantity of concrete per square meter needed. For a given discharge, the question is to know which of the above possibilities demands the lowest concrete volume to achieve the desired safety factor. After computation of several examples it was concluded that the second alternative is the best in view of concrete consuming. To check if the assumptions made for the model result in reasonable changes of geometry and weight, a design safety factor SF2 value of 1.5 was used. Reasonable would mean that for this increase in the safety margin, the roughness height or the foundation slab thickness variations would be in the order of 1-2 times the initial values.

Foundation thickening corresponds to the addiction of a slab of constant thickness with exactly the same base length and width of the initial element - Figure 5.9.

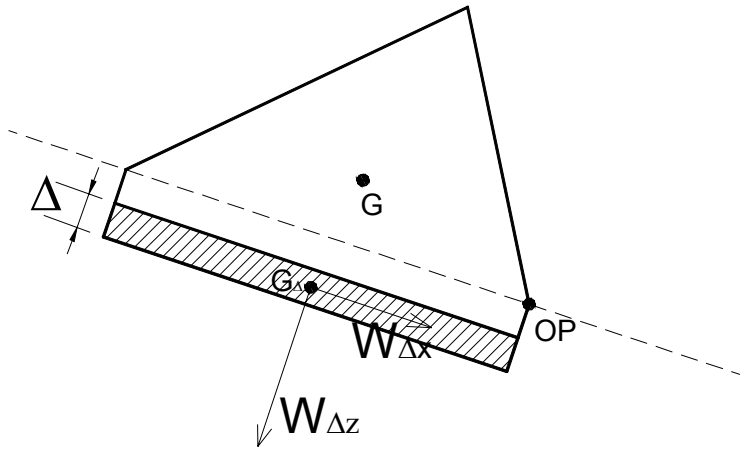

Figure 5.9 – Additional forces due to foundation thickening

A stabilising moment should be added to (5.18), so that the new stabilising moment is:

$$(\sum M_{stabilisng})_{\Delta} = R_z \cdot (b - x_G) + W_{\Delta X} \cdot (h_f + \frac{\Delta}{2}) + (W_{\Delta Z} - L_{\Delta}) \cdot \frac{L_B}{2} \tag{5.20}$$

and

$$(\sum M_{stabilising})_{\Delta} = SF2 \cdot \sum M_{Overturning} \tag{5.21}$$

The weight component are given by (5.22) and (5.23):

$$W_{\Delta x} = L_B \cdot \Delta \cdot \rho_s \cdot g \cdot \sin\alpha \tag{5.22}$$

$$W_{\Delta z} = L_B \cdot \Delta \cdot \rho_s \cdot g \cdot \cos\alpha \tag{5.23}$$

For tests without drainage, L_Δ is given by (5.9), substituting A by A_Δ. For tests with drainage, L_Δ is zero and R_z is given by equation 5.15b.

The value of Δ is obtained by solving the 2nd order polynomial equation coming out from (5.20) and (5.21) and choosing the positive root (5.24).

$$\Delta = \frac{-b + \sqrt{b^2 - 4 \cdot a \cdot c}}{2 \cdot a} \tag{5.24}$$

where:

$$a = \frac{L_B}{2} \cdot \rho_s \cdot g \cdot \sin\alpha \tag{5.25}$$

$$b_{without\_drainage} = L_B \cdot \rho_s \cdot g \cdot \sin\alpha \cdot h_f + \frac{L_B^{\,2}}{2}(\rho_s \cdot g \cdot \cos\alpha - \rho_w(1 - C_{mean})) \tag{5.26a}$$

$$b_{with\_drainage} = L_B \cdot \rho_s \cdot g \cdot \sin\alpha \cdot h_f + \frac{L_B^{\,2}}{2}(\rho_s \cdot g \cdot \cos\alpha) \tag{5.26b}$$

$$c = R_z \cdot (b - x_G) - (\sum M_{stabilisng})_\Delta = (1 - SF2)\sum M_{stabilising} \tag{5.27}$$

For a given unit discharge, Δ will be naturally the largest for k_s=k_{smin} (SF1=1.0). The safety gap to overcome till the final safety factor equals 1.5 is also the largest. Δ reduces progressively for increasing k_s values (SF1>1.0).

5.4.1.5 Model adjustment for element type 3

In the case of the pyramids all computations are done not by *meter of width* but by element. Thus, the previous equations 5.12/5.22/5.23/5.25/5.26a/5.26b, depending from the surface (of elements or of water column) should be multiplied by the width, *b*.

5.4.2 In below-Limit Equilibrium State

5.4.2.1 Introduction

If for a given discharge a roughness bigger than the minimum is chosen, design is made under below limit-state conditions (h_{cr}/k_s<$h_{cr}/k_{s\ max}$). This is also the case when SF1 is increased by roughness height increase, in opposition to foundation thickening.

In below-LES conditions, the direction of the resultant is not known and the reasoning done in §5.4.1 is not adequate. It should be kept in mind that:

- If h_{cr}/k_s<$h_{cr}/k_{s\ max}$ then k_s>$k_{s\ min}$ of the given discharge *q*.

- For same q the cavity size will increase and the skimming flow depth and velocity will be slightly reduced. To know the new corresponding Y_{mean}/k_s further tests with larger blocks would be necessary. Nevertheless, even if these values could be obtained, the acting forces could not be determined since the direction of the resultant force for conditions below LES is unknown.

5.4.2.2 Assumptions for the stability model

5.4.2.2.1 <u>On flow velocity and flow depth</u>

The mean flow depth and mean flow velocity will certainly be slightly reduced in comparison to $h_{cr}/k_{s\ max}$ conditions (LES). As they cannot be computed, the LES values $(U_w)_{ksmin}$ and $(h_w)_{ksmin}$ are used. These are the highest values that these two flow characteristics can assume for the given discharge (5.28 and 5.29). These assumptions are conservative in stability terms.

$$(U_w)_{ks\min\_q} = (U_{w\max})_q \tag{5.28}$$

$$(h_w)_{ks\min\_q} = (h_{w\max})_q \tag{5.29}$$

Furthermore, the relation between the kinetic head and the elements size is also the maximum for LES conditions. This relation can be represented by K* as defined in (5.8). Its value computed for $k_{s\ min}$ is used.

In resume, for $h_{cr}/k_s<h_{cr}/k_{s\ max}$ conditions, F* should be computed from (5.30) and R_x from (5.16). Lastly, R_z can be obtained after computation of the hydrostatic lift.

$$(F^*)_{ks>ks\min} = (K^*)_{ks\min} \cdot k_s \cdot \rho_w \cdot g \cdot \frac{(U_w{}^2)_{ks\min}}{2 \cdot g} \tag{5.30}$$

5.4.2.2.2 <u>On the hydrostatic lift</u>

For computations without drainage, the hydrostatic lift can be computed from equation (5.9), entering the surface (or volume if pyramid) corresponding to the actual roughness. For computations with drainage, hydrostatic lift can be computed with equation 5.12 using $(h_w)_{ksmin}$.

5.4.2.3 Safety factor definition (SF1)

Once all the forces in stake are known, the sums of stabilising and overturning moments can be computed using (5.18) and (5.19). As for the same discharge the roughness height was increased, the computed safety factor is naturally larger than unity (SF1>1 for $h_{cr}/k_s<h_{cr}/k_{s\ max}$).

5.4.2.4 Recommended safety factor definition (SF2)

SF1 is larger than unity, but it might be:

1. higher than required, thus generating an overestimation of the needed element weight and concrete quantities, acceptable or not;

2. lower than required, being suggested to either re-initiate the procedure of §5.4.1 with a slightly smaller roughness height or, increase the foundation thickness until the required safety factor is achieved, as described in §5.4.1.4. A SF2 value of 1.5 is recommended.

5.5 DEVELOPMENT OF COMPUTATION TOOLS

5.5.1 Spread sheet development

An EXCEL spreadsheet was developed for repetitive computations with the described stability model. The procedure is presented in Table 5.3. Any user will just have to insert six parameters, and eventually a seventh one:

- the design unit discharge;
- the type of lining (following indications given on Figure 4.5, Figure 4.6, Figure 5.1, Figure 5.2 and Table 5.1);
- if the stability evaluation should be performed with/without drainage;
- the roughness height (which will define h_{cr}/k_s and hence the design conditions);
- the mean air concentration (from suggestions or any other for sensitivity analysis);
- the density of the envisaged concrete;
- an eventual value of additional foundation thickening, Δ^*, if needed or desired.

In brief, the user is asked to fill in the previous information in cells highlighted in blue, leaving all the red cells to be computed without user-interference. The spreadsheet was divided in three pages. The first page is used to gather the information concerning the design scenario, including user-input and geometry computations. In the following, and depending on design conditions (h_{cr}/k_s), the user can obtain the result from page 2 (LES conditions) or page 3 (Below LES conditions). The seventh, and last, input will correspond to the final adjustment of the safety factor and foundation slab thickness.

5.5.2 Synopsis design charts

Design chart presenting the value of SF1 can be obtained with the described stability model by following the procedures previously presented. The design chart allows a rapid comparison of alternative roughness heights and associated safety factors.

In Appendix 5 the obtained synoptic design charts for the element types 1, 2, 2ES, 3 and 3+ are presented, for concrete density of 2400 kg/m^3, in non-drained conditions (the most unfavourable) and for weights up to 30 kN. Trend-lines were adjusted to the computed values. The correlation factors are higher than 0.999. Some examples are described in §5.7.

For each value of SF1 and unit discharge q, the minimum roughness height (precision at *cm*) is presented as well as the corresponding weight. However, this might not correspond to the minimum quantity of concrete for the given SF1. As an alternative, the recommended procedure is to initially use a low value of SF1 (preferably 1.0) and obtain a higher SF by increase in foundation thickness (see §5.4.1.4) instead of increasing the element's size (roughness height).

Also in Appendix 5, one resume table of the values used for one of the charts is included (2ES), being possible to compare the design scenarios of SF1=1.0 for which a final SF value of 1.5 is achieved with additional foundation thickness and, for the same discharge, the scenario of SF1=1.5 with a larger element.

Table 5.3 – Description of Stability Model spreadsheet procedure

Flow chart	Description
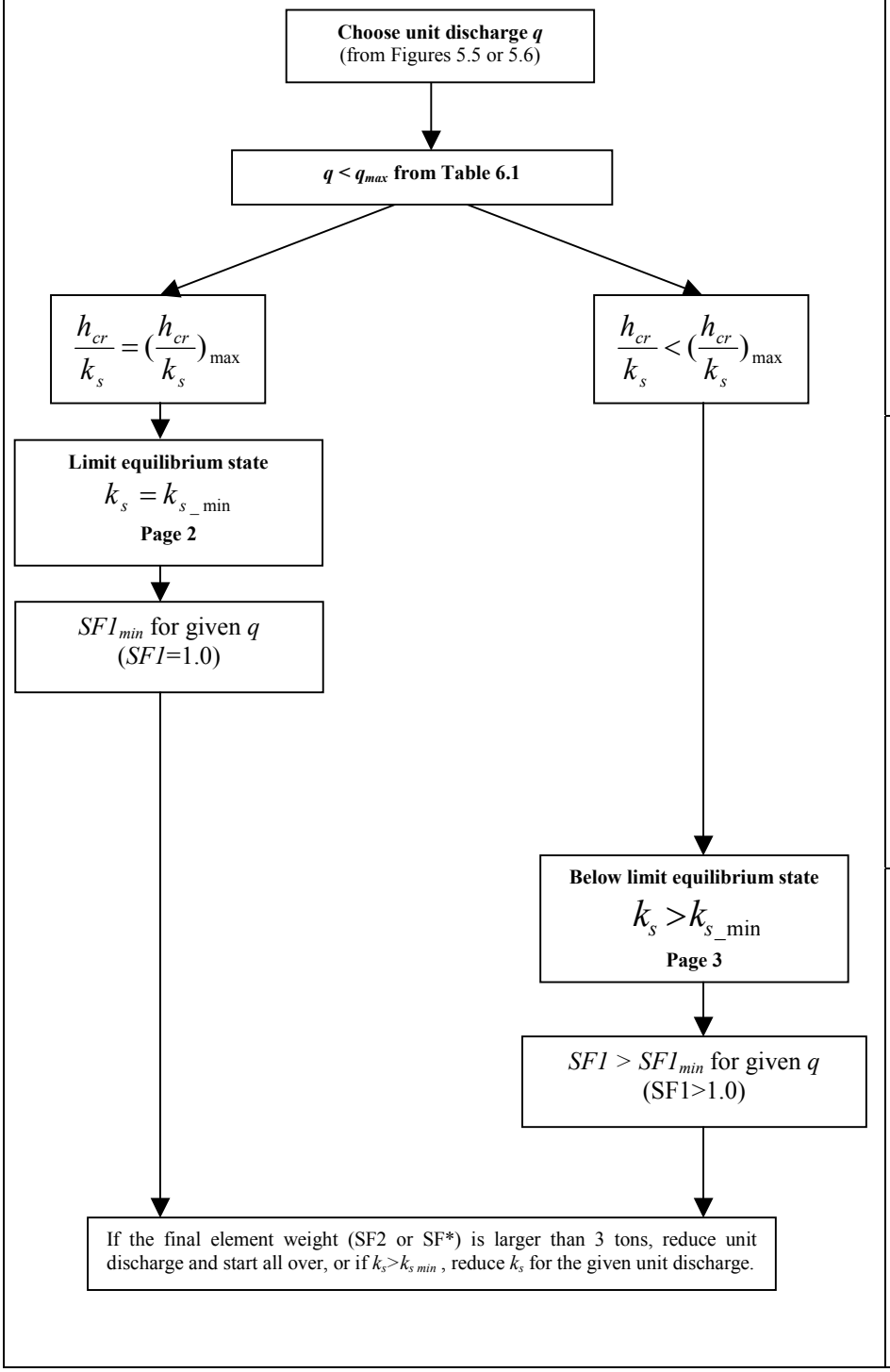	**Page 1** • q can be higher that values of Figures 4.5/6 if $h_{cr}/k_s \le h_{cr}/k_{smax}$ (Figures 5.1/2)and weight <3 ton (see Table 5.1). • Once ks has been chosen, all geometrical parameters are computed, according to expression presented in Appendix 5.1. If design is being made in LES conditions then **page 2** and if not **page 3**. **Page 2** • Computation of loads • Computation of K* • Computation of SF1 • Computation of SF2 • Quantification of concrete quantities and element weight. (higher/lower than 3 tons?) • Adjustment of Δ and SF2, including concrete quantities estimation (Δ*, SF*) The last step is not compulsory according to recommendations, but allows a sensitivity analysis. If Δ*= –Δ, SF*=SF1. **Page 3** • Auxiliary computation of LES conditions for k_{smin}, including geometry, loads and K* • Computation of loads for k_s • Computation of SF1 • If SF1 <1.5, computation of SF2 • Quantification of concrete quantities and element weight. (higher/lower than 3 tons?) • Adjustment of Δ and SF2, including concrete quantities estimation (Δ*, SF*) The last step is not compulsory according to recommendations, but allows a sensitivity analysis. If Δ*= –Δ, SF*=SF1.

5.6 DISCUSSION OF THE RESULTS OF THE ANALYTICAL STABILITY MODEL

5.6.1 Safety factor computation

The model is calibrated to assign a safety factor of 1.0 for limit equilibrium conditions. For other conditions the computed SF obtained was always superior to unity, showing accordance. Furthermore, for a given discharge, if the roughness height is increased, the safety factor follows progressively this increase. For instance, for values of $h_{cr}/k_s < max$ the SF does not double or triple but stays within *reasonable* results.

On the other hand, by increasing the foundation thickness, as strongly recommended in this work, additional thickness remains within *reasonable* values. For instance, to bridge the difference between SF1=1.0 and SF2=1.5 in LES conditions, additional foundation thickening is likely to be less than ¼ the roughness height.

5.6.2 Assumptions

5.6.2.1 On the hydrodynamic forces

Drag and lift coefficients are not known for these elements. They vary with velocity, fluid viscosity, density (function of the air concentration) and projection areas A_D and A_L. For the most studied element - the sphere - only one reference was found (Aksoy, 1973). For a sphere close to a boundary, the projection areas are equal and $C_D \sim 3$ times C_L (mean values).

Contrarily to the sphere, all the tested elements have unequal A_D and A_L. Drag and lift can even be of the same order of magnitude. At this stage of research it is simply not known.

Verifying this assumption was tried using pressure coefficients taken from the EUROCODE 1, concerning wind loads acting on prismatic constructions. The hydrodynamic loads were defined based on pressure coefficients for wind actions over industrial building with saw-like multi-span roofs. The dynamic load scenario considered a single local pressure close to the element tips (similar to the highest points of a roof), on the leeside of the flow (downstream), with a pressure coefficient (C_{pe}) of –1.5. No positive, stabilising, pressure was taken for the upstream surface.

In resume, the load case at LES conditions considered the weight, the hydrostatic lift and a single hydrodynamic force (normal to the downstream surface). The hydrodynamic force (F_{hid}) was computed from:

$$F_{hid} = C_{pe} \cdot A_{hid} \cdot \rho_w \cdot \frac{V^2}{2} \qquad (5.31)$$

where A_{hid} is the acting surface (proportional to 10% of the base length) and V is a reference mean flow velocity. The chosen load scenario was considered to be the most unfavourable for stability.

Taking the video recording velocity measurements as reference, the equilibrium of moments was obtained for cases where failure had occurred in the experiments (e.g. elements 1/a and 2/a). The same procedure was tried for lining Type 2 (step), which did not fail during tests. In the drained case, balance of moments was not achieved, as required, being the stabilising moment larger than the overturning one (as expected). However, for the non-drained test the situation is inverse, showing the limitation of the assumed load scenario. In fact, wind pressure coefficients are

defined for buildings with a certain height above ground, which does not fully correspond to the macro-roughness concrete element surface. Thus, these coefficients might not faithfully account for the limited exposure of each element due to the hiding effect of the preceding ones. All matters considered this methodology has also its limitations.

In resume, the assumption made for the development of the stability model is one amongst many possible approaches, all having limitations and disadvantages. It was considered to be the most reasonable. It contributed positively to the consistency of the conceived model.

5.6.2.2 On the hydrostatic lift

Eliminating totally the foundation pressures for computations with drainage is a conservative procedure. Not having the possibility to reduce such pressures by fractions[23], a total reduction was assumed. At LES conditions, this reduction results in a high value of R_z, and by consequence of F^* and K^*. The imposed SF1 equals unity and all other design conditions will be computed relatively to this very safety-side K^* reference. Oversize might even be the result. All matters considered, design should be done in LES for the most unfavourable scenario (non-drained).

5.6.2.3 On air concentration

Air concentration was accounted for in the stability model by means of the mean air concentration. Suggestions were made based on former studies and formulae. An important simplification done was assuming quasi-uniform flow conditions for all discharges. This might have not always been the case, especially for very the highest discharges. The use of other instrumentation would have been necessary, but the risk of damaging, for instance, an optic probe, in destructive tests is very high.

The model was calibrated for the C_{mean} recommended. For LES conditions, variations of some *mm* in the final thickness Δ, needed to assure a SF2=1.5 were detected for C_{mean} values between 0.20 and 0.40. Below LES conditions, variation of C_{mean} values relatively to the suggestion used might result in differences around 10% in the necessary additional thickness.

For lower discharges, C_{mean} might be higher than the given recommendations, as the skimming flow regime may not yet have achieved such a regular unidirectional pattern.

5.7 DESIGN EXAMPLE

This design example is valid for the same conditions assumed for the stability model development (see sections 5.1).

The methodology follows the reasoning of the flow chart of Table 5.3. If design is made for LES conditions it consists of:

1. Defining the design unit discharge.
2. Choose element type by analysis of the design charts (Appendix 5)
3. Compute the element's weight using the definition drawings (Appendix 5) and equations (5.3) and (5.4).
4. Choose a design scenario, preferably without drainage (recommended), and compute the hydrostatic lift using (5.5), mean flow depth values from Figure 5.1 or 5.2, and a mean air concentration given by (2.9), (2.10) or (2.11).

[23] The experimental set-up did not include pressure measurements in the foundation, which might be one suggestion for further research and model optimisation.

5. Compute the stabilising moment with the help of (5.18) and use (5.17) to obtain the overturning moment.
6. To obtain a higher safety factor, increase the thickness of the foundation slab (and thus the stabilising moment) using equations (5.20) to (5.27).

If design is not done for LES conditions, meaning that a higher safety margin is to be obtained by defining a larger block, another procedure should be followed:

1. All the steps of the previous LES procedure should have been performed, for the given unit discharge and for the minimum roughness for failure conditions, defining the maximum values of the equivalent clear-water velocity and the corresponding hydrodynamic loads.
2. For a given roughness (higher than the minimum used in step 1) compute the geometry and weight.
3. Compute the hydrostatic lift (5.5).
4. Compute the hydrodynamic force F^* with (5.8), using the values of K^* and U_w obtained in step 1.
5. Compute the stabilising and overturning moments to obtain the initial safety factor SF1.
6. If this factor is considered insufficient, a larger roughness height can be chosen and the procedure repeated. Alternatively, the thickness of the foundation slab can be increased in order to achieve the required safety.

Additionally, if quasi-uniform conditions are achieved at the toe, the equivalent mean depth averaged clear-water velocity might be used to pre-design the energy dissipation facilities at the toe. Furthermore, the drainage layer can be design to drain up to 1% of the overflow discharge.

For instance, if an element type 2+ES is to be designed for a unit discharge of 6 m^2/s, the minimum roughness acceptable is 0.7 m (LES conditions => max h_{cr}/k_s=2.19) to which corresponds a block of 14 kN. Taking 0.30 as mean air concentration in quasi-uniform conditions and using a design scenario without drainage, a safety factor of 1.0 is obtained (initial assumption). To achieve a higher safety margin of 1.5 the foundation thickness should be increased of 0.18 m, less than twice the initial foundation thickness. Notice should be the fact that the solution of the 2^{nd} order polynomial equation might not be the optimal solution, the lowest value, than Δ has to assume so that SF2=1.5. In point 11 of the spreadsheet, the estimate of Δ is optimised. In Appendix 5, the spreadsheet output for this case is presented.

If just the drainage conditions are changed, rendering the design scenario less unfavourable, the chosen roughness will provide an initial safety value (SF1) larger than 1.0. On the other hand, this also means that a higher discharge can be considered.

If just the roughness height is increased (for instance to 0.84 m), lowering h_{cr}/k_s to below-LES conditions, the increase of weight will increase the safety margin (SF1) for the given unit discharge. Naturally, SF1>1.0 and the needed Δ to achieve SF2=1.5 are lower than that needed previously for 0.70 m. In this case, the loads are first computed for a roughness height of 0.7 m (minimum), to obtain the hydrodynamic parameters for LES conditions, being then used to compute SF1 for the new roughness height. The desired final safety factor can be obtained either by further increasing the roughness height or by additional foundation thickening.

Graphically, one example can be presented for the lining type 3, for which tests with different foundation thickness were performed. In Figure 5.10, one example of such synoptic design chart

is presented, for a concrete density of 2400 kg/m^3, in non-drained conditions. The example can be read in several ways:

- For a given unit discharge of 2.30 m^2/s, a minimum safety factor of 1.0 would be achieved for an element type 3 with k_s=0.50 m or an element type 3+ with k_s=0.42 m, the latter being lighter than the former.

- On the other hand, for k_s = 0.50 m an element type 3+ will either have a SF1 close to 1.25 for 2.30 m^2/s (approximately the same weight of an element type 3), or will be able to withstand a higher discharge (as shown) for SF=1.0.

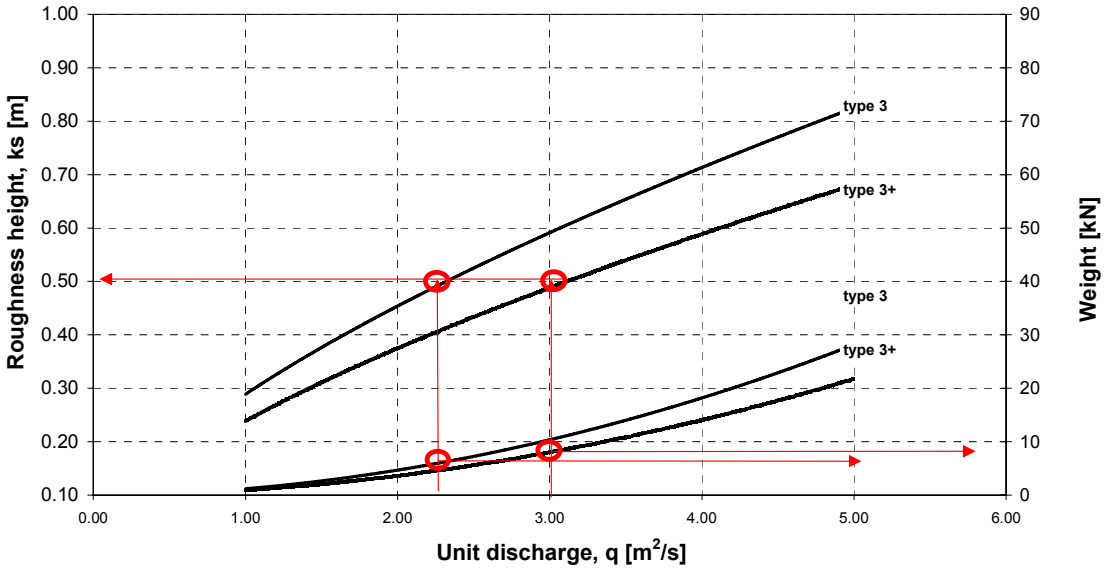

Figure 5.10 - Design example of a pyramid element using the design charts for elements 3 and 3+ without drainage (concrete density is 2400 kg/m^3).

From computation it was shown that, generally, for a given discharge, lighter blocks could be achieved if the safety factor was raised by increasing the foundation's thickness rather than by increasing the roughness height.

6 DESIGN RECOMMENDATIONS

6.1 INTRODUCTION

The conceived lining system might be of use for the rehabilitation of existing dams, for the design and construction of low dams, as well as for the protection of cofferdams. It has been developed for use over earth embankment of moderate slopes, about 1/3 (V/H). In the following Chapter a review of important features to keep in mind during design of an overflow lining is done. It does not have the pretension to be exhaustive.

6.2 DESIGN FRAMEWORK

An overflow lining can be designed to be a face protection against erosion caused by overflow or also to increase the efficiency of energy dissipation along the dam's face. Any one or other way, it acts as a spilling channel. Its width, slope, surface characteristics, foundation, wall height, crest transition and toe transition, among other features, are the main issues discussed hereafter.

The design conditions should be defined on the basis of the required level of safety, being dependent on the hydrology, on the reservoir storage capacity, on the occupation of the downstream areas and on the potential consequences of failure.

6.2.1 Site conditions

Site conditions will determine the availability of space for an intervention, the availability of material for dam construction, the foundation quality, the downstream riverbed adequacy for energy dissipation and the risk associated to flooding of downstream areas. These issues will restrain considerably the alternatives for embankment constitution (material, slope, height, internal constitution, etc.) and for overflow energy dissipation. Moreover, road access might play an important role in the definition of design alternatives and construction procedures.

6.2.2 Hydrology

Depending on the schemes characteristics the overflow lining can be used either as a main spillway or as an auxiliary spillway. Its crest elevation, crest length and unit discharge are closely depending on the reservoir capacity, on the existing freeboard (if any) and on the incoming floods.

Estimation of the design flood depends on the scheme's purpose, catchment characteristics (surface, hydrographic network density, infiltration, land occupation, etc.), rainfall characteristics, existing hydrological data records (extension, quality, consistency, observed flood events, etc.), downstream conditions and associated risk to flooding. Lastly, the hydrological studies will depend on the chosen/available hydrological methods and its interpretation. Overflow events should be analysed in what concerns their magnitude (discharge peak, volume, time of rise, etc.), their duration and their frequency.

Once a series of incoming events (with associated estimates of frequency) has been identified, flood routing should be made for different spillway configurations (crest length, crest shape, crest width, crest elevation), in quest for the best alternative in terms of flood storage (and delay) and of spillway's design unit discharge.

6.2.3 The design unit discharge vs. crest dilemma

Definition of spillway crest characteristics is always a compromise. On the one hand, crest elevation defines the normal operational reservoir level for non-gated spillways. It defines the normal storage volume, the evolution of reservoir level rise during flood events and contributes to the definition of the overflow head.

On the other hand, the crest width has direct implications on the channel width, on the visual observation conditions of embankment behaviour and safety assessment, and on the unit discharge. A larger crest is likely to mean a larger channel, supposedly more costly, but lower unit discharge (for the same crest elevation) and lower loads on the lining. Smaller lining elements can be envisaged. Moreover, to such a lower unit discharge corresponds, in similar conditions, lower residual energy at the toe per meter of width. If a dissipation basin is designed, it will be shorter, and eventually less deep. If energy is dissipated in the downstream riverbed, the jet impact pressures will be lower reducing the scouring potential. However, by doing a convergent section, unadvised for certain flow regimes, the cost rise associated with increased width might be reduced. These procedures reduce cost on the one side to increase it on other. Decisions are quite dependent on local conditions. Moreover, crest design is decisive in the definition of the overflow head and overflow duration, both parameters having close link with crest protection and infiltration rates and drainage efficiency.

Consider should also be the quality of the downstream foundation and the available river width in natural state. In fact, restitution conditions might reveal to be the determinant decision point, if the unit discharge is governed not by the spillways chute conditions as seen above, but by the cost of the energy dissipation device.

One decision criterion for this dilemma was found in literature, where a minimum cost per m^3 of unit discharge is adopted (Pravdivets, 1987). However, not only the initial cost of the structures should be in stake, but consider should also be the expected frequency of operation and consequent maintenance cost. Placing a vegetation cover to enhance the landscape integration of the scheme is another possibility to consider. These features are becoming more and more important in public acceptance of dam construction or rehabilitation interventions, with consequent increasing weight in the overall cost.

6.2.4 Selection of lining geometry

6.2.4.1 Stability

Element stability should be evaluated as described in Chapter 6, with the design flood unit discharge (pre-design). For extreme floods unit discharge the safety margin will be reduced. Failure might occur. Therefore, verifying stability for the safety check unit discharge should complete the pre-design. In these conditions, the final safety factor should be at least 1.0.

6.2.4.2 Construction and operation

Selection of a lining's geometry depends also on construction and operation demands. For an equal geometry, larger elements (and higher discharges and narrower channel width) might be more advantageous if, for instance, concrete is a non-decisive cost factor. On the other hand,

smaller elements are easier to carry in limited space construction sites. Some of the factors in stake are resumed in Table 6.1. For elements of different geometry, the relative complexity of the formwork and the production rates needed/possible might be the decisive points. The most important parameters influencing cost and lining geometry are: manpower's cost, concrete cost, access to site, possibility of machinery displacement and maintenance cost. The latter is quite dependent on construction quality, operation frequency and exposure to vandalism.

Table 6.1 - Factors affecting the choice of element size in what concern construction and operation

Size	Advantages	Disadvantages
Larger	Withstand larger discharges than other linings Less prone to vandalism Self-stable	More material needed More sensible to settlement Probably need site crane
Smaller	Easier to carry and install Flexible in view of settlement	Lighter, withstand low discharges entering domain of competition with other lining systems More blocks are needed for an equal length.

6.2.4.3 Energy dissipation

Numerous doubts still exist in what concerns energy dissipation over such macro-roughness surfaces as the ones conceived. To start, the length needed to achieve uniform conditions and the energy losses in the non-fully-aerated region are not precisely known. This length is considerably reduced for macro-roughness (see section 2.3) when compared to smooth chutes. In what concerns the energy dissipation in uniform or quasi-uniform conditions, some expressions have been developed for stepped regular macro-roughness. They might provide a first indication for design. For conditions of limit equilibrium state $h_{cr}/k_{s\ max}$, the measurements done in laboratory provide good estimates of quasi-uniform flow characteristics. A brief review of some of these laws is included in Appendix 1. Energy dissipation is out of the scope of this work. Energy dissipation and friction laws for some of the selected geometries are under study at the LCH.

6.3 CONSTRUCTION

The wall height can be estimated having the values of Y_{max} presented in Appendix 4 for each lining type as reference.

For crest design, toe design and foundation layers design, the methods reviewed in Chapter 2 are recommended. Important features have been highlighted in sections 2.4.3, 2.4.4 and 2.5.5.

A design unit discharge of about 1% of the overflow design unit discharge seems to be a fairly safe design recommendation, recalling that drainage flow was measured in the laboratory for a permeability of 10^{-3}, whereas prototype permeability are more likely to be around 10^{-5} m/s.

7 CONCLUSIONS

7.1 CONCLUSIONS

1° Several lining systems for overflow dams exist already albeit their use is still not widespread. Known linings have been used for discharges up to 3 m^3/s/m and velocities of up to 13 m/s. Only roller compact concrete systems and wedge concrete elements seem to be interesting in more stringent conditions. However, the first demand for heavy machinery displacement, site access roads and good stable foundation (dam's face), whereas the second owe their stability to a combination of complex geometry and equilibrium of pressures acting on each element.

2° The elements presented herein broaden the range of existing overflow lining alternatives. The studied lining is composed of individual concrete blocks placed on a drainage layer. These elements have simple geometry and are stable mainly due to their own weight. This system bridges both the need to withstand more severe hydraulic conditions and the demand for reliable systems that are easy to produce, to carry and to handle. Further, by allowing covering with vegetation the conceived system can even improve the scheme's integration in the landscape.

3° Experimental tests were led and showed that linings type 1, 2, 2ES and 3 should be kept as interesting solutions, as they withstood to higher, or at least equivalent, discharges than the already existing lining systems. The results from this experimental work can be used to design elements of any size and for a 1/3 slope, by use of similarity laws and of the dimensionless tools herein presented. Elements designed according with the methodology presented can also be used for slopes tender than 1/3 (V/H); the contrary is not advisable. For instance, when transposing the results for prototype scale, a lining type 2 made of 3-tons elements might withstand a unit discharge of 15 m^3/s/m.

4° The 44° negative inclined step (Type 1) is the larger element and does not present any considerable advantage in terms of stability regarding other stepped-like elements, at least, not within the range of discharges tested. The 30° negative inclined step (Type 2) is clearly the least concrete consuming solution that withstands the highest discharge. On the other hand, the 30° negative inclined step with end sill (Type 2+ES) increases considerably the cavity size and might lead to significant gains in energy dissipation for a small increase in concrete quantity. The extra formwork required might be substituted with pre-cast end sills that can be later incorporated in the system. The pyramid elements (Type 3) might represent a good alternative for not so high discharges. They create a highly complex flow pattern and presented the lowest velocity values for equal discharges. The relation between the energy dissipation efficiency of these pyramids and its concrete consume seems quite promising and should be enlightened.

5° This system is envisaged for application in the rehabilitation of existing dams, for the design and construction of low height dams, as well as for protection of cofferdams. It might be economically competitive with overflow linings that withstand similar flow conditions when concrete and manpower are not a critical cost factor. Other advantages are the low demand for maintenance, the possibility to be produced in site, with even conventional formwork, and their low vulnerability to acts of vandalism.

6° Drainage was proven to be of crucial importance for stability. It is a key feature of the lining system and should be carefully designed. Drainage efficiency is critical to prevent pressure built-up in the element's foundation and the rise of the seepage flow net inside the embankment. It should be able to drain about 1% of the lining's design unit discharge.

7° The stability model developed has proven to provide good estimates for the minimum safety factor and for increased safety margins. This model is composed of principles and assumptions, intending to simulate the physical process under study. A minimum safety factor corresponds to the observed failure conditions. Additional safety is proportional to the assumptions made. The assumptions made for the hydrostatic pressures, for the hydrodynamic forces and for air concentration are considered to have positively contributed to the development of a reasonable, coherent and consistent model.

8° It was proven to be highly interesting to design elements for limit equilibrium state conditions, based on the most unfavourable conditions tested in the laboratory (inefficient drainage layer) and further increase their safety margin by merely increasing the thickness of their foundation and not by changing the whole dimensions. It is the least concrete consuming solution.

9° During laboratory tests, measurements were taken for flow characteristics, using straightforward measuring techniques. They have proved to provide sufficient information with reasonable accuracy to allow for stability analysis and for comparison of flow pattern and flow characteristics over the conceived elements. At the present state it was more important to identify the most promising configurations regarding stability and define trends, than to exhaustively study just a particular geometry.

7.2 OUTLOOK AND FURTHER RESEARCH

Follow up research can comprise:

1. Calibration of the developed stability model can be achieved by leading experiments with elements of different roughness heights. At present, the stability model is based on one single observation and on dimensional analysis.

2. To complete the already-initiated analysis of the adequacy of using currentmeter readings to estimate velocity profiles, by making side-to-side measurements together with an optic probe. Local air concentration values and corresponding local flow velocities could thus be compared. The aim would be to develop a simple methodology to define the limits of validity of currentmeter readings and to back-compute the mean air concentration and obtain a reasonable velocity profile, without the need for expensive instrumentation.

3. To test other stability approaches, notably a Shield like approach. This approach is only meaningful if experiments with the same elements but with different roughness height are led.

4. To broaden the range of application of these linings to other slopes;

5. To characterise the pseudo-bottom created over the pyramids;

6. To develop design-assisting computation tools for flow modelling over macro–roughness linings;

7. To improve knowledge about the infiltration process and dependency of embankment stability from the seepage flow net variations, having overflow duration as one key parameter;

8. Improve the herein presented stability model's assumption in what concerned pressures in the element's foundation, by measuring pressures in the under-drain layer;

9. To test and further develop interlocking measures for lining elements, in particular for the toe and the crest blocks.

10. To test the stability of the conceived elements to flash floods, characterised by a rapid and sudden increase of the discharge;

11. To test the collapse pattern for after-first-departure conditions using unaligned joints, by fixing the halves somehow to the side walls or to the channel bottom;

12. To try another stability approach for the pyramids, where these would be substitutes by half-spheres in the stability model, for which drag and lift form factors might be available in literature. Comparison with the herein model would be interesting.

13. To evaluate the use of composite elements, for example, to test the use of expanded clay in large size blocks.

In what concerns energy dissipation and friction laws, research work is well underway at LCH (results expected in the coming year). Some of the selected geometries are being considered, not as single blocks but as part of RCC linings. Other topics included are:

a) the discussion on the applicability and relative agreement of existing formulae for friction loss computation, based on velocity measurements, over macro-roughness surfaces (as those created by the presented concrete element linings);
b) the hydraulic of flows;
c) the establishment of correlations between the energy loss for a given lining geometry and the flow characteristics.

NOTATION

a	$[MT^{-2}]$	-	Auxiliary variable for equation 5.24
A	$[L^2]$	-	Cross-section area of the element
A_D	$[L^2]$	-	Drag force application surface, projected in perpendicular direction to force
A_L	$[L^2]$	-	Lift force application surface, projected in perpendicular direction to force
A_{Hid}	$[L^2]$	-	Surface of wind incidence in multi-span roofs in the load case of local pressures.
b	$[MLT^{-2}]$	-	Auxiliary variable for equation 5.24 (with drainage/without drainage)
b	[L]	-	Element width
c	$[ML^2T^{-2}]$	-	Auxiliary variable for equation56.24
C	[-]	-	Discharge coefficient (in equations 2.2, 3.1, 3.2 and 3.3)
C	[-]	-	Local air concentration of skimming flow (in equation 3.4)
C	[-]	-	Drainage reduction factor (in equation 5.10)
C_D	[-]	-	Drag coefficient
C_L	[-]	-	Lift coefficient
C_{mean}	[-]	-	Mean air concentration
C_{pe}	[-]	-	Wind pressure coefficient
D	[L]	-	Diameter of pipe
D_h	[L]	-	Hydraulic diameter
D_{15}	[L]	-	Characteristic diameter of a grain sample corresponding to 15 percent of retained material at a thieve openings of this size – the capital D corresponds to a drainage layer of larger granular size.
d_{85}	[L]	-	Characteristic diameter of a grain sample corresponding to 15 percent of retained material at a thieve openings of this size – the small d corresponds to a drainage layer of smaller granular size.
D_{84}	[L]	-	Characteristic diameter of a grain sample corresponding to 84 percent of retained material at a thieve openings of this size.
Dh	[L]	-	Height of body in Figure 6.6
$f_{\text{Darcy-Weisbach}}$	[-]	-	Darcy-Weisbach friction factor
F_D	$[MLT^{-2}]$	-	Hydrodynamic drag force
F_{Hid}	$[MLT^{-2}]$	-	Hydrodynamic force (computed with wind pressure coefficients)
F_L	$[MLT^{-2}]$	-	Hydrodynamic lift force
F_R	$[MLT^{-2}]$	-	Hydrodynamic resultant force
F_L*	$[MLT^{-2}]$	-	Equivalent hydrodynamic lift force applied in the gravity centre
F_D*	$[MLT^{-2}]$	-	Equivalent hydrodynamic drag force applied in the gravity centre
F*	$[MLT^{-2}]$	-	Resultant hydrodynamic force in x-direction
$(F^*)_{ks>ksmin}$	$[MLT^{-2}]$	-	Equivalent hydrodynamic force in x-direction for a roughness height larger than the minimum roughness height of the given discharge q (below LES conditions).
g	$[LT^{-2}]$	-	Gravitational acceleration
h	[L]	-	Flow depth
H	[L	-	Specific energy head
h_p	[L]	-	Element type 3 roughness height
h_{cr}	[L]	-	Critical flow depth (rectangular section)
h_d	[L]	-	LCH facility step height
h_f	[L]	-	Element foundation thickness
h_{obs}	[L]	-	Mean observed flow depth
h_s	[L]	-	Element type 2+ES end sill height
h_w	[L]	-	Equivalent clear-water depth
h_{bottom}	[L]	-	Depth of bottom surface of body in Figure 5.6
h_{top}	[L]	-	Depth of top surface of body in Figure 5.6

$(h_w)_{ksmin\_q}$	[L]	-	Equivalent clear-water depth computed for the element of minimum size (k_{smin}) for a given discharge q
$(h_{w\,max})_q$	[L]	-	Maximum equivalent clear-water depth for a given discharge q
k	[L]	-	Equivalent absolute roughness
k_s	[L]	-	Roughness height
k_{smin}	[L]	-	Minimum roughness height required for a given q and SF=1.0
K^*	[-]	-	Coefficient for hydrodynamic force F^*
$(K^*)_{ksmin}$	[-]	-	Coefficient for hydrodynamic force F^* computed for the minimum roughness height of the given discharge q at LES conditions
L	[L]	-	Upstream overflow *Bazin* weir crest width (equation 3.4)
L	[MLT^{-2}]	-	Hydrostatic Lift
L_B	[L]	-	Element longitudinal length
L_Δ	[MLT^{-2}]	-	Hydrostatic lift corresponding to the additional foundation thickness
M_{OP}	[ML^2T^{-2}]	-	Moment at point OP
$M_{stabilising}$	[ML^2T^{-2}]	-	Stabilising moment created at OP
$M_{overturning}$	[ML^2T^{-2}]	-	Overturning Moment created at OP
$(M_{stabilising})_\Delta$	[ML^2T^{-2}]	-	Stabilising moment created at OP by additional foundation thickness
n_{Manning}	[$L^{1/2}T^{-1}$]	-	Manning's roughness parameter
p	[L]	-	Reservoir depth immediately upstream of the overflow weir
Q	[L^3T^{-1}]	-	Flow discharge
q_w	[L^2T^{-1}]	-	Unit discharge
q_{max}	[L^2T^{-1}]	-	Maximum unit discharge withstood by an element weighting 30 kN.
R_Z	[MLT^{-2}]	-	Component of the resultant of acting forces in the z-axis (perpendicular direction)
R_X	[MLT^{-2}]	-	Component of the resultant of acting forces in the x-axis (longitudinal direction)
s	[L]	-	LCH facility step length
s_s	[L]	-	Element type 2+ES end sill length
S_{mean}	[L]	-	Mean observed surface level
S_{max}	[L]	-	Maximum observed surface level
$SF1$	[-]	-	Minimum safety factor
$SF2$	[-]	-	Recommended safety factor
SF^*	[-]	-	Final safety factor after refining of foundation thickness
U_w	[LT^{-1}]	-	Mean clear-water velocity
U_{LES}	[LT^{-1}]	-	Average velocity computed from measurements for LES conditions
U_{prot}	[LT^{-1}]	-	U_{LES} at prototype scale
$(U_w)_{ksmin\_q}$	[L]	-	Mean clear-water velocity computed for the element of minimum size (k_{smin}) for a given discharge q
$(U_{w\,max})_q$	[L]	-	Maximum mean clear-water velocity for a given discharge q
V_{cr}	[LT^{-1}]	-	Critical flow velocity of rectangular section
V_v	[LT^{-1}]	-	Mean velocity of coloured front propagation measured by video recording
W_w	[MLT^{-2}]	-	Weight of equivalent static water column above element
W_x	[MLT^{-2}]	-	Component of element's self weight in x-axis (longitudinal direction)
W_z	[MLT^{-2}]	-	Component of element's self weight in z-axis (perpendicular direction)
$W_{\Delta x}$	[MLT^{-2}]	-	Component of additional foundation's self weight in x-axis (longitudinal direction)
$W_{\Delta z}$	[MLT^{-2}]	-	Component of additional foundation's self weight in z-axis (perpendicular direction)
x_A	[L]	-	x-co-ordinate of the hydrodynamic forces application point A at LES conditions
x_G	[L]	-	x-co-ordinate of element's gravity centre
x_{OP}	[L]	-	x-co-ordinate of the overturning point OP
Y_{mean}	[L]	-	Mean observed flow depth
Y_{max}	[L]	-	Maximum observed flow depth
Y_{90}	[L]	-	Flow depth in skimming regime at which the local air concentration is 90%
z_A	[L]	-	z-co-ordinate of the hydrodynamic forces application point A at LES conditions
z_{OP}	[L]	-	z-co-ordinate of the overturning point OP
z_G	[L]	-	z-co-ordinate of element's gravity centre
α	[-]	-	Angle of slope with horizontal reference
β	[-]	-	Angle of sloped upstream surface of element type 1 with dam face's slope
Δ	[L]	-	Additional foundation thickness

ε	[-]	-	Relative roughness
λ_L	[-]	-	Scale factor for length in Froude's similarity
θ	[-]	-	Angle of triangular weir opening
ρ	$[ML^{-3}]$	-	Fluid density
ρ_w	$[ML^{-3}]$	-	Water density
ρ_s	$[ML^{-3}]$	-	Element density
τ	$[ML^{-1}T^{-2}]$	-	Shear stress

ABBREVIATIONS

LCH	-	Laboratory of Hydraulic Constructions
EPFL	-	Swiss Institute of Technology - Lausanne

REFERENCES

(*) not consulted directly by the author

ALBERT, R., GAUTIER, J. (1992) – "Spillways founded on earth fill /*Evacuateurs fondés sur remblai*", La Houille Blanche, N°2, 3, pp. 147-157.

ANDRE, S. (2000) - "Hydraulics of stepped spillways /*Hydraulique des évacuateurs de crue en escalier*", "*Wasser, energie,luft –eau, énergie,air"*, N°7/8, pp. 199-202.

ANDRE, S, BOILLAT, J.-L., SCHLEISS, A. (2001) – « High velocity two-phase turbulent flow over macro-roughness stepped chutes: Focus on dynamic pressures », Proceedings of the 2001 International Symposium on Environmental Hydraulics (in CD).

AKSOY, SAHAP. (1973) - "Fluid force on a sphere near a solid boundary" IAHR Congress in Instambul, A29, pp. 217-224.

BAKER, R. (1989) – "Pre-cast concrete blocks for dam spillways", Water Power & Dam Construction, pp. 60-66, July.

BAKER, R. (2000) – "Field testing of Brushes Clough stepped block spillway", in *Hydraulics of Stepped Spillways*, Edited by Minor & Hager, pp.13-20, Balkema, Rotterdam.

BATHURST, J.C. (1978) - "Flow resistance of large-scale roughness", Journal of the Hydraulics Division, Vol. 104, N° HY12, December, pp. 1587-1603.

BOES, R. M. (2000) – "Scale effects in modelling two-phase stepped spillway flow ", in *Hydraulics of Stepped Spillways*, Edited by Minor & Hager, pp.53-60, Balkema, Rotterdam.

BOES, R. M. (2000) – "Two-phase flows and energy dissipation over stepped spillways / *Zweiphasenströmung und energieumsetzung an Grosskaskaden* », Technical Publication n°166, VAW, Swiss Federal Institute of Technology, Zurich.

BOSSHARD, M (1991) – "Overflow small dams /*Überflutbarkeit kleiner Dämme*", VAW, Swiss Federal Institute of Technology, Zurich.

CHANSON, H. (1994) – "Hydraulic design of stepped cascades, channels, weirs and spillways », Pergamon.

DUBOIS, J. (1998) – "Hydraulic behaviour and modelling of surface runoff /*Comportement hydraulique et modélisation des écoulements de surface"*, PhD Thesis, Communication 8, LCH-EPFL, Lausanne.

DUBOIS, J. (2000) – "Implementation of resistance laws / *Implémentation des lois de comportement* », Lecture notes from the Postgraduate studies in Hydraulic Schemes, Lausanne.

EUROCODE 1 (1993) – "Basis of Design and Actions on Structures. Part 2.3: Wind Actions", CEN/TC250/SC1.

FRITZ, H., HAGER, W. (1998) – "Hydraulics of embankment weirs", Journal of Hydraulic Engineering, pp. 963-971, September.

FRIZELL, K.H., MEFFORD, B.W., VERMEYEN, T.B., MORRIS, D. I (1996) – "US5544973: Concrete step embankment protection", Delphion Intellectual Property Network, Patent Plaques, pp. 1-8, (http://www.delphion.com).

FRIZELL, K.H., MATOS, J., PINHEIRO, A.N. (2000) – "Design of concrete stepped overlay protection for embankment dams", in *Hydraulics of Stepped Spillways*, Edited by Minor & Hager, pp.179-186, Balkema, Rotterdam.

GRAF, W.H., ALTINAKAR, M. (1998) - "Fluvial Hydraulics – Flow and transport processes in channels of simple geometry", Wiley & Sons.

HAGEN, V.K. (1982) – "Re-evaluation of design floods and dam safety", XIV ICOLD Congress on Large Dams, Q.52 / R.29., pp. 475-491, Rio de Janeiro.

*HARTUNG, F., SCHEUERLEIN, H (1970) - "Design of overflow rock fill dams" XV ICOLD Congress on Large Dams, Q.36 R.35, pp. 578-598, Montreal.

HENDERSON, F. M. (1966) - "Open Channel Flow", MacMillan, New York.

HEWLETT, H.W.M., BAKER, R., MAY, R.W.P., PRAVDIVETS, Y. (1997) – "Design of stepped-block spillways", Special publication 142, Construction Industry Research and Information Association (CIRIA).

ICOLD (1984) – "River control during dam construction", Bulletin 48.

ICOLD (1993) – "Reinforced rock fill and reinforced fill for dams", Bulletin 89.

ICOLD (1995) – "Dam Failures – Statistical Analysis", Bulletin 99.

ICOLD (1997) – "Dams less than thirty metres high - cost savings and safety improvements", Bulletin 109.

*IZBACH, S.V., KHALDRE, K.Y. (1959) – "Hydraulics of river channel closure", Butterworths, London.

LAFITTE, R. (1985) – " Rehabilitation of dams to ensure safety / *Mesures pour renforcer la securité des barrages*", XV ICOLD Congress on Large Dams, GR. Q.59, pp. 974-1003, Lausanne.

LEMPERIERE, F. (1993) – "Dams that have failed by flooding: an analysis of 70 failures", Water Power & Dam Construction, pp.19-24, September/October.

MANSO, P.A., SCHLEISS, A.J. (2002). "Stability of linings by concrete elements for surface protection of overflow earthfill dams", paper submitted to the Canadian Journal of Civil Engineering.

MATOS, J. (1999) – "Air entrainment and energy dissipation on stepped spillways/ *Emulsionamento de ar e dissipação de energia do escoamento em descarregadores em degraus* », Research Report, IST, Lisbon.

MATOS, J. (2000) – "Hydraulic design of stepped spillways over RCC dams", in *Hydraulics of Stepped Spillways*, Edited by Minor & Hager, pp.187-194, Balkema, Rotterdam.

MATOS, J., QUINTELA, A., SANCHEZ JÚNY, M., DOLZ, J. (2000) – "Air entrainment and safety against cavitation damage in stepped spillways over RCC dams", in *Hydraulics of Stepped Spillways*, Edited by Minor & Hager, pp. 69-76, Balkema, Rotterdam.

MARTINS, R., MARANHA DAS NEVES, E. (1993) – "Pervious rock fill dams", Technical Communication n° 790, LNEC (*Laboratório Nacional de Engenharia Civil*), Lisbon.

MARTINS, R., VISEU, T. (1994) – "Unconventional flood discharge / *Descarga não convencional de cheias*", communication at II APRH Water Congress, Lisbon.

MARTINS, R. (1996) - "Design criteria for rock fill structures subjected to flow", Technical Communication N° 807, LNEC -Laboratório Nacional de Engenharia Civil, Lisbon, 14 p.

MAYNORD, S.T., RUFF, J.F, ABT, S.R. (1989) – "Riprap Design", JHE, Vol. 115, No. 7, July, pp. 937-949.

MCLEAN, F.G., HANSEN, K.D. (1993) – "Roller compacted concrete for embankment overtopping protection", Proc. Conference on Geotechnical Practice in Dam Rehabilitation, ASCE, New York, pp. 188-209.

MINOR, H.-E. (1998) - "Report of the European R&D Working Group "Floods", in "Dam Safety", Edited by BERGA, L., A.A. Balkema, Rotterdam.

NEILL, C. R. (1967) – "Mean velocity criterion for scour of coarse uniform bed-material", Proceedings of the XII Congress of the IAHR, Vol. I, C6, pp. 46-54.

NIGUS, L.A., STEIGER, K.M., MARTI, C. (2000) – "Ashton stepped spillway - design and construction", in *Hydraulics of Stepped Spillways*, Edited by Minor & Hager, pp.35-41, Balkema, Rotterdam.

ODENDAAL, W.A., VAN ZYL, F.C - "Failure of a cofferdam due to overtopping" XII ICOLD Congress on Large Dams, Q.49 R.11, pp. 141-156, New Delhi, 1979.

OLIVIER, H. - "Through and overflow rock fill dams – new design techniques" Proceedings Institution of Civil Engineers, Paper n° 7012, 36 (March), pp. 433-471, London, 1967.

*PARKIN, A.K. - "Rock fill dams with built-in spillways. Hydraulic characteristics" Water Research Foundations of Australia, Bulletin No. 6, March, 1943.

PEYRAS, L., ROYET, P., DEGOUTTE, G. (1991) – "Flows and dissipation of energy on gabion weirs / *Ecoulement et dissipation sur les déversoirs en gradins de gabions*", La Houille Blanche, N° 1, pp.37-47.

PINHEIRO, A.N., RELVAS, A.T. – "Non-conventional spillways over earth dams. The present and the future of their application in Portugal / *Descarregadores de cheias não convencionais sobre barragens de aterro. O presente e o futuro da sua aplicação em Portugal*", Recursos Hídricos, APRH, Vol. 20, pp.19-26, Lisbon, 1998.

PINHEIRO, A.N., FAEL, C. (2000) – "Nappe flow in stepped channels – occurrence and energy dissipation", in « Hydraulics of Stepped Spillways », Edited by Minor & Hager, pp.119-127, Balkema, Rotterdam.

POWLEDGE, G.R., SVEUM, D.L. (1988) - "Overtopping embankment dams – an alternative in accommodating rare floods?" XVI ICOLD Congress on Large Dams, Q.63 R.35, pp. 555-581, San Francisco.

POWLEDGE, G.R., RALSTON, D.C., MILLER, P., CHEN, Y.H., CLOPPER, P.E., TEMPLE, D.M. (1989) - "Mechanics of overflow erosion on embankments. I: research activities", Journal of Hydraulic Engineering, Vol. 115, N° 8, , August, pp. 1040-1055.

POWLEDGE, G.R., RALSTON, D.C., MILLER, P., CHEN, Y.H., CLOPPER, P.E., TEMPLE, D.M. (1989)- "Mechanics of overflow erosion on embankments. II: hydraulic and design considerations", Journal of Hydraulic Engineering, Vol. 115, N° 8, pp. 1056-1075, August.

PRAVDIVETS, Y.P. (1987) - "Industrial design of an earth overflow dam", Gidrotekhnicheskoe Stroitel'stvo, N°12, pp. 15-18, December (translated by Plenum Publishing Corporation 1988).

PRAVDIVETS, Y.P., BRAMLEY, M.E. (1989) - "Stepped protection blocks for dam spillways", Water Power & Dam Construction, pp. 49-56, July.

PRAVDIVETS, Y.P., SLISSKY, S.M. (1981) - "Passing floodwaters over embankments dams", Water Power & Dam Construction, pp. 30-32, July.

SAMORA, M.G. (1993) - "Use of rip-rap for channel protection / *Utilização de enrocamento para protecção de canais* ", Master Thesis, Universidade Técnica de Lisboa, Lisbon.

SÁNCHEZ JUNY, Martí (2001) – "Hydraulic behaviour of stepped spillways in RCC dams. Analysis of pressure fields/*Comportamento hidráulico de los aliviaderos escalonados en presas de hormígon compactado. Análisis del campo de presiones*", PhD thesis, Universitat Politècnica de Catalunya, Spain

SÁNCHEZ JUNY, Martí (2000) - "Pressure field in skimming flow over a stepped spillway ", in « Hydraulics of Stepped Spillways », Edited by Minor & Hager, pp.137-146, Balkema, Rotterdam.

SCHNITTER, N. J. (1994) - "A History of Dams – The useful pyramids", A.A. Balkema, Rotterdam, Brookfield.

SERAFIM, J. LAGINHA (1981) - "Safety of dams judged from failures", Water Power & Dam Construction, pp. 32-35, December.

SINGH, B., VARSHNEY, R.S. (1995) - "Engineering for embankment dams", A.A. Balkema, Rotterdam, Brookfield.

STROBL, T (2000) - "Embankment dams", Notes of Postgraduate Course in Hydraulic Schemes, Swiss Institute of Technology (EPFL), Lausanne.

TIMBLIN Jr., L.O, GREY, P.G., MORRISON, W.R. (1988) - "Emergency spillways using geomembranes" XVI ICOLD Congress on Large Dams, Q.61 R.28, San Francisco.

WHITTAKER, J., JÄGGI, M. (1986) – "Protection of river beds with large boulders / *Blockschwellen*", Communication n° 81, VAW, Zurich.

WOOD, I. R. (1991) – "Air entrainment in free-surface flows", IAHR Hydraulic Structures Design Manual 4 . Balkema, Rotterdam, The Netherlands.

YALIN (1971) – "Theory of Hydraulic Models", MacMillan.

ACKNOWLEDGEMENTS

Those who quest for knowledge
might occasionally have the blessing of reaching it,
though never really realising this privilege,
so overwhelming is their thirst.

I wish to thank the *Fundação para a Ciência e Tecnologia* (Portugal) for their financial support, in the form of the scholarship PRAXIS XXI / BM / 20621 / 99, which allowed for 12 months of study and active research. I did my best to honour it.

The work was led at the Laboratory of Hydraulic Construction of the Swiss Institute of Technology where I came about a group of enthusiastic and pragmatic research engineers. I would like to thank all LCH collaborators for their suggestions. I address a particular thanks to my Supervisor, Prof. Anton Schleiss, who welcomed me and supported this research work at the Laboratory. A word is due also to Marc Soldini, Louis Schneiter and Marc-Eric Pantillon for their collaboration.

This dissertation is the ending stage of an enriching 2-year experience in the Postgraduate Studies on Hydraulic Schemes, during which I met remarkable individuals of very different backgrounds with whom I learned considerably. To them: "*um grande abraço*".

Many colleagues and friends have contributed with their suggestions, comments and remarks. I thank them with my friendship and retribution.

To my family I address my deepest feelings. They were restless in their warm support and wise advice. This work is dedicated to them. *Muito obrigado*.

Lausanne, 20 September 2001 (reviewed in June 2002 for publication)

Appendix 1: Review of friction laws for skimming flow over a macro-roughness surface

For skimming flow over a macro-roughness surface the expressions used for smooth surfaces have are no longer applicable; they have either to be modified or corrected to account for the high air content and for an increasing role of the form friction. The resistance on the pseudo-bottom can be considered conceptually equivalent to a certain roughness.

Former studies on stepped surfaces and on riprap surfaces have led to the establishment of friction laws still not unanimously accepted or widely applied and verified. These laws are suited for quasi-uniform flow conditions, for which the unit head loss, the hydraulic gradient and the pseudo-bottom slope are almost identical. Their use is the state of the art practice. A resume is presented in the Table A.1.

The presented laws where derived from the Colebrooke-White expression for free-surface flow and use the Darcy-Weisbach friction factor. In fact, in turbulent rough flow the friction factor f is proportional to the square of the mean flow velocity. Most design engineers rather use the empirical Gauckler-Manning-Strickler law, so commonly used for river hydraulics. However, this formula has proven to be valid only for a single value of relative roughness ($\varepsilon = 0.00917$), even if its straightforward application provides results with a reasonable error, less than 5 per cent, for most of the river hydraulic problems (Dubois, 1998, 2000). For the design of conventional smooth spillways the Colebrooke-White expression for free-surface flow has been adopted.

In conclusion, due to the inexistence of a clearly accepted friction law for skimming flow over macro-roughness engineers should compare several alternative laws, for instance those presented in Table A.1, remembering their limitations in what concerns form friction and air entrainment.

Table A.1 – Review of friction laws for research fields related with flow over macro-roughness

	Friction laws	**Domain**	**Reference**
Macro-roughness (general)	$\sqrt{\frac{8}{f}} = 5.62\log(\frac{d}{D_{84}}) + 4$ or, transformed as, $\frac{1}{\sqrt{f}} = -1.987\log(\frac{D_{84}}{5.15d})$		Bathurst (1985) Dubois (1998)
	$\sqrt{\frac{8}{f}} = 5.62\log(\frac{d}{D_{84}}) + 3.13 \cdot s^{-0.613}$ s- density of elements in section		Dubois (1998)
Stepped surfaces	$f = 8gd\sin\theta / U^2$	Uniform flow	Mateos Iguácel *et al.* (2000)
	$f = 8gD_h\sin\theta / U_w^{\ 2}$	U_w, mean water velocity Slopes of 22°, 26.6°	Frizell *et al.,* Matos, Boes, Chamani (2000)
Open channel Flow	$\frac{1}{\sqrt{f}} = 2.03\log(\frac{4}{\varepsilon}) + 2.2$	Turbulent flow Re>2x 10^{-4}	GRAF et *al.* (1998)
	$\sqrt{\frac{8}{f}} = 5.62\log(\frac{d}{D_{84}}) + 3.25$	Rough turbulent flow, for large channels and $d/D_{50} \leq 10$	Adapted from GRAF et al. (1998), equation 3.13c
Rip-rap surfaces	$\frac{1}{\sqrt{f}} = 2(1 - 0.8\varepsilon)\log(\frac{1.5}{\varepsilon})$	High relative roughness	Samora (1993) Martins (1996)

Appendix 2: Froude similarity scale factors

Condition of dynamic similarity for flow in model and prototype exclusively governed by gravity

Parameter	Symbol	Dimension	Scale factor	
Length	l	L	λ_L	10
Velocity	u	LT^{-1}	$\lambda_V=\lambda_L^{1/2}$	3.16
Time	t	T	$\lambda_t=\lambda_L^{1/2}$	3.16
Unit discharge	q	L^2T^{-1}	$\lambda_q=\lambda_L^{3/2}$	31.62
Discharge	Q	L^3T^{-1}	$\lambda_Q=\lambda_L^{5/2}$	316.23
Mass	m	M	$\lambda_m=\lambda_L^3\lambda\rho$	1000
Area	A	L^2	$\lambda_A=\lambda_L^2$	100
Volume	V	L^3	$\lambda_V=\lambda_L^3$	1000
Acceleration	a	LT^{-2}	1	10
Angular velocity	w	T^{-1}	$\lambda_w=\lambda_L^{-1/2}$	0.32
Force	F	MLT^{-2}	$\lambda_F=\lambda_L^3\lambda\gamma$	1000
Specific pressure	p	$ML^{-1}T^{-2}$	$\lambda_p=\lambda_L\lambda\gamma$	10
Impulse and momentum	i	MLT^{-1}	$\lambda_i=\lambda_L^{7/2}\lambda\rho$	3162.28
Energy and work	e	ML^2T^{-2}	$\lambda_e=\lambda_L^4\lambda\gamma$	10000
Power	N	ML^2T^{-3}	$\lambda_N=\lambda_L^{7/2}\lambda\gamma$	3162.28

For $\gamma_p=\gamma_m=\gamma$ then $\lambda\gamma=\lambda\rho$

For the same liquid in model and prototype $\lambda\gamma=\lambda\rho=\lambda\mu=\lambda\nu=1$

Appendix 2 (suite): Element Catalogue (drawings and photos)

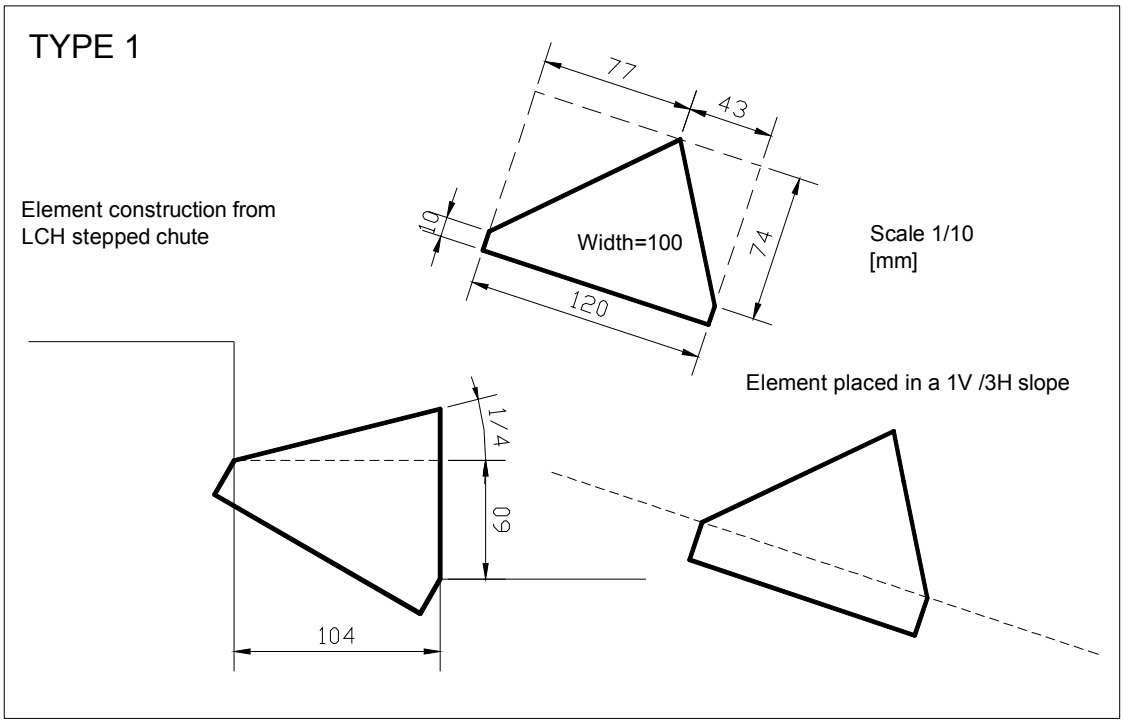

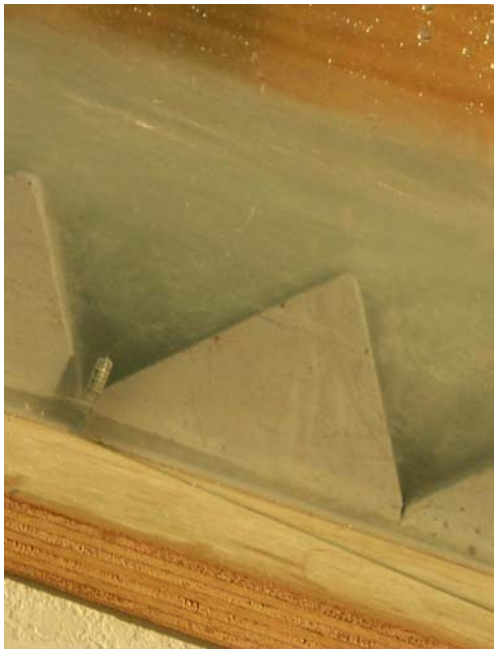

TYPE 2

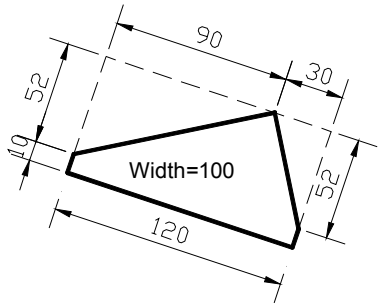

Element construction from
LCH stepped chute

Scale 1/10
[mm]

Element placed in a 1V /3H slope

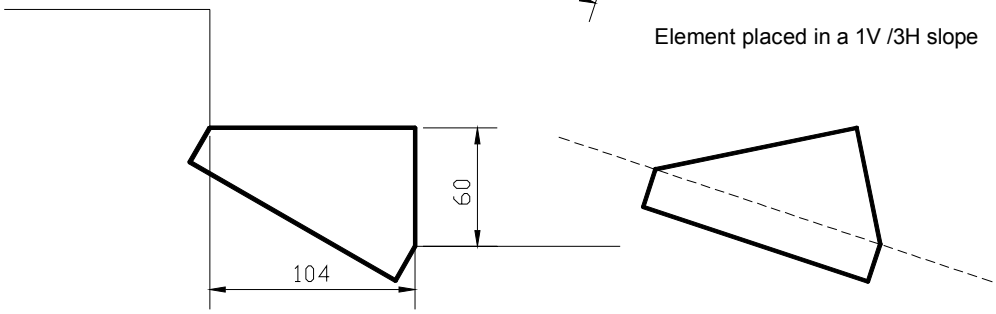

TYPE 2 + ES

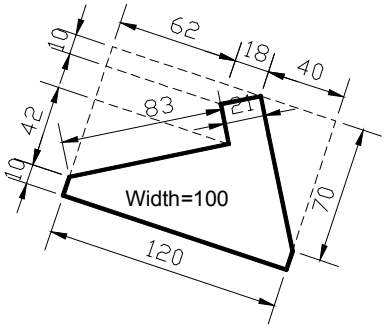

Element construction from
LCH stepped chute

Scale 1/10
[mm]

Element placed in a 1V /3H slope

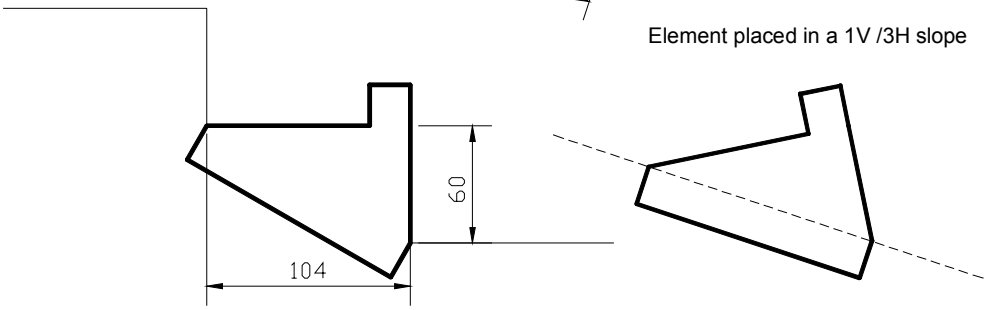

TYPE 3

Cross section at highest point

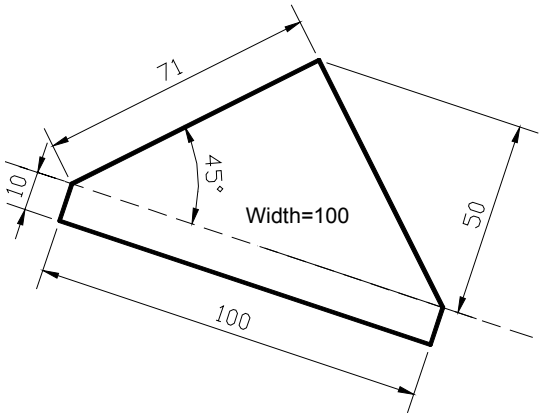

3D schematic view

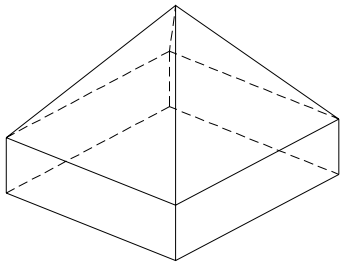

Scale 1/10
[mm]

Appendix 3 – Experimental facility

Photo A3.1 – Entrance of channel. View from downstream. Reach of metallic triangular macro-roughness in the foreground and the dividing wall (inside the head tank) in the background.

Photo A3.2 – Entrance of channel. View from upstream: dividing wall in the foreground; downstream zone of head tank; the overflow weir with rounded approach transitions and the chute (with metallic triangular macro-roughness)

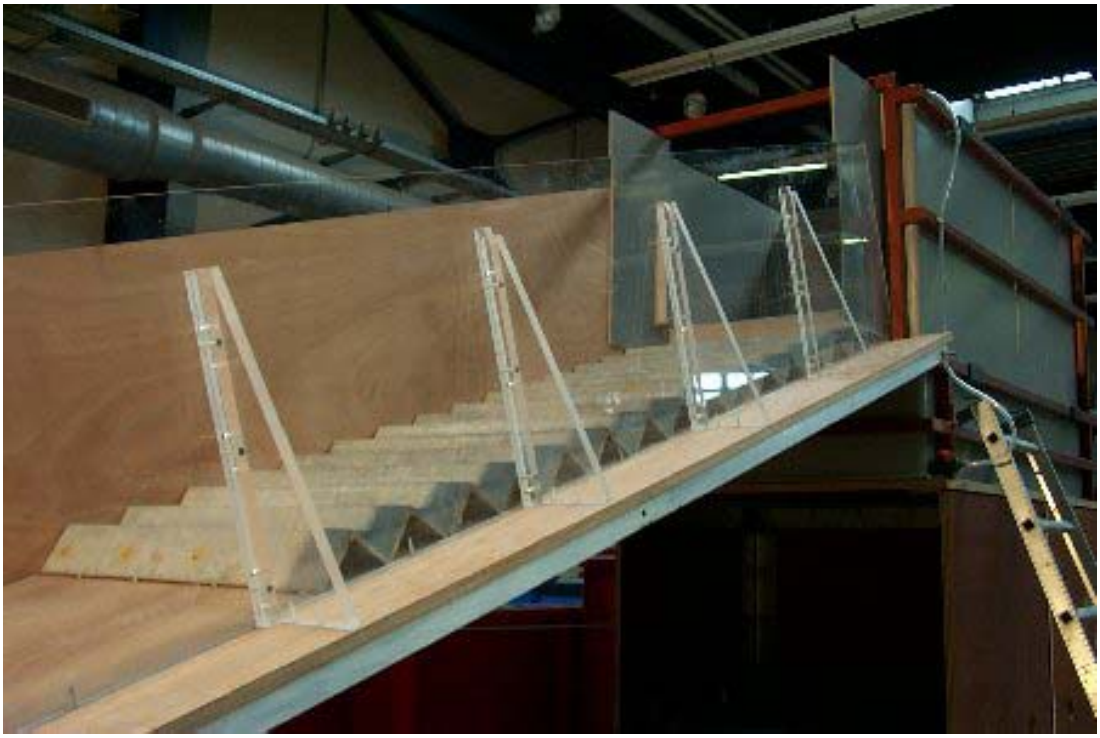

Photo A3.3 – Metallic profiles fixed at the bottom of the chute, creating a triangular macro-roughness surface. Triangular reinforcements for Plexiglas side wall

Photo A3.4– View of toe block: large wooden beam fixed to the channel bottom. The joints were water-tightened with (yellow) putty.

Photo A3.5 – General view of drainage devices, including the drainage layer (of blue) foam, the wooden transition and the collecting PVC basin.

APPENDIX 4. 1 - Experiment n° 1 – 44° NEGATIVE INCLINED STEP (1, without drainage, aligned joints)

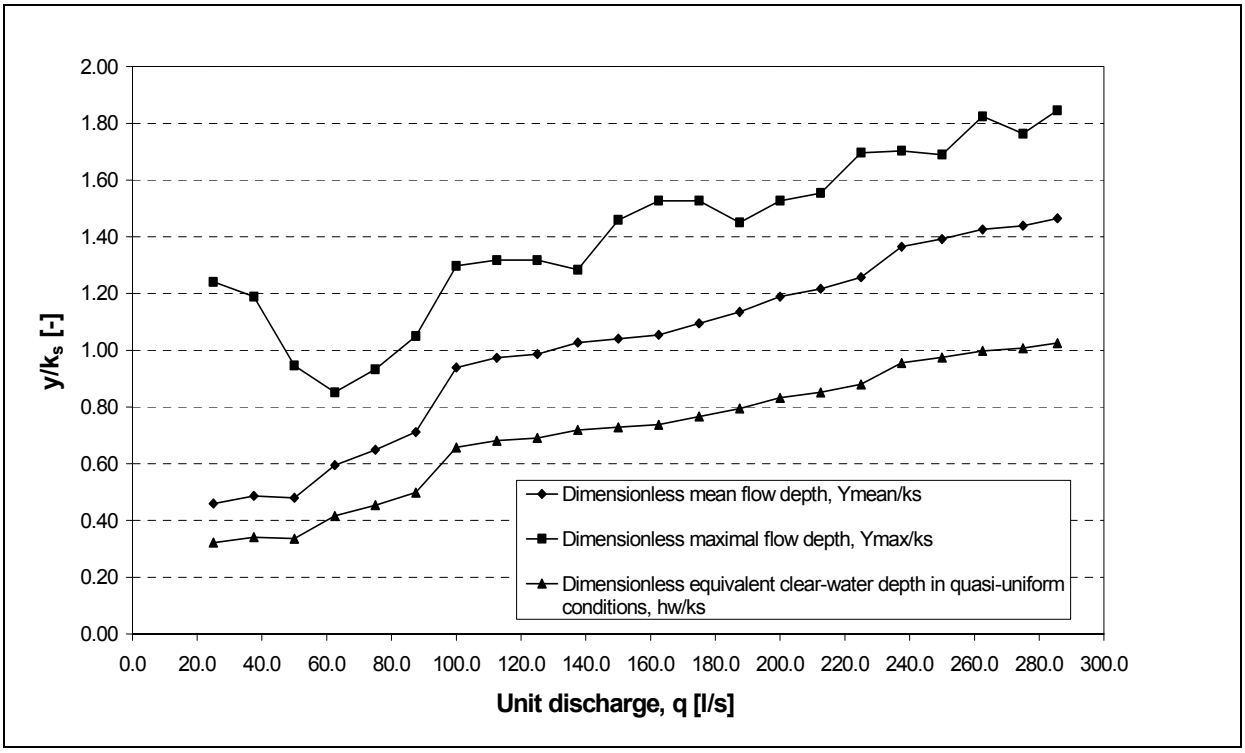

Figure A4.1a – Dimensionless- mean flow depth Y_{mean}/k_s, maximum flow depth Y_{max}/k_s and equivalent Clear-water depth h_w/k_s (with C_{mean}=0.30)

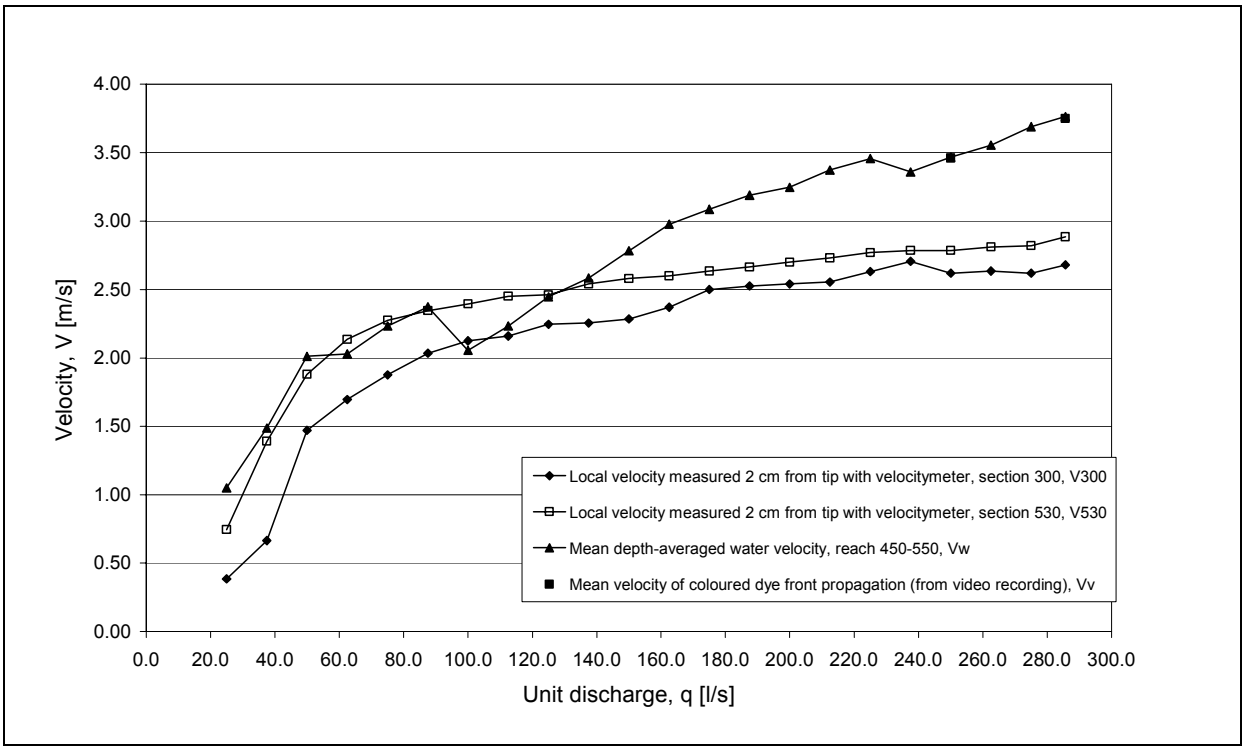

Figure A4.1b - Local velocity measurements using currentmenter, section 300 and 530, mean flow velocity estimated from coloured dys propagation (video), and computed clear-water mean depth-averaged velocity.

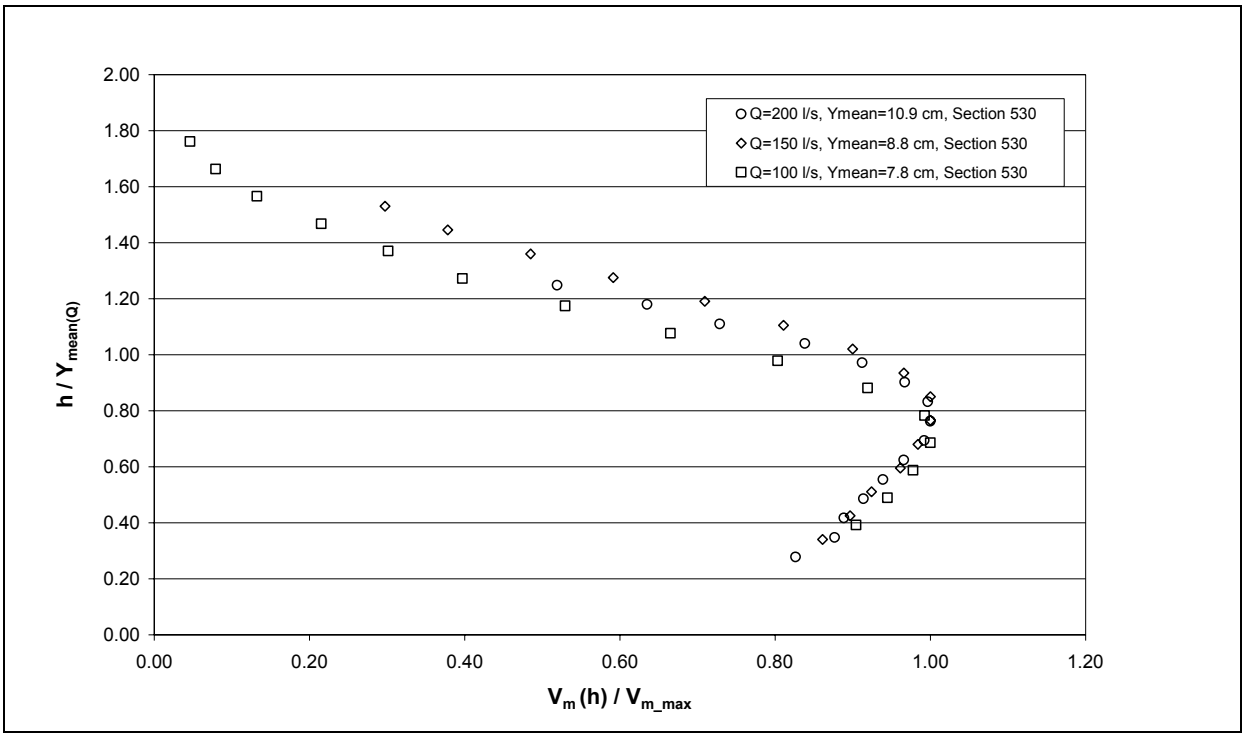

Figure A4.1a - Dimensionless velocity profiles for 100, 150 and 200 l/s at section 530. Water velocity measurements made using water currentmeter (Vm) throughout the depth. Flow depth rendered dimensionless through division by the observed mean flow depth for the given flow ($Ymean_Q$). Type 1 element (ks=74 mm), 1/3 channel slope (α=18.43°).

APPENDIX 4. 1 (suite) - Experiment n° 3 – 45° PYRAMIDS (3, without drainage, unaligned joints)

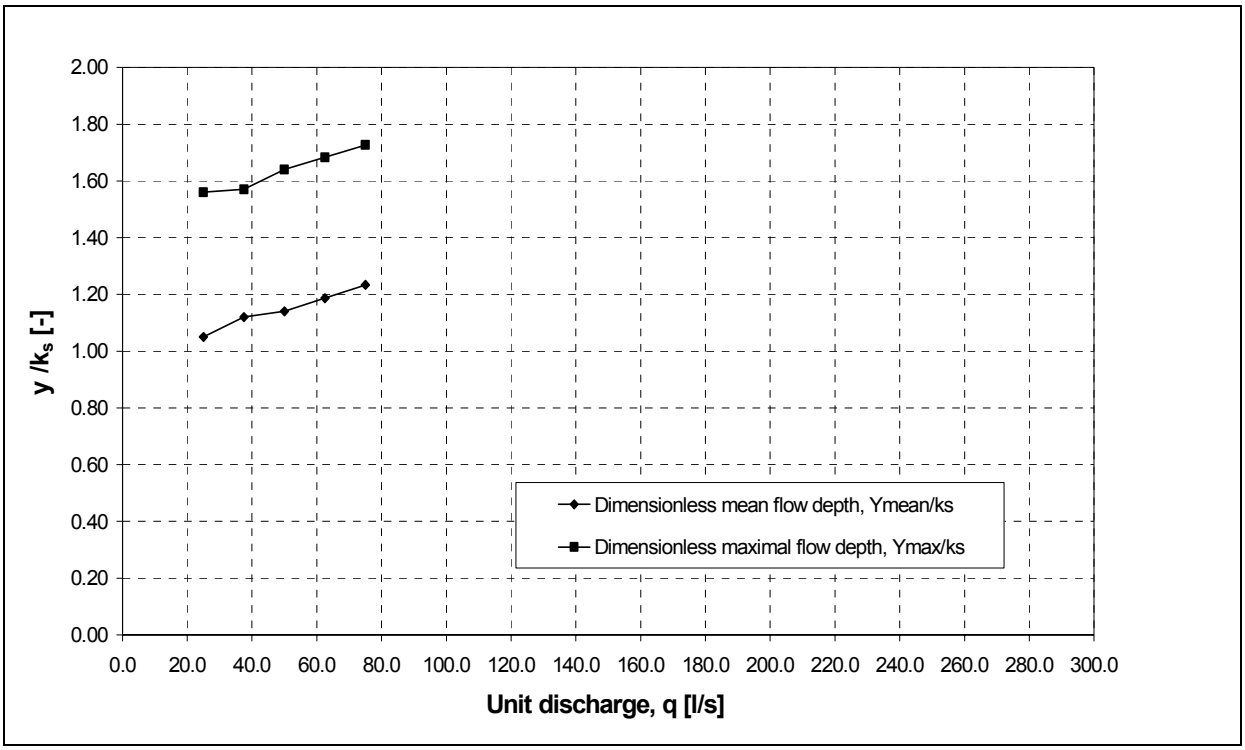

Figure A4.3a – Dimensionless- mean flow depth Y_{mean}/k_s and maximum flow depth Y_{max}/k_s.

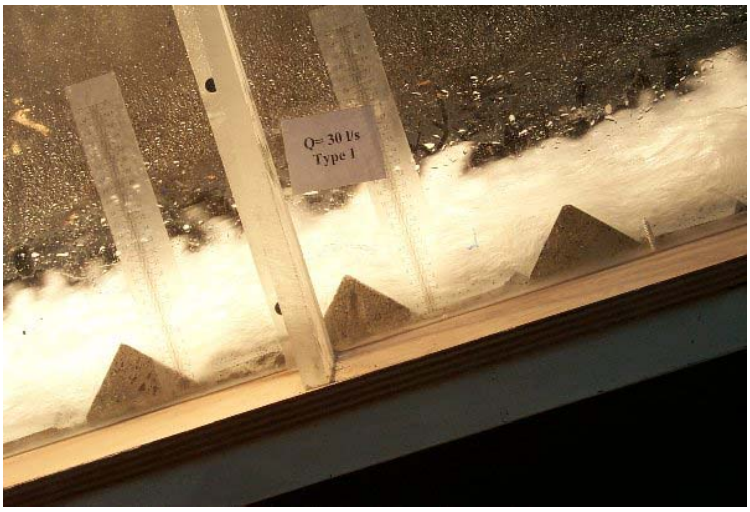

Lining type 3, test 3, Q= 30 l/s

Lay-out of lining type 3 after failure for Q=60 l/s

APPENDIX 4. 1 (suite) - Experiment n° 4 – 45° PYRAMIDS (3+, without drainage, unaligned joints)

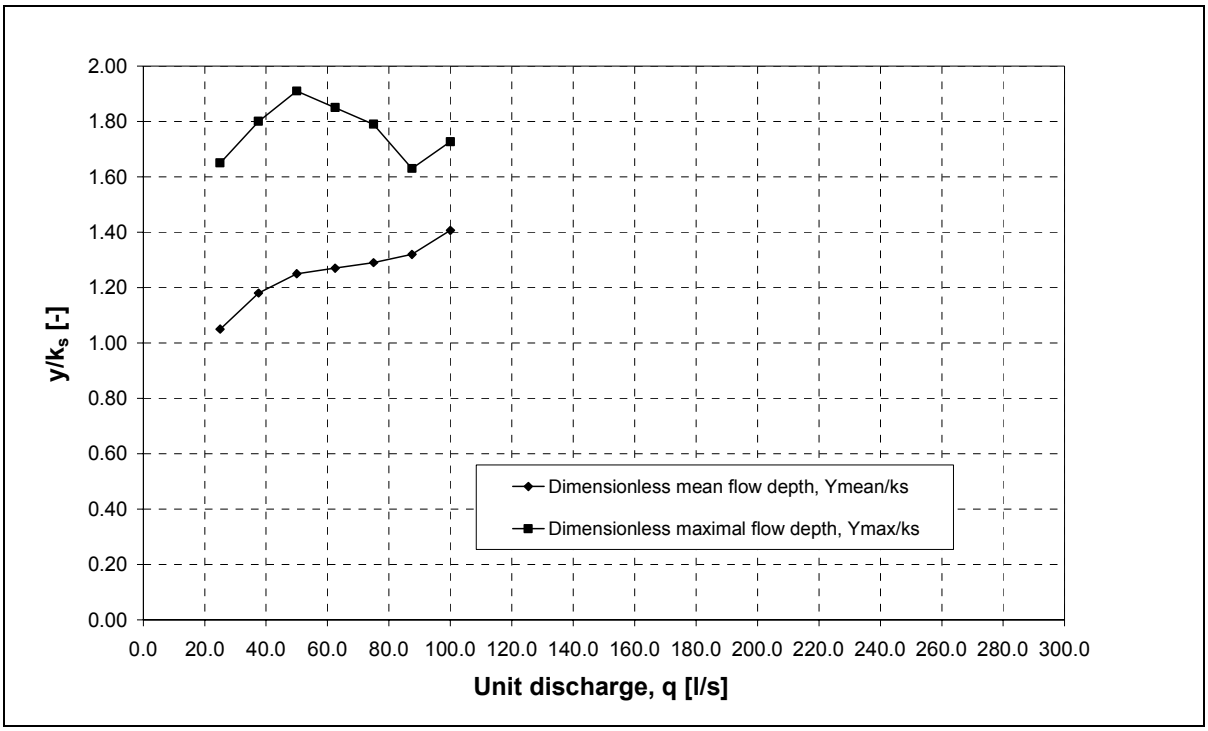

Figure A4.3a – Dimensionless- mean flow depth Y_{mean}/k_s and maximum flow depth Y_{max}/k_s

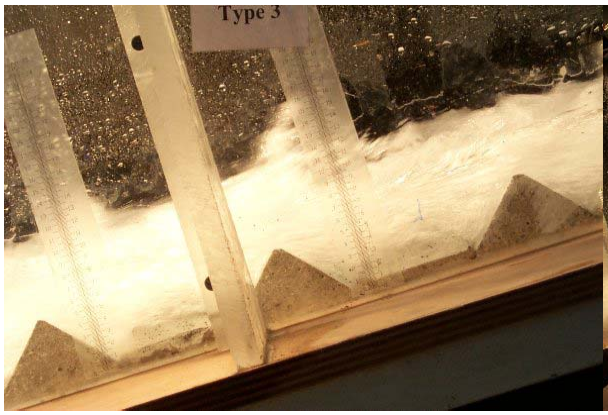

Lining type 3+, test 4, Q= 30 l/s

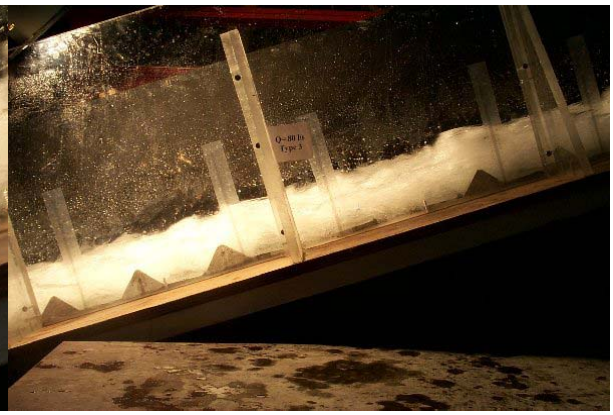

Lining type 3+, test 4, Q= 80 l/s

(notice that some halves close to the wall have already failed)

APPENDIX 4. 1 (suite) - Experiment n° 6 – INVERTED 44° NEGATIVE INCLINED STEP (1a, without drainage, aligned joints)

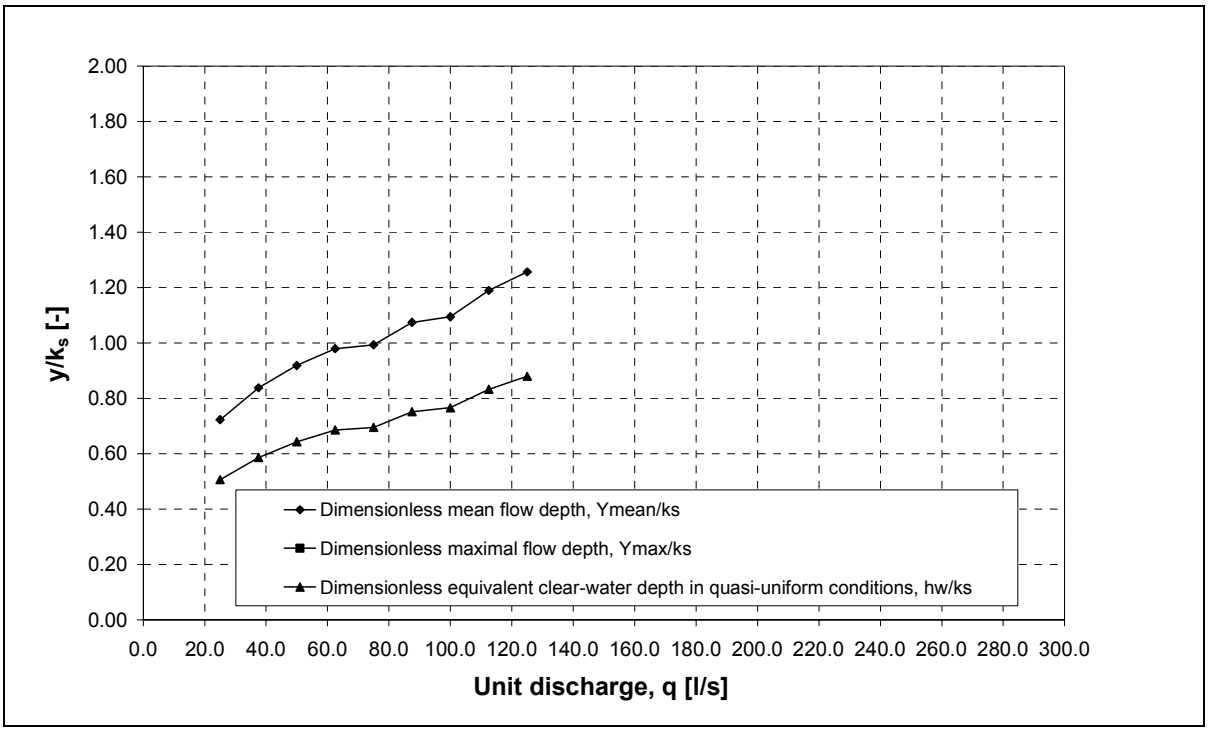

Figure A4.6a - Dimensionless- mean flow depth Y_{mean}/k_s, maximum flow depth Y_{max}/k_s and equivalent Clear-water depth h_w/k_s (with C_{mean}=0.30)

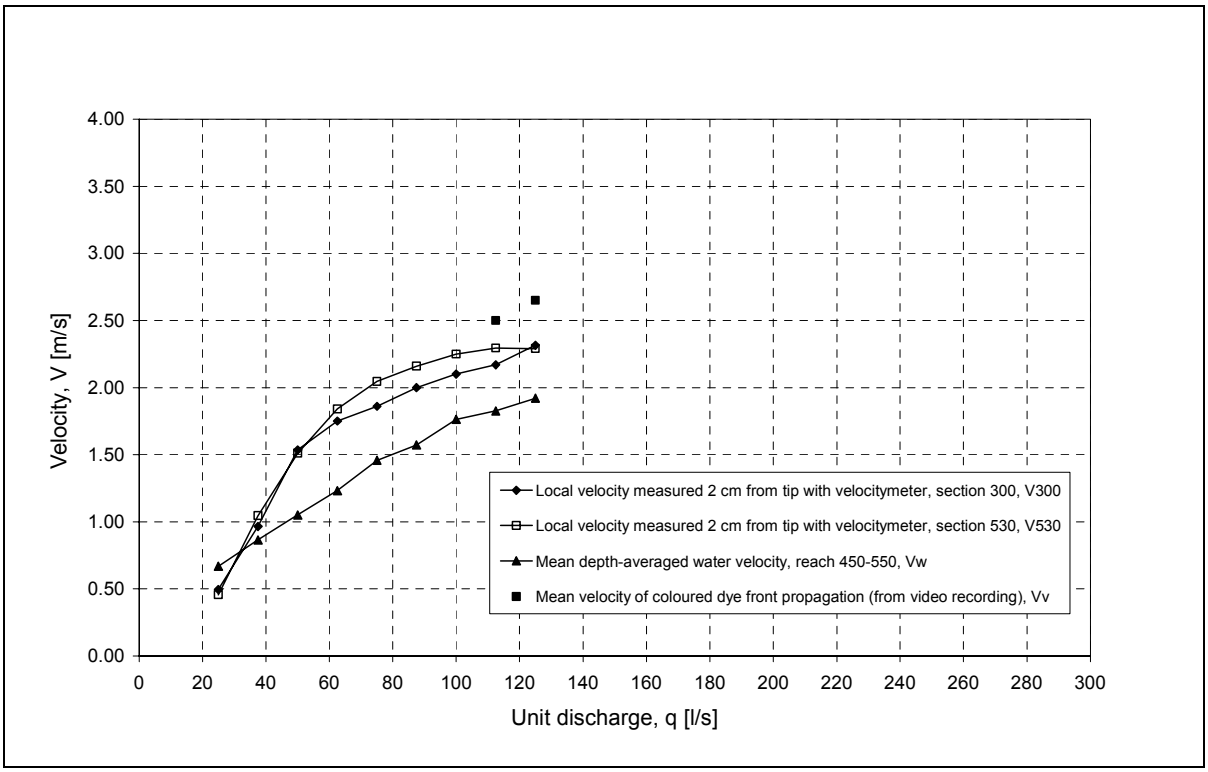

Figure A4.6b - Local velocity measurements using currentmenter, section 300 and 530, mean flow velocity estimated from coloured dye propagation (video), and computed clear-water mean depth-averaged velocity.

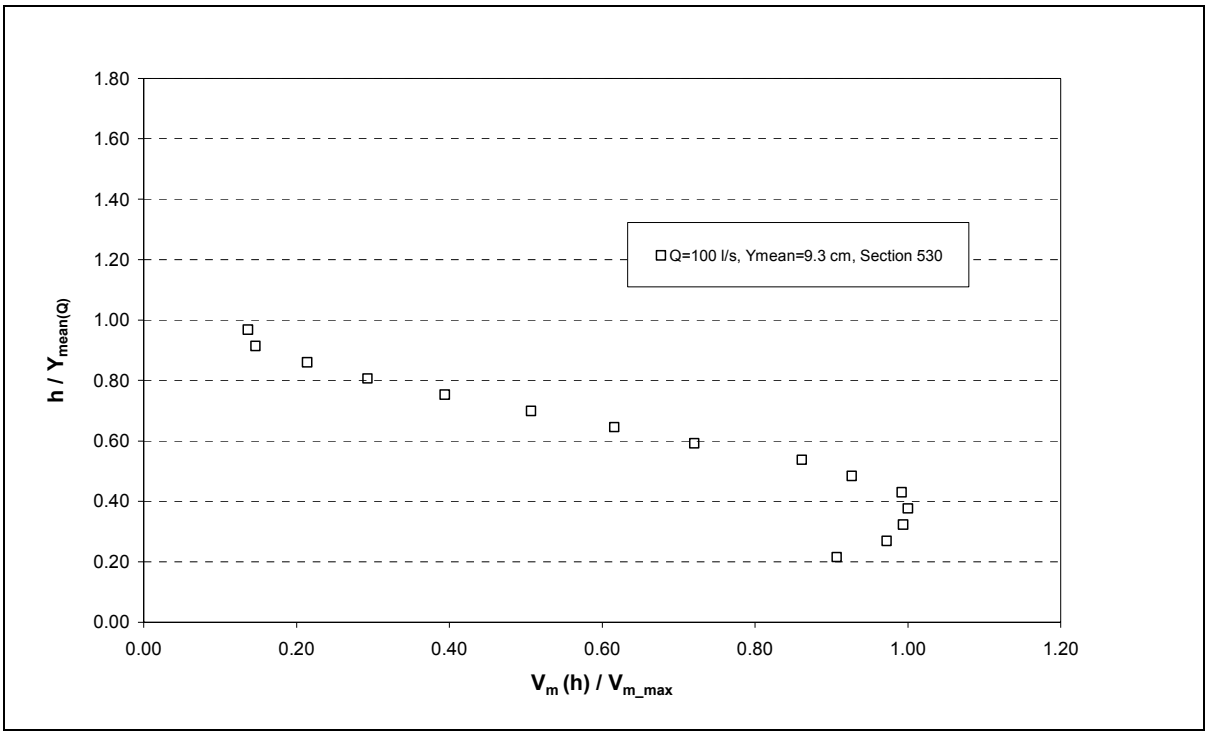

Figure A4.6a - Dimensionless velocity profile for 100 l/s, at section 530. Water velocity measurements made using water currentmeter (Vm) throughout the depth. Flow depth rendered dimensionless through division by the observed mean flow depth for the given flow ($Ymean_Q$). Type 1 element (ks=74 mm), 1/3 channel slope (α=18.43°).

Lining type 1a, test 6, after failure lay-out

Lining type 1a, test 5, after failure lay-out

APPENDIX 4. 1 (suite) - Experiment n° 7 – 30° NEGATIVE INCLINED STEP (2, without drainage, aligned joints)

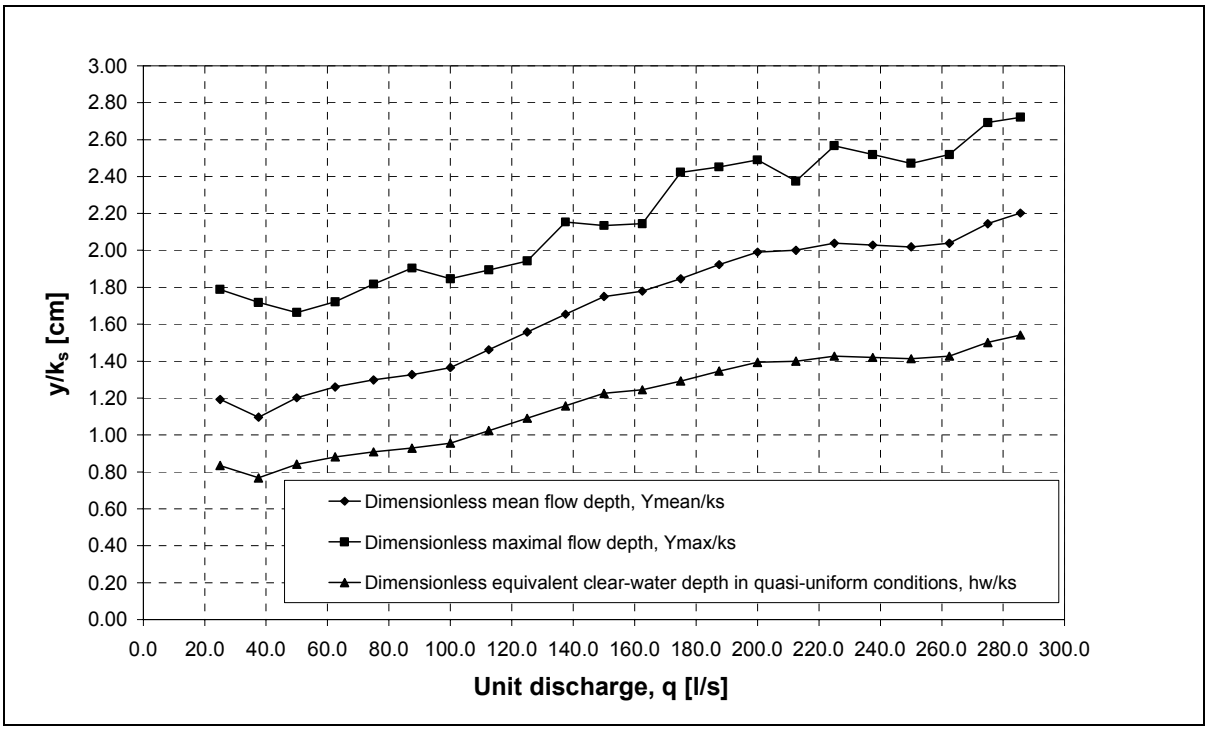

Figure A4.7a - Dimensionless- mean flow depth Y_{mean}/k_s, maximum flow depth Y_{max}/k_s and equivalent Clear-water depth h_w/k_s (with C_{mean}=0.30)

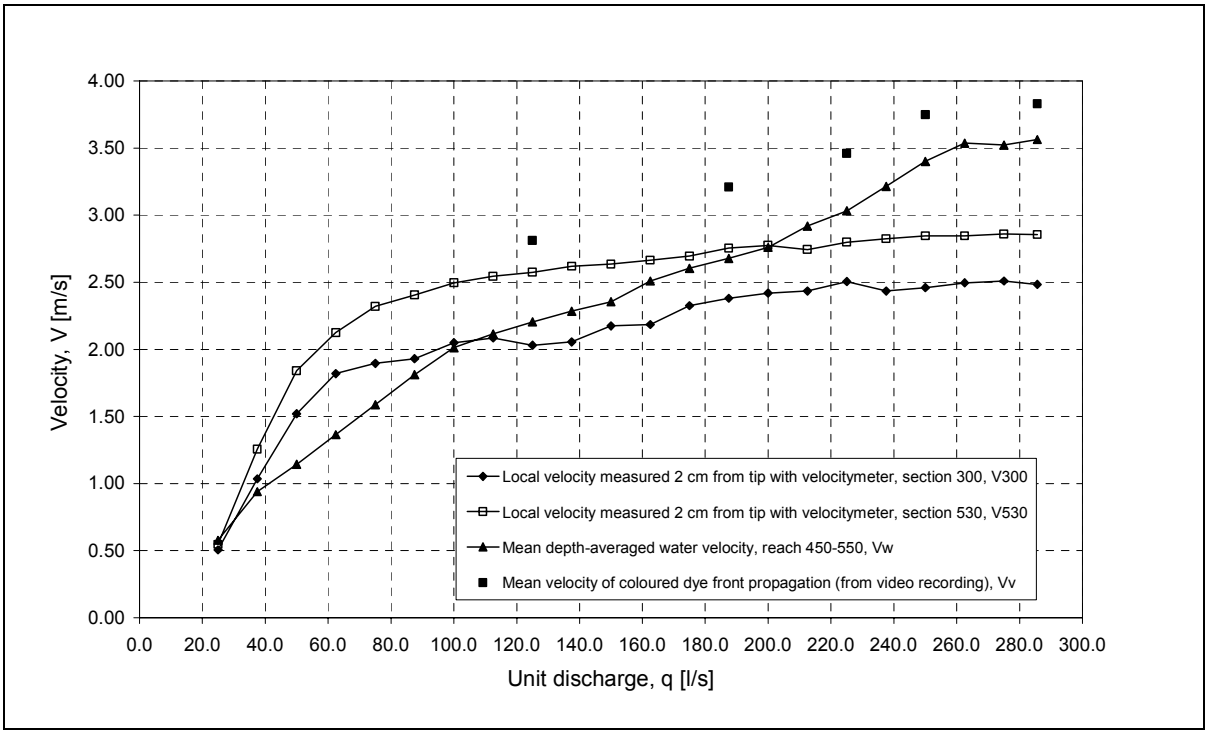

Figure A4.7b - Local velocity measurements using currentmenter, section 300 and 530, mean flow velocity estimated from coloured dye propagation (video), and computed clear-water mean depth-averaged velocity.

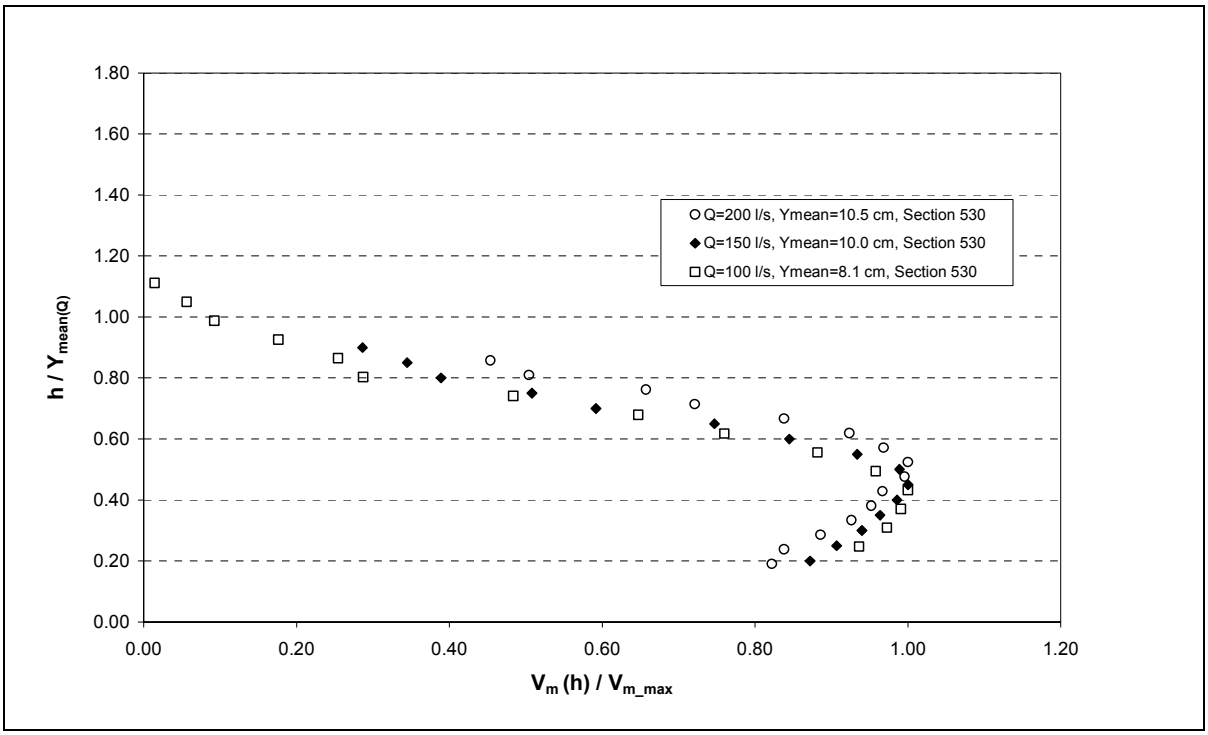

Figure A4.7c - Dimensionless velocity profiles for 100, 150 and 200 l/s at section 530. Water velocity measurements made using water currentmeter (Vm) throughout the depth. Flow depth rendered dimensionless through division by the observed mean flow depth for the given flow ($Ymean_Q$). Type 2 element (ks=52 mm), 1/3 channel slope (α=18.43°).

APPENDIX 4. 1 (suite) - Experiment n° 8 – INVERTED 30° NEGATIVE INCLINED STEP (2a, without drainage, aligned joints)

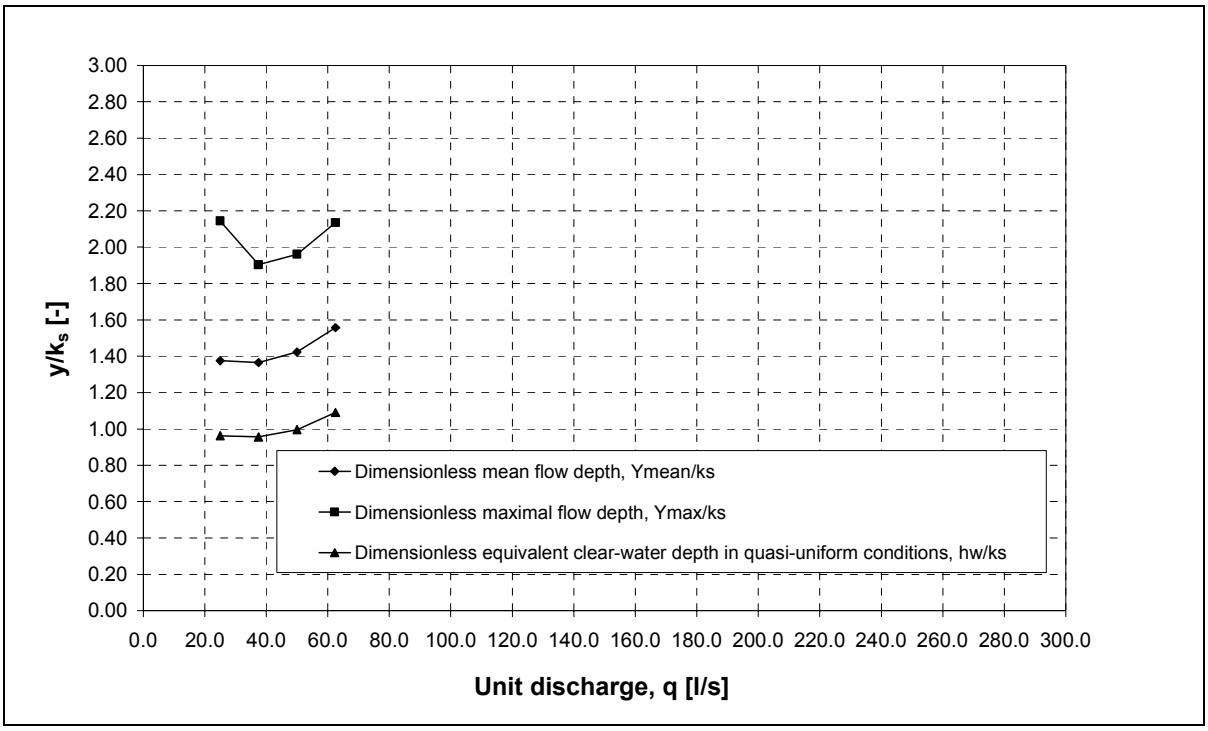

Figure A4.8a - Dimensionless- mean flow depth Y_{mean}/k_s, maximum flow depth Y_{max}/k_s and equivalent Clear-water depth h_w/k_s (with C_{mean}=0.30)

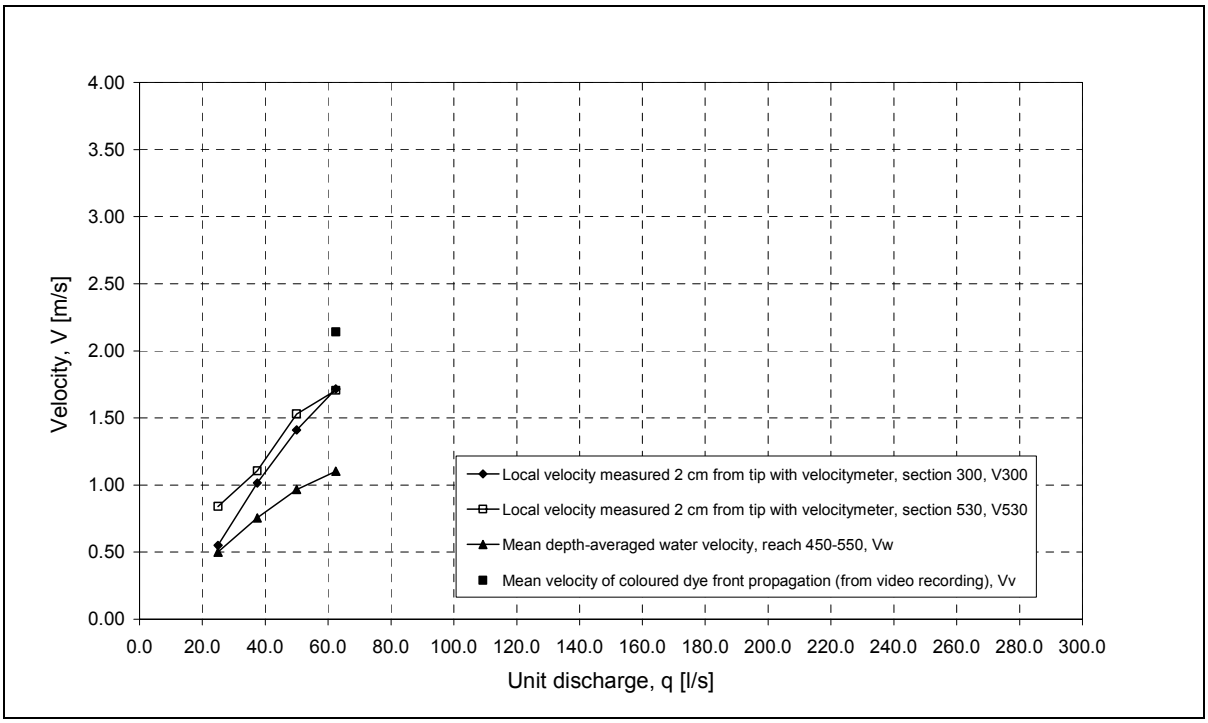

Figure A4.8b - Local velocity measurements using currentmenter, section 300 and 530, mean flow velocity estimated from coloured dye propagation (video), and computed clear-water mean depth-averaged velocity.

APPENDIX 4. 1 (suite) - Experiment n° 9 – 30° NEGATIVE INCLINED STEP WITH END SILL (2+ES, without drainage, aligned joints)

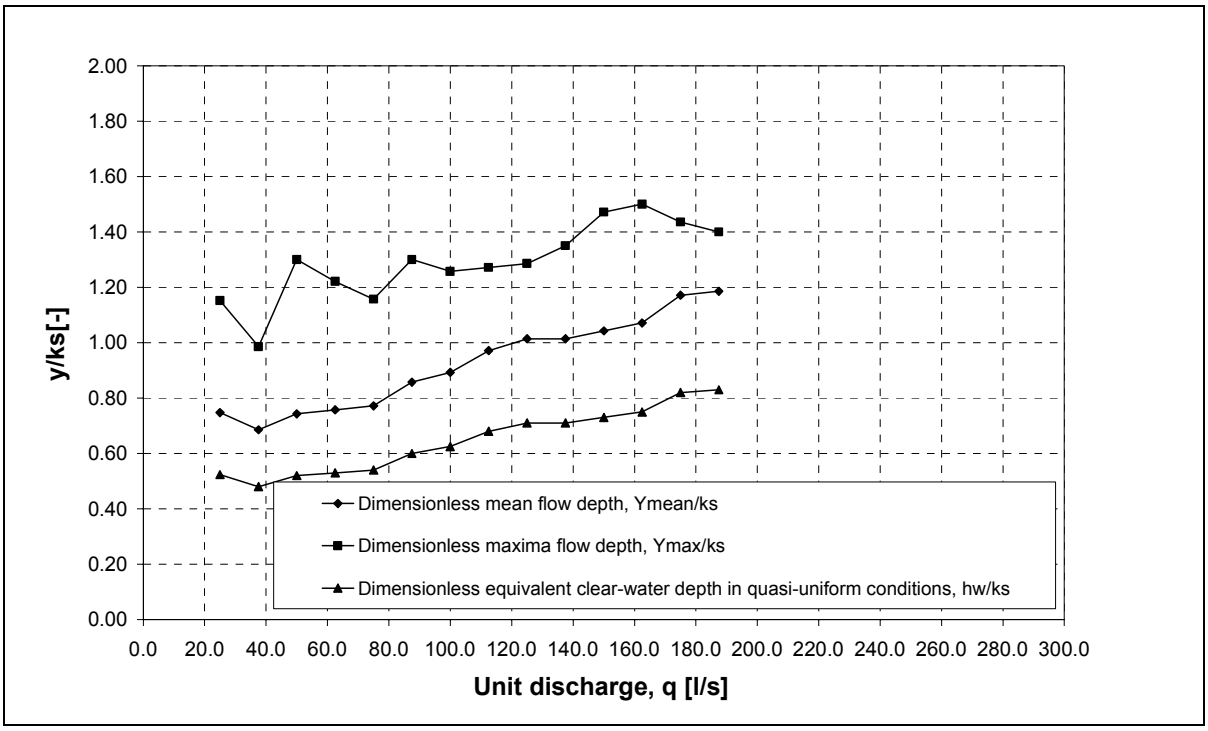

Figure A4.9a - Dimensionless- mean flow depth Y_{mean}/k_s, maximum flow depth Y_{max}/k_s and equivalent Clear-water depth h_w/k_s (with C_{mean}=0.30)

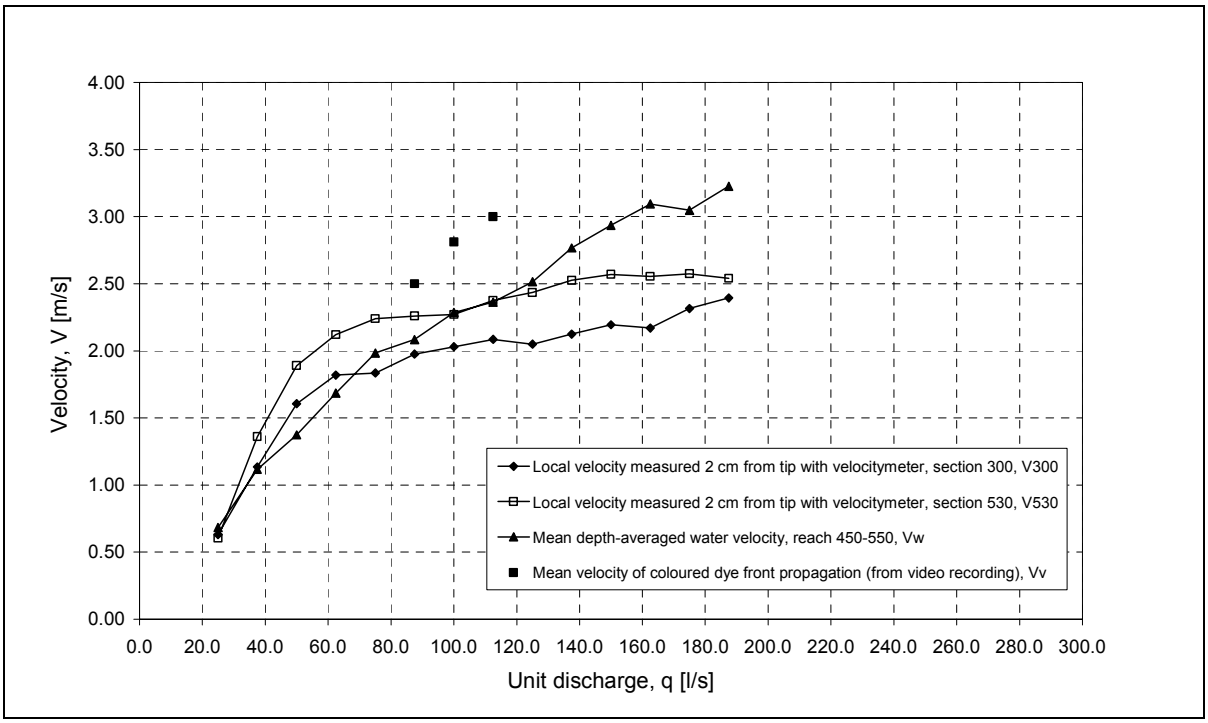

Figure A4.9b - Local velocity measurements using currentmenter, section 300 and 530, mean flow velocity estimated from coloured dye propagation (video), and computed clear-water mean depth-averaged velocity.

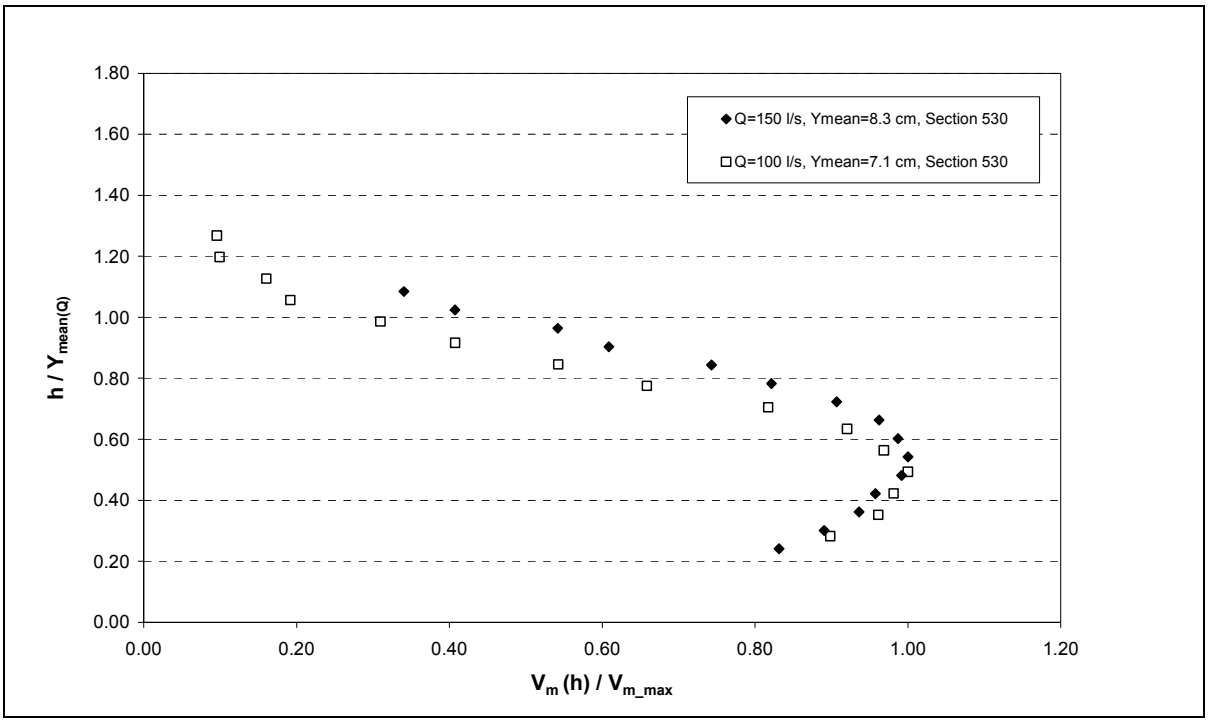

Figure A4.9c - Dimensionless velocity profiles for 100 and 150 l/s at section 530. Water velocity measurements made using water currentmeter (Vm) throughout the depth. Flow depth rendered dimensionless through division by the observed mean flow depth for the given flow ($Ymean_Q$). Type 2ES element (ks=70 mm), 1/3 channel slope (α=18.43°).

APPENDIX 4. 1 (suite) - Experiment n° 10 – INVERTED 30° NEGATIVE INCLINED STEP WITH END SILL (2+ES, without drainage, aligned joints)

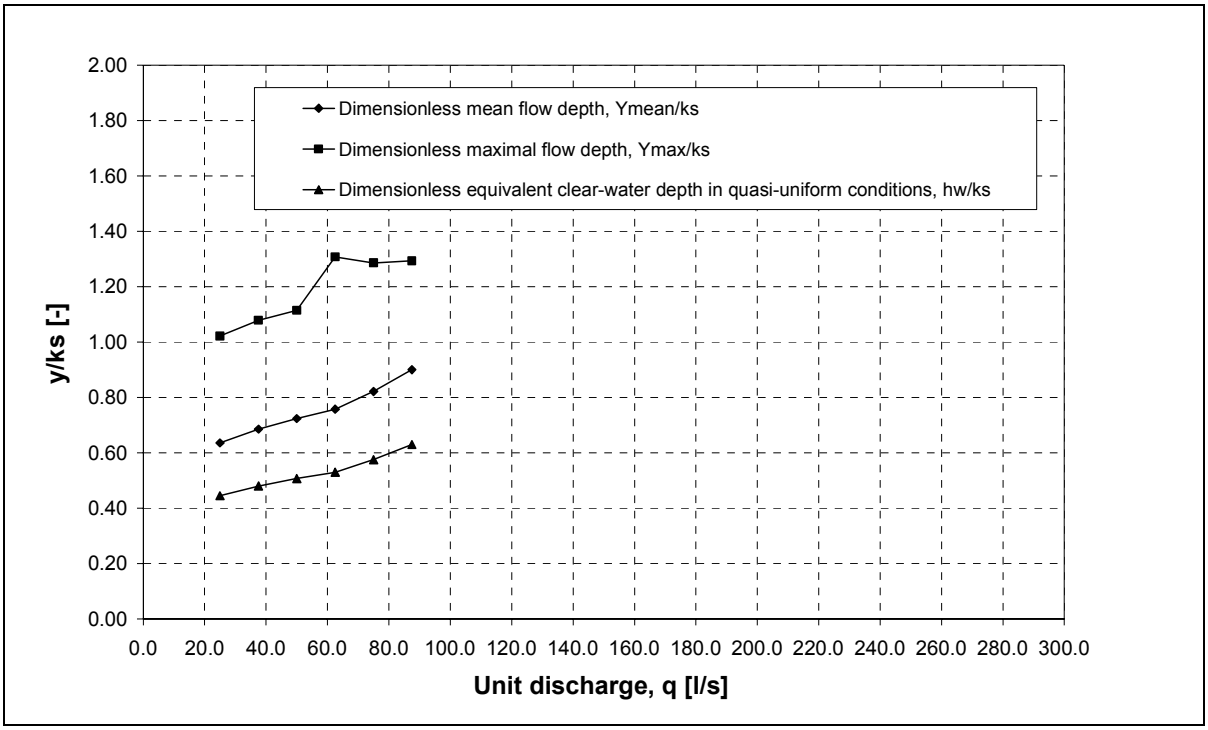

Figure A4.10a - Dimensionless- mean flow depth Y_{mean}/k_s, maximum flow depth Y_{max}/k_s and equivalent Clear-water depth h_w/k_s (with C_{mean}=0.30)

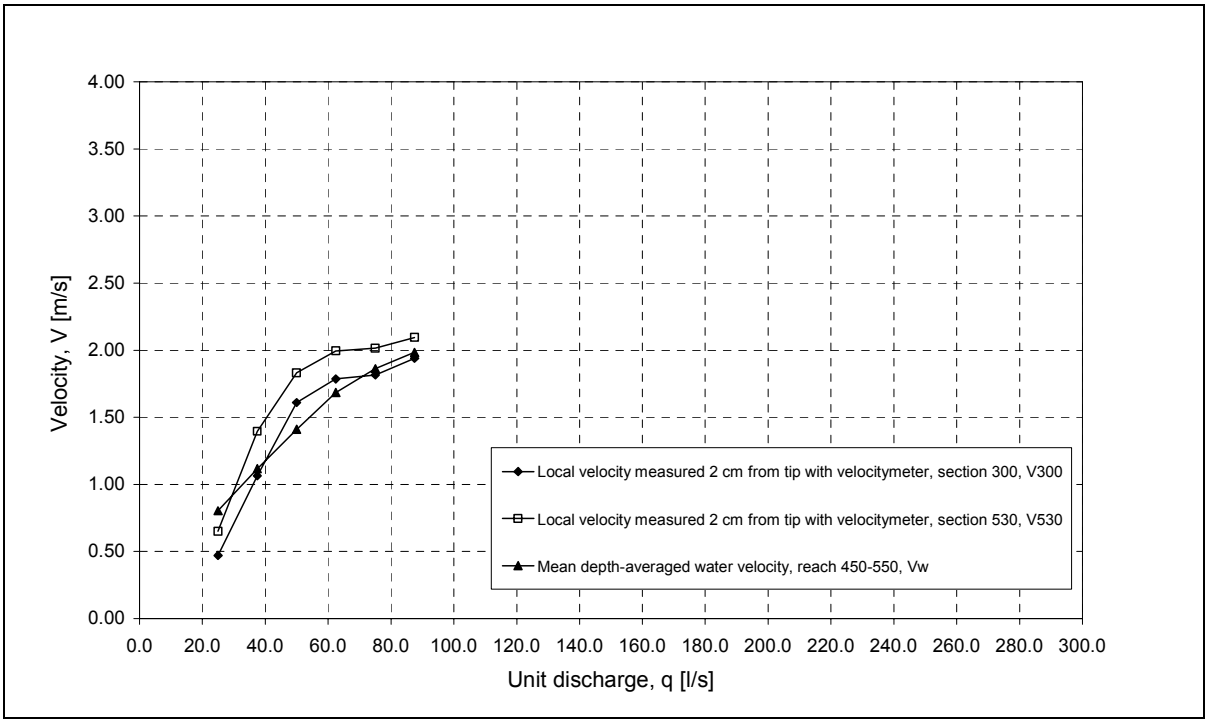

Figure A4.10b - Local velocity measurements using currentmenter, section 300 and 530, mean flow velocity estimated from coloured dye propagation (video), and computed clear-water mean depth-averaged velocity.

APPENDIX 4. 1 (suite) - Experiment n° 11 – 30° NEGATIVE INCLINED STEP WITH END SILL (2+ES, with drainage, aligned joints)

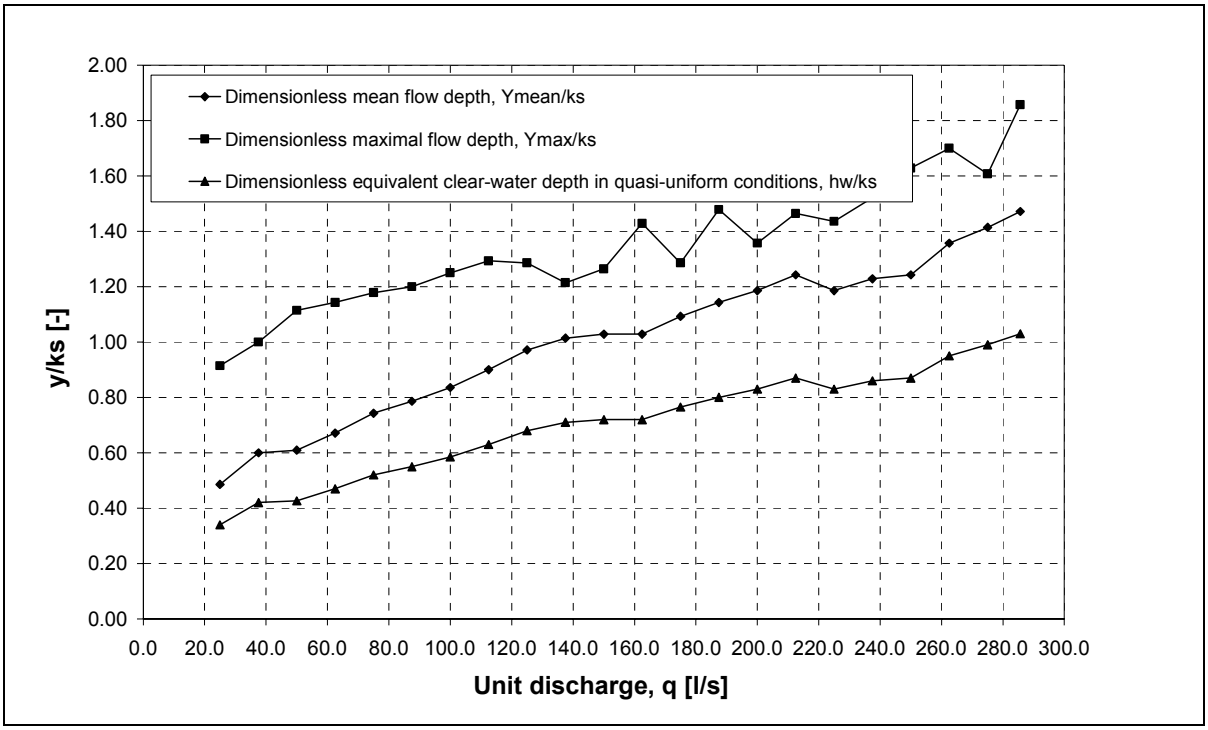

Figure A4.11a - Dimensionless- mean flow depth Y_{mean}/k_s, maximum flow depth Y_{max}/k_s and equivalent Clear-water depth h_w/k_s (with C_{mean}=0.30)

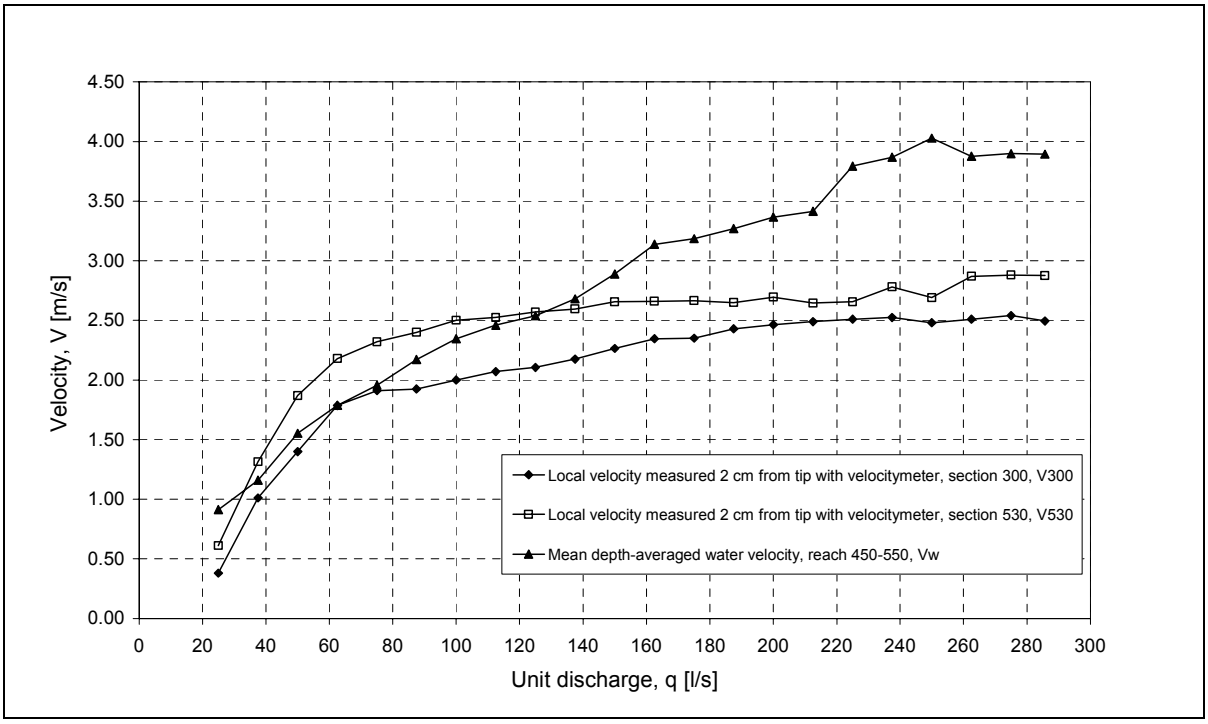

Figure A4.11b - Local velocity measurements using currentmenter, section 300 and 530, and computed clear-water mean depth-averaged velocity.

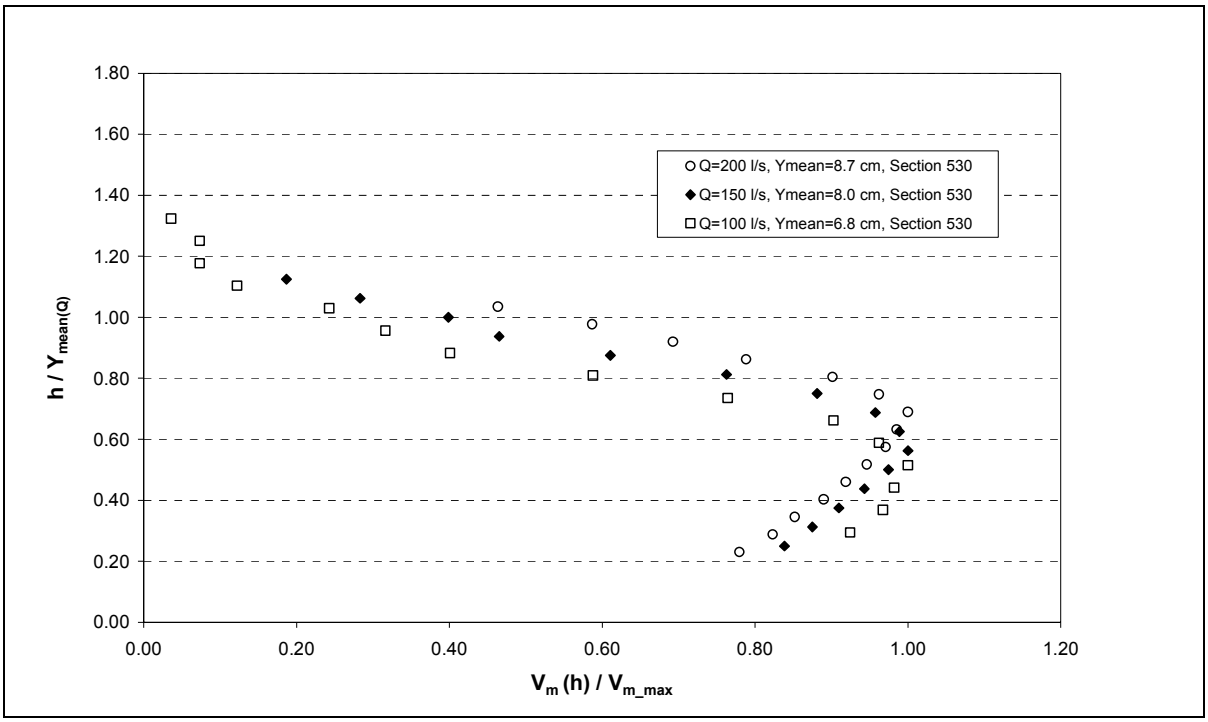

Figure A4.11c - Dimensionless velocity profiles for 100 and 150 l/s at section 530. Water velocity measurements made using water currentmeter (Vm) throughout the depth. Flow depth rendered dimensionless through division by the observed mean flow depth for the given flow ($Ymean_Q$). Type 2ES element (ks=70 mm), 1/3 channel slope (α=18.43°).

APPENDIX 4. 1 (suite) - Experiment n° 12 – 44° NEGATIVE INCLINED STEP (1, with drainage, aligned joints)

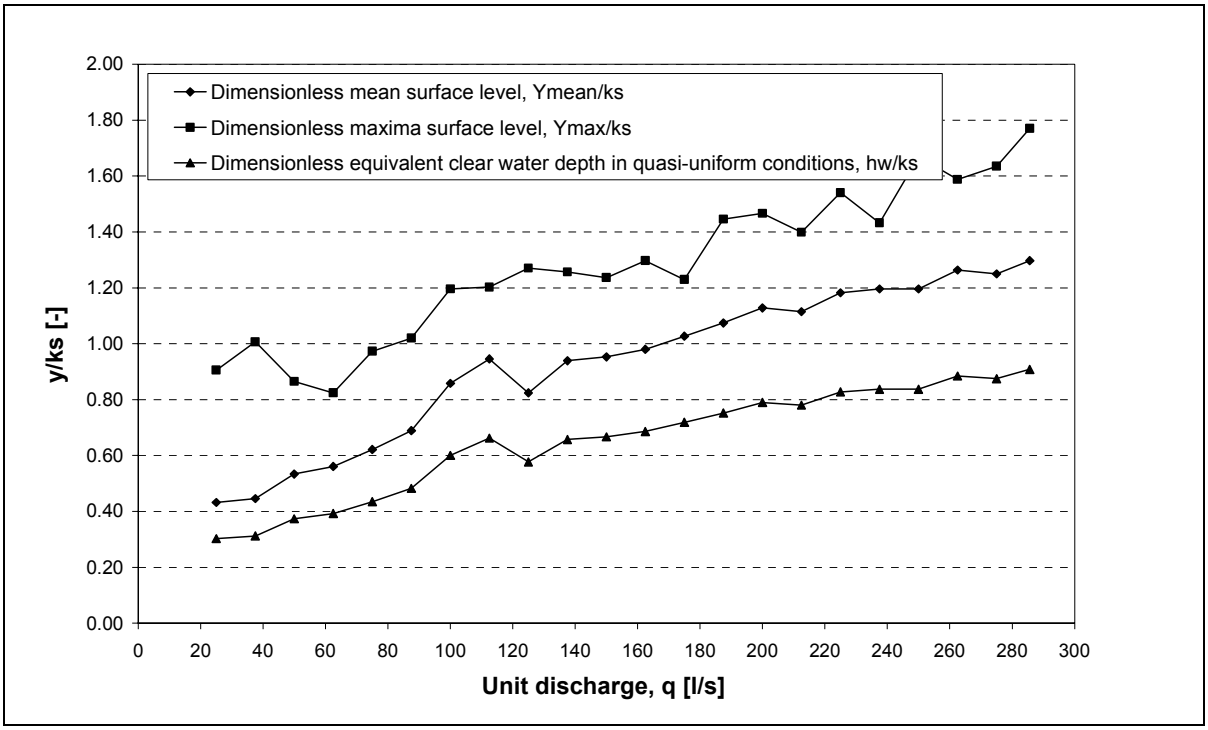

Figure A4.12a - Dimensionless- mean flow depth Y_{mean}/k_s, maximum flow depth Y_{max}/k_s and equivalent Clear-water depth h_w/k_s (with C_{mean}=0.30)

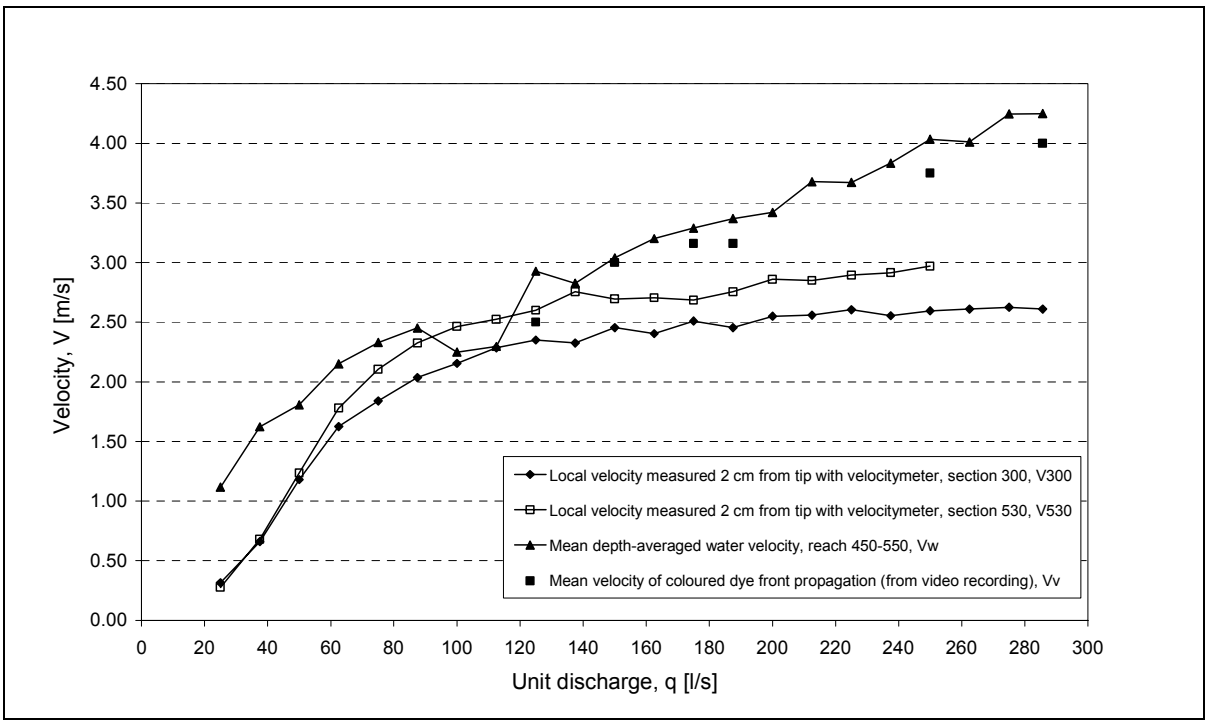

Figure A4.12b - Local velocity measurements using currentmenter, section 300 and 530, mean flow velocity estimated from coloured dys propagation (video), and computed clear-water mean depth-averaged velocity.

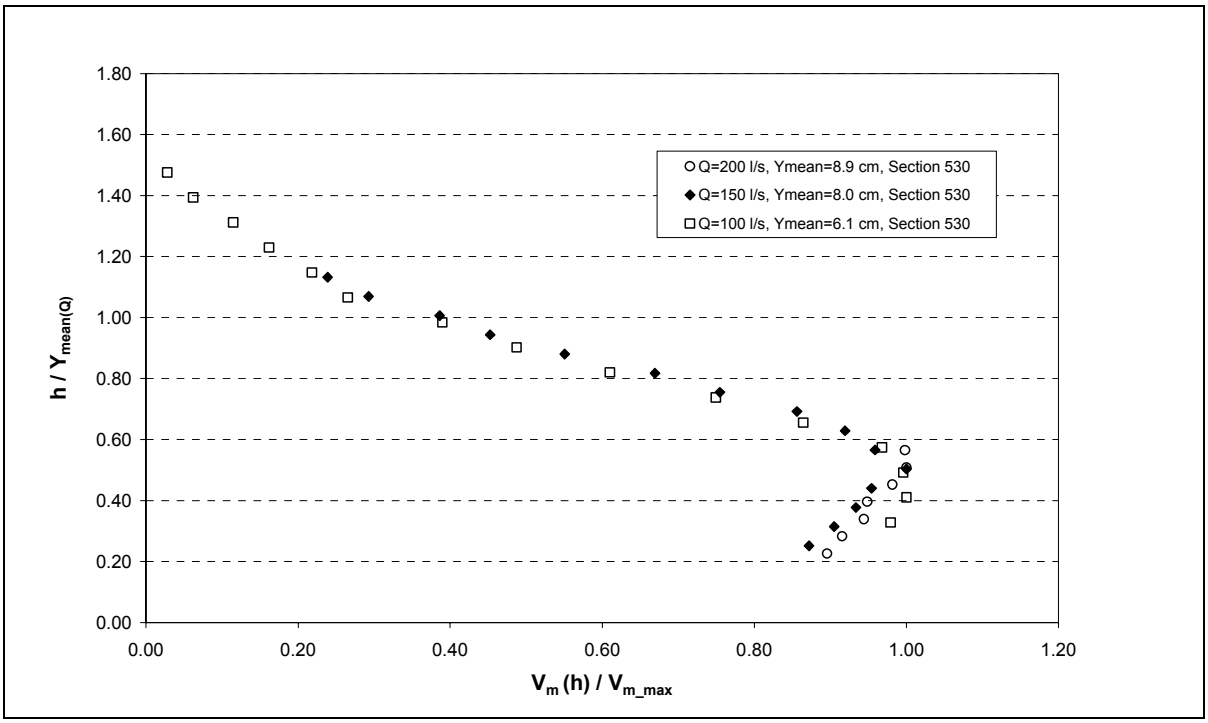

Figure A4.12c - Dimensionless velocity profiles for 100 and 150 l/s at section 530. Water velocity measurements made using water currentmeter (Vm) throughout the depth. Flow depth rendered dimensionless through division by the observed mean flow depth for the given flow ($Ymean_Q$). Type 1 element (ks=74 mm), 1/3 channel slope (α=18.43°).

APPENDIX 4. 1 (suite) - Experiment n° 13 – INVERTED 44° NEGATIVE INCLINED STEP (1a, with drainage, aligned joints)

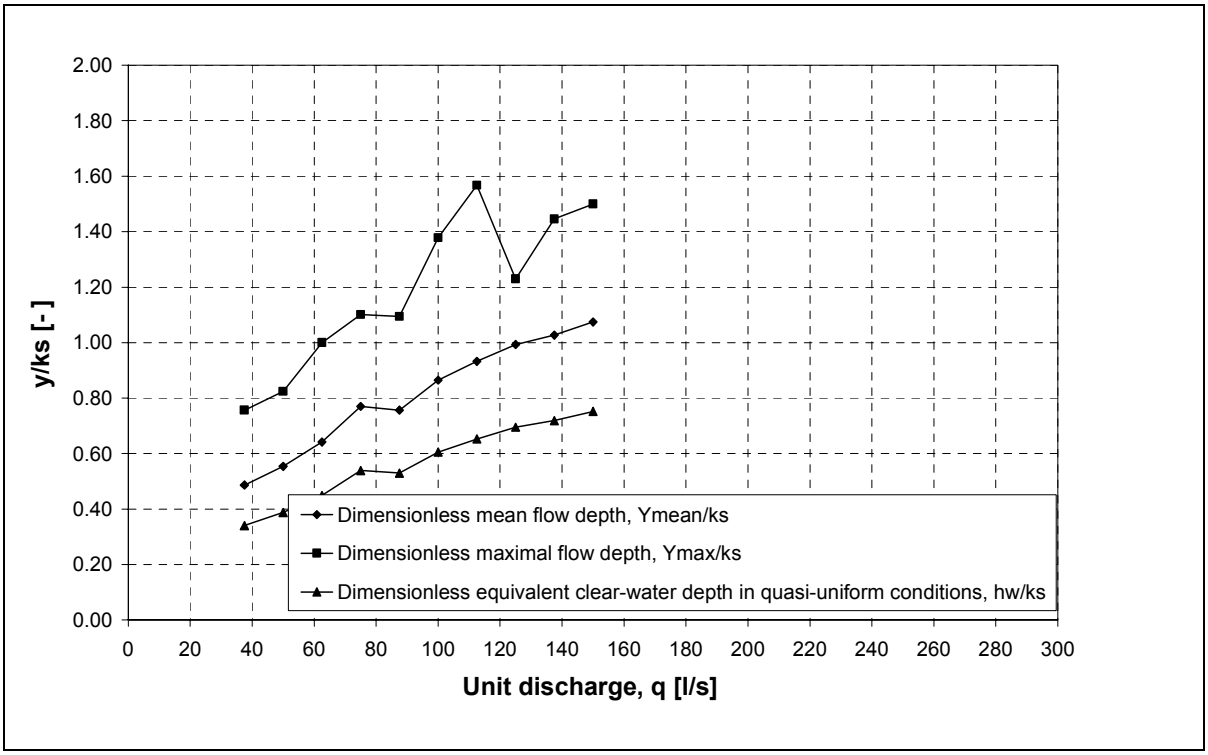

Figure A4.13a - Dimensionless- mean flow depth Y_{mean}/k_s, maximum flow depth Y_{max}/k_s and equivalent Clear-water depth h_w/k_s (with C_{mean}=0.30)

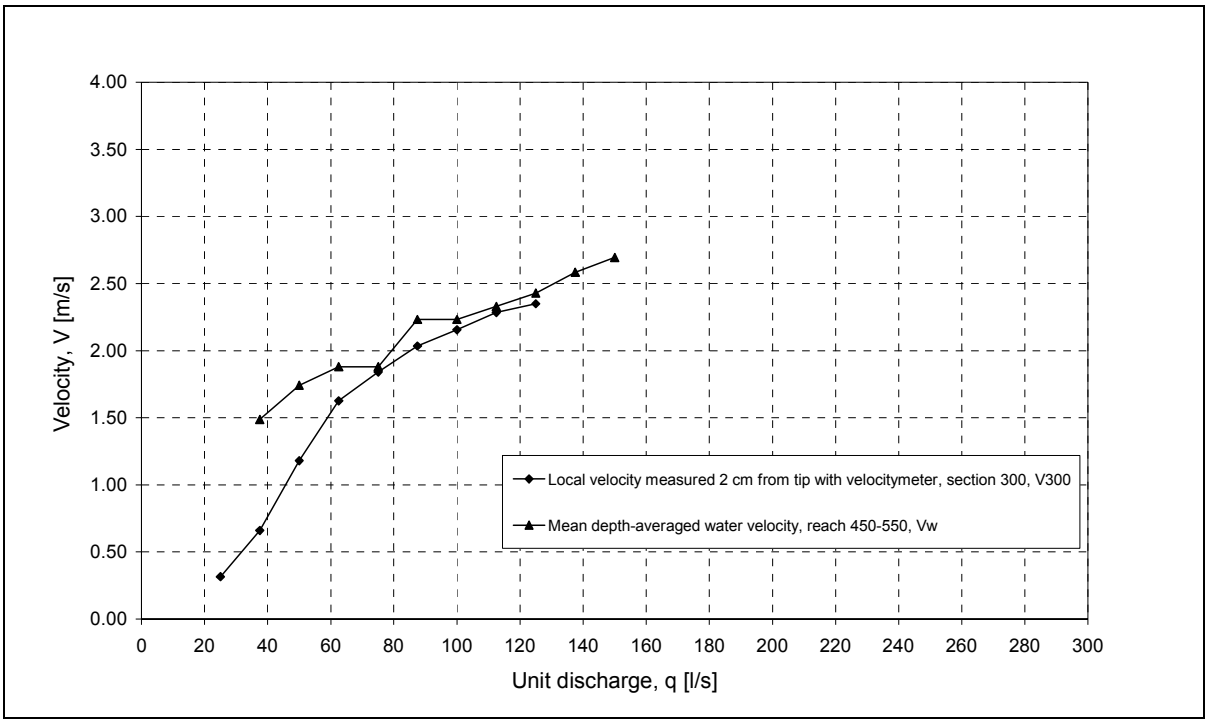

Figure A4.13b - Local velocity measurements using currentmenter, section 300, and computed clear-water mean depth-averaged velocity.

APPENDIX 4. 1 (suite) - Mean flow depth vs. unit discharge at *prototype* scale (scale factor 10)

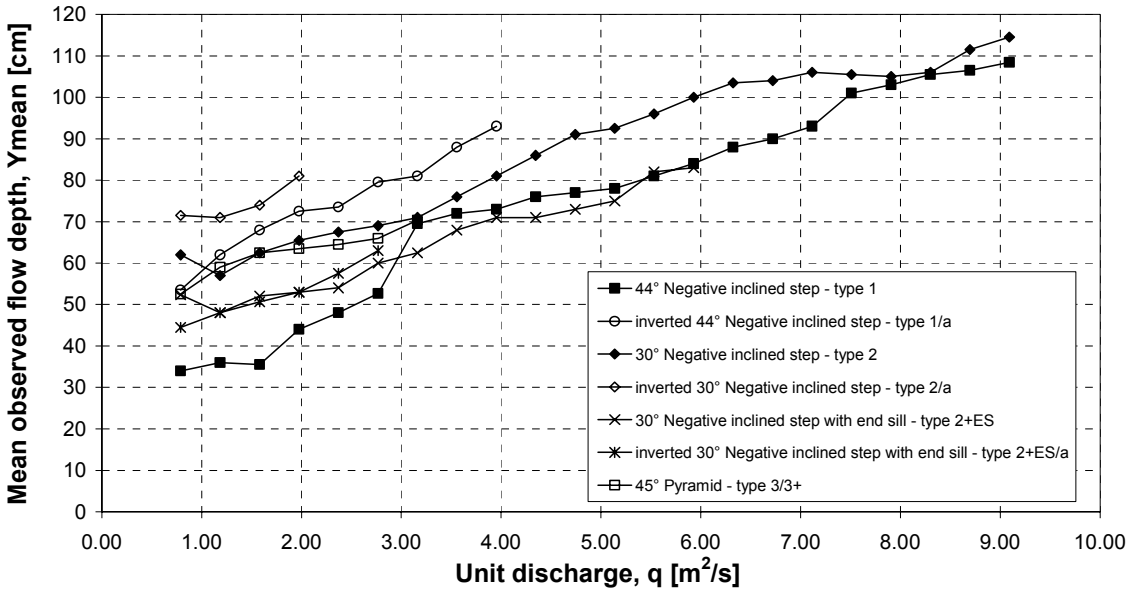

Mean observed flow depth, Y_{mean}, for all tested linings and discharges, WITHOUT DRAINAGE. Linings types 1/1a (ks=74 cm, weight 1.36 ton), types 2/2a (ks=52 cm, weight 1.05 ton), types 2ES and 2Es/a (ks=70 cm, weight 1.10 ton), types 3/3+ (ks=50 cm, weight 0.57 and 0.82 ton). PROTOTYPE scale 1:10.

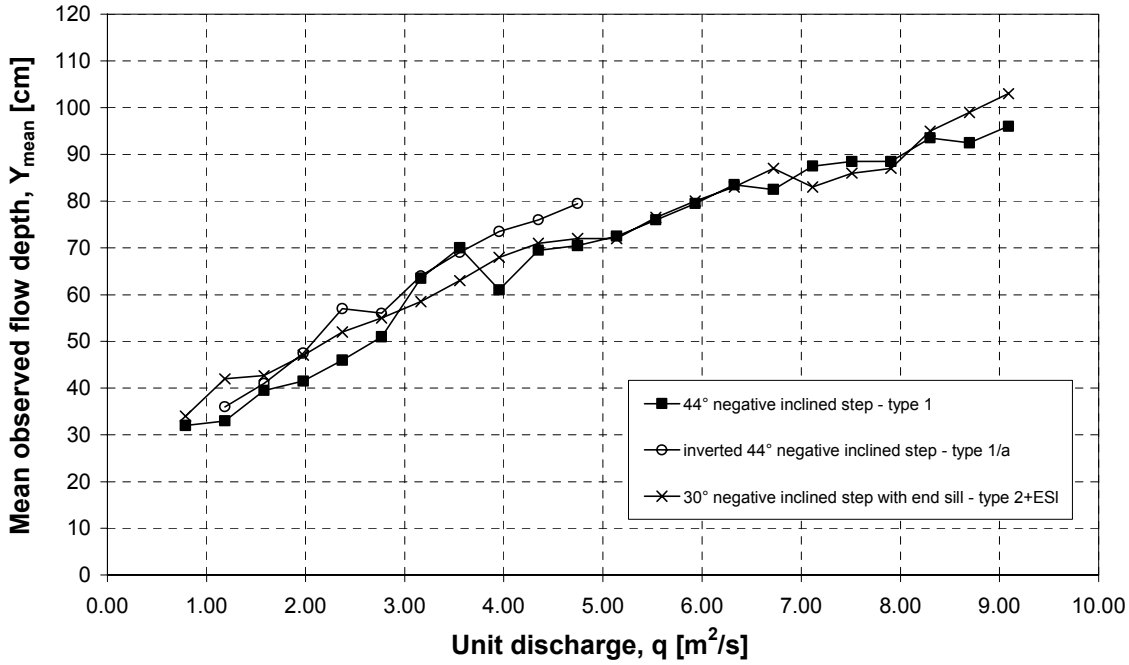

Mean observed flow depth, Y_{mean}, for all tested linings and discharges, WITH DRAINAGE. Linings types 1/1a (ks=74 cm, weight 1.36 ton), type 2ES (ks=70 cm, weight 1.10 ton). PROTOTYPE scale 1:10.

Appendix 5 – Stability assessment of concrete elements (design drawings, design charts, design examples)

Computation of *x*-co-ordinate of gravity centre	$x_G = \frac{\sum_{i=1}^{n} A_i \cdot x_{Gi}}{\sum_{i=1}^{n} A_i}$, subdividing the element in *n* known geometrical shapes $x_{G\,type3} = \frac{base}{2}$
Computation of *z*-co-ordinate of gravity centre	$z_G = \frac{\sum_{i=1}^{n} A_i \cdot z_{Gi}}{\sum_{i=1}^{n} A_i}$, replacing the areas by volumes for element type 3
Computation of the cross section area surface	$A = f(k_s, type)$ $A_{type1/1a} = (\frac{1200}{74^2} + \frac{120}{148}) \cdot k_s{}^2$ $A_{type2/2a} = (\frac{1200}{52^2} + \frac{120}{104}) \cdot k_s{}^2$ $A_{type2ES/2ESa} = (\frac{1200 + 0.5 \cdot 52 \cdot 120 + 21^2}{70^2}) \cdot k_s{}^2$
Computation of the volume	$V = f(k_s, type)$ $V_{type1/1a/2/2a/2ES/2ES1} = A_{type1/1a/2/2a/2ES/2ESa} \cdot b_{type1/1a/2/2a/2ES/2ESa}$ $V_{type3} = (\frac{100}{50} k_s)^2 \cdot (\frac{k_s}{3} + \frac{10}{50} \cdot k_s)$

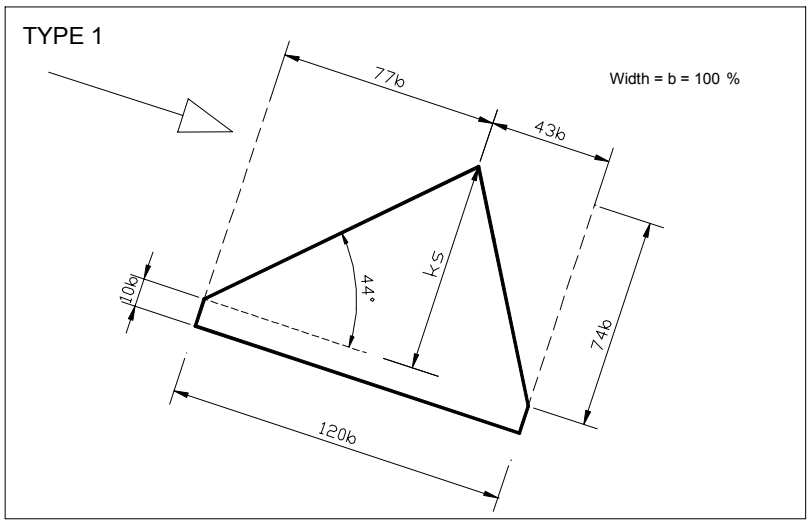

TYPE 2

Width = b = 100 %

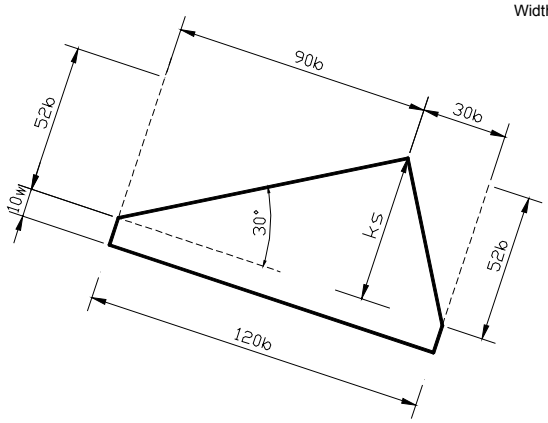

TYPE 2 + ES

Width = b = 100 %

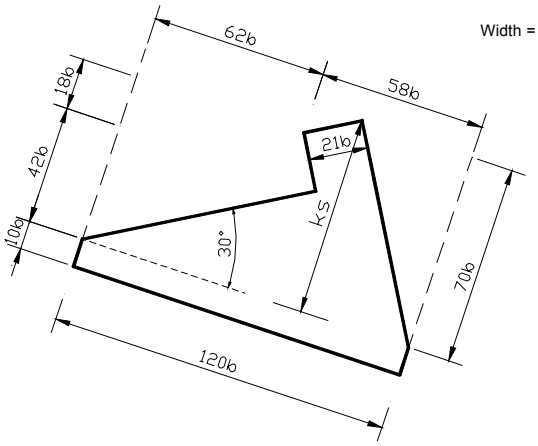

TYPE 3

Cross section at highest point

3D View

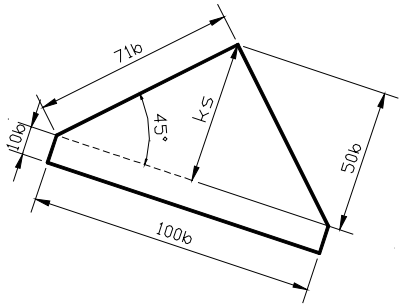

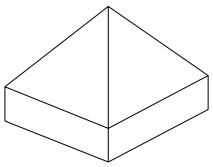

Width = b = 100 %

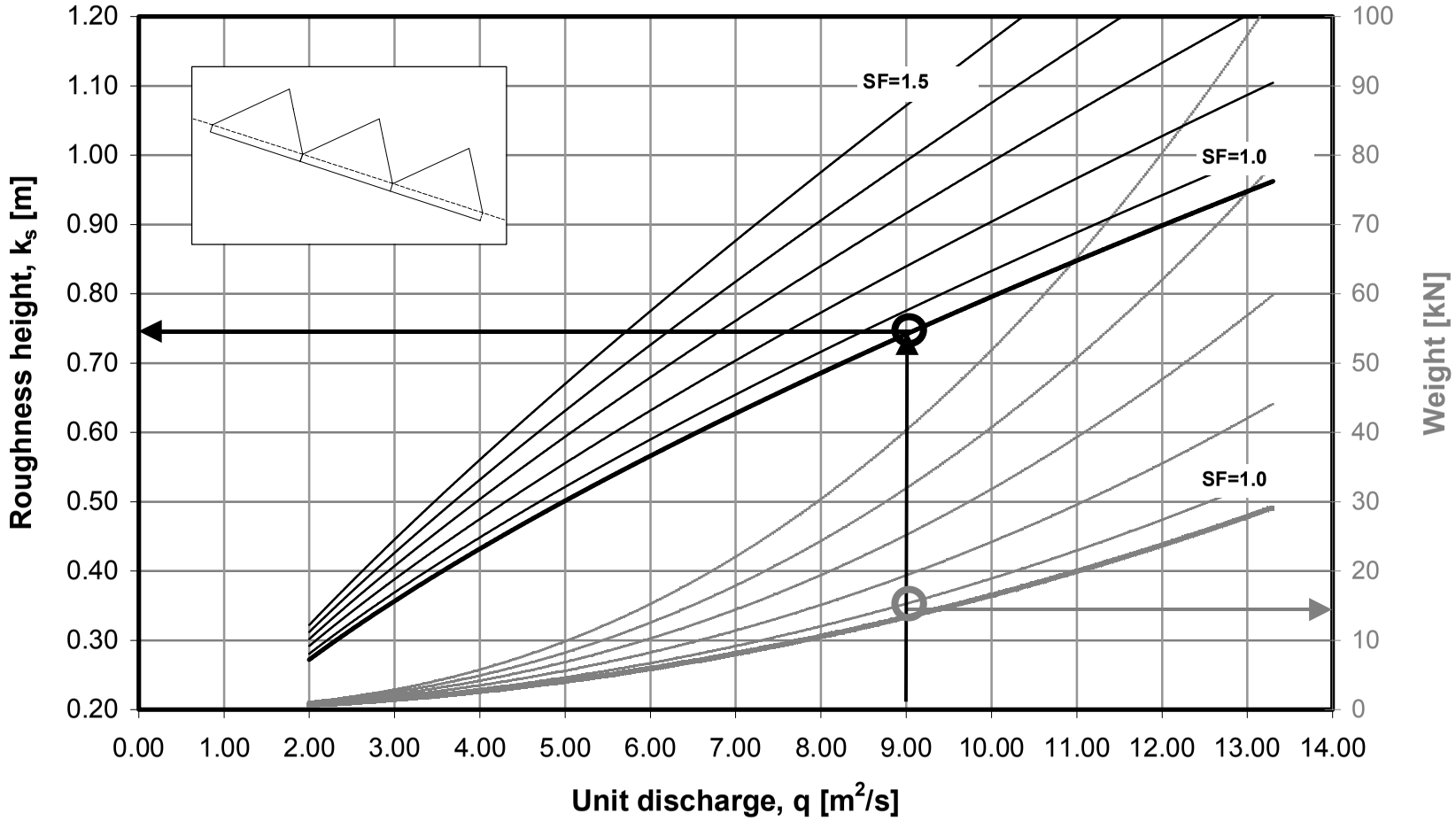

Figure 1 - Design chart for the 44° NEGATIVE INCLINED STEP (type 1). Minimum safety factor values, SF1 between 1.0 and 1.5, without drainage. Concrete density of 2400 kg/m^3. The experimental observation corresponds to the value marked with a circle.

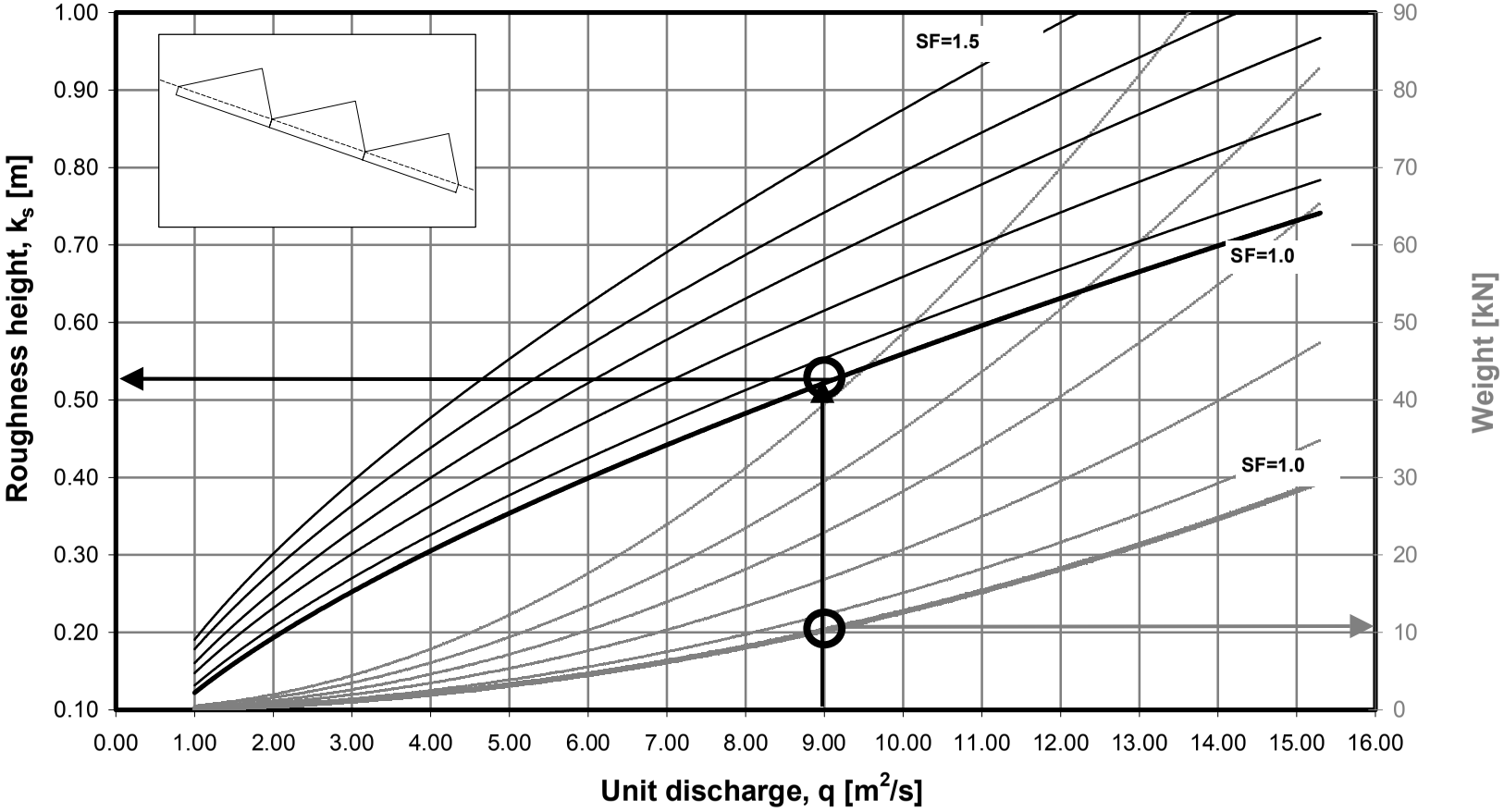

Figure 2 - Design chart for the 30° NEGATIVE INCLINED STEP (type 2). Minimum safety factor values, SF1 between 1.0 and 1.5, without drainage. Concrete density of 2400 kg/m^3. The experimental observation corresponds to the value marked with a circle.

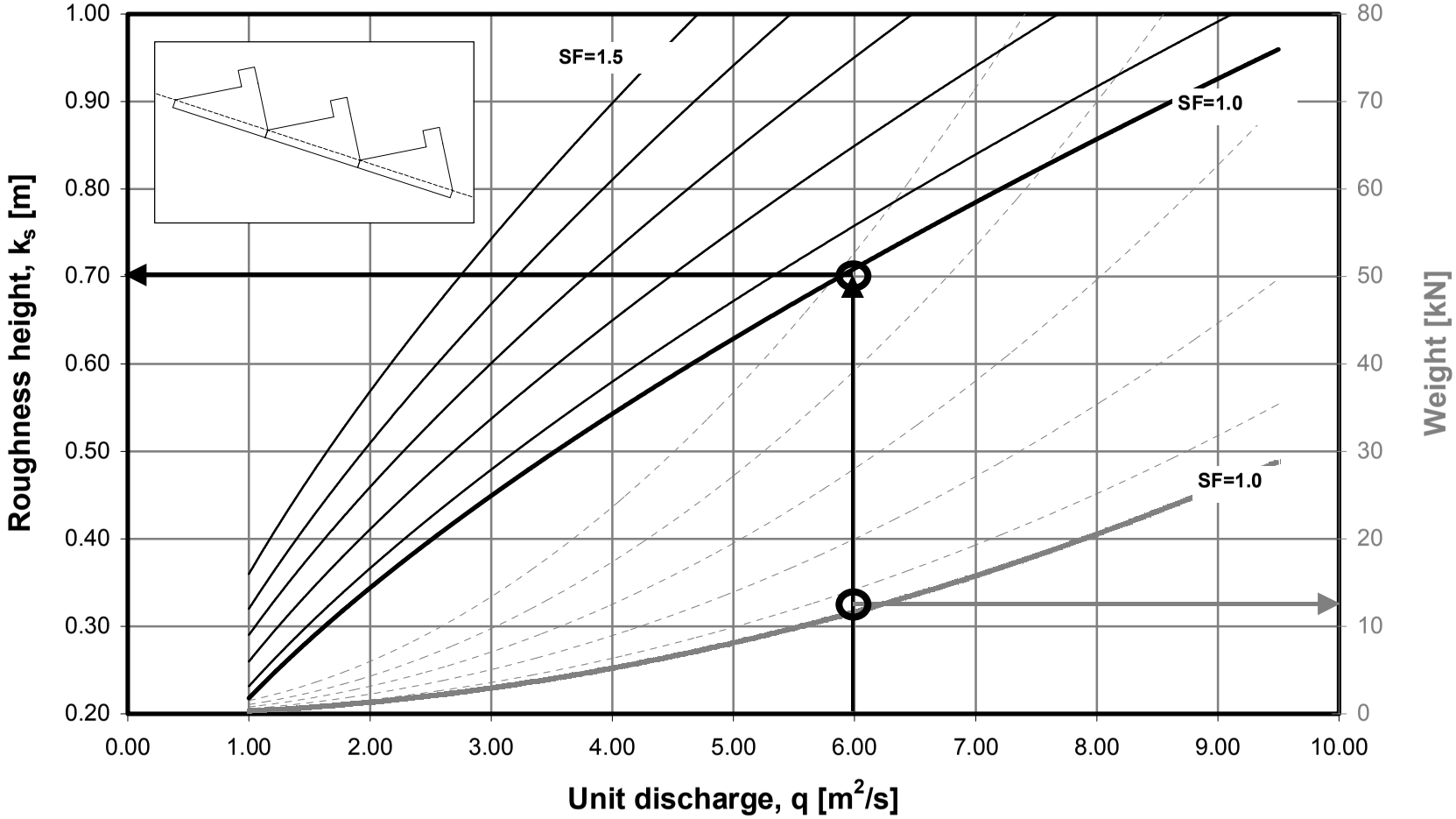

Figure 3 - Design chart for the 30° NEGATIVE INCLINED STEP WITH END SILL (type 2+ES). Minimum safety factor values, SF1 between 1.0 and 1.5, without drainage. Concrete density of 2400 kg/m^3. The experimental observation corresponds to the value marked with a circle.

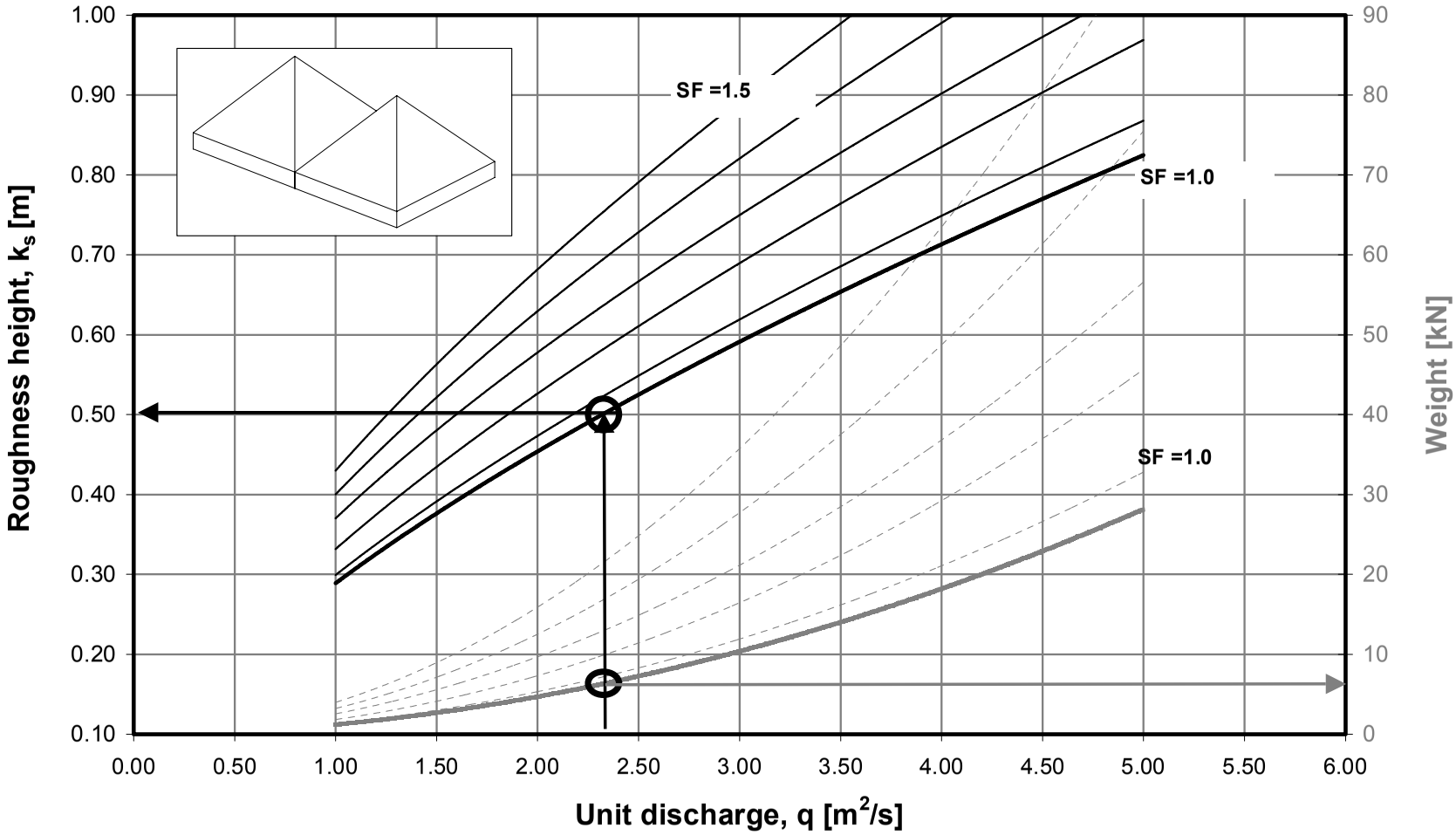

Figure 4 - Design chart for the 45° PYRAMIDS (type 3). Minimum safety factor values, SF1 between 1.0 and 1.5, without drainage. Concrete density of 2400 kg/m^3. The experimental observation corresponds to the value marked with a circle.

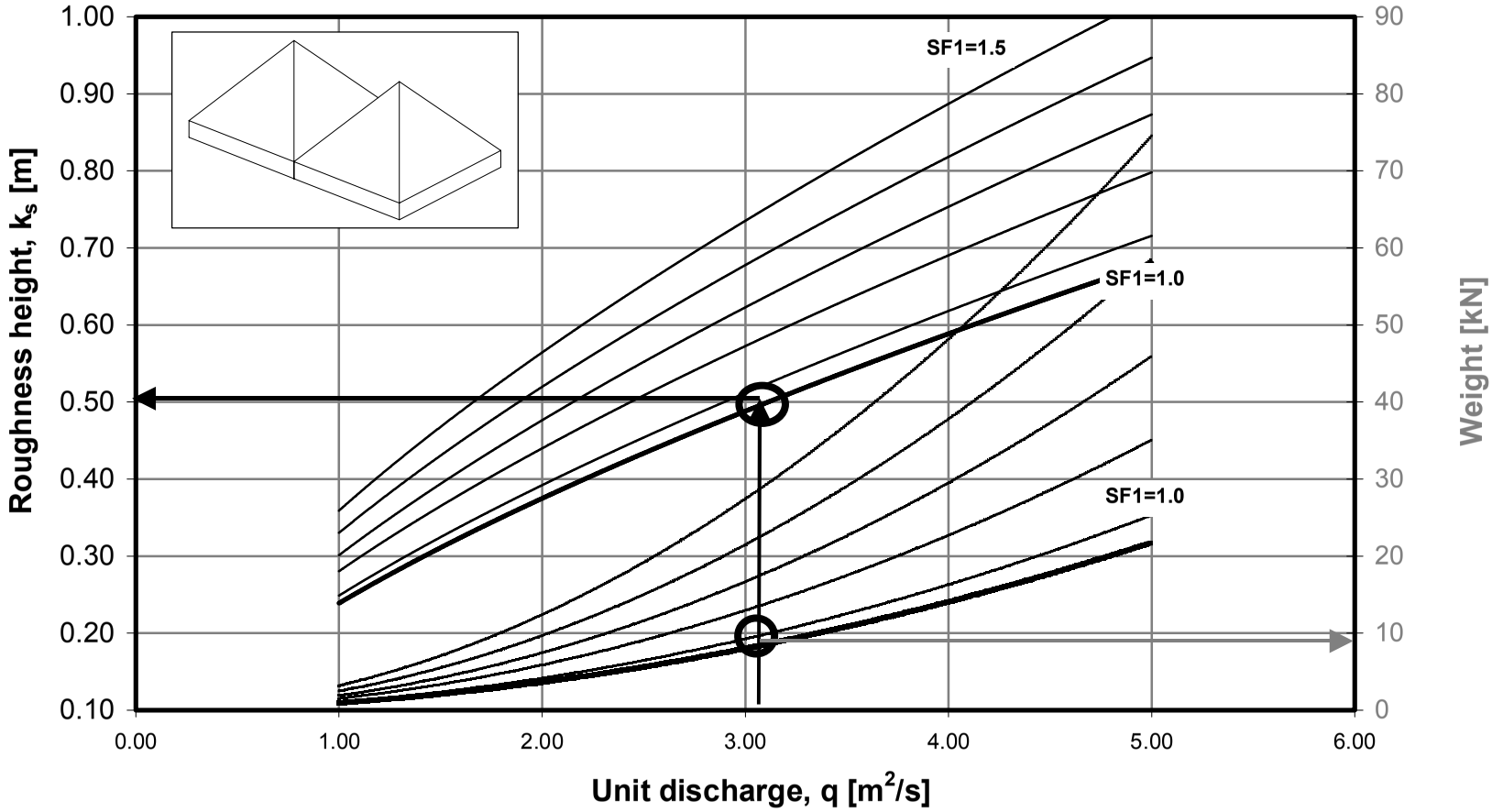

Figure 5 - Design chart for the 45° PYRAMIDS WITH ADDITIONAL SLAB (type 3+). Minimum safety factor values, SF1 between 1.0 and 1.5, without drainage. Concrete density of 2400 kg/m^3. The experimental observation corresponds to the value marked with a circle.

STABILITY OF CONCRETE ELEMENT LININGS

This worksheet was developed to evaluate the stability of overflow embankment linings made of concrete elements.
Its application range is limited to earthfill dam slopes (around 1V/3H)
The design is made for fully aerated uniform flow conditions in skimming regime.
author: Pedro Manso, August 2001, Laboratoire de Construction Hydrauliques, EPFL

blue text = Fill in BY USER red=computed
Note : Before start, erase all text written in blue, concerning former use of this worksheet

Description **Example 1: Element type 2ES, without drainage, for hcr/ks max conditions**

1° Design discharge

Unit discharge	q	[m^2/s]	**5.9**	
Critical water depth	hcr	[m]	1.53	eq.2.1

Note: From Figures 5.5/5.6 the type of element can be selected, for computation with drainage or without drainage.
The maximum unit discharge, *q max*, can be slightly higher than the maximum value on these figures.
Check Table 5.1 for values of qmax to which correspond a weight equal to the maximum capacity of site cranes, 30 kN.
Computation of safety including drainage are available for element type 1/1a/2ES.

2° Element type

Type		**2ES**	
Drainage	(yes/no)	**no**	>>> more unfavourable is "no"

Note: Select element height (ks) according to limits of hcr/ks (Figures 5.1 or 5.2) and limit weight for use of site cranes
If for chosen unit discharge hcr/ks is higher than maximum of Figures 5.1 or 5.2 => increase roughness height
If by increasing roughness weight the blocks become too heavy => reduce unit discharge (increase channel width)
In Figures 5.5 and 5.6 the mean skimming flow water depth (Ymean) is also presented.
The following Table computed the geometry features needed (equations in **Appendix 5**)

Type	hcr/ks max (Fig. 5.5/6)	Ymean/ks max	ks [m]	hcr/ks	xg [m]	zg [m]	base [m]
1	2.74	1.46		define other block	-	-	-
1a	1.58	1.26		define other block	-	-	-
2	3.90	2.20		define other block	-	-	-
2a	1.42	1.56		define other block	-	-	-
2ES	2.19	1.19	**0.70**	2.18	0.697	0.233	1.20
2ESa	1.32	0.90		define other block	-	-	-
3	1.66	1.29		define other block	-	-	-
to be used			0.70		0.6974	0.2328	1.20

Mean air concentration	Cmean	**0.30**	>> follow suggestions

Suggestions: Compute Cmean from the formulae of Matos and Chanson for stepped-like elements, and from Hartung and Scheuerlein for the pyramids. Those formulae are valid for skimming flow over macro-roughness in quasi-uniform flow conditions and depend only on the slope. For a slope of 1/3, averaged values of Cmean = 0.30 for stepped-like elements and Cmean =0.38 for pyramids, are suggested. Sensitivity analysis is recommended.

3° Geometry

cross-section surface	A	[m2]	0.5841
element base	base	[m]	1.20
element width	b	[m]	1.00
volume	V	[m3]	0.5841
density	ρs	[kg/m3]	**2400**
mass		[kg]	1402
weight		[kN]	13.74
gravity centre coordinate-x	xg	[m]	0.6974
gravity centre coordinate-z	zg	[m]	0.2328
foundation thickness	hf	[m]	0.100

4° Computation procedure

If hcr/ks = hcr/ks max => move to page 2, limit equilibrium state calculation
If not => move to page 3

BELOW LIMIT EQUILIBRIUM CONDITIONS

hcr/ks < hcr/ks max

The limit equilibrium state (LES) assumption is adequate for conditions just before failure of the lining (hcr/ks is maximum).

For values of hcr/ks lower than the maximum the element should be stable. If LES was assumed for hcr/ks<hcr/ks max an artificial overestimation of the hydrodynamic forces would be made.
In fact, the hydrodynamic forces have their maximum values for hcr/ksmax (LES conditions) where they just counterbalance the weight, together with the lift force.

For hcr/ks < max it is not possible to evaluate the hydrodynamic forces. Nevertheless, if their maximum values are taken (for LES conditions with same discharge) the minimum safety factor corresponding to the chosen ks can be computed.

5° Given data

slope	α	[°]	18.43
gravitacional acceleration	g	[m/s-2]	9.81
water density	ρw	[kg/m3]	1000
kynematic water viscosity	ν	[m/s]	1.16E-06

6° Auxiliary calculation of LES conditions (hcr/ks max => ks min for given q) to compute K*

type of block			2ES	
specific discharge	q	[m2/s]	5.90	
hcr/ks max			2.19	(from Table page 1)
Ymean/ks max			1.19	(from Table page 1)
ks min for given q		[m]	0.70	
Ymean max for given ks		[m]	0.83	
Mean air concentration	Cmean	[m]	0.31	see sugestions for Cmean at page 1
hw max for given ks	hw	[m]	0.57	Max value for given q
Mean depth-averaged water velocity	Uw	[m/s]	10.32	Max value for given q

Type	A [m2]	xg [m]	zg [m]	base [m]	b [m]
1	-	-	-	-	-
1a	-	-	-	-	-
2	-	-	-	-	-
2a	-	-	-	-	-
2ES	0.5782	0.694	0.232	1.19	0.99
2ESa	-	-	-	-	-
3	-	-	-	-	-
to be used	0.5782	0.6939	0.2316	1.19	0.99

mass		[kg]	1381		
Weight - x direction	Wx	[N/m]	4305		eq.5.3
Weight - z direction	Wz	[N/m]	12915		eq.5.4
Hydrostatic lift	L	[N/m]	3713		eq.5.9/5.12
Direction of resultant force	θ	[°]	24.9		eq. 5.13
Resulting force in z-direction	Rz	[N/m]	9202		eq. 5.15
Resulting force in x-direction	Rx	[N/m]	19864		eq. 5.14
Hydrodynamic force in flow direction	Fx*	[N/m]	15559		eq.5.16
Factor for F*	K*	[-]	0.42	AD=ks	eq. 5.8

7° Basic equation and Loads (per meter width)

i) for hcr/ks < hcr/ks max the ΣMs >Σmus, meaning SF1>1.0

ii) Using the same value of K* computed for LES the hydrodynamic force F* will have the most unfavourable proportion towards the kynematic energy head ($Uw^2/2g$).

iii) All forces are at the gravity center, G.

Weight - x direction	Wx	[N/m]	4349		eq.5.3
Weight - z direction	Wz	[N/m]	13046		eq.5.4
Hydrostatic Lift	L	[N/m]	3805	h=hw LES	eq.5.9/5.12/5.29
Mean depth-averaged water velocity	Uw	[m/s]	10.32	Uw=Uw LES	eq.5.28
Hydrodynamic force in flow direction	F*	[N/m]	15638		eq.5.30

8° Safety factor computation (SF1)

Resulting force in z-direction	Rz	[N/m]	9241	eq. 5.15 a/b
Resulting force in x-direction	Rx	[N/m]	19987	eq. 5.16
Direction of resultant force	θ	[°]	24.81	eq. 5.14
Sum of stabilising moments	ΣMs	[Nm/m]	4644.51	eq.5.18
Sum of overturning moments	ΣMo	[Nm/m]	4653.37	eq.5.19
Safety factor at LES conditions	SF1		**1.00**	eq.5.17

Suggestion: If SF1 > 1.5 then reduce the roughness height

9° Computation of a recommended safety factor, SF2

i) To assign additional safety to a certain blcoks geometry and for a given flow, an increase in the foundation thickness, Δ, is advised.
ii) Increase of foundation thickness is advised untill SF2 assumes a minimum value of 1.5.
ii) Every additional increase in foundation thickness represents a non-neglegible increase in weight (and cost).

Recomended minimum safety factor	SF2		**1.50**	
Sum of stabilising moments (with Δ)	ΣMs +MWΔ	[Nm/m]	6975.61	eq. 5.20/5.21
Moment of additional weight at OP	MW_Δ	[Nm/m]	2331.09	eq. 5.20/5.21
Additional thickness	Δ	[m]	**0.182**	eq.5.24
auxiliary variable	a	[N/m2]	4467.16	eq.5.25
auxiliary variable	b	[N/m]	12031.0	eq.5.26 a/b
auxiliary variable	c	[Nm/m]	-2331.09	eq.5.27

Note: The computed Δ might not be the lowest possible value for SF2=1.5. This conditions is verifies for a range of values. It is suggested to follow step 11 to refine Δ's estimation.

10° Quantities of concrete

total lateral area	At	[m2]	0.8019	
total volume	Vt	[m3]	0.802	
mass of one block		[kg]	1924.6	
mass/m2		[ton/m2]	1.60	
weight of one block		in [N]	18861.3	
		in [kN]	18.86	

11° Refine estimation of the safety factor and its consequence on concrete quantity

This step is not compulsory.

			If SF1<1.5	If SF1>1.5
Extra increase in foundation (SF>1.5)	Δ*	[m]	**-0.015**	**0.005**
Moment of extra weight	MWΔ*	[Nm/m]	-206.6	-
sum of moments with extra increase in foundation	ΣMs*	[Nm/m]	6769.02	-
	SF*		**1.45**	**-**
total volume	Vt*	[m3]	0.784	0.590
mass/m2		[ton/m2]	1.57	1.18
weight of one block		in [kN]	18.44	13.88
Total additional foundation thickness		[m]	**0.167**	**0.005**

Suggestion:

a) if Δ* is set to as -Δ the quantities for the initial laboratory scenario are presented

b) Δ* can be defined to correct the oversize due to Δ so that a high SF does not become uneconomic

STABILITY OF CONCRETE ELEMENT LININGS

This worksheet was developed to evaluate the stability of overflow embankment linings made of concrete elements.
Its application range is limited to earthfill dam slopes (around 1V/3H)
The design conditions correspond to fully aerated uniform flow in skimming regime
author: Pedro Manso, August 2001, Laboratoire de Construction Hydrauliques, EPFL

blue text = Fill in BY USER red=computed
Note : Before start, erase all text written in blue, concerning former use of this worksheet

Description **Example 2: Element type 2ES, without drainage, for below hcr/ks max conditions**

1° Design discharge

Unit discharge	q	[m^2/s]	**5.9**	
Critical water depth	hcr	[m]	1.53	eq.2.1

Note: From Figures 5.5/5.6 the type of element can be selected, for computation with drainage or without drainage.
The maximum unit discharge, *q max* , can be slightly higher than the maximum value on these figures.
Check Table 6.1for values of q max to which correspond a weight equal to the maximum capacity of site cranes, 30 kN.
Computation of safety including drainage are available for element type 1/1a/2ES.

2° Element type

Type		**2ES**	
Drainage	(yes/no)	**no**	>>> more unfavourable is "no"

Note: Select element height (ks) according to limits of hcr/ks (Figures 5.1 or 5.2) and limit weight for use of site cranes
In Figures 5.5 and 5.6 the mean skimming flow water depth (Ymean) is also presented.
The following Table computed the geometry features needed (equations in **Appendix 5.1**)

Type	hcr/ks max (Fig. 5.5/6)	Ymean/ks max	ks [m]	hcr/ks	xg [m]	zg [m]	base [m]
1	2.74	1.46		define other block	-	-	-
1a	1.58	1.26		define other block	-	-	-
2	3.90	2.20		define other block	-	-	-
2a	1.42	1.56		define other block	-	-	-
2ES	2.19	1.19	**0.84**	1.82	0.837	0.279	1.44
2ESa	1.32	0.90		define other block	-	-	-
3	1.66	1.29		define other block	-	-	-
to be used			0.84		0.8369	0.2794	1.44

Mean air concentration	Cmean	**0.30**	>> follow suggestions

Suggestions: Compute Cmean from the formulae of Matos or Chanson for stepped-like elements, and from Hartung & Scheuerlein for the pyramids. Those formulae are valid for skimming flow over macro-roughness in quasi-uniform flow conditions and depend only on the slope. For a slope of 1/3, averaged values of Cmean = 0.30 for stepped-like elements and Cmean =0.38 for pyramids, are suggested. Sensitivity analysis is recommended.

3° Geometry (formulae in Appendix 5.1)

cross-section surface	A	[m2]	0.8411
element base	base	[m]	1.44
element width	b	[m]	1.20
volume	V	[m3]	1.0093
density	ρs	[kg/m3]	**2400**
mass		[kg]	2422
weight		[kN]	23.74
gravity centre coordinate-x	xg	[m]	0.8369
gravity centre coordinate-z	zg	[m]	0.2794
foundation thickness	hf	[m]	0.120

4° Computation procedure

If hcr/ks = hcr/ks max => move to page 2, limit equilibrium state calculation
If not => move to page 3

BELOW LIMIT EQUILIBRIUM CONDITIONS

hcr/ks < hcr/ks max

The limit equilibrium state (LES) assumption is adequate for conditions just before failure of the lining (hcr/ks is maximum).

For values of hcr/ks lower than the maximum the element should be stable. If LES was assumed for hcr/ks<hcr/ks max an artificial overestimation of the hydrodynamic forces would be made.
In fact, the hydrodynamic forces have their maximum values for hcr/ksmax (LES conditions) where they just counterbalance the weight, together with the lift force.

For hcr/ks < max it is not possible to evaluate the hydrodynamic forces. Nevertheless, if their maximum values are taken (for LES conditions with same discharge) the minimum safety factor corresponding to the chosen ks can be computed.

5° Given data

slope	α	[°]	18.43
gravitacional acceleration	g	[m/s-2]	9.81
water density	ρw	[kg/m3]	1000
kynematic water viscosity	ν	[m/s]	1.16E-06

6° Auxiliary calculation of LES conditions (hcr/ks max => ks min for given q) to compute K*

type of block			2ES	
specific discharge	q	[m2/s]	5.90	
hcr/ks max			2.19	(from Table page 1)
Ymean/ks max			1.19	(from Table page 1)
ks min for given q		[m]	0.70	
Ymean max for given ks		[m]	0.83	
Mean air concentration	Cmean	[m]	0.31	see sugestions for Cmean at page 1
hw max for given ks	hw	[m]	0.57	Max value for given q
Mean depth-averaged water velocity	Uw	[m/s]	10.32	Max value for given q

Type	A [m2]	xg [m]	zg [m]	base [m]	b [m]
1	-	-	-	-	-
1a	-	-	-	-	-
2	-	-	-	-	-
2a	-	-	-	-	-
2ES	0.5782	0.694	0.232	1.19	0.99
2ESa	-	-	-	-	-
3	-	-	-	-	-
to be used	0.5782	0.6939	0.2316	1.19	0.99

mass		[kg]	1381		
Weight - x direction	Wx	[N/m]	4305		eq.5.3
Weight - z direction	Wz	[N/m]	12915		eq.5.4
Hydrostatic lift	L	[N/m]	3713		eq.5.9/5.12
Direction of resultant force	θ	[°]	24.9		eq. 5.13
Resulting force in z-direction	Rz	[N/m]	9202		eq. 5.15
Resulting force in x-direction	Rx	[N/m]	19864		eq. 5.14
Hydrodynamic force in flow direction	Fx*	[N/m]	15559		eq.5.16
Factor for F*	K*	[-]	0.42	AD=ks	eq. 5.8

7° Basic equation and Loads (per meter width)

i) for hcr/ks < hcr/ks max the ΣMs >Σmus, meaning SF1>1.0

ii) Using the same value of K* computed for LES the hydrodynamic force F* will have the most unfavourable proportion towards the kynematic energy head ($Uw^2/2g$).

iii) All forces are at the gravity center, G.

Weight - x direction	Wx	[N/m]	6262		eq.5.3
Weight - z direction	Wz	[N/m]	18787		eq.5.4
Hydrostatic Lift	L	[N/m]	5479	h=hw LES	eq.5.9/5.12/5.29
Mean depth-averaged water velocity	Uw	[m/s]	10.32	Uw=Uw LES	eq.5.28
Hydrodynamic force in flow direction	F*	[N/m]	18765		eq.5.30

8° Safety factor computation (SF1)

Resulting force in z-direction	Rz	[N/m]	13307	eq. 5.15 a/b
Resulting force in x-direction	Rx	[N/m]	25028	eq. 5.16
Direction of resultant force	θ	[°]	28.00	eq. 5.14
Sum of stabilising moments	ΣMs	[Nm/m]	8025.72	eq.5.18
Sum of overturning moments	ΣMo	[Nm/m]	6992.45	eq.5.19
Safety factor at LES conditions	SF1		**1.15**	eq.5.17

Suggestion: If SF1 > 1.5 then reduce the roughness height

9° Computation of a recommended safety factor, SF2

i) To assign additional safety to a certain blcoks geometry and for a given flow, an increase in the foundation thickness, Δ, is advised.
ii) Increase of foundation thickness is advised untill SF2 assumes a minimum value of 1.5.
ii) Every additional increase in foundation thickness represents a non-neglegible increase in weight (and cost).

Recomended minimum safety factor	SF2		**1.50**	
Sum of stabilising moments (with Δ)	ΣMs +MWΔ	[Nm/m]	10852.62	eq. 5.20/5.21
Moment of additional weight at OP	MW_Δ	[Nm/m]	2826.90	eq. 5.20/5.21
Additional thickness	Δ	[m]	**0.156**	eq.5.24
auxiliary variable	a	[N/m2]	5360.59	eq.5.25
auxiliary variable	b	[N/m]	17324.6	eq.5.26 a/b
auxiliary variable	c	[Nm/m]	-2826.90	eq.5.27

Note: The computed Δ might not be the lowest possible value for SF2=1.5. This conditions is verifies for a range of values. It is suggested to follow step 11 to refine Δ's estimation.

10° Quantities of concrete

total lateral area	At	[m2]	1.0653	
total volume	Vt	[m3]	1.278	
mass of one block		[kg]	3068.0	
mass/m2		[ton/m2]	1.78	
weight of one block		in [N]	30066.3	
		in [kN]	30.07	**ATTENTION: heavier than 30 kN**

11° Refine estimation of the safety factor and its consequence on concrete quantity

This step is not compulsory.

			If SF1<1.5	If SF1>1.5
Extra increase in foundation (SF>1.5)	Δ*	[m]	**-0.020**	**0.005**
Moment of extra weight	MWΔ*	[Nm/m]	-382.9	-
sum of moments with extra increase in foundation	ΣMs*	[Nm/m]	10469.73	-
	SF*		**1.50**	**-**
total volume	Vt*	[m3]	1.244	-
mass/m2		[ton/m2]	1.73	-
weight of one block		in [kN]	29.25	-
Total additional foundation thickness		[m]	**0.136**	**-**

Suggestion:

a) if Δ* is set to as -Δ the quantities for the initial laboratory scenario are presented

b) Δ* can be defined to correct the oversize due to Δ so that a high SF does not become uneconomic

Appendix 5 (suite): Resume table of values needed to plot the Design Chart of element type 2+ES

Type 2ES		SF1=1.0		SF1=1.1		SF1=1.2		SF1=1.3		SF1=1.4		SF1=1.5							
q	hcr/ks	ks	W	ks	W	ks	W	ks	W	ks	W	ks	W	SF1	SF2	SF*	Δ	Weight (initial)	Weight (with Δ)
[m^2/s]		[m]	[kN]	[m]	[kN]	[m]	[kN]	[m]	[kN]	[m]	[kN]	[m]	[kN]				[m]	[kN]	[kN]
9.50	2.18	0.96	28.88											1.00	1.5	1.50	0.205	28.88	**39.75**
9.10	2.19	0.93	26.26											0.99	1.5	1.50	0.200	26.26	**36.23**
9.00	2.17	0.93	26.26											1.00	1.5	1.50	0.197	26.26	**36.07**
8.00	2.17	0.86	20.77											1.00	1.5	1.50	0.182	20.77	28.52
8.00	2.05			0.91	24.60									1.05	1.5	1.50	0.169	24.60	**32.67**
7.10	2.18	0.79	16.10											1.00	1.5	1.50	0.169	16.10	22.19
7.10	2.03			0.85	20.05									1.05	1.5	1.50	0.154	20.05	26.47
7.10	1.82					0.95	27.99							1.15	1.5	1.50	0.127	27.99	**34.58**
7.00	2.16	0.79	16.10											1.00	1.5	1.50	0.165	16.10	22.03
7.00	2.03			0.84	19.35									1.05	1.5	1.50	0.153	19.35	25.57
7.00	1.82					0.94	27.12							1.15	1.5	1.50	0.125	27.12	**33.46**
6.00	2.17	0.71	11.68											1.00	1.5	1.50	0.150	11.68	16.04
6.00	2.03			0.76	14.33									1.05	1.5	1.50	0.137	14.33	18.89
6.00	1.81					0.85	20.05							1.15	1.5	1.50	0.112	20.05	24.72
6.00	1.62							0.95	27.99					1.25	1.5	1.50	0.084	27.99	**32.37**
5.93	2.19	0.70	11.20											1.00	1.5	1.50	0.150	11.20	15.44
5.00	2.17	0.63	8.16											1.00	1.5	1.50	0.133	8.16	11.20
5.00	2.04			0.67	9.82									1.05	1.5	1.50	0.122	9.82	12.97
5.00	1.82					0.75	13.77							1.15	1.5	1.50	0.100	13.77	17.01
5.00	1.63							0.84	19.35					1.25	1.5	1.50	0.074	19.35	22.38
5.00	1.45									0.94	27.12			1.35	1.5	1.50	0.045	27.12	**29.42**
4.00	2.18	0.54	5.14											1.00	1.5	1.50	0.115	5.14	7.08
4.00	2.03			0.58	6.37									1.05	1.5	1.50	0.105	6.37	8.40
4.00	1.81					0.65	8.97							1.15	1.5	1.50	0.085	8.97	11.04
4.00	1.61							0.73	12.70					1.25	1.5	1.50	0.063	12.70	14.63
4.00	1.45									0.81	17.35			1.35	1.5	1.50	0.040	17.35	18.85
4.00	1.31											0.90	23.80	1.45	1.5	1.50	0.012	23.80	24.37
3.00	2.16	0.45	2.97											1.01	1.5	1.50	0.143	2.97	4.64
3.00	2.02			0.48	3.61									1.06	1.5	1.50	0.125	3.61	5.27
3.00	1.80					0.54	5.14							1.16	1.5	1.50	0.092	5.14	6.69
3.00	1.62							0.60	7.05					1.25	1.5	1.50	0.063	7.05	8.37
3.00	1.45									0.67	9.82			1.35	1.5	1.50	0.034	9.82	10.69
3.00	1.31											0.74	13.23	1.45	1.5	1.50	0.010	13.23	13.55
2.00	2.18	0.34	1.28											1.00	1.5	1.50	0.073	1.28	1.77
2.00	2.00			0.37	1.65									1.06	1.5	1.50	0.065	1.65	2.17
2.00	1.81					0.41	2.25							1.15	1.5	1.50	0.054	2.25	2.77
2.00	1.61							0.46	3.18					1.25	1.5	1.50	0.040	3.18	3.66
2.00	1.45									0.51	4.33			1.35	1.5	1.50	0.026	4.33	4.72
2.00	1.30											0.57	6.05	1.46	1.5	1.50	0.007	6.05	6.17
1.00	2.12	0.22	0.35											1.02	1.5	1.50	0.044	0.35	0.47
1.00	2.03			0.23	0.40									1.05	1.5	1.50	0.042	0.40	0.52
1.00	1.80					0.26	0.57							1.16	1.5	1.50	0.034	0.57	0.70
1.00	1.61							0.29	0.80					1.25	1.5	1.50	0.025	0.80	0.92
1.00	1.46									0.32	1.07			1.35	1.5	1.50	0.017	1.07	1.17
1.00	1.30											0.36	1.52	1.46	1.5	1.50	0.004	1.52	1.56

Communications du Laboratoire de constructions hydrauliques
Ecole Polytechnique Fédérale de Lausanne
Editeur: Prof. Dr A. Schleiss

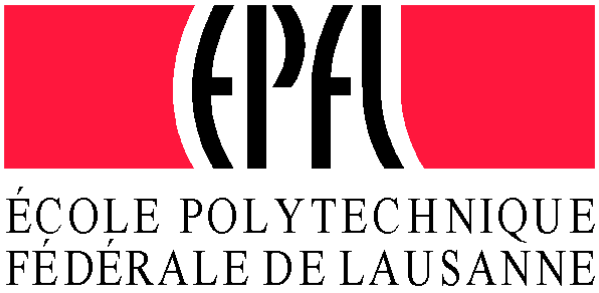

Prof. Dr A. Schleiss
Laboratoire de constructions hydrauliques - LCH
EPFL, CH-1015 Lausanne
http://lchwww.epfl.ch
e-mail: secretariat.lch@epfl.ch